AD

USAAVLABS TECHNICAL REPORT 66-49

DESIGN AND TEST EVALUATION OF A SUPERCRITICAL SPEED SHAFT

By

Robert Baier
John Mack

June 1966

U. S. ARMY AVIATION MATERIEL LABORATORIES
FORT EUSTIS, VIRGINIA

CONTRACT DA 44-177-AMC-161(T)
VERTOL DIVISION
THE BOEING COMPANY
MORTON, PENNSYLVANIA

Disclaimers

The findings in this report are not to be construed as an official Department of the Army position unless so designated by other authorized documents.

When Government drawings, specifications, or other data are used for any purpose other than in connection with a definitely related Government procurement operation, the United States Government thereby incurs no responsibility nor any obligation whatsoever; and the fact that the Government may have formulated, furnished, or in any way supplied the said drawings, specifications, or other data is not to be regarded by implication or otherwise as in any manner licensing the holder or any other person or corporation, or conveying any rights or permission, to manufacture, use, or sell any patented invention that may in any way be related thereto.

Trade names cited in this report do not constitute an official endorsement or approval of the use of such commercial hardware or software.

Disposition Instructions

Destroy this report when no longer needed. Do not return it to the originator.

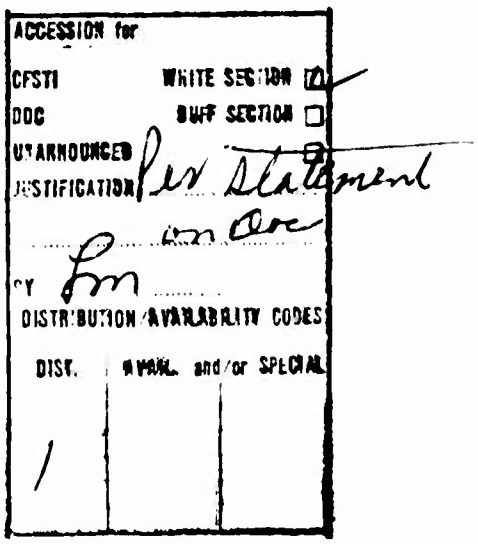

DEPARTMENT OF THE ARMY
U. S. ARMY AVIATION MATERIEL LABORATORIES
FORT EUSTIS, VIRGINIA 23604

This report presents the results of a continuing research program for the investigation of high-speed drive-system concepts for use in V/STOL aircraft. The main efforts of this program are directed toward:

1. Design of a full-scale supercritical speed shaft system utilizing design criteria established with small-scale model shafts.

2. Dynamic bench tests of a full-scale shaft system.

3. Correlation of results of full-scale model tests with small-scale model tests.

The extensive testing conducted under this program has successfully demonstrated the capability of slender and highly loaded power transmission shafting to operate safely at speeds significantly above the first critical speed.

Task 1M121401D14414
Contract DA 44-177-AMC-161(T)
USAAVLABS Technical Report 66-49
June 1966

DESIGN AND TEST EVALUATION OF A SUPERCRITICAL SPEED SHAFT

R-458

by

Robert Baier
and
John Mack

Prepared by

VERTOL DIVISION
THE BOEING COMPANY
Morton, Pennsylvania

for

U.S. ARMY AVIATION MATERIEL LABORATORIES
Fort Eustis, Virginia

SUMMARY

This report concludes a study performed by Boeing-Vertol Division on the supercritical speed shaft. It presents the results of design and test parameters used to build a full-size helicopter interconnect shaft for USAAVLABS under Contract DA 44-177-AMC-161(T).

Program objectives were: (1) to relate presently developed supercritical shaft and model test results to a full-size helicopter interconnect shaft; (2) to develop a specification and preliminary design for a supercritical shaft damper suitable for aircraft installation; and (3) to develop a systematic procedure and theoretical background for the balancing of supercritical speed shafts.

A full-size supercritical speed shaft was built, and the modeling procedures and design criteria previously developed, using small size shafts, were applied. The full-size damped shaft operated satisfactorily and demonstrated its capability by running successfully through the entire speed range (0 to 8900 revolutions per minute) and beyond this to 9500 revolutions per minute.

A number of damper design types were tested on the supercritical shaft. A viscous damper appears to be a good choice for an aircraft type damper.

Criteria of successful operation were established. When the test results were analyzed by these criteria (shown on page 132 in Figure 76), the following points were evident:

The supercritical shaft is feasible for helicopter operation.

The supercritical shaft will be advantageous to the helicopter.

It can therefore be concluded that the development of the supercritical shaft could proceed toward a helicopter flight evaluation.

FOREWORD

This report covers the development and testing by Boeing-Vertol Division of a supercritical speed shaft for eventual use in helicopters. It concludes the work authorized under USAAVLABS Contract DA 44-177-AMC-161(T) to develop a full-size synchronizing shaft system for the CH-47A helicopter.

The work on the supercritical speed shaft began on receipt of the contract on 6 July 1964. The principal investigators at Vertol Division were: R. Baier, Project Engineer; and J. C. Mack, Supervising Engineer. Acknowledgment is made to personnel of Battelle Memorial Institute, Messrs. R. Prouse, H. Meacham and J. Vorhees, for the assistance and contribution they provided, on a subcontract effort, during the program. Acknowledgment of appreciation is made to the USAAVLABS representative, Mr. Wayne Hudgins, for his aid in this program.

TABLE OF CONTENTS

TABLE OF CONTENTS (Continued)

LIST OF ILLUSTRATIONS

LIST OF TABLES

LIST OF SYMBOLS

$\bar{a}$	absolute acceleration of mass-center of cross section
A	cross-sectional area
c	damping coefficient per unit span of shaft
C	required damping coefficient (lb-sec/in)
d	inside diameter
D	outside diameter
e	weight offset from shaft geometric center
E	Young's modulus
$\bar{F}_e$	net elastic force vector acting on a unit span of shaft
g	acceleration of gravity, 32.2 feet per second per second
h	gap width (inches)
$\bar{i},\bar{j},\bar{k}$	a set of unit vectors fixed in space, with $\bar{k}$ along the line of supports
I	moment of inertia of shaft about a diameter
K	spring stiffness (lb/inch), shaft stiffness at the unbalance location
ℓ	length
m	mass (lb sec^2/inch)
m(x)	mass per unit length of shaft
M	unbalance weight
$\bar{n}_1,\bar{n}_2$	unit vectors fixed in the shaft and rotating with it
O	the line between the end supports of the shaft

O'	the position (at rest) of the center of any cross section
O''	the position at any instant of the center of the cross section when an elastic displacement has taken place
P	the position of the mass-center of the cross section when no elastic displacement is present
P'	the instantaneous deflected position of the cross-center of the cross section
r	elastic deflection
R	end load (pounds)
$\overline{R}$	position vector of mass-center of cross section at any instant
$\overline{R}_o$	position vector of cross-section center with respect to line of support due to initial deflection
t	time
$\overline{V}$	absolute velocity of mass-center of cross section
$\overline{V}_o$	absolute velocity of geometric center of cross section
W	weight
$\overline{W}$	displacement vector of cross section center due to shaft flexibility
x	coordinate along line of supports of shaft
x,y	fixed axis system
X	motion of the mass
X_1	nagnitude of the support motion
y	deflection (inches)
δ	radius of deflection at that speed (inches)

$\bar{\eta}$	position vector of mass-center of cross section with respect to center of cross section
μ	viscosity (reyns) at the temperature of interest
μ_n	n^{th} mode damping ratio (external damping)
ρ	mass-density of shaft material
ω	angular velocity of critical speed of interest (radians per second), rate of rotation of shaft
ω_n	n^{th} mode natural frequency
ω_1	rotational speed
Ω	shaft rotational speed
$\bar{\Omega}$	angular velocity vector for shaft
$\bar{\Omega}_f$	angular velocity vector for any rotating frame of reference

INTRODUCTION

This report concludes a program by the Vertol Division to develop, test, and evaluate a full-size supercritical rotor interconnect shaft for the CH-47A helicopter. The program was authorized by USAAVLABS Contract DA 44-177-AMC-161(T), dated 6 July 1964.

Vertol Division's awareness of the advantages of a supercritical shaft system is evidenced by proposals for analytical study, construction and testing of a supercritical shaft system early in 1959. Actual fabrication and testing of a company-funded model was under way in 1961. The results of this early work pointed out the need for the development of a damper to successfully allow a shaft to operate directly at its critical speed for extended periods of time.

Battelle Memorial Institute of Columbus, Ohio, was awarded an Air Force contract for model testing of supercritical shafting in May 1961. A procedure was developed which allowed modeled shafts to be related to shafts of any material, size and length in a dynamically similar manner. An analogy between shafts operating at their critical speeds and electrical transmission lines was formulated. This analogy gave promise of being the basis upon which optimum damper parameters could be calculated for any shaft. Shafts designed by the electrical analogy method were subjected to variables such as torque, curvature, axial force, external vibration, eccentricity, and moment restraint.

The excellent performance obtained in model tests by the use of this new design technique resulted in establishing a high degree of confidence that a full-size shaft could be designed using these same techniques (transmission line analogy) and that the full-size supercritical speed shaft would perform in a satisfactory manner.

Previous Battelle model investigation revealed that the damper exerted the primary influence in controlling shaft vibrations during testing. Additionally, it was found that variables of torque, curvature, or external vibration were of secondary importance because a damper could control a shaft through numerous critical speeds.

The electrical analogy, past empirical results, and model shaft testing constituted the tools available to Vertol to design the full-scale shaft.

This report presents an evaluation of the design tools, the modifications to these tools made necessary by test experience, and the final results of the modified approach.

DISCUSSION

GENERAL

This study covers the first recorded attempt wherein developed theory and design criteria obtained from model-size shaft investigation were applied to a full-size interconnect helicopter shaft. Refer to Figure 1.

The weight and reliability of a shaft system for a given length and horsepower capacity are responsive to two areas of improvement:

1. For weight - An increase in rotational speed with consequent lower torque, provided this is not accompanied by the increase in shaft supports typical of subcritical systems.

2. For reliability - A decrease in shaft discontinuities such as reduced sections, splines, riveted joints, bearings and couplings.

The supercritical shaft concept encompasses both areas of improvement, in that a successful system is capable of operation with greatly increased length of unsupported shaft. Figure 2 indicates the improvements realized by substituting a supercritical shaft for a subcritical shaft while maintaining the same rotational speed and torque capacity.

Further improvements in the future will be realized if intermediate gear reductions are eliminated as a result of the usable high-speed capability of the supercritical shaft concept.

The full-size supercritical design applies to a CH-47A helicopter shaft system, potentially operable in all respects except for the use of a laboratory damper.

The supercritical speed shaft under investigation is of the same diameter, and turns at the same speed, as an existing subcritical shaft system. Diameter, length and shaft speeds are dictated by present transmission ratios and torque requirements.

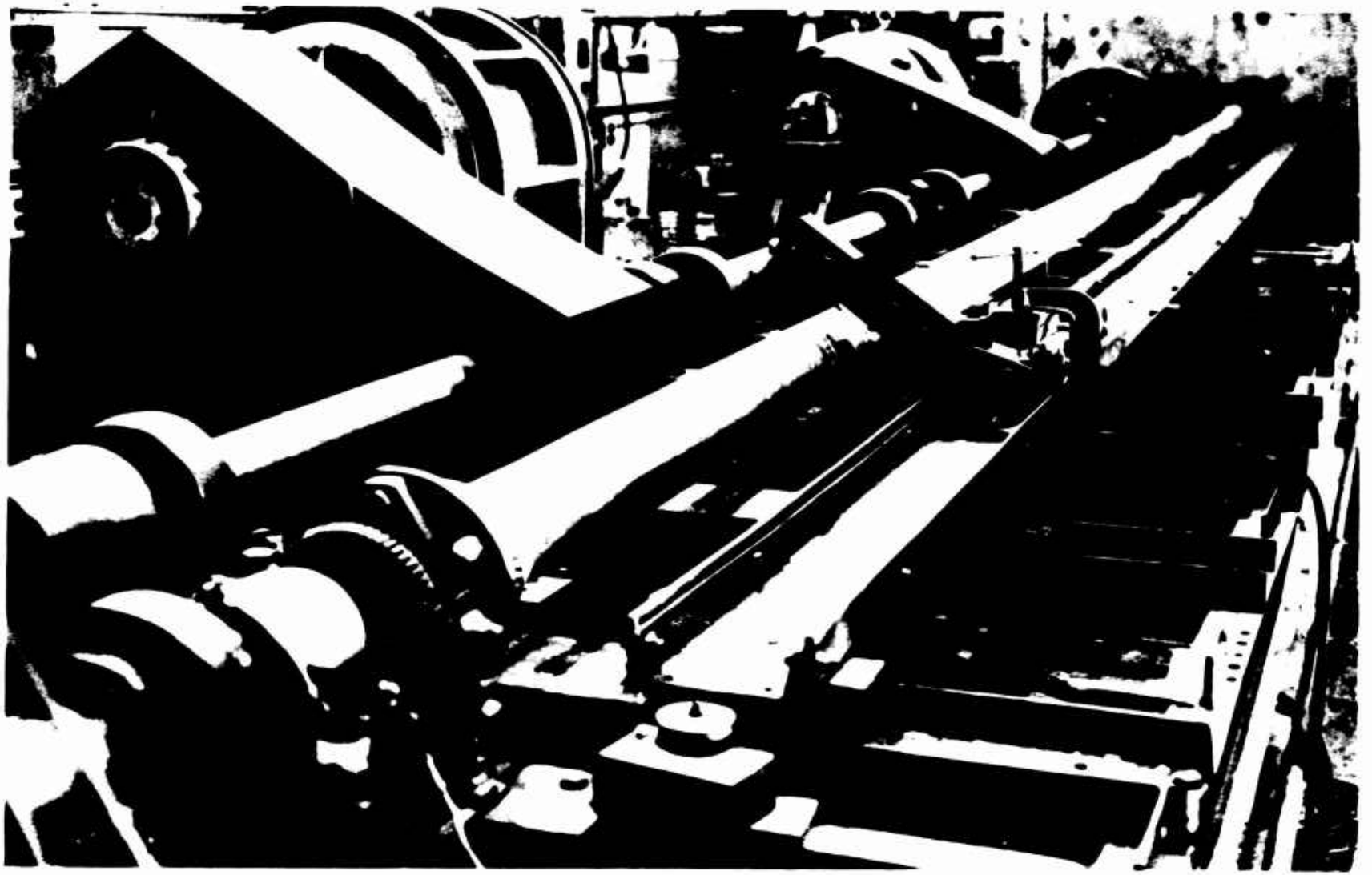

FIGURE 1. SUPERCRITICAL SPEED SHAFT - OPTICAL PICKUP AND TRACK.

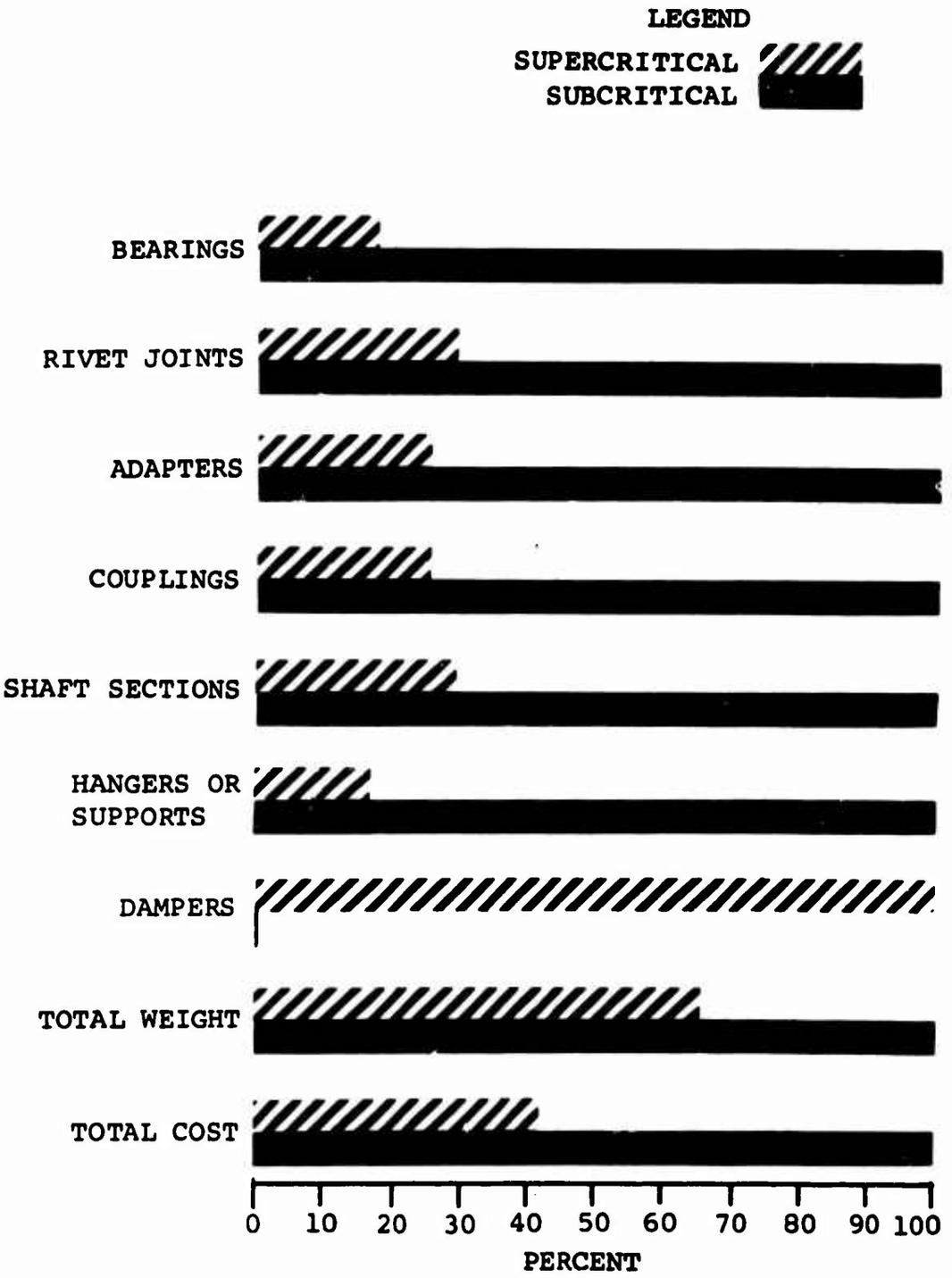

FIGURE 2. COMPARISONS (PARTS, COST, WEIGHT).

A separate area of study developed a specification and a preliminary design for a supercritical speed shaft damper system, one suitable for the environmental conditions encountered in actual aircraft service. A final area of study included a theoretical approach and a tabulated or empirical approach to shaft balance. Observation of a full-size, damped, supercritical shaft system checked the validity of developed design criteria and determined the relation of model shaft results with full-size shaft performance.

ANALYSIS OF PROBLEM

Supercritical Definition

For this report, a supercritical or hypercritical shaft is defined as a shaft operating above the first critical speeds (lateral bending resonant frequency). Functional operation of a supercritical shaft is explained by the vibration theory of resonance given in Linear System Operation.

Linear System Operation - Resonance concepts are reviewed in reference to a single-degree-of-freedom, spring-mass damper system. The response of an undamped spring-mass system when excited by a sinusoidal motion of the support is represented by the differential equation

$$m\ddot{x} + K\ (X-X_1) = 0$$

$$m\ddot{x} + KX = KX_1 \qquad (1)$$

where m = mass (lb sec^2/inch)

K = spring stiffness (lb/inch)

X = motion of the mass

X_1 = magnitude of the support motion

The solution to the differential equation, the relative response as a function of excitation frequency, is shown in Figure 3. At very slow speeds, as at A shown in Figure 3, the forcing function P moves slowly and the mass follows with no extension of the spring. At B the motion of the top is very rapid; therefore, the mass cannot follow and stands still in space. Then the relative motion is equal to the motion of the top $y_o/a_o=1$. At point C there is resonance, so the extensions of

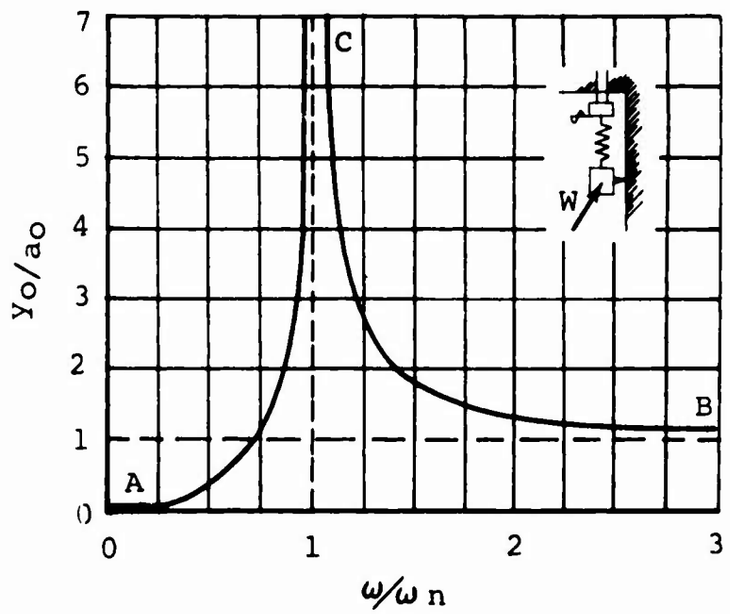

FIGURE 3. AMPLITUDE VS CRITICAL FREQUENCY RATIO.

the spring become, theoretically, infinitely large in an undamped system and result in failure. Resonance of a system is often determined by noting the frequency at which the phase shift reaches 90 degrees.

Rigid Shaft Operation - When one relates the linear system to a rotating shaft, first, there is the mass or rigid body of the shaft; second, there are the spring supports to structure; third, part of the linear system is a forcing function which, in this case, is an unbalance in the rigid shaft; and fourth, the damping, which is inherent or which is added to the system, controls the vibrations at resonance.

Phase shifts can be readily understood by the graphical illustration of the system used in the balancing machine.

When a shaft rotates slowly, the unbalance will force the shaft to move against the spring support in line with the unbalance. A piece of chalk will mark the heavy side as shown in Figure 4(A). As the shaft's speed is increased, the deflection will lag behind the unbalance according to the phase shift. Directly at critical speed, the chalk will mark the shaft 90 degrees behind the unbalance. See Figure 4(B). As speed is increased beyond critical, the deflection lags still further until it is 180 degrees behind the unbalance and the shaft is rotating about its mass center. At this point the chalk will mark the light side of the shaft, or the side opposite the unbalance. See Figure 4(C).

Flexible Shaft Operation - To develop the classical concept of a flexible shaft, consider a weightless shaft of uniform cross section with an unbalance at the center running, at an angular speed, between two bearings. See Figure 5.

If the undeflected shaft is rotating about the centerline, there would be a rotating centrifugal force $M\omega^2 e$ acting on the shaft. As for an elastic deflection of the shaft (r), an additional centrifugal force $M\omega^2 r$ acts on the shaft. Balancing the centrifugal force, the elastic restoring force maintains the equilibrium of the rotating mass as illustrated in section AA of Figure 5.

x, y = fixed axis system

ω_1 = rotational speed

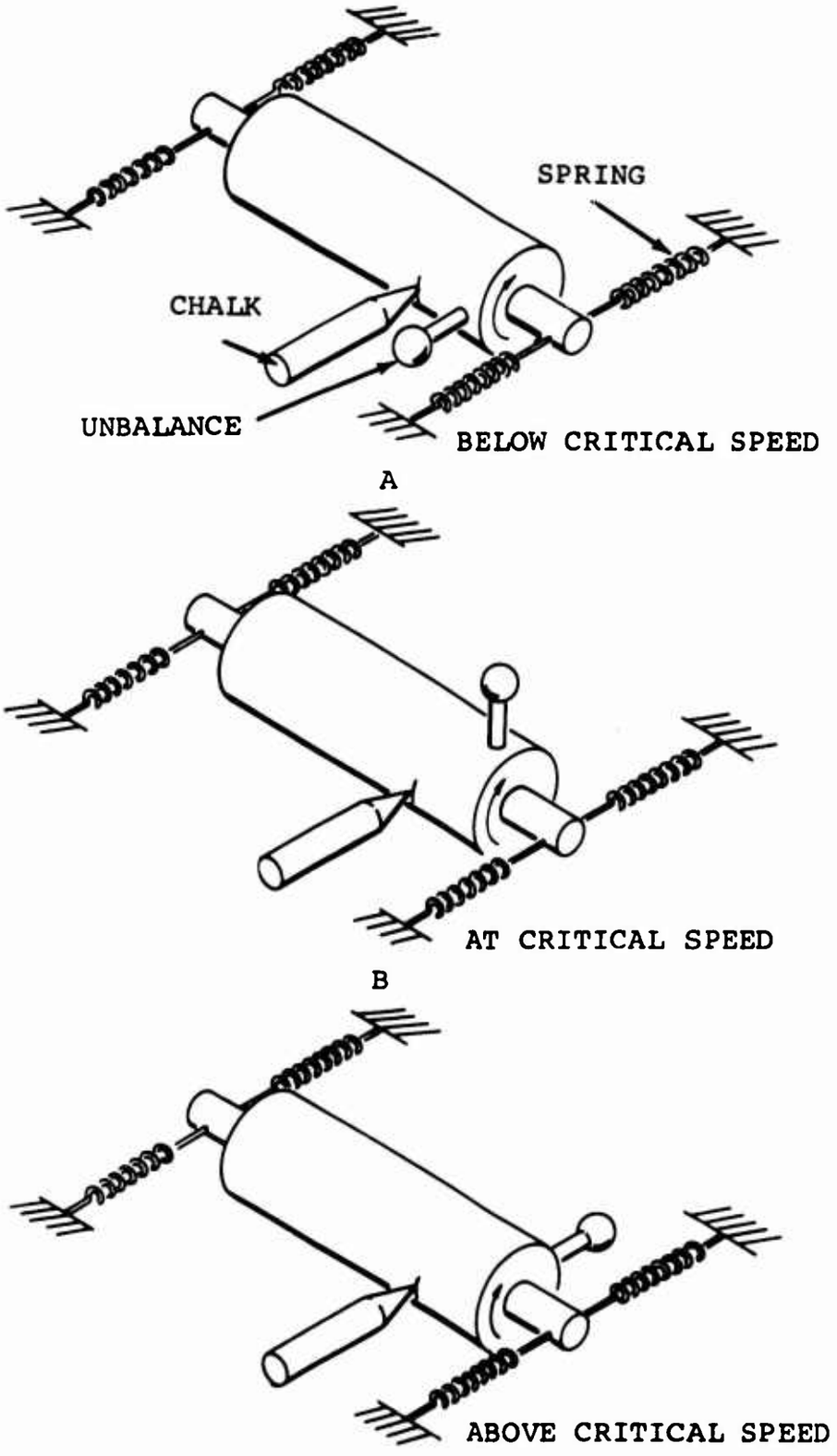

FIGURE 4. PHASE SHIFT OF RIGID SHAFT.

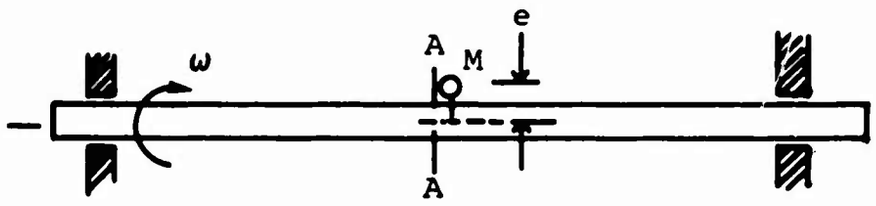

WEIGHTLESS SHAFT WITH UNBALANCE AT CENTER

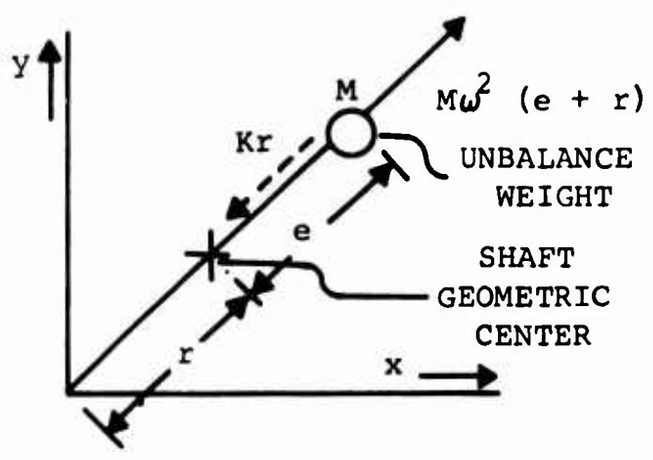

FIGURE 5. FORCE - BALANCE DIAGRAM.

r = elastic deflection

e = weight offset from shaft geometric center

K = shaft stiffness at the unbalance location

M = unbalance weight

Summing the forces acting on mass M,

$$Kr = M\omega^2 e + M\omega^2 r. \tag{2}$$

Solving for the elastic deflection,

$$(K-M\omega^2)r = M\omega^2 e \tag{3}$$

$$r = \frac{\omega^2}{\frac{K}{M} - \omega^2} e \ .$$

Since $(K/M)^{1/2}$ is the natural frequency (ω_n) of the shaft-mass system,

$$r = \frac{(\omega/\omega_n)^2}{1 - \left(\frac{\omega}{\omega_n}\right)^2} e. \tag{4}$$

The above equation can be extended to a uniform shaft by considering (e) as the effective modal unbalance. It is noted that this formula coincides with that of a simple spring-mass system excited by a force proportional to the square of the frequency. Relative positions of the geometric shaft center, effective modal center of gravity, and the centerline between bearings are illustrated in Figure 6.

Shown in the diagram for slow rotations ($\omega = 0$), the radius of whirl is practically zero. At the rotating speed equal to the shaft natural frequency the radius becomes infinite; and at frequencies above natural, the shaft rotates about the effective center of gravity. The rotational speed at which the radius of whirl becomes infinite is known as the critical speed, and this speed is the same as the non-rotating natural frequency of the shaft in lateral bending. In practice, a critical speed exists for each of the natural modes, and excitation results from the modal unbalance of the shaft distributed weight.

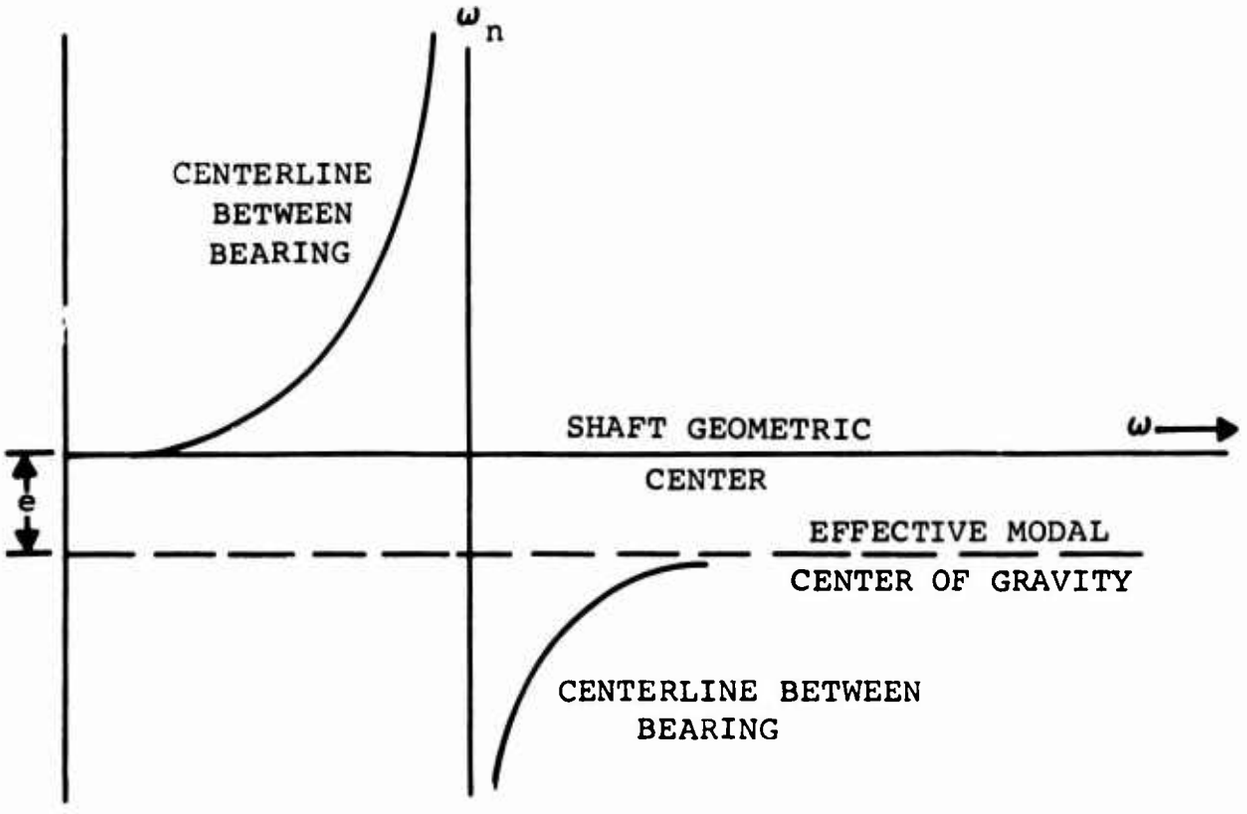

FIGURE 6. SHAFT CENTERLINE DEFLECTION.

FIGURE 7. DEMONSTRATION MODEL.

Flexible Shaft Demonstration - The photographs in Figure 7 show a supercritical speed shaft demonstration model in operation. It is driven by a small, variable-speed electric motor. Amplitudes are controlled by a model multiple plate viscous shear damper. The damper is located at the extreme end of the shaft in one case, and in the other case the damper is located at 8 or 10 percent of the shaft length.

The classical loops can be clearly seen on the shaft as it rotates at the 5th and 6th critical speeds, respectively.

The natural sag is apparent and does not influence the formation of whirling modes. Several of these demonstration shafts have been made to fail. It was interesting to note that each bending failure occurred at the peak of each bend or antinode, and that the plane was the same for all loops. During testing, as the bending failure occurred, power of the demonstration motor was insufficient for the increased wind resistance. No further damage resulted. See Figure 8.

Problem Statement - At the inception of the program, the primary task was to determine whether previously developed supercritical design techniques could be applied to the full size helicopter drive shaft. The physical characteristics and operational speeds of the full-scale shaft were predetermined by selection of the vehicle. The task was considered necessary because the available information had been developed on models whose maximum length was a fraction of that required for the proposed application. Therefore, confirmation of the design approaches and scaling effects was essential to the full-size utilization of the previous efforts.

It was found during the program that the sub-scale design techniques available did not completely predict the dynamic behavior of the full-size shaft. The full-size test specimen could not attain the required maximum rpm because of excessive amplitudes encountered at the higher criticals. This problem was solved by development of a method for dynamic balancing. Maximum rpm was then met and exceeded.

The secondary task defined at program inception was to determine the design of a supercritical shaft damper suitable for helicopter use. It appeared that environmental conditions, weight, and reliability might present such problems as to make the damper a restrictive factor to practical usage. After design study, a damper has been devised with characteristics

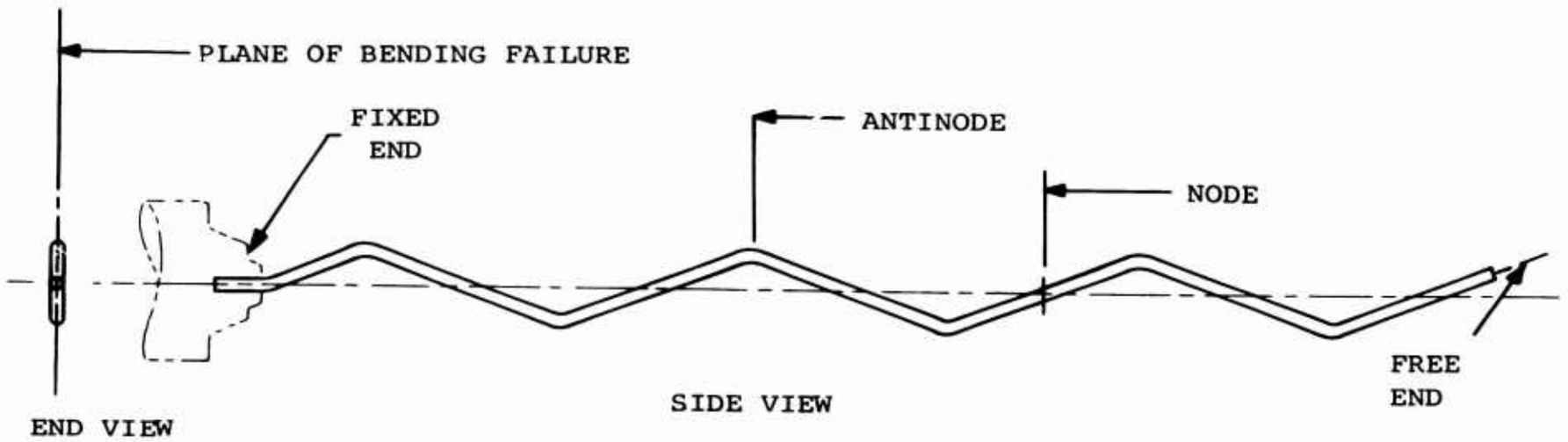

FIGURE 8. DEMONSTRATION MODEL SHAFT.

which appear to be well suited to operational helicopter supercritical shafting. Expansion of the solution will be discussed under DESIGN.

Problem Solution

The selection of the initial design parameters was assisted by the previously developed techniques.* These determined the four damper parameters, namely, location, coefficient, mass, and spring rate, by using shaft characteristics of length, stiffness and weight. Unbalance was not initially included in the shaft characteristics considered. Past work has averaged calculated damper parameters for the critical speeds of interest. For the most part, this approach has resulted in dynamic performance, as measured by whirl amplitude that has been acceptable. In this investigation, it became apparent after running the full-size shaft that the dynamic behavior was not predictable from the model tests and that a further solution would be necessary. The alternatives that presented themselves were to increase the damping effectiveness or to reduce the forcing function as it was revealed in shaft unbalance. The first alternative constituted a major design change, in that the most feasible approach would increase the number of dampers to two or more. The second alternative, which would not increase shaft weight or complexity, was therefore implemented by an attempt to balance the shaft. This was successful, and the shaft after balancing was run to speeds in excess of the maximum required rpm.

As a result of the marked improvement provided by balancing, a further study to refine and systematize the procedure was indicated if other large shafts were to be built and operated.

Two methods of shaft balancing were investigated. The first, an experimental method, directed that selected balance weights be added at stations along the shaft lengths. The balance weights would correct the mode under consideration but would not affect the other modes. Selecting a balancing station which would influence one mode without affecting the other modes became more and more difficult as the number of critical speeds was increased.

*Electrical Transmission Line Analogy (Appendix I) and Design Manual Solution (Appendix II).

The second method was an analytical balancing approach in which the deflections and phase of each mode were used as inputs to determine modal unbalance of the shaft. A mathematical balance in all modes can be accomplished by the addition of balance weights of computed magnitude and phase at predetermined shaft stations. Theoretically, any number of critical speeds could be handled by the analytical balancing method. However, the analytical method proved to have limitations, as discussed later.

Experimental Procedure Development - The experimental balancing procedure for mode-by-mode balancing has been formalized for balancing of the third, fourth, and fifth critical speeds of the full-size test specimen shaft. The balancing planes are located at three shaft stations. The stations are selected so that balance weights added for a specific critical will have a minimum effect on the other two criticals of interest. Each mode is successively balanced by the use of two charts; these indicate the correct weights and phase which correspond to the amplitude and phase of shaft distortion measured at Station 300. Station 300 is located away from the nodes of all critical speeds, and therefore observed deflections at this station can be related to a true indication of shaft performance over the entire speed range without shifting the amplitude measuring device. The charts have been prepared to provide the balance weights at the correct stations from the deflections observed, even though Station 300 will not necessarily show maximum deflections. This method has been used to balance the CH-47A shaft in several different degrees of initial unbalance, and all results indicate that the procedure will be practical and reliable for production balancing.

Analytical Procedure Development - The balancing of a supercritical shaft by the experimental methods used in the past is a difficult process. It is expected that such balancing would become more and more delicate as additional whirling modes are involved. Therefore, it is desirable to develop an analytical tool which can serve as a guide for interpreting experimental data and form the basis for a systematic balancing procedure. This is the objective of the theoretical work undertaken on this project.

The theoretical problem involved here consists of two distinct but related parts; namely, the interpretation of experimental data to determine the unbalance present, and the development of a method to calculate balancing corrections. The methods

developed during this program to solve these problems are briefly described below, and the complete theoretical developments are presented in Appendix IV of this report.

For a rotating system with distributed mass, such as a shaft, it is necessary to consider the unbalance as a set of two unknown functions; namely, the distance and the angular position of the mass center. Thus we must, by proper interpretation of experimental data, determine these two unknown functions. In the development of Appendix IV, the equations of motion of a whirling and vibrating shaft are derived in any arbitrary coordinate system, including the effect of viscous damping as well as an arbitrary distribution of mass unbalance and initial deflection. These equations are then specialized to the case of a steady, whirling motion referred to a set of axes and rotating with the shaft. The choice of these axes was dictated by the experimental technique adopted by Batt lle Memorial Institute, which provided all measurements with respect to such axes. The resulting differential equations of motion are solved in the form of a series in terms of "whirling modes" (which are identical to the bending modes) of the shaft. The solution provides this amplitude of the whirling motion in each mode in terms of the amplitude of the initial deflection and unbalance in the corresponding mode. It is then shown that the solution can be used to determine the unbalance from experimental measurements of whirling deflection at any point of the shaft (not a node). Measurements are taken at as many rotational speeds as the number of modes desired in the solution for unbalance. Thus, if the shaft is designed to operate through five critical speeds, the unbalance in at least the first five modes should be determined and eliminated. These measurements should be taken at five speeds of the two components of the whirling deflection. These measurements should, if possible, be taken at speeds covering the entire desired range, as this will improve the accuracy. This is not necessarily at critical speeds. One interesting feature of the solution obtained is that it demonstrates a fact little understood previously; namely, that at a given critical speed, the whirling shape is not necessarily the pure mode corresponding to that speed, but is in fact a contribution of many whirling modes, the relative amounts of which are determined by the modal content of the unbalance. This coupling is precisely the feature that tends to limit the experimental balancing method. It should be noted that previous analytical work in this area has been limited to the determination of whirling mode shapes and critical speeds. Previous methods did not provide the relationship between unbalance,

whirling amplitude and angle, which is essential to a proper interpretation of experimental data.

The second part of the analytical work is concerned with the analytical determination of suitable balance corrections. It is shown that, if it is desired to eliminate the unbalance in (n) of the whirling modes, this can always be accomplished by a system of (n) weights which can be located arbitrarily (but not all at nodes). One fairly effective system is to locate weights at one of the antinodes of each mode of interest; however, this solution is not necessarily an optimum one. It is often possible to balance a shaft to an acceptable degree by using a number (k) of masses smaller than the number of modes of interest ($k < n$). The development of a suitable method to optimize the number and location of such weights should be an objective of future work in this area.

The calculations required to determine unbalance from experimental data and to select suitable balancing corrections are rather complex to carry out by hand. It was therefore necessary, during the course of the present program, to carry out only approximate solutions which were based on the use of idealized rather than actual mode shapes. The results have been somewhat mixed, in that successful balancing of the test shaft through the fifth critical speed was accomplished in one case, but an attempt to balance five modes simultaneously was not demonstrated in a satisfactory manner.

It would be desirable to develop a computer program to carry out the necessary balancing calculations exactly and rapidly. This would allow a closer integration of experimental and theoretical work. Thus, experimental data presented as whirling amplitudes would be fed into the computer, which would calculate suitable balance corrections based upon actual rather than idealized shaft characteristics. The corrections would then be available immediately so that their effect could be verified in the laboratory. This seems to be the form that a future balancing procedure suitable for production operation of supercritical shafts should take.

DESIGN

Design Data Supplied

The rotor interconnect shaft of the CH-47A medium transport helicopter was chosen as the subject of investigation. See

Figure 9 The reasons for the selection of this aircraft were:

1. The present subcritical system is in existence for comparison of performance, cost analysis, weight, reliability, etc.

2. A demonstration vehicle is available for complete evaluation of final design.

3. This shaft is the longest, and has the highest continuous horsepower capacity, of any high-speed shaft in the military aircraft inventory.

Design requirements based on an existing subcritical system allow evaluation of a supercritical speed system without major and costly changes in the drive train. In a new supercritical design it may prove to be advantageous to run the shafting at much higher speed, without the intermediate gear reduction from engine speed. Supercritical operation can be achieved by running at higher speeds or by removing some of the supports. Since shaft speed is dictated by the present transmission, removing the supports was the approach followed. See Figure 10.

The design and test program was based on the following requirements of the system as it exists in the helicopter and on the environmental requirements expected by the aircraft in service.

Shaft length between gearboxes . . . . . 338.8 inches

Shaft outside diameter (maximum) . . . . 4.50 inches

Operating speed range

Ground idle . . . . . minimum 2900 rpm
maximum 3240 rpm

Normal flight range . . . . . minimum 7050 rpm
maximum 7555 rpm

Extended flight range . . . . minimum 6600 rpm
maximum 8270 rpm

Normal operational torque . . . . . 15,000 inch-pounds

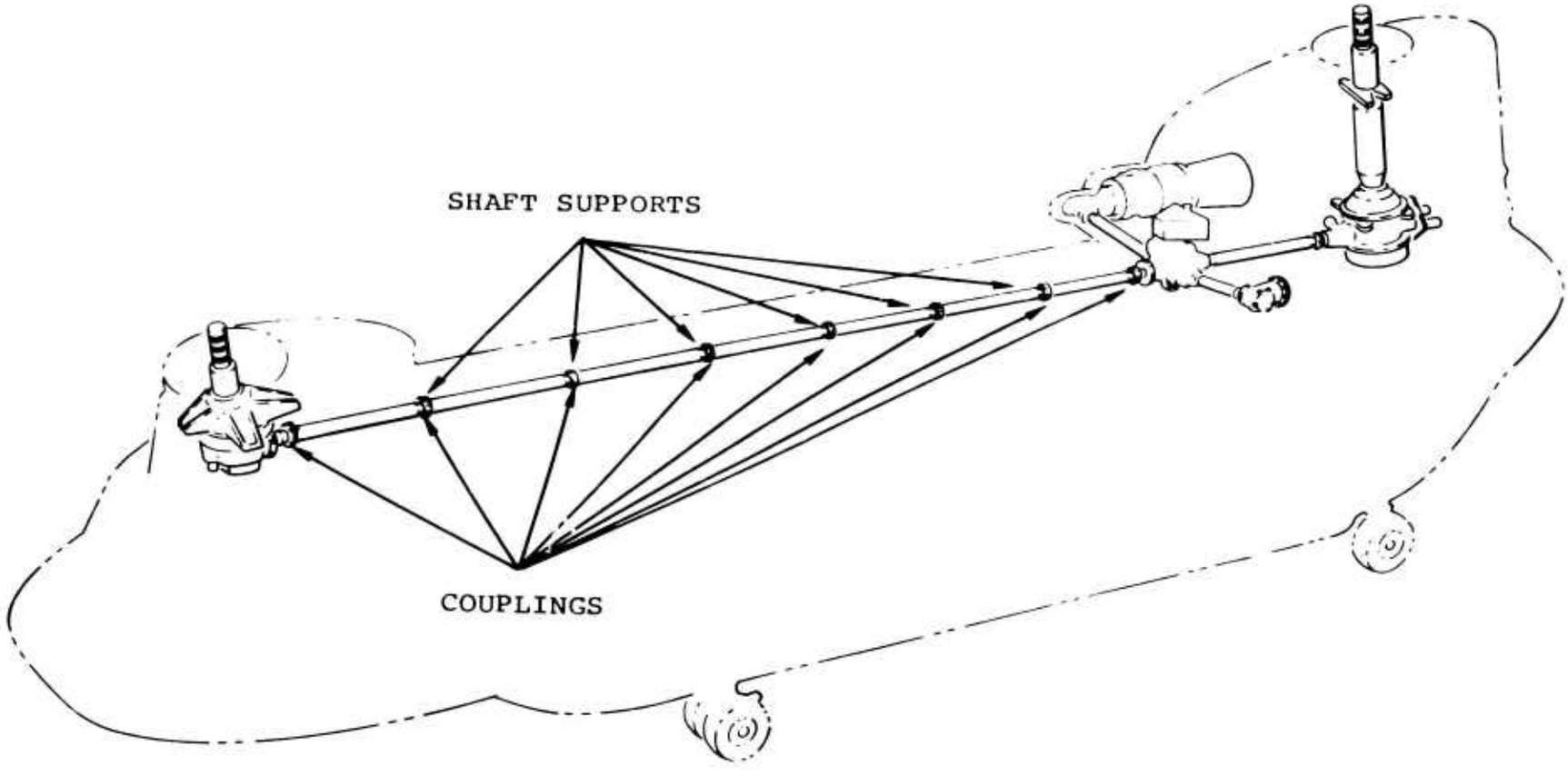

FIGURE 9. INSTALLATION OF SUBCRITICAL SHAFT SYSTEM.

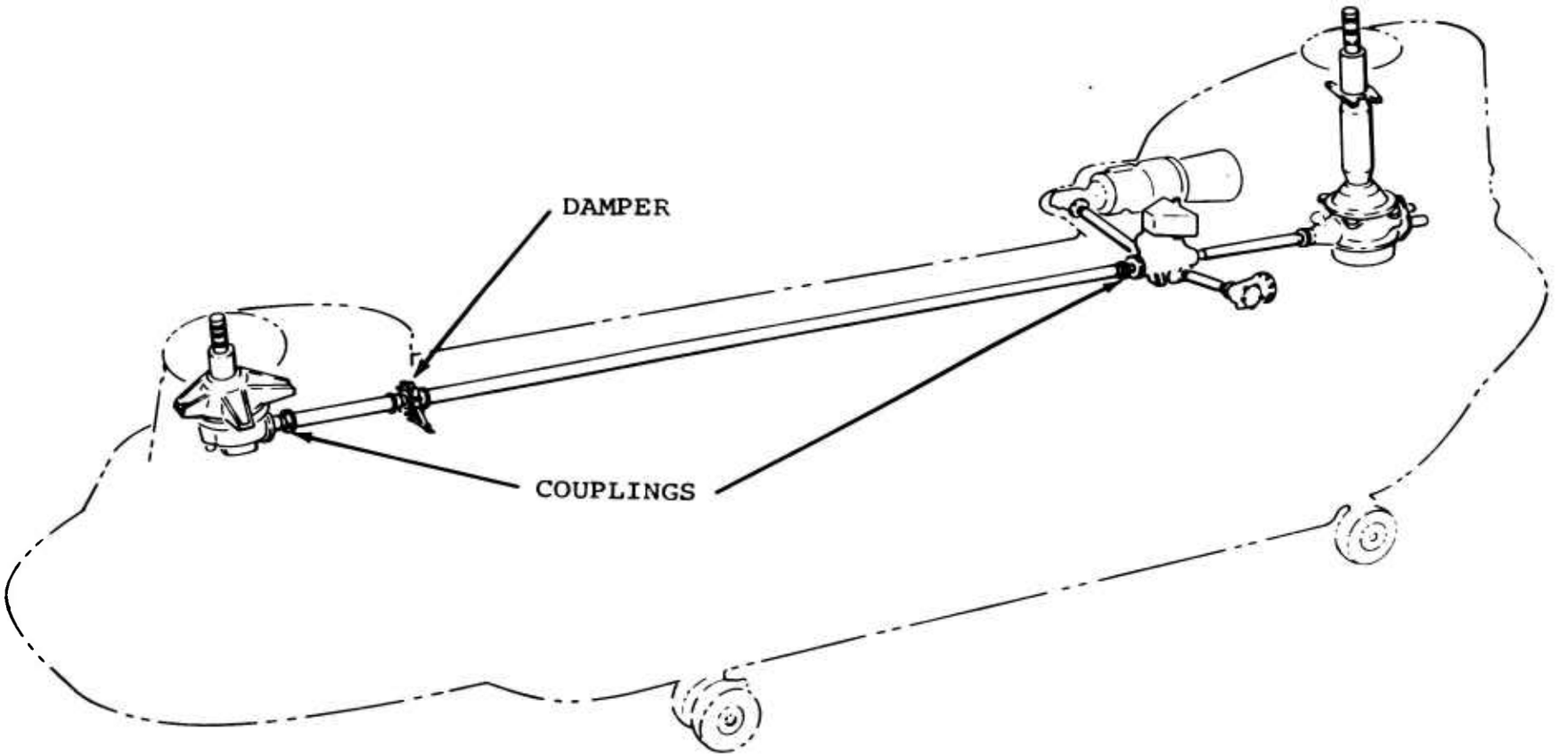

FIGURE 10. INSTALLATION OF SUPERCRITICAL SHAFT SYSTEM.

Design fatigue torque . . . . . 26,500 inch-pounds ± 15%

Ultimate torque . . . . . 60,000 inch-pounds

Relative motions . . . . . Angular ± 0°4'
from fuselage deflections
at limit load . . . . . Length -0.216 inch

Angular tolerances on blade phasing . . . ±1° at rotor

Starting time (approximate)

0 to 3200 (ground idle) . . . . . 7 seconds

3200 to design speed . . . . . 4 seconds

g Loadings

Flight . . . . . +2.67

Flight . . . . . -0.50

Landing . . . . . +2.80

Crash .... 8g all directions, acting separately

Data Derived

Below are listed the design requirements of the supercritical test shaft:

1. Torque capacity to duplicate the operational shaft.

2. Safe speed range to meet or exceed the operational requirements.

3. Physical dimensions to be compatible with the CH-47 helicopter.

4. Environmental temperature range to be restricted to laboratory room temperatures.

5. Number of dampers to be a minimum.

The torque capacity requirement was met by designing the supercritical tube to the same torsional stress criteria as the present subcritical tube. Restrictions on outside diameter resulted in identical tube diameter and wall thickness. Length between transmissions also duplicates the CH-47 shaft system length. The remaining data to be derived for design of the supercritical shaft were the damper variables, damper positions, and accurate critical speeds.

These data were obtained by applying the previously developed electrical transmission line analogy (see Appendix I) or by using the charts and graphs given in the Design Manual (Reference 5). Model tests were necessary to supplement these design approaches and to verify the results prior to actual design of the full-size shaft. Table I shows results obtained from three methods of solving the design problem.

TABLE I
DESIGN APPROACH

Design Inputs	Methods			Comparison Full Size
	Electrical Analogy	Design Manual	Model Tests	
Damper Coefficient	3Z to 4Z	3Z	6Z to 10Z	3Z optimum
Damper Mass	Maximum ½ shaft wt.	Maximum 1/3 shaft wt.	Maximum 1/3 shaft wt.	Maximum 1/3 shaft wt.
Damper Spring Rate	Estimated minimum	Estimated minimum	Minimum	Minimum
Damper Location (Percent of Shaft Length)	1.1%	5%	9% optimum	9%
Damper Type	Viscous shear type used throughout			
Shaft Amplitude	Not determined		Measured but not to scale	
Critical Speeds (rpm)	Calculated	Similar to calculated	Measured but not comparable to calculated	Measured and comparable to model
Z = Impedance (See Reference 4.)				

Table I exhibits the fact that most damper characteristics from the electrical analogy or from the Design Manual (refer to Appendix I or II) are similar. Damper location is an exception in which the electrical theory positions the damper very close to the end of the shaft. This damper position may be the optimum for the fifth critical, but it is doubtful if the damper would suppress the amplitudes of the first critical within acceptable limits to allow the shaft to ever run at that speed. Therefore, model test results were used to establish damper location on the full-size shaft. See Figure 11.

Damper Investigation

Design Objectives - In considering the design of a damper suitable for an aircraft installation, the following objectives were set:

1. The characteristics of the damper must be matched with the requirements of the shaft under all conditions of speed expected in actual operation.

2. The damper should have the capability of fail-safe operation.

3. It should operate with or without engine power available. It should not depend on any other aircraft system (electrical, hydraulic, pneumatic) for its safe and continued performance.

4. It must be able to operate under environmental conditions expected by the aircraft. It must operate from -65°F to +180°F ambient temperature extremes.

Design Comparison - A common problem of all damper types is to utilize the whirling motion of the shaft to actuate the elements of the damper and thereby dissipate the unwanted energy. This is a fairly simple problem at low speeds where the amplitudes are relatively high with low inertia forces. As high speeds are approached, the amplitudes are reduced to very small values, and loss-motion between the shaft and the damper elements, together with the high inertia loads, may prevent the damper's performing in a satisfactory manner.

This problem becomes more severe when links or fittings are

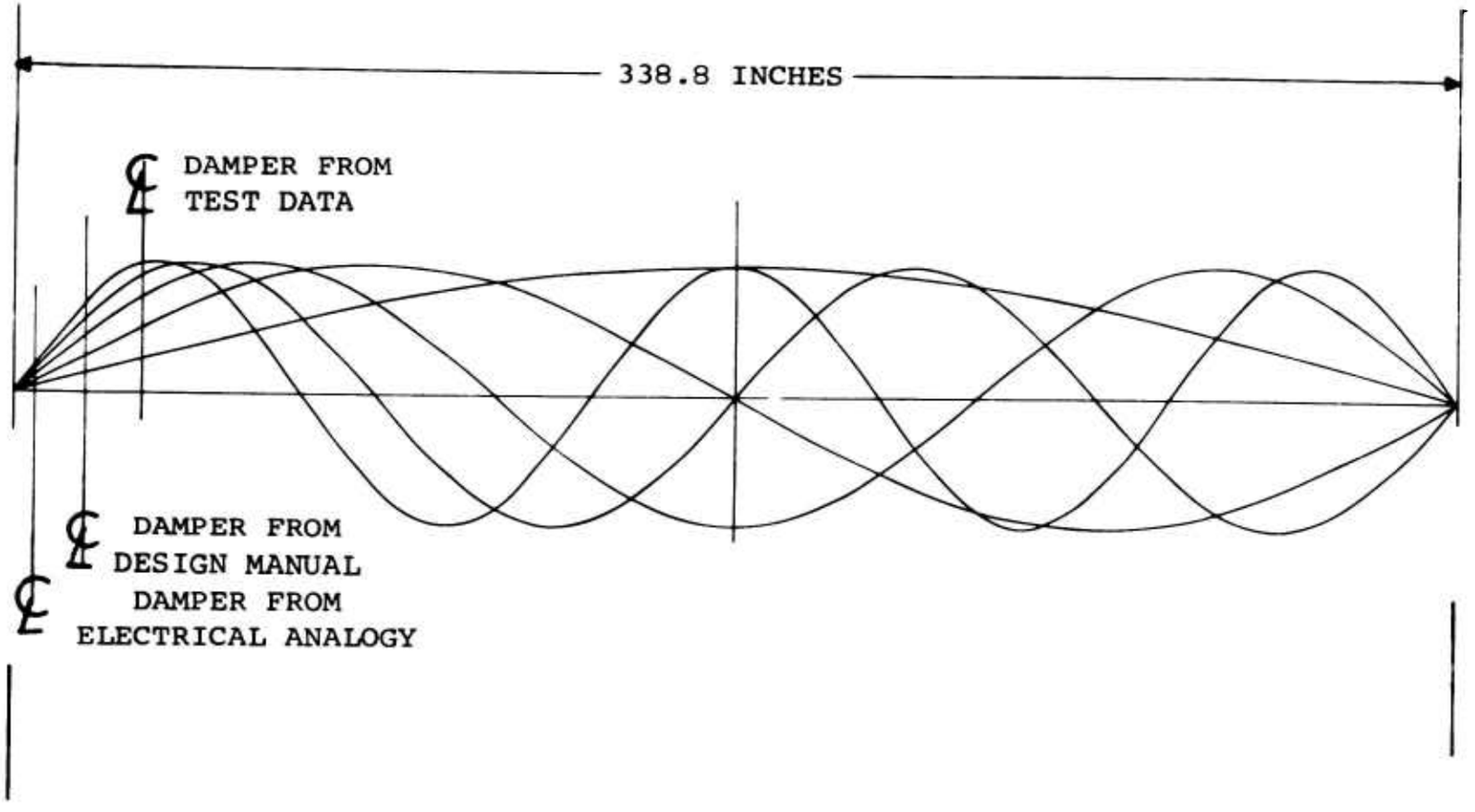

FIGURE 11. DAMPER LOCATION USING DESIGN METHODS.

added between the whirling shaft and the energy-absorbing section of the damper body.

Design types considered were (see Table II):

1. Viscous shear
2. Orifice
3. Concentric ring (squeeze film)
4. Immersion body (heart pump)

TABLE II
COMPARISON OF DAMPER CHARACTERISTICS

Type	Figure	Moving Weight (pounds) (1)	Damper Weight (pounds) (2)	Temperature Correction	Comment
Immersion Body "A"	15	9.85	1.56	No	Laboratory test would require temperature correction for service
Immersion Body "B"	16	11.50	5.20	Yes	Not tested; preliminary design only
Orifice	13	11.35	4.47	Yes	Not tested; preliminary design only
Viscous Shear	12	13.00	10.04	Yes	Similar to test damper, but includes temperature correction

(1) Moving weight includes damper parts moving with shaft and shaft adapter assembly (9.10 pounds constant).

(2) Damper weight includes all damper parts except bearing and supports to airframe. Weight includes oil.

Viscous Shear Damper (Figure 12) - The viscous shear damper derives its damping characteristics from the resistance offered by shear of a liquid film between two surfaces in close proximity. The resistance depends on the viscosity of the liquid and the relative velocity or shear rate. The viscous shear damper coefficient has a linear response to velocity. It has the disadvantage of also being sensitive to viscosity changes due to temperature variations.

One of the moving surfaces of the viscous shear damper is attached directly to the whirling shaft through a bearing from which it receives its orbiting motion. There is a minimum of loss-motion in this arrangement.

Orifice Damper (Figure 13) - The orifice damper derives its damping characteristics from the resistance offered by fluid passing through a sharp-edged orifice. The resistance is proportional to the velocity squared. The damping coefficient is insensitive to temperature changes when the flow through the orifice is in the turbulent region.

The orifice damper is basically a piston mounted directly to the whirling shaft through a bearing from which it receives a translating motion. To prevent binding, it is attached to the bearing housing with a pin or ball joint which removes out-of-plane motion.

The axial motion moves the piston relative to the cylinder, mounted with another pin or ball joint to the structure, and forces damper fluid through the sharp-edged orifice.

This design has a number of joints which may have sufficient clearance to reduce the effectiveness of the damper, especially at the higher frequencies.

Concentric Ring Damper (Figure 14) - The concentric ring works on the principle of squeeze-film action. It derives its characteristics from the resistance offered the approach of two surfaces when separated by a film of viscous fluid. A further characteristic of this type is the inertia effect of each concentric ring. At the higher frequencies, the greater mass of the larger rings helps to react the load and, by tending to stand still in space, changes the damping action. A properly designed squeeze-film damper would match the action of the ring masses and the remaining damping coefficient so that it would exactly match the requirements of the system. This

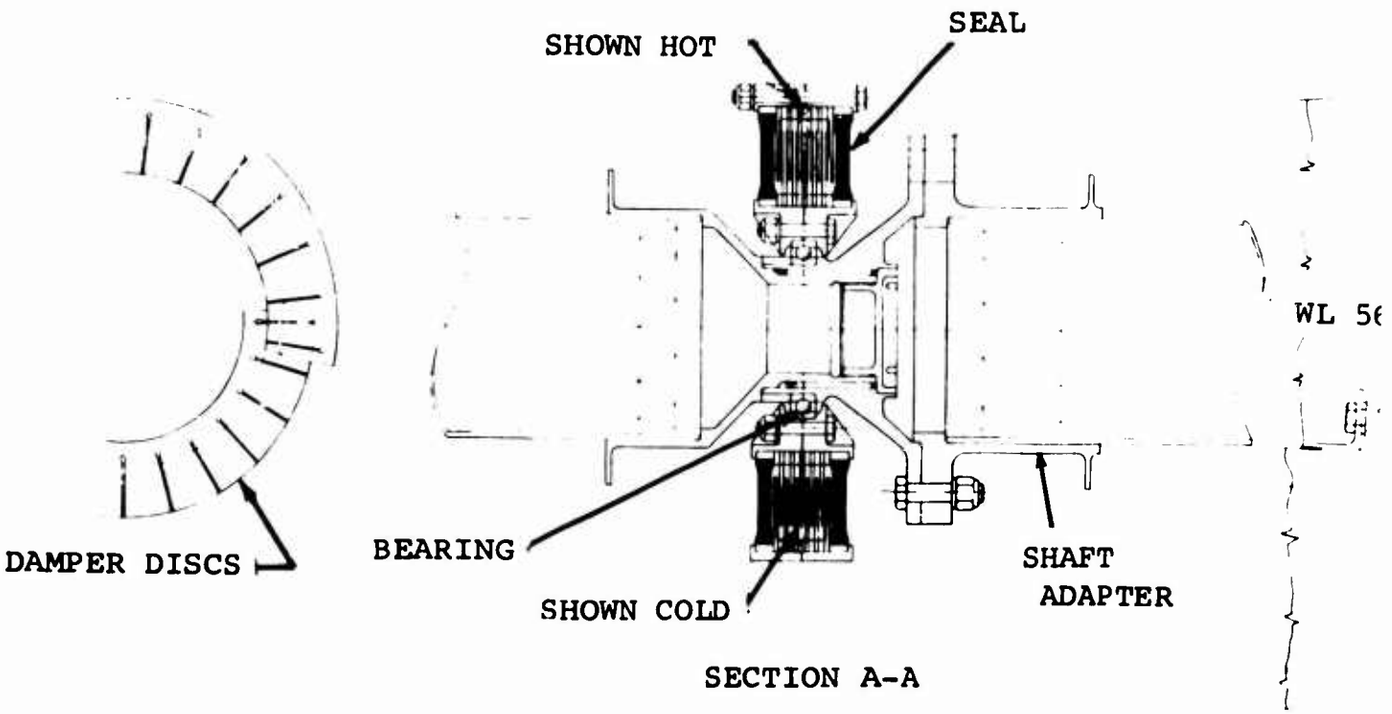

FIGURE 12. VISCOUS SHEAR DAMPI

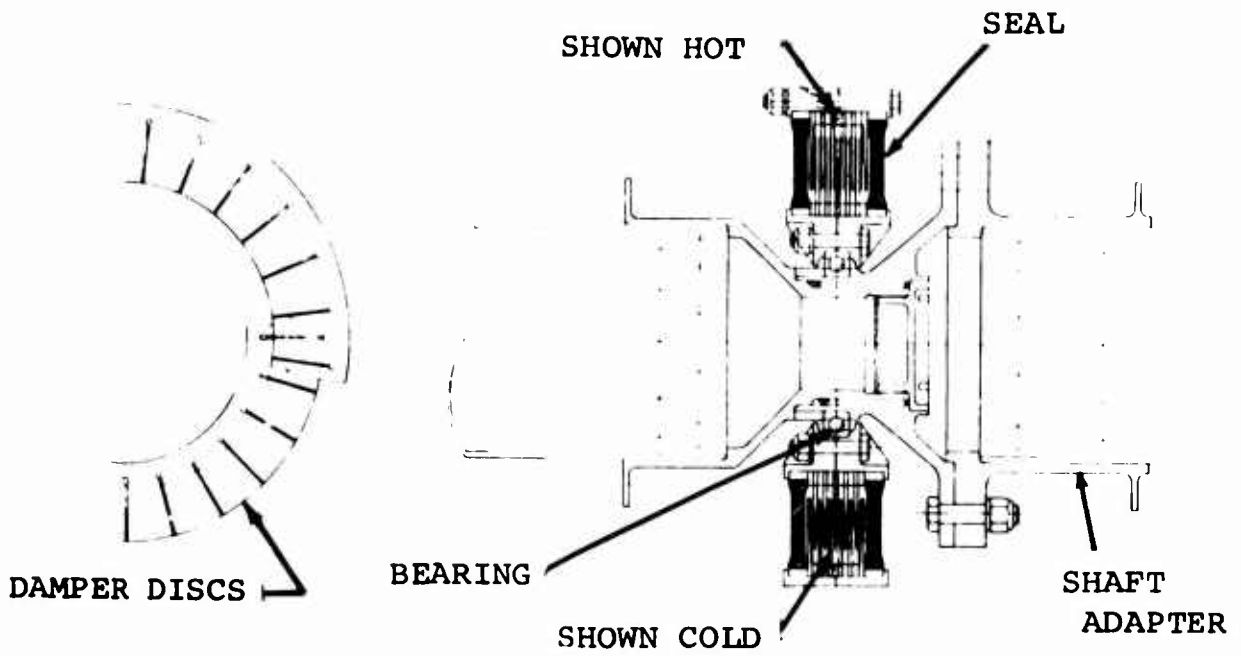

FIGURE 12. VISCOUS SHEAR DAMPER

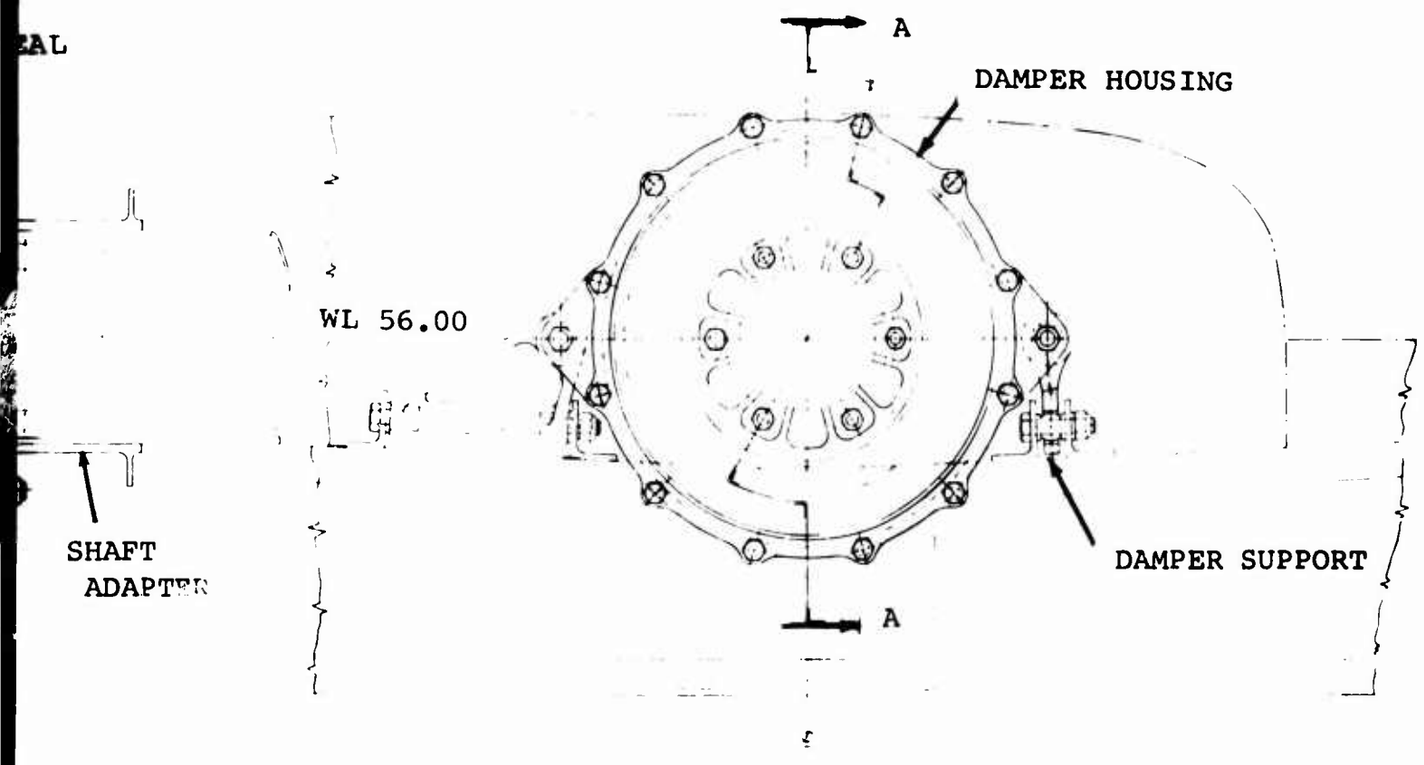

VISCOUS SHEAR DAMPER

B

Damper design by Utica
Division, The Bendix Corporation

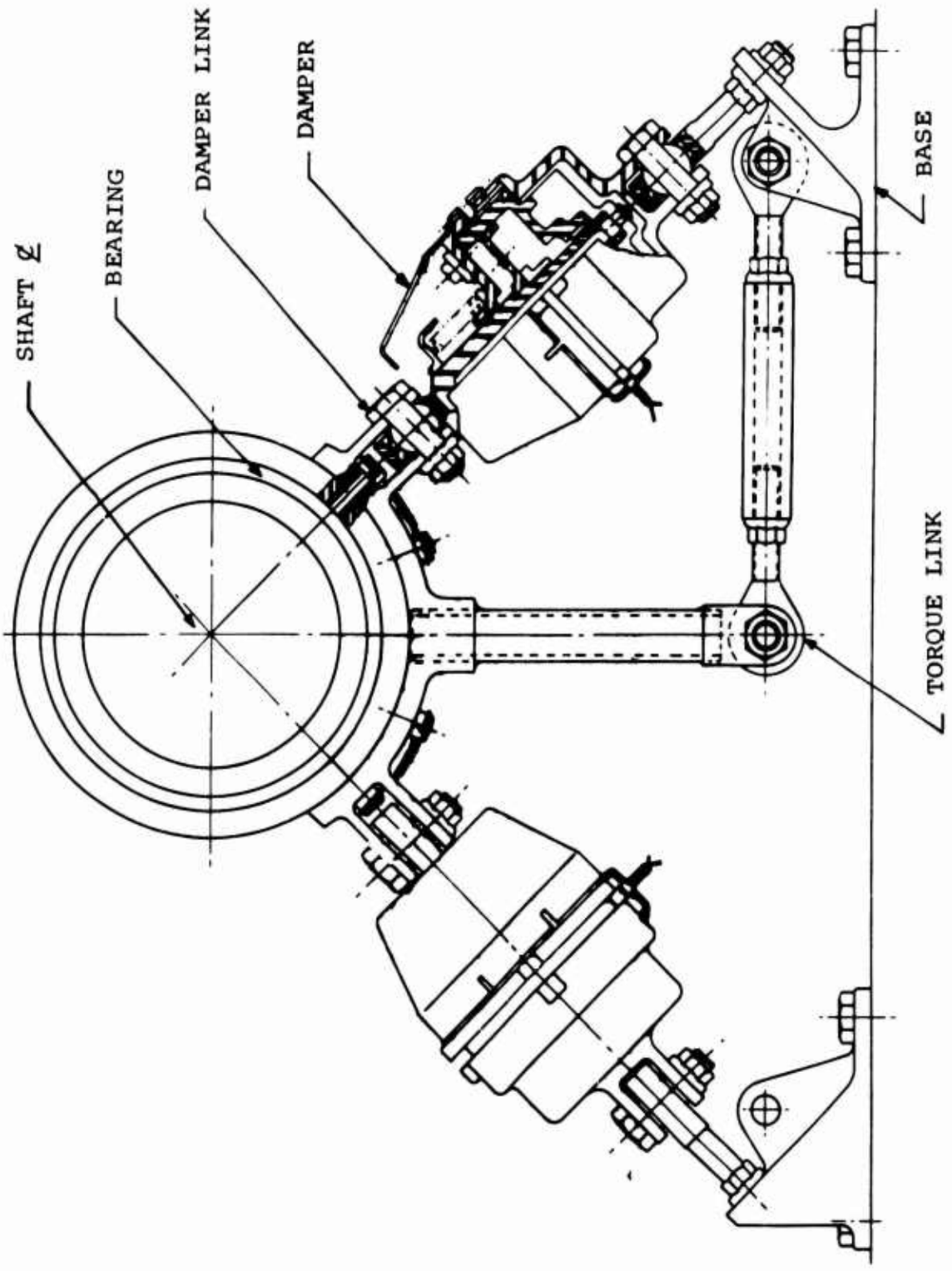

FIGURE 13. ORIFICE DAMPER.

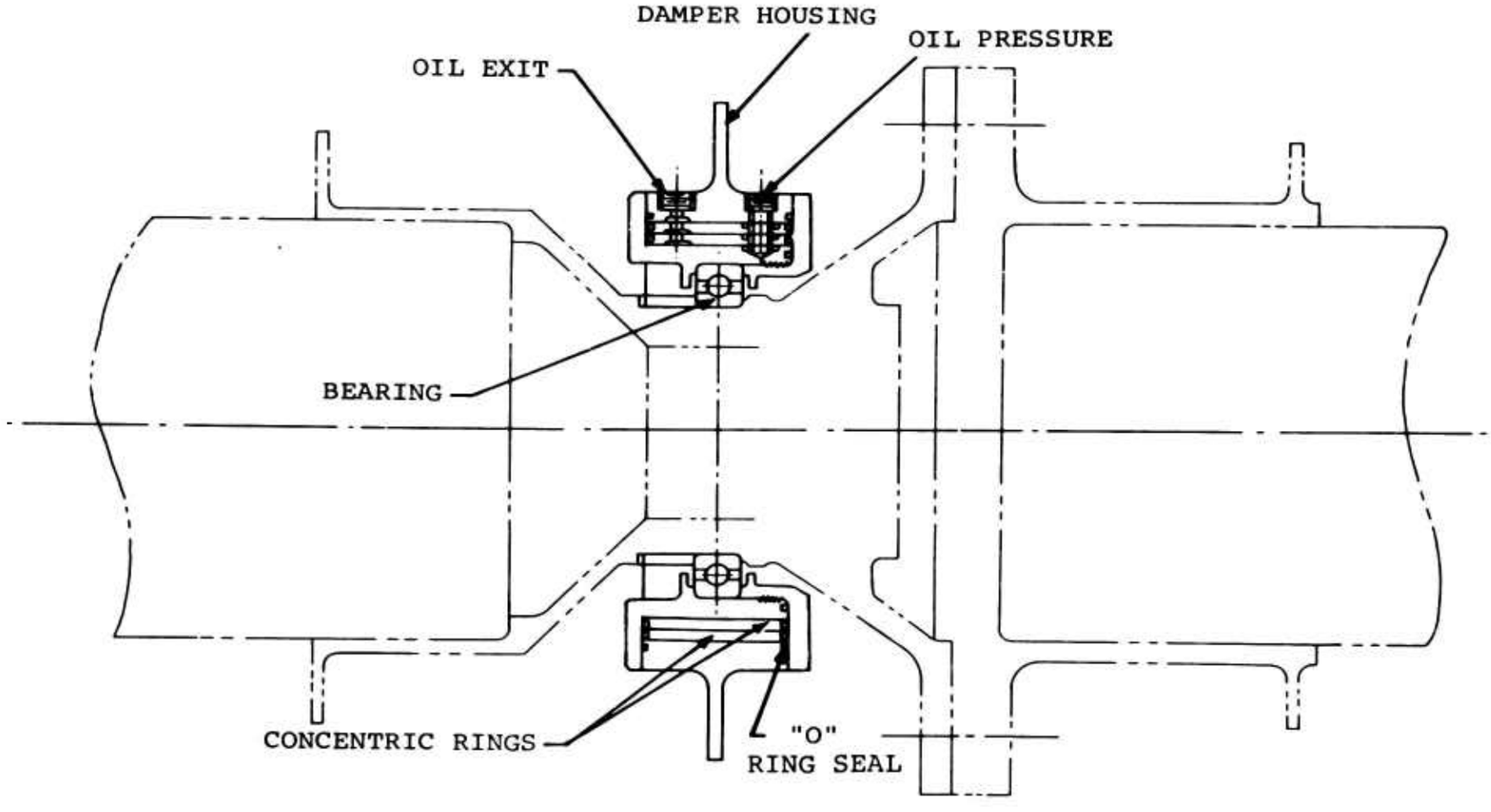

FIGURE 14. SQUEEZE-FILM DAMPER.

tuned damper would be considerably heavier than the one reported (see Reference 8). Cavitation in the film is a problem, and fluid under pressure must be supplied for satisfactory operation.

The inner ring of this system is attached directly to the whirling shaft through a bearing. The bearing transmits the orbiting action of the whirling shaft to the ring without causing rotation of the ring. A number of rings make up the damper and together provide the desired motion and damping coefficient. The rings must be keyed together to prevent individual whirling or rotation. The final external ring makes up the housing and is attached to structure.

There is a minimum of loss-motion in this arrangement.

Immersion Body (Figures 15 and 16) - The immersion body damper consists of a pump (heart pump principle). It derives its damping characteristics by pumping the fluid around the periphery as the shaft orbits. The characteristics are determined by the area of the fluid chamber, the type of fluid used and the frequency.

This damper is attached directly to the whirling shaft through a bearing from which it receives its orbiting motion. The bearing housing flexes the elastomeric fluid chamber in the same orbiting motion, forcing the fluid around the chamber in proportion to the amplitude and frequency.

Restrictions are sometimes added in such a manner that the area of the restriction will change with variations in the temperature, thus producing a more constant damping action.

There is a minimum of loss-motion in this arrangement.

Early tests indicate a nonlinear response of this type of damper. The change in response was most pronounced in the higher frequency range (above 80 cps).

Damping Comparison - The relationship between the theoretical damping necessary with a given amplitude and that obtained using various types of dampers is shown in Figure 17.

The viscous shear damper with its linear characteristics follows very closely the requirements of the shaft. The orifice damper matches the shaft requirements at only two points.

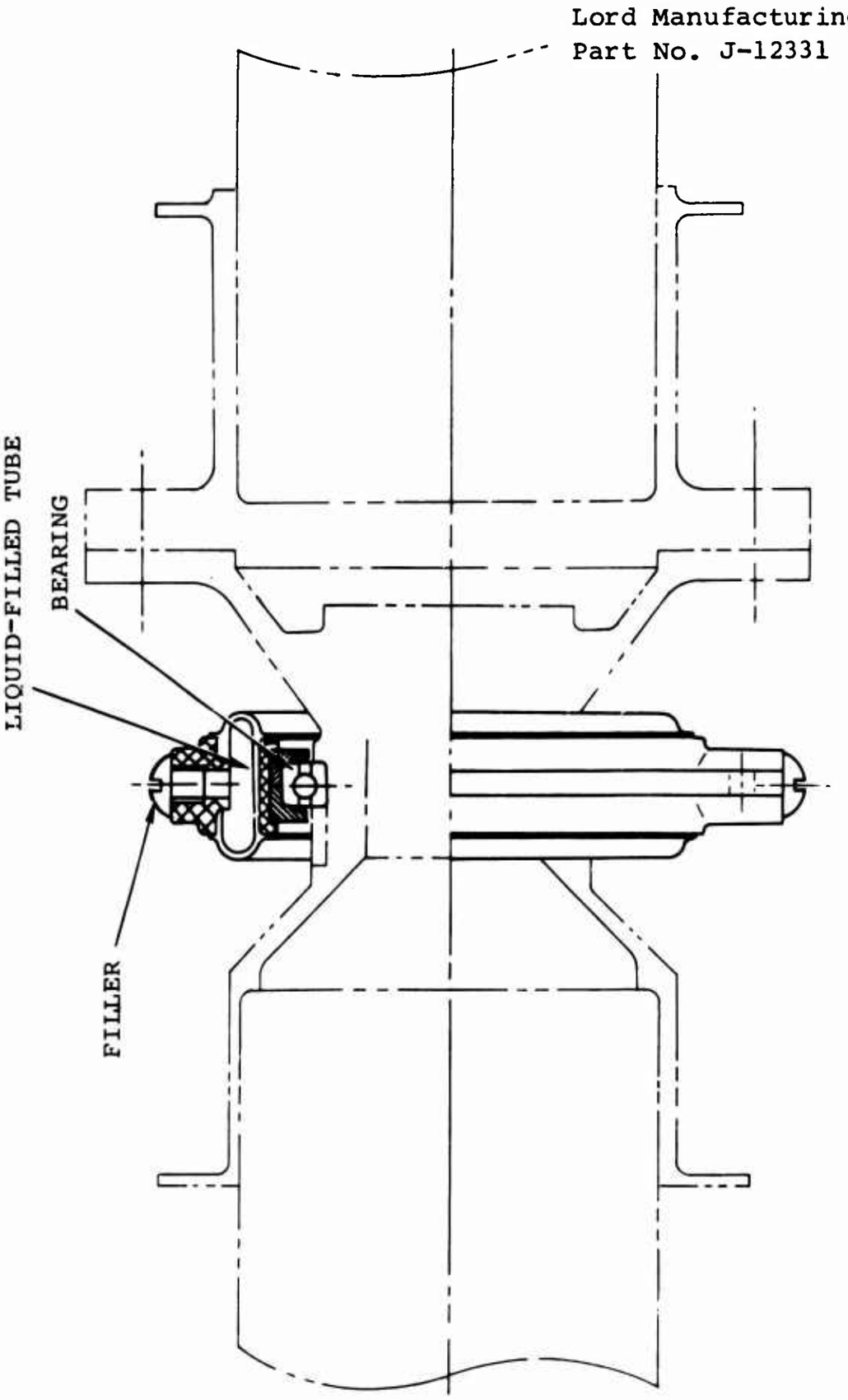

FIGURE 15. IMMERSION BODY DAMPER "A".

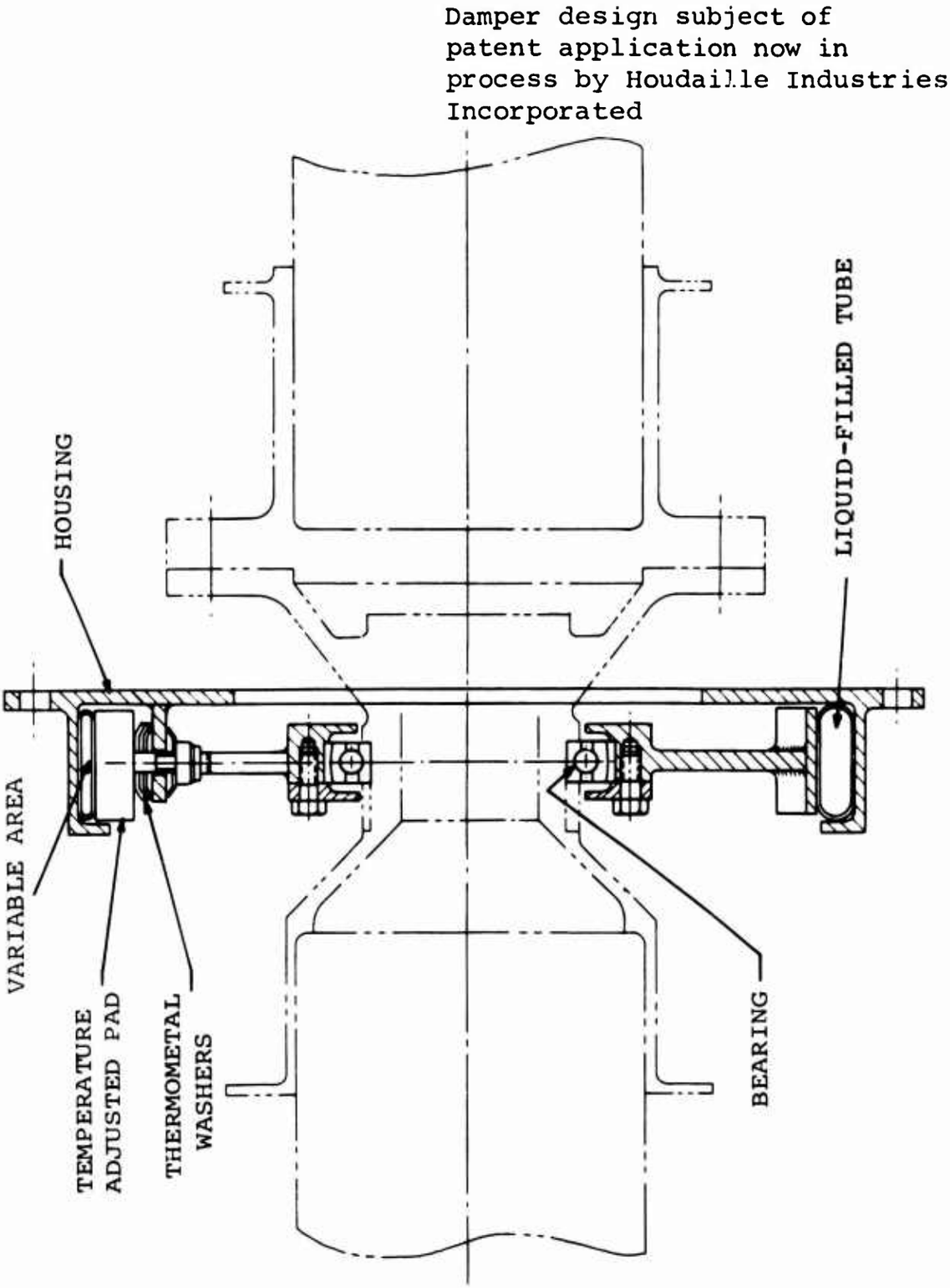

FIGURE 16. IMMERSION BODY DAMPER "B".

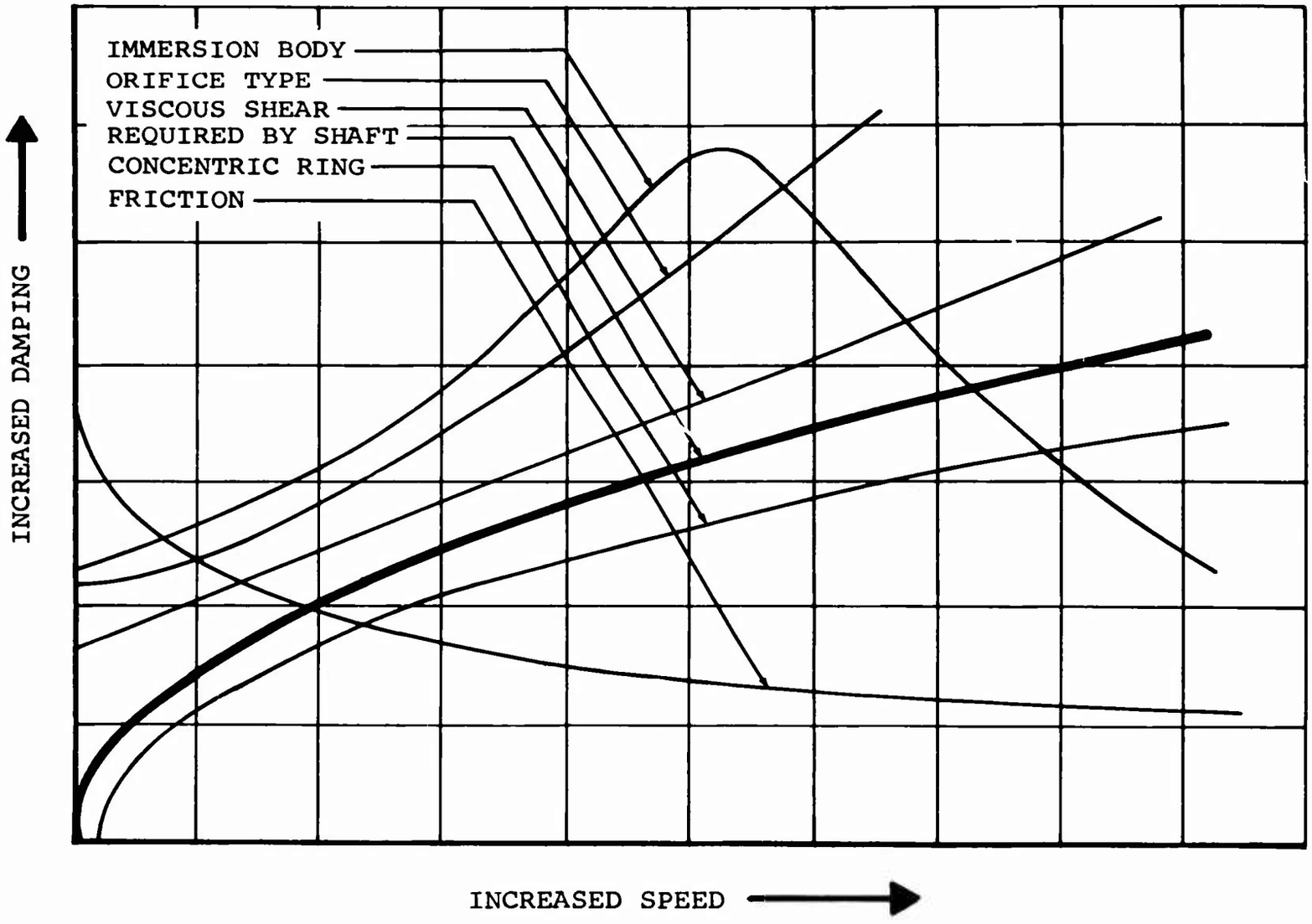

FIGURE 17. DAMPER CHARACTERISTICS.

The characteristics deviate rapidly at any substantial speed above or below these and may seriously limit the number of critical speeds through which this damper can control vibration. A pure friction damper was not seriously considered because of several factors: first, because of the obvious deviation from the shaft requirements as shown by the chart; second, because of undesirable characteristics displayed by some model shafts when friction inadvertently was present in the viscous shear plate damper in the laboratory.

It can be seen that the concentric ring squeeze-film damper most closely follows the requirements of the supercritical speed shaft.

The immersion body dampers show a fairly good response in the lower frequency range, with a sharp drop in the higher range.

These curves show general trends for the various types of dampers as they exist today, and all can possibly be modified for improvement to better match the requirements of a specific design.

Selected Design - Any of the damper types discussed above could be developed to meet the requirements of a supercritical speed shaft under the environmental conditions expected in an aircraft installation. Some of the dampers have been built and tested, while others represent design concept only.

The viscous shear damper selected for preliminary design was a variation of the damper used so successfully in the laboratory. This design should therefore enhance the probability of immediate successful operation. It was felt that minimum development would be required to provide a solution to the damping coefficient - temperature variation problem. Metal-to-metal mounting of the shear plates provides an efficient path to transfer the heat, and a large metal housing will provide adequate area to dissipate heat without additional fans or coolers.

Damper Requirements:

Damping coefficient	minimum	6 lb/sec/in.
	maximum	40 lb/sec/in.
Spring rate	minimum	5 lb/in.
	maximum	1000 lb/in.

Allowable damper mass maximum	20 lb
Shaft speed	0 to 8900 rpm
Temperature ranges minimum	-65°F
maximum	+180°F

The calculated design damper shear area required is:

Viscosity (centistokes)	Viscosity (reyns)	Required Shear Area (square inches)
100	1.4×10^{-5}	21400.0
1,000	1.4×10^{-4}	2140.0
10,000	1.4×10^{-3}	214.0
100,000	1.4×10^{-2}	21.4

The above viscosities and areas are required at the upper temperature limit expected in service. Maximum ambient temperature is 180 degrees Fahrenheit.

A damper with an area of about 200 square inches is not unreasonable in the configuration being considered.

Therefore, the fluid to use would have an apparent viscosity of 10,000 centistokes at 180 degrees Fahrenheit. The 30,000-centistoke silicone fluid is near this requirement at 180 degrees Fahrenheit. At -65 degrees Fahrenheit, this same fluid has a viscosity of 200,000 centistokes, a change temperature of 20 to 1. This change from maximum to minimum temperature indicates that if adequate damping is provided at the high-speed range under hot conditions, the system will be over-damped when it is cold. The system will be over-damped still further when compared with the requirements at low speed in the cold condition.

To reduce the change in damping coefficient with temperature variations as much as possible, it is desirable to design using a fluid that has minimum percentage of change with the temperature extremes encountered.

The following shows the variations and the ratios of a representative group of silicone fluids.

Fluid	Viscosity at 180°F (centistokes)	Viscosity at -65°F (centistokes)	Ratio
100,000	30,000	700,000	23/1
30,000	10,000	200,000	20/1
10,000	3,000	90,000	30/1
1,000	350	9,000	26/1
100	37	1,100	30/1

The ratios shown are indicative of the change in damping coefficient. They are beyond the range of coefficients investigated in the laboratory test program. Thus, a compensating device will be required for satisfactory operation under the temperature extremes expected. It is interesting to note that transmission oil (MIL-L-7808) which has a low viscosity would require 7500 square inches of plate area and a 0.001-inch gap to provide the required damping coefficient at 70 degrees Fahrenheit. The ratio of viscosity change is over 1000 to 1 in the range of -65 to +180 degrees Fahrenheit. Other lubricating oils display a far higher ratio.

Test results have indicated that a permissible variation in the damping coefficient exists. Therefore, the temperature compensation may not need to accommodate the full viscosity range.

The conclusion is that for a damper to operate in the normal aircraft environment, a temperature-compensated unit filled with a silicone viscous fluid should be used. The compensation must cover a range of 30 to 1 to provide a constant damping coefficient. With a constant plate area, this implies a change of this order in gap width.

A description of the suggested damper design is shown in Figure 12 . The damper is attached to the shaft by means of the bearing in the center. The bearing is grease-lubricated in a manner similar to the bearings of the existing drive system supports. The outside housing of the bearing provides the support around its periphery for the inner leaves of the viscous shear elements. These elements intermesh with the outer shear elements much in the same manner as the fingers of the left and right hands intermesh when the hands are

folded or clasped.

Clearance between the intermeshing elements is provided for the viscous fluid in an axial direction. Clearance is provided for motion of the elements relative to each other in a radial or lateral direction. The outer shear elements are attached around their outside diameters to a housing which contains the fittings for attaching the damper assembly to the aircraft structure.

The inner and outer housings are free to move relative to each other. The damper fluid is held in contact with the shear plates by flexible diaphragms on each side of the plates which make a fluid-tight joint where they contact the inner and outer housings. The diaphragms serve three purposes: they provide a liquid-tight, flexible container for the damper fluid, yet allow free damper action; they provide a spring rate to the assembly which tends to center the damper elements; they provide the reaction torque necessary to overcome friction in the bearing.

The fittings on the housing are provided with self-aligning bearings attached to links. The links secure the damper to the structure, but at the same time will allow it to shift in an axial direction as well as provide it with angular misalignment features in two planes. It is free to float in an axial direction; it is free to align itself with the shaft in an angular direction; but it is not free to move in either the vertical or the horizontal direction. It is also held from rotating. This freedom will allow it to function properly and to align itself on the shaft.

The effect of viscosity changes with variations of temperature, either environmental or due to operational heat, is compensated for by having the shear elements change their relative positions, thus varying the gap between the working surfaces. The gap between the shear elements as set up by the design is from the calculations with the temperature of the damper fluid at 70 degrees Fahrenheit. If this temperature goes up or down, the gap will change by the action of the thermometal, shear-element material. The rate of change is calculated to agree with the change in viscosity in such a way as to maintain a constant damper coefficient.

The design objectives are fulfilled as follows:

1. The viscous shear damper matches the requirements of the shaft.

2. Failsafe operation in the event of a sealing ring or housing leak is inherent due to the heavy fluid and labyrinth arrangement of the plates. For example, the laboratory damper operates without seals, depending only upon occasional oiling. The fluid film remains upon the plates. Should testing prove that an additional barrier is required, a vertical wall through the center of the damper is contemplated.

3. The damper is independent of the aircraft systems for lubrication.

4. Temperature compensation will accommodate the full range of environmental conditions.

Damper Design Equations

The following relationships were used in the preliminary design of the viscous shear damper:

1. Shear velocity = $\omega\delta$ (inches per second) (5)

   where ω = angular velocity of critical speed of interest (radians per second)

   δ = radius of deflection at that speed (inches)

2. Gap width (minimum) = $\frac{\text{Shear Velocity}}{\text{Limit Shear Rate}}$ (6)

   where Limit Shear Rate is defined by the maximum acceptable drop in apparent viscosity of the damping fluid

3. Shear area = $\frac{Ch}{\mu}$ (square inches) (7)

where C = required damping coefficient (lb-sec/in)
h = gap width (inches)
μ = viscosity (reyns) at the temperature of interest

DESCRIPTION OF TEST ITEMS

Model Shaft

The model shaft was made dynamically similar to the full-size shaft system as determined by the application of the modeling equations of Reference 4. The model was used to determine optimum damping coefficient and to establish the best damper location for successful full-scale operation. The characteristics of the model shaft are given below. Wall thickness measurements are provided in Table III.

Model Shaft Characteristics

Length	135.60 inches
Outside diameter	1.50 inches
Inside diameter	1.37 inches
Material	Aluminum alloy tube
Weight	3.86 pounds

The scaling factors of the model shaft were such that the calculated critical speeds occurred at twice the revolution per minute of the calculated critical speeds for the full-scale shaft.

The model damper was a single plate viscous shear type, similar, except for size, to that used in the full-scale tests. The model damper moving weight was varied from 1.2 to 1.5 pounds, corresponding to 18 to 22 pounds of damper weight on the full-scale shaft.

TABLE III

MODEL SHAFT WALL THICKNESS MEASUREMENTS

1.50 DIAMETER x .064 WALL x 135.6 INCHES LENGTH				
Station	0-degree Index	90 degrees	180 degrees	270 degrees
A	.064	.064	.0635	.064
B	.063	.0635	.064	.064
C	.064	.0635	.064	.064
D	.064	.064	.064	.064
E	.064	.064	.064	.0645
F	.064	.0635	.064	.064
G	.064	.064	.0635	.064
H	.064	.064	.064	.064
I	.064	.064	.064	.064
J	.064	.064	.064	.0645
K	.064	.064	.0635	.064
L	.0635	.0635	.064	.064
AVERAGE WALL THICKNESS				
	.063875	.063833	.063875	.064033

The model damper was designed to be mounted on the model shaft tube without requiring a reduced diameter section. Thus, damper position was infinitely variable.

Shaft end connections were designed to simulate the bending stiffness of the flexible metal disc couplings of the full-scale shaft, based upon the same ratio of K L/EI, where K equals the moment stiffness and L is the total shaft length. The required, calculated section was 0.160 inch in diameter for a length of 0.50 inch. Final model tests were made with this end condition, while the initial tests were made with a somewhat stiffer end connection having a 0.250-inch diameter. Test results provide a comparison of the two sections tested.

Full-Size Shaft

The full-size shaft was designed to the physical dimensions

dictated by data supplied and by model tests.

Full-Size-Shaft Characteristics:

Length	338.50 inches
Outside diameter	4.50 inches
Inside diameter	4.26 inches
Material	Aluminum alloy tube
Weight	56.0 pounds

Description of Shaft - The full-size test specimen shaft used a standard extruded tube as it came from the mill. No attempt was made to straighten or initially to balance the test specimen. Maximum runout was ± 0.165 inch in the 338.8-inch length of tube, less than half the standard tolerance of ± 0.010 inch per foot of length. Figure 18 shows shaft stations referred to throughout the report and rotations. Figure 19 shows physical characteristics of the shaft.

The full-scale test shaft is supported at each end through a flexible metal disk coupling. This coupling introduces a low moment restraint and thus provides end conditions that approach an ideal "simply supported" configuration. The full-scale shaft is uniform in weight along its length except at 30 inches from one end, which is the damper location.

The joint at the damper must be relatively rigid. The more rigid the joint, the more effective will the damper be in controlling the amplitude of the turning shaft.

The original intention was to bolt the fingers of the flexible coupling adapters together after removing the flexible coupling plates and thereby use existing standard hardware for this point.

Two sections of standard drive shaft tubing were bolted together at the adapters and tested to determine the deflection and bending stiffness of the assembly.

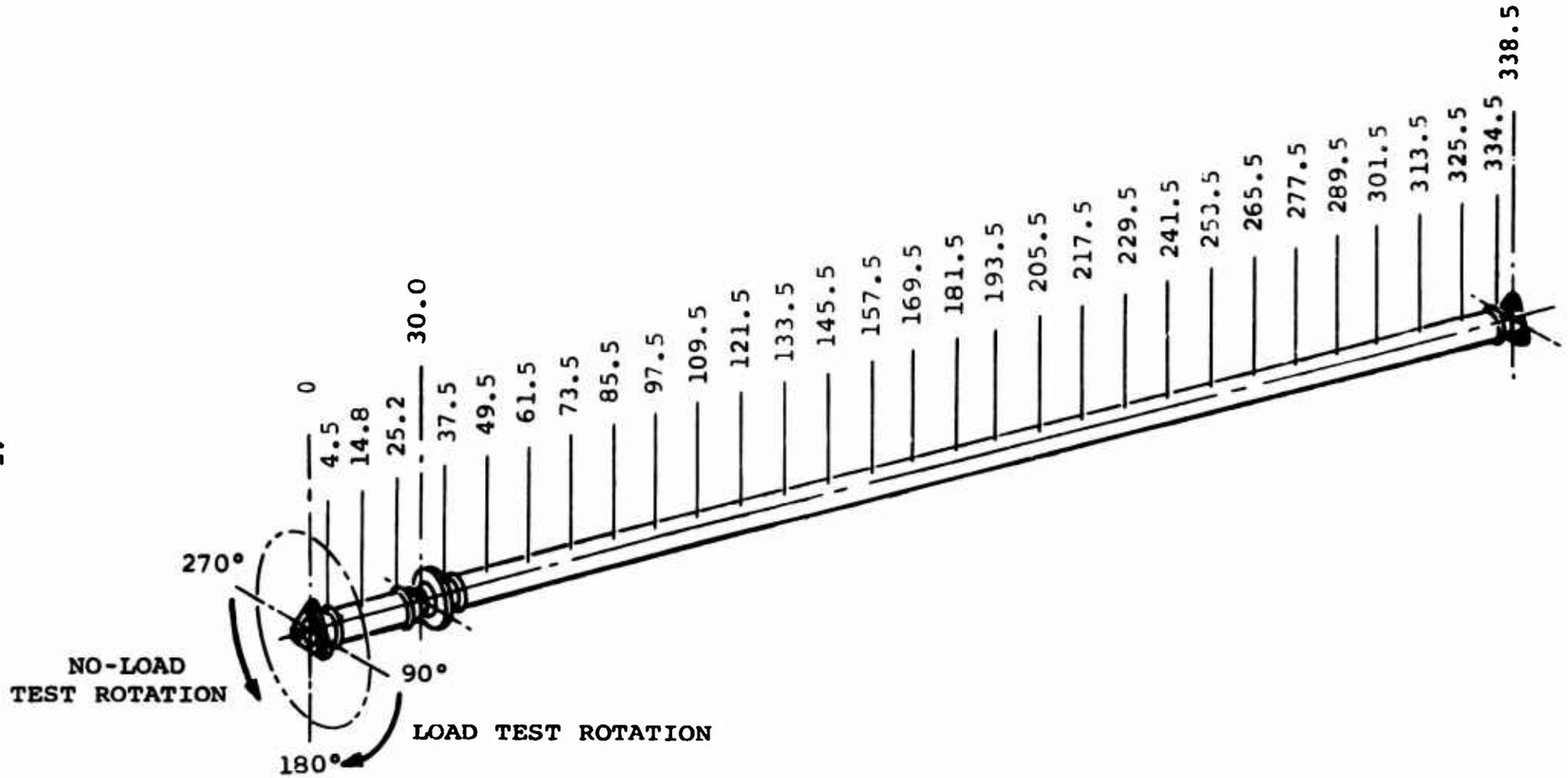

FIGURE 18. SHAFT STATIONS AND ROTATION.

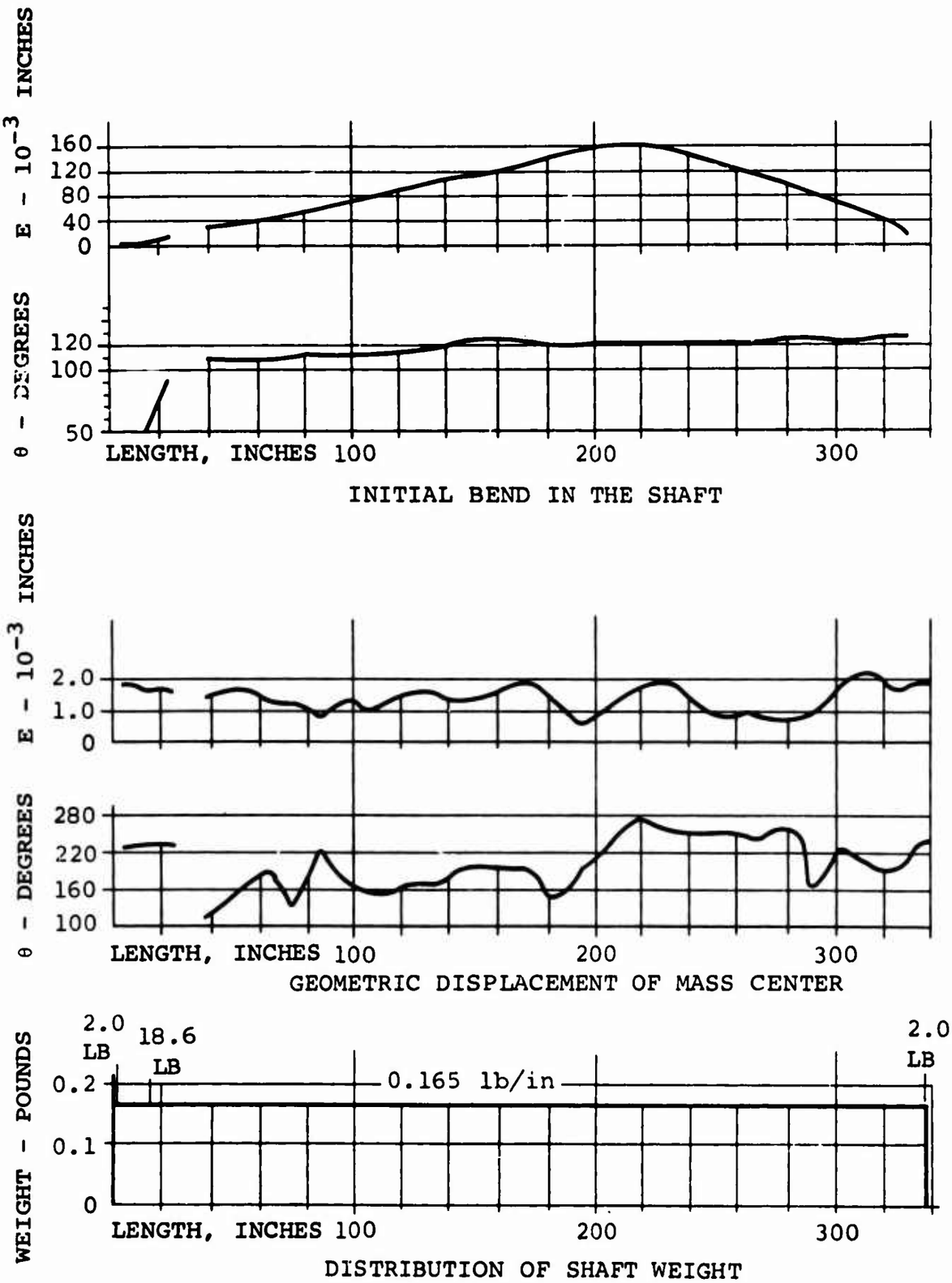

FIGURE 19. PHYSICAL CHARACTERISTICS OF TEST SHAFT.

TABLE IV

SUPERCRITICAL SHAFT WALL THICKNESS MEASUREMENTS

	Degrees							
Station	15	60	105	150	195	240	285	330
4.5	.1185	.1180	.1185	.1200	.1210	.1215	.1205	.1190
14.8	.1180	.1175	.1185	.1195	.1210	.1210	.1205	.1185
25.2	.1180	.1175	.1185	.1190	.1195	.1205	.1190	.1185
37.5	.1185	.1195	.1205	.1210	.1210	.1190	.1200	.1185
49.5	.1180	.1195	.1195	.1210	.1205	.1195	.1185	.1180
61.5	.1170	.1180	.1185	.1200	.1200	.1195	.1190	.1180
73.5	.1180	.1190	.1195	.1200	.1200	.1185	.1180	.1170
85.5	.1170	.1185	.1190	.1190	.1200	.1195	.1190	.1180
97.5	.1180	.1190	.1190	.1205	.1205	.1195	.1190	.1180
109.5	.1190	.1185	.1200	.1205	.1205	.1195	.1190	.1185
121.5	.1180	.1185	.1205	.1210	.1210	.1200	.1190	.1180
133.5	.1180	.1185	.1190	.1205	.1200	.1195	.1185	.1180
145.5	.1180	.1190	.1180	.1200	.1195	.1200	.1190	.1185
157.5	.1180	.1180	.1185	.1200	.1200	.1200	.1180	.1185
169.5	.1175	.1180	.1190	.1205	.1205	.1205	.1175	.1190
181.5	.1185	.1185	.1195	.1205	.1210	.1190	.1180	.1180
193.5	.1185	.1195	.1200	.1205	.1220	.1205	.1195	.1200
205.5	.1180	.1175	.1190	.1190	.1205	.1200	.1190	.1180
217.5	.1195	.1190	.1195	.1190	.1205	.1215	.1215	.1205
229.5	.1180	.1175	.1180	.1180	.1195	.1205	.1195	.1185
241.5	.1180	.1180	.1185	.1185	.1195	.1200	.1190	.1185
253.5	.1185	.1175	.1195	.1190	.1200	.1200	.1205	.1190
265.5	.1185	.1175	.1190	.1185	.1190	.1195	.1185	.1185
277.5	.1185	.118	.1185	.1185	.1195	.1195	.1190	.1185
289.5	.1180	.118	.1190	.1195	.1200	.1190	.1185	.1180
301.5	.1170	.1175	.1175	.1185	.1195	.1200	.1185	.1175
313.5	.1170	.1175	.1175	.1195	.1195	.1200	.1170	.1175
325.5	.1165	.1175	.1180	.1195	.1195	.1195	.1185	.1175
334.5	.1180	.1185	.1195	.1190	.1205	.1210	.1185	.1180

It was found that the arms of the adapters were flexible and that the joint was only 5 percent as stiff as the tube.

Special adapters were then designed and made in order to maintain tube stiffness through the reduced diameter section at the damper location.

Figure 20 shows the specially designed cone adapter and flange adapter, both joined by a circle of bolts through a continuous flange. Calculations and tests indicated that the stiffness at the joined adapters was equivalent in bending to the basic tube stiffness. The measured deflection of the entire shaft as assembled and supported at the ends was within 1 percent of the deflection calculated by simple beam theory. It was concluded that a uniform EI value of 43.1×10^6 pounds per square inch described the full-scale test specimen.

A problem was encountered with the splined section of the damper adapter. Initially, a straight spline with cylindrical land at one end was found to provide an inadequate centering effect. When a conical land at the opposite end was added, unexpected performance changes during operation were eliminated. However, it was found that despite careful indexing, a disassembly of the shaft resulted in changes in dynamic characteristics. A still more positive centering effect is desirable for a production design shaft.

Laboratory-Type Damper - The damper was a single-plate viscous-shear type having a center spherical joint. This permits damper-to-shaft angular alignment with a minimum radial clearance. See Figure 20. The damper (Figure 21) was designed so that multiple plates could be used to raise the damping coefficient. Also, the damper was constructed so that variations in damping coefficient were obtainable by changing spacing between the plates. This could be done by changing the shims which maintain the gaps between the plates. The shims could be added or removed quickly and easily without removing the damper from the machine or disturbing its location on the shaft. The damper liquid used was 250W oil. Damper plate area was 176 square inches per plate. Plate clearance to produce the range of coefficients was 0.002 to 0.012 inch.

Damping coefficient of 17.2 pounds/second/inch at 50 cycles per second rose to 21.0 pounds/second/inch at the higher frequency of 150 cycles per second. The ambient temperature was 80 degrees Fahrenheit. A damper plate clearance of 0.004 inch was used to obtain these coefficients.

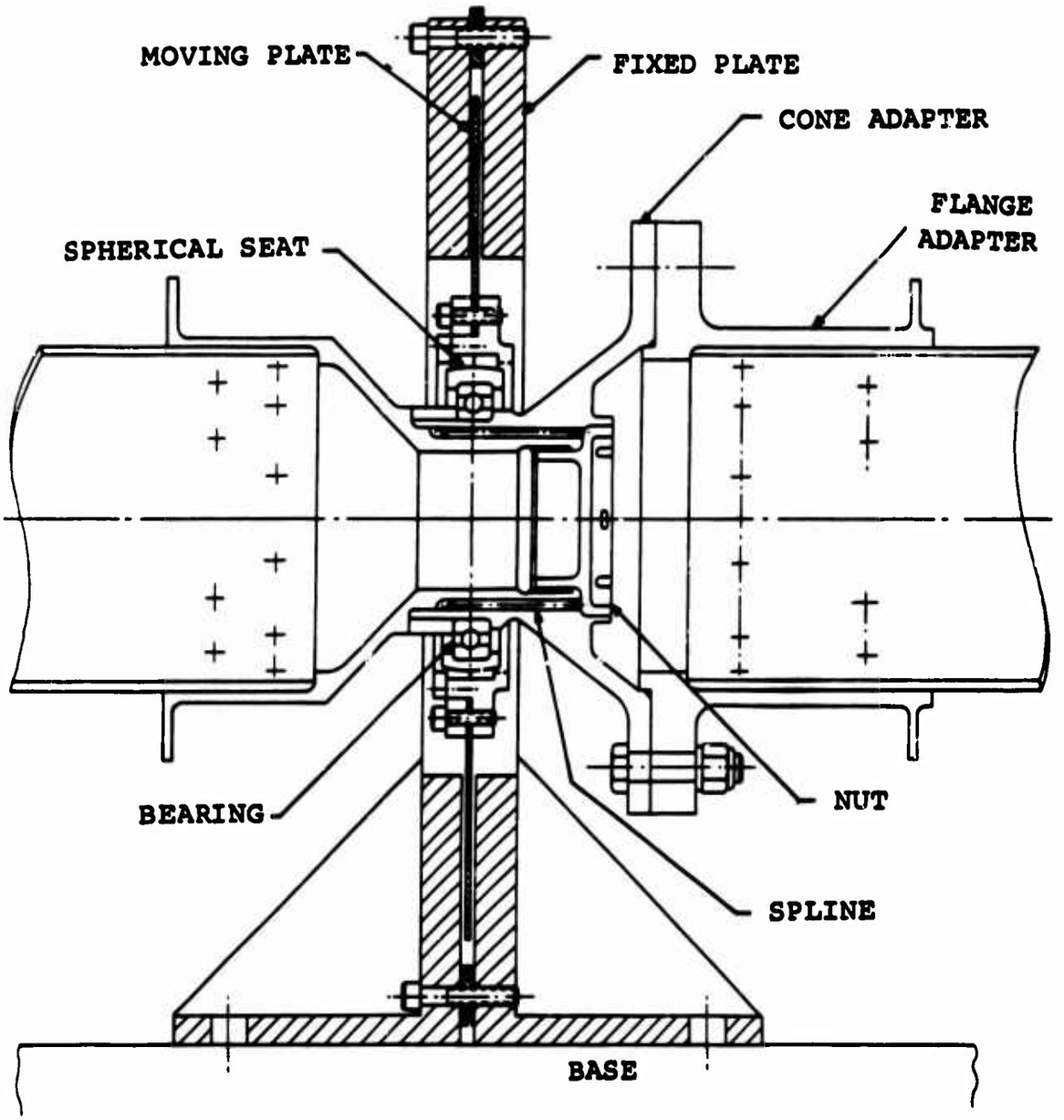

FIGURE 20. LABORATORY DAMPER AND ADAPTERS.

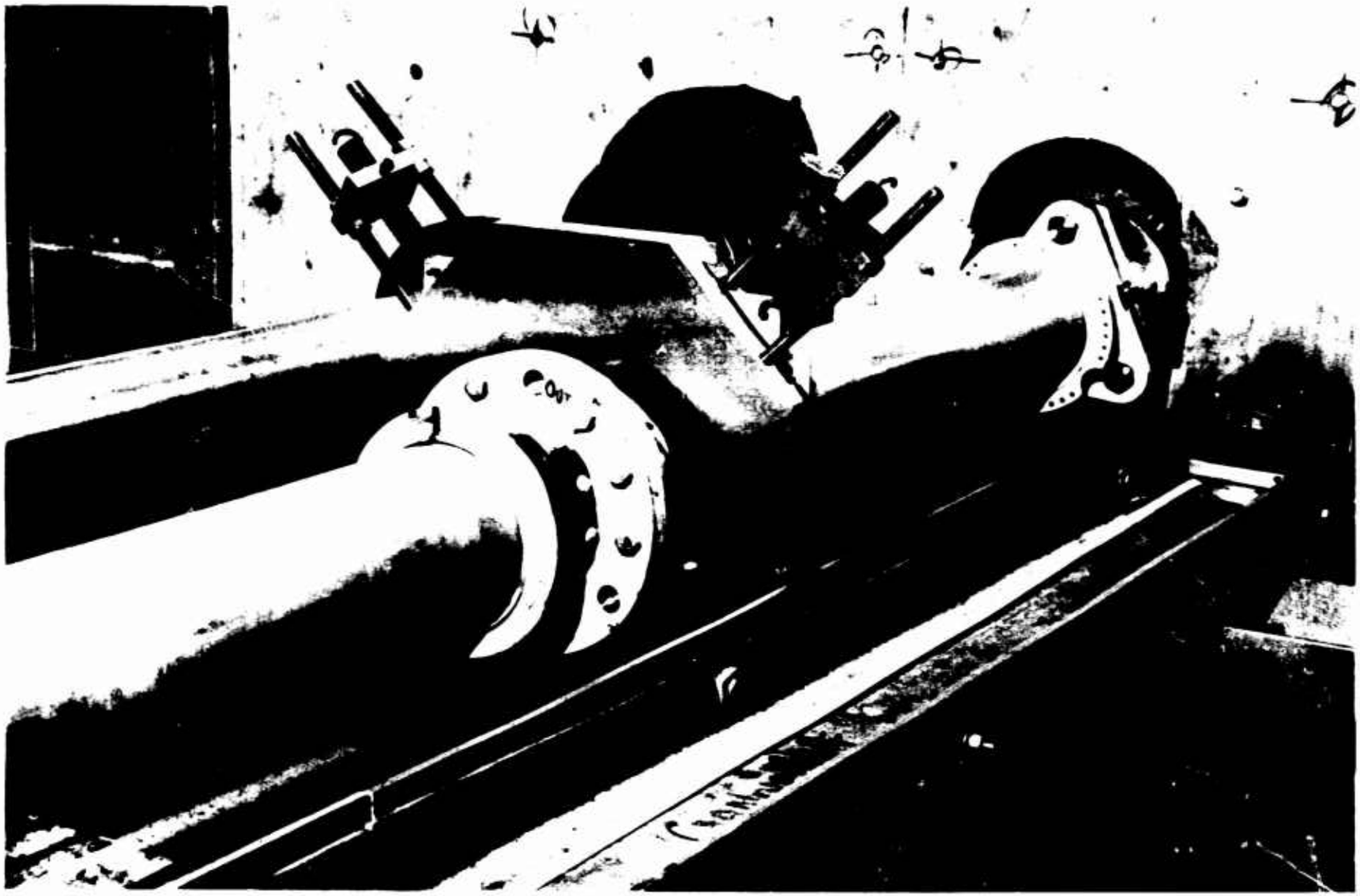

FIGURE 21. LABORATORY DAMPER.

EXPERIMENTAL PROCEDURES

Test evaluation of the model and full-size shafts was accomplished in part at Battelle Memorial Institute, Columbus, Ohio, under subcontract to the Vertol Division, and in part at the Vertol Division test facility. The test program investigated a series of design and environmental variables. Conclusions as to the effect of each variable were drawn from observations of shaft motion and shaft stress as the shaft was rotated. One model and one full-size test specimen were used in the program.

MODEL AND NO-TORQUE TEST STAND

The model and no-load test stand are driven by a 15-horsepower direct-current motor equipped with variable speed control and a governor that precisely holds a speed at any desired setting. The flat belt-driven test spindle has the capability of turning small-size shafts at speeds as high as 50,000 revolutions per minute. With a large shaft, such as the full-size specimen tested, the windage and friction of the larger bearings plus the power requirements of the damper limit the top speed obtainable. The shaft is supported by a headstock and a tailstock. The tailstock is adjustable to accommodate various shaft lengths.

TORQUE TEST STAND

The load test machine is a four-square, regenerative torque apparatus having two fixed-speed motors of 75 horsepower each. The motors are connected through clutches to the low-speed balance shaft by V-belts. The gearboxes on each end drive the high-speed test spindles. The test specimen (shaft) is connected between the high-speed spindles and makes up the four-square system. Extended periods of operation at variable speeds are not possible with the present configuration of this machine. Maximum circulatory horsepower is 2000, as determined by the capacity of the gearboxes. See Figure 22.

INSTRUMENTATION

The final performance of the shaft will be evident in the amplitudes of the vibration loops on the shaft. A method was developed to observe the motions of the shaft without disturbing or touching the surface. An optical system was used wherein a shadow of the shaft fell on a light-sensitive element of a

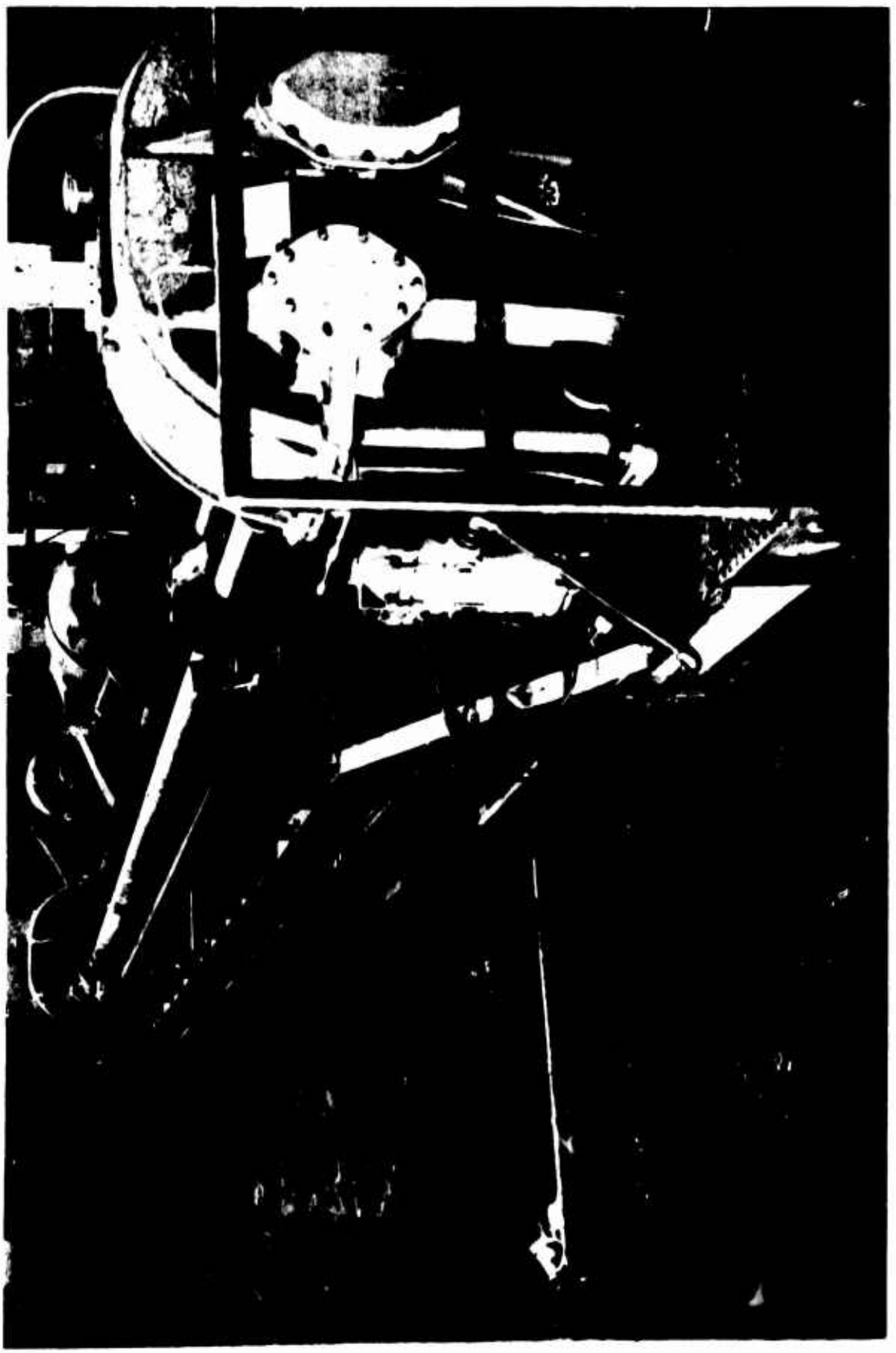

FIGURE 22. LOAD TEST MACHINE.

photocell. The position of the shaft was used to determine the amount of light striking the cell, and in this way the voltage in the system was regulated. The change in voltage was calibrated with a known deflection. Calibration of the system was accomplished with a dynamic shaker as well as with the shaft running. Figure 23 shows a chart of calibration response. Figure 24 shows the method used to obtain dynamic calibration, using measured rods clamped to the shaft near one end. Figure 25 shows the optical pickup installed in position on the test machine track.

The optical pickup unit was mounted on a track located parallel to the test shaft. This arrangement enables the optical pickup to traverse the full length of the shaft and to define the mode shapes by measuring the amplitudes as it progresses. See Figure 1.

A second optical unit was used to scan an eccentric on the tailstock spindle in order to obtain index data for the shaft angular position. The signal obtained from the optical unit was electronically compared with the signal from the rotating deflected shaft for phase angle information.

Strain gages were installed at points of expected maximum bending for testing under torque loading conditions. A slip-ring was used to transfer gage readings to indicating and recording equipment.

The additional instrumentation used in conjunction with the primary sensing devices was as follows:

Item	Description	Manufacturer
Oscillograph	Model 5-124	CEC
Amplifier	Frequency response flat 0-20 kc	Kintel
X-Y Plotter		Mosely
Accelerometers		Endevco
Oscilloscope	Model 502 dual beam	Tektronics
Electronic Counter	Model 523	Hewlett-Packard

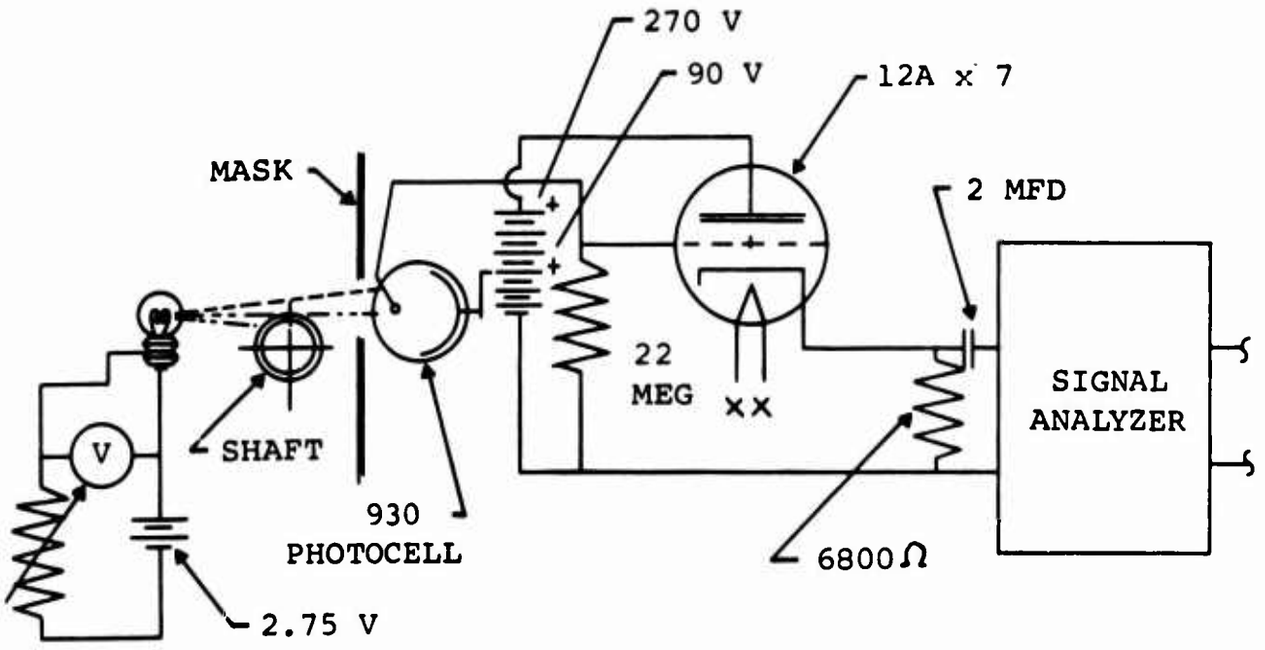

SCHEMATIC OF SHAFT AMPLITUDE TRANSDUCER

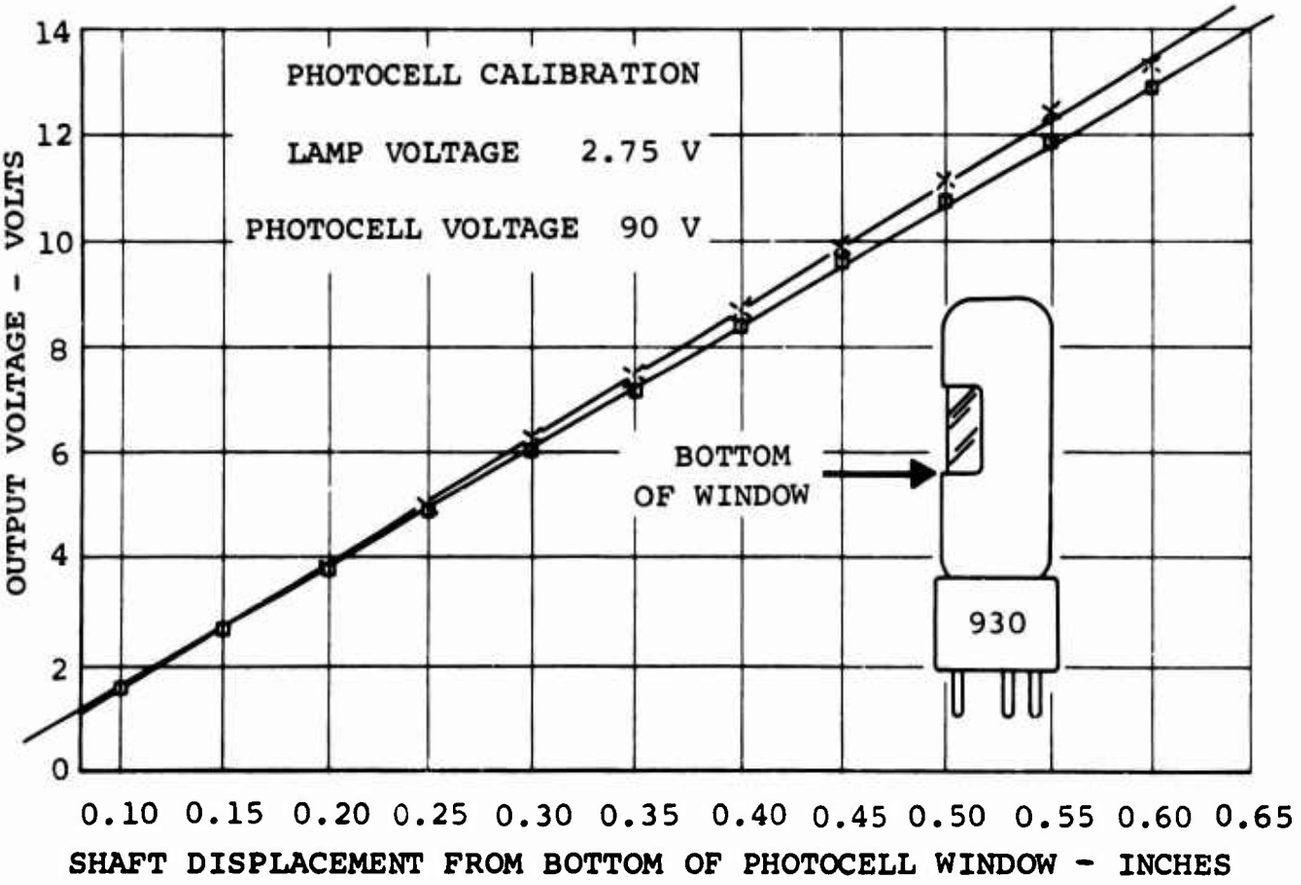

FIGURE 23. OPTICAL PICKUP CALIBRATION CURVE

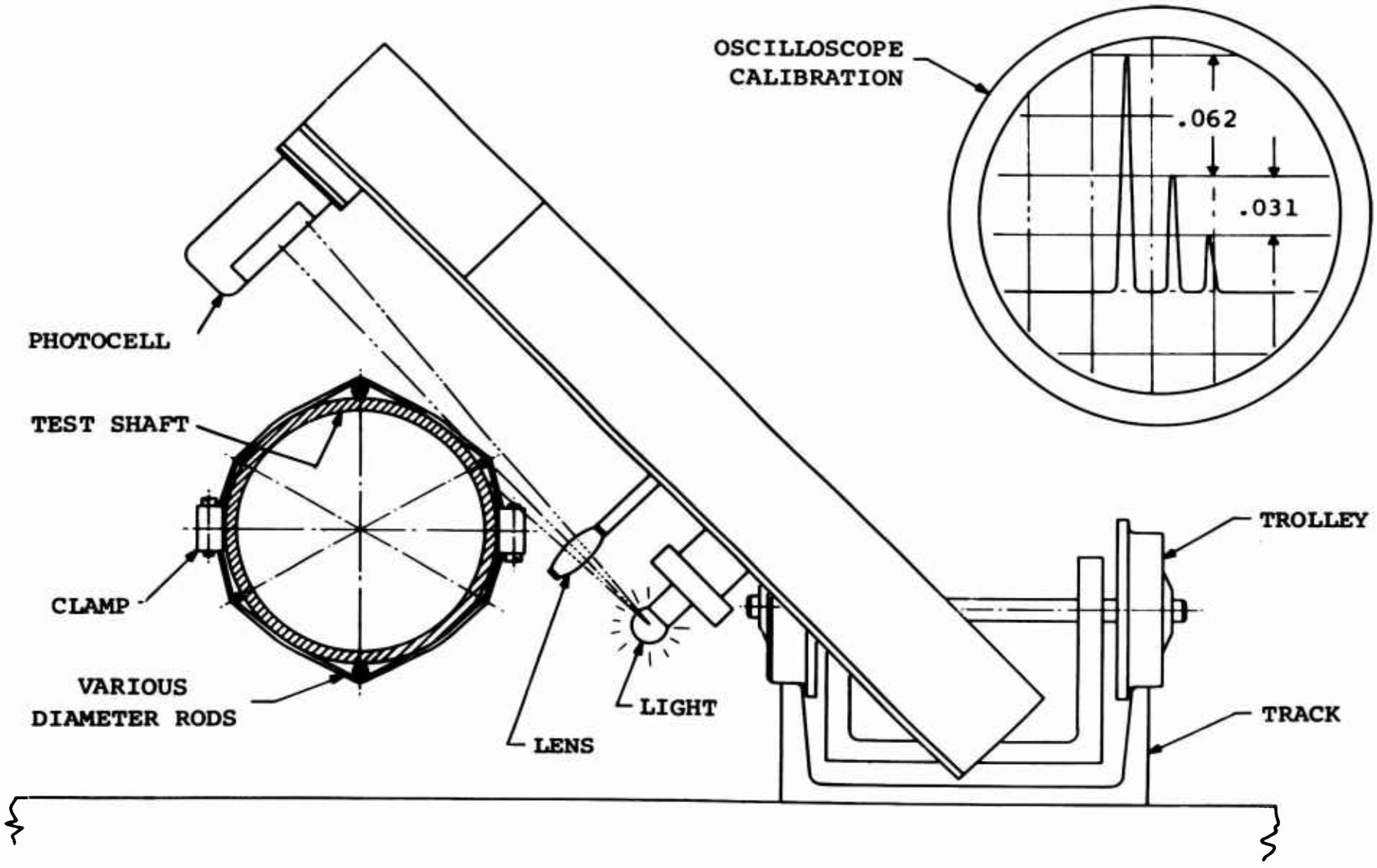

FIGURE 24. OPTICAL PICKUP DYNAMIC CALIBRATION.

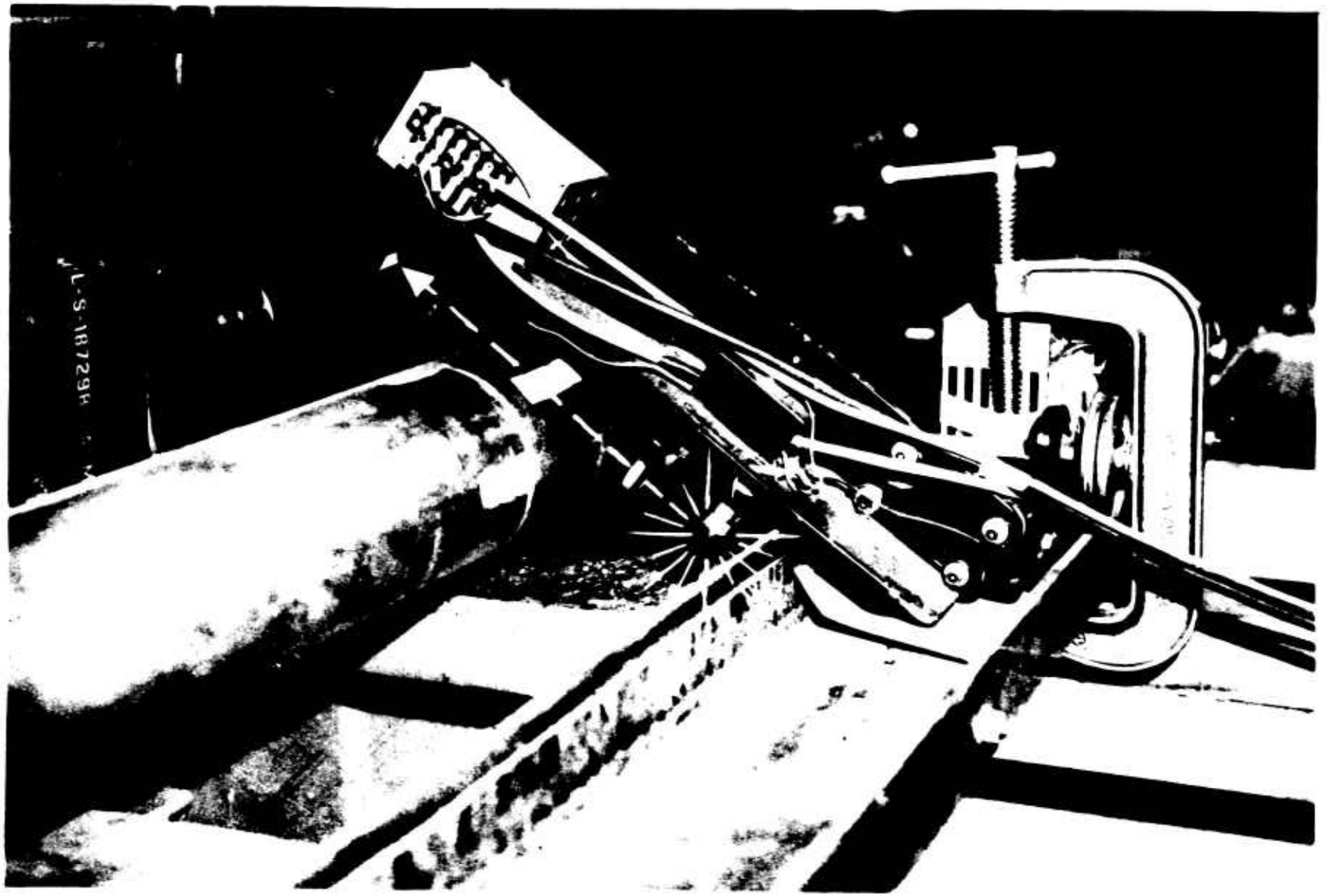

FIGURE 25. OPTICAL PICKUP INSTALLATION.

TEST PROCEDURE

During tests of the full-scale shaft, the following test parameters were monitored and recorded:

1. Damper temperature
2. Damper support spring rate
3. Shaft revolutions per minute
4. Shaft amplitude at a given shaft station or, alternatively, shaft modal shape for various revolutions per minute
5. Shaft bending stress (when strain gages were fitted)
6. Shaft torque (when applicable)

BALANCING PROCEDURE

Balance weights were added to the shaft by using standard aircraft-type hose clamps. See Figure 26. The clamp adjusting screw provided the balance mass. This enabled quick adjustment or transfer of the balance weights to any station or angle on the test shaft.

Dynamic performance or characteristic modal shape amplitude, and phase of deflection are all required for the balancing procedure. The modes were obtained from the test shaft when it was excited with a 50-pound electrodynamic shaker. Both damped and undamped responses, and the modal shapes and frequencies of the damped rotating system, are reported in the Experimental Results section.

The Experimental Balancing Method is a step-by-step procedure by which the test shaft is balanced at each of its critical speeds. The balance weights are distributed so that a previously balanced critical will not be affected. The experimental balancing is based on the assumption that at speeds very near a critical speed, the shaft amplitude is due to a single mode, and application of this balancing method only requires knowing the mode shapes for the shaft. The selection of the location for balancing planes is, according to the experimental theory, rather arbitrary, and the minimum number

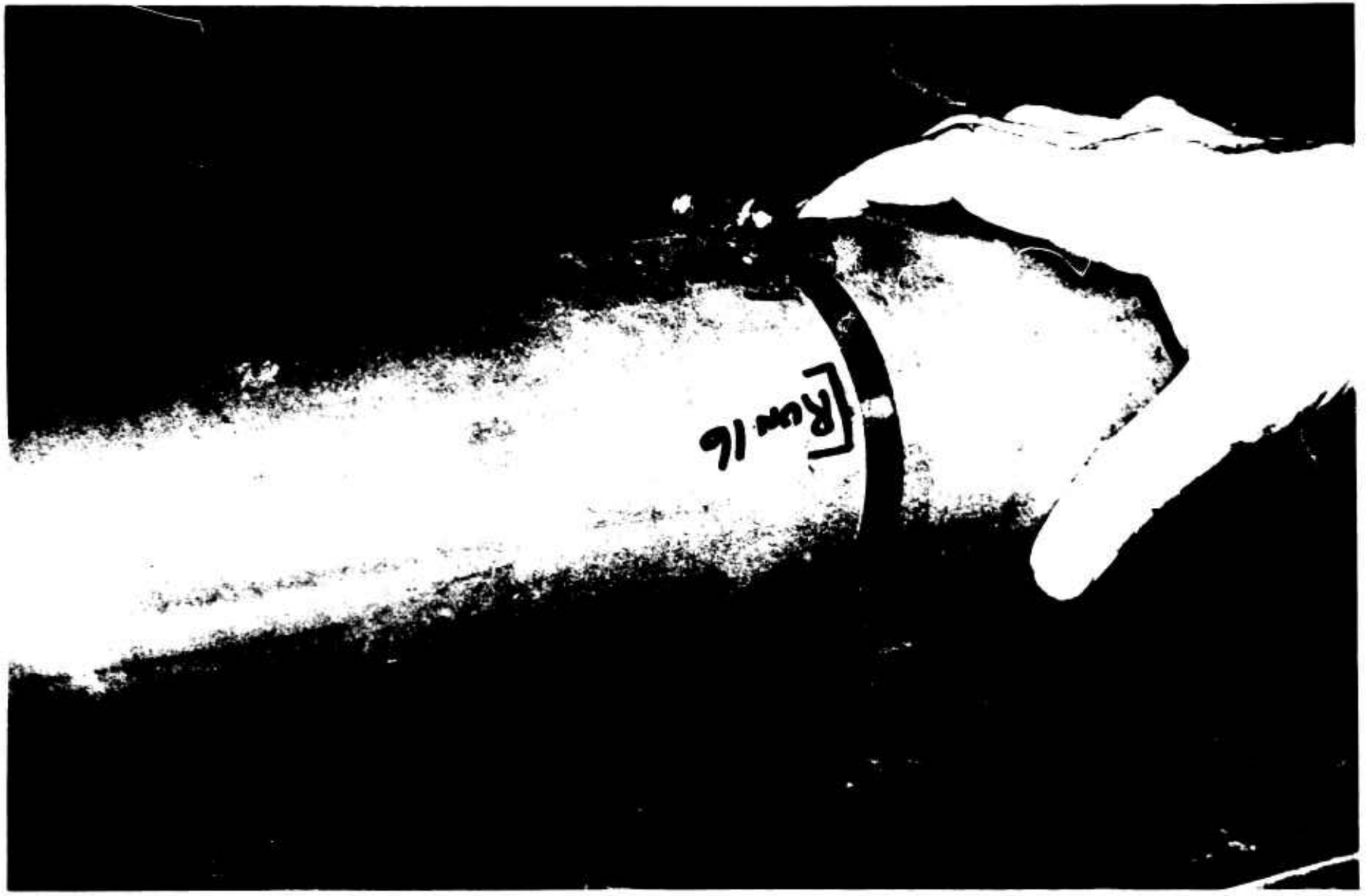

FIGURE 26. EXPERIMENTAL BALANCE WEIGHT.

of balancing planes required is equal to the number of modes to be balanced. In addition to distributing the balance weights to avoid unbalancing a previously balanced mode, it is best to distribute the weights in a way that will have a minimal effect on the modes which are to be balanced in the next successive steps. A more detailed discussion of the Experimental Balancing theory and the choice of balance planes is included in Appendix III.

The higher modes require balance weights of a size which has little effect on the lower modes. Since the lower modes are less important to satisfactory shaft operation, the practical objectives of the balancing procedures are to balance the third, fourth, and fifth critical speeds mode-by-mode. The following balance planes were selected for these objectives:

Mode	Balance Plane
3	Station 185
4	Station 222
5	Stations 140 and 222

Equal weights were used at Stations 140 and 222 for the fifth mode, and the weights were placed at the same angular location.

The correct weight and angular positions for each critical were determined from the vector effect of an initial trial mass at the critical speeds. A limited number of trials were required at each critical to achieve a successful balance.

In order to formalize this method for a production procedure, a set of calibration curves has been made for the selected balance positions when the amplitude and phase measurements are made at Station 300. Figures 27 and 28 display these calibration curves.

A summary of the production balancing procedure for the test shaft utilizing Figures 27 and 28 would be:

1. Place the shaft and damper in the machine and position the displacement transducer at Station 300.

2. Run the shaft to 3200 revolutions per minute and record the shaft amplitude and phase of the distortion at this speed.

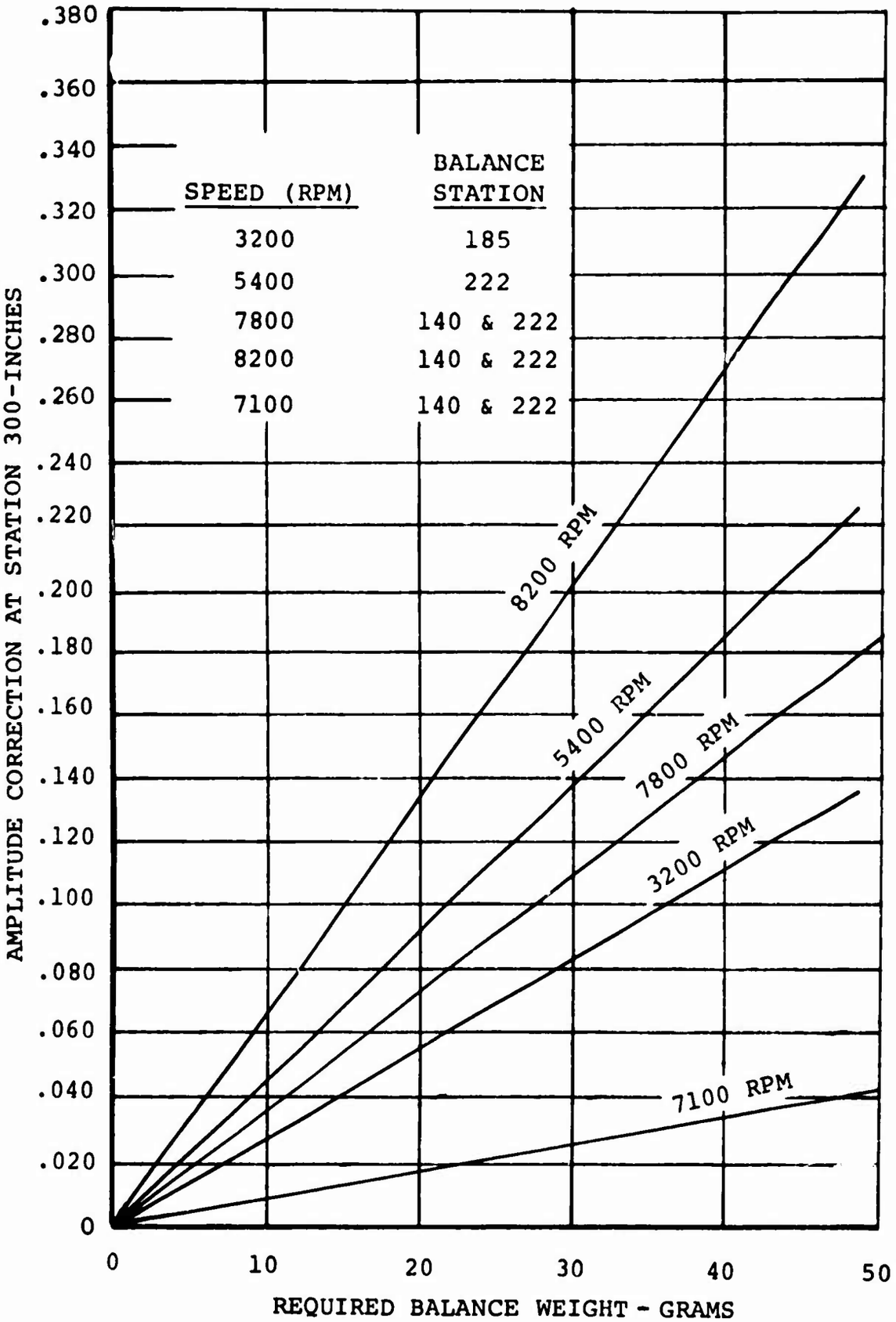

FIGURE 27. MAGNITUDE - BALANCE WEIGHT.

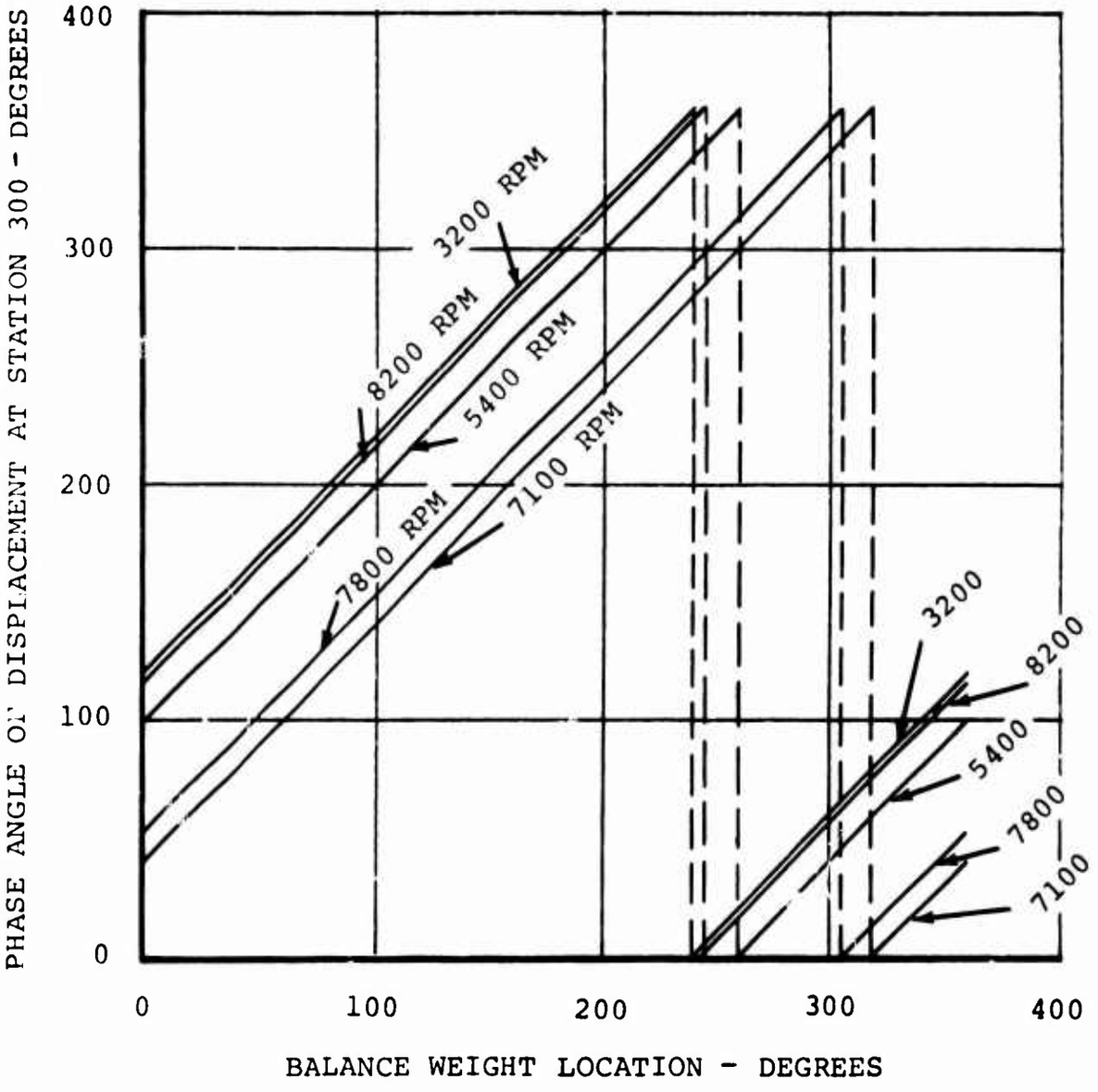

FIGURE 28. ANGLE - BALANCE WEIGHT.

3. Attach the weight indicated from Figure 27 at Station 185 at the angular position from Figure 28. Repeat (2) and (3), if necessary.

4. Run the shaft to 5400 revolutions per minute and record the shaft amplitude and phase of the distortion at this speed.

5. Attach the weight indicated from Figure 27 at Station 222 at the angular position from Figure 28. Repeat items (4) and (5), if necessary.

6. Run the shaft to 8200 revolutions per minute if possible, or to the next highest balance speed possible for the fifth critical (7100 or 7800 revolutions per minute), and record the amplitude and phase of the distortion.

7. Attach the weight indicated from Figure 27 at each of Stations 140 and 222 at the angular position on the shaft from Figure 28. Repeat items (6) and (7), if necessary.

The test procedure for the Analytical Balancing Method, Appendix IV, was as follows:

1. Run the shaft at five different rotational speeds, preferably, though not necessarily, at the five critical speeds.

2. Measure phase angle, amplitude, and mode shape at these speeds.

3. Supply these data to the mathematical solution. Solve for amount of balance at predetermined shaft stations.

4. Rerun the shaft and check results with weights added.

EXPERIMENTAL RESULTS

MODEL TESTS

The objectives of the model tests were as follows:

1. To verify the design calculations.
2. To determine if a single damper would effectively control vibration.
3. To predict optimum damper location and damping coefficient for the full-scale shaft.

Variables investigated in model tests were as follows:

1. Damper location
2. Damping coefficient
3. Number of dampers
4. End support stiffness

Results of model tests are shown in the accompanying figures and tables. The results of experiments in which damper location was varied from 6 to 12 inches from the shaft end are shown in Figure 29. Vibration amplitudes at the first and fifth critical speeds were lowest with the 12-inch location. Damper weight was 1.2 pounds.

The results of damper locations up to 15 inches, with a slightly heavier damper moving weight (1.5 pounds), are shown in Figure 30. There was a sharp increase in amplitude at the 15-inch position.

Variations in the damping coefficient are shown in Figure 31. The highest tested damping coefficient showed best control of amplitude at the higher critical speeds, while the lowest tested coefficient best controlled the first three critical speeds.

The effects of the two values of end connection stiffness are shown in Figure 32. The smaller diameter, which more closely approached the estimated stiffness of the full-size flexible

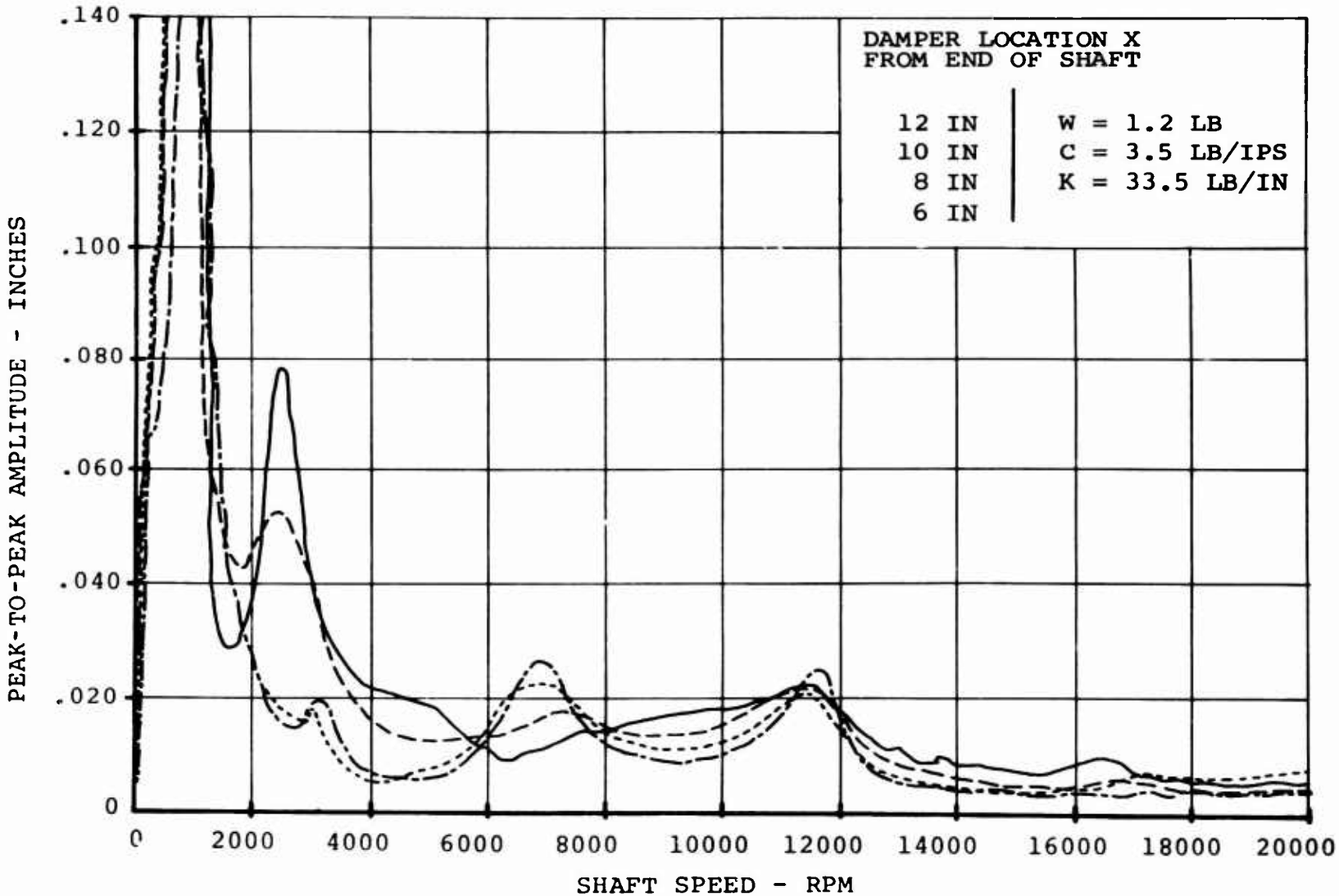

FIGURE 29. DAMPER LOCATION 1.

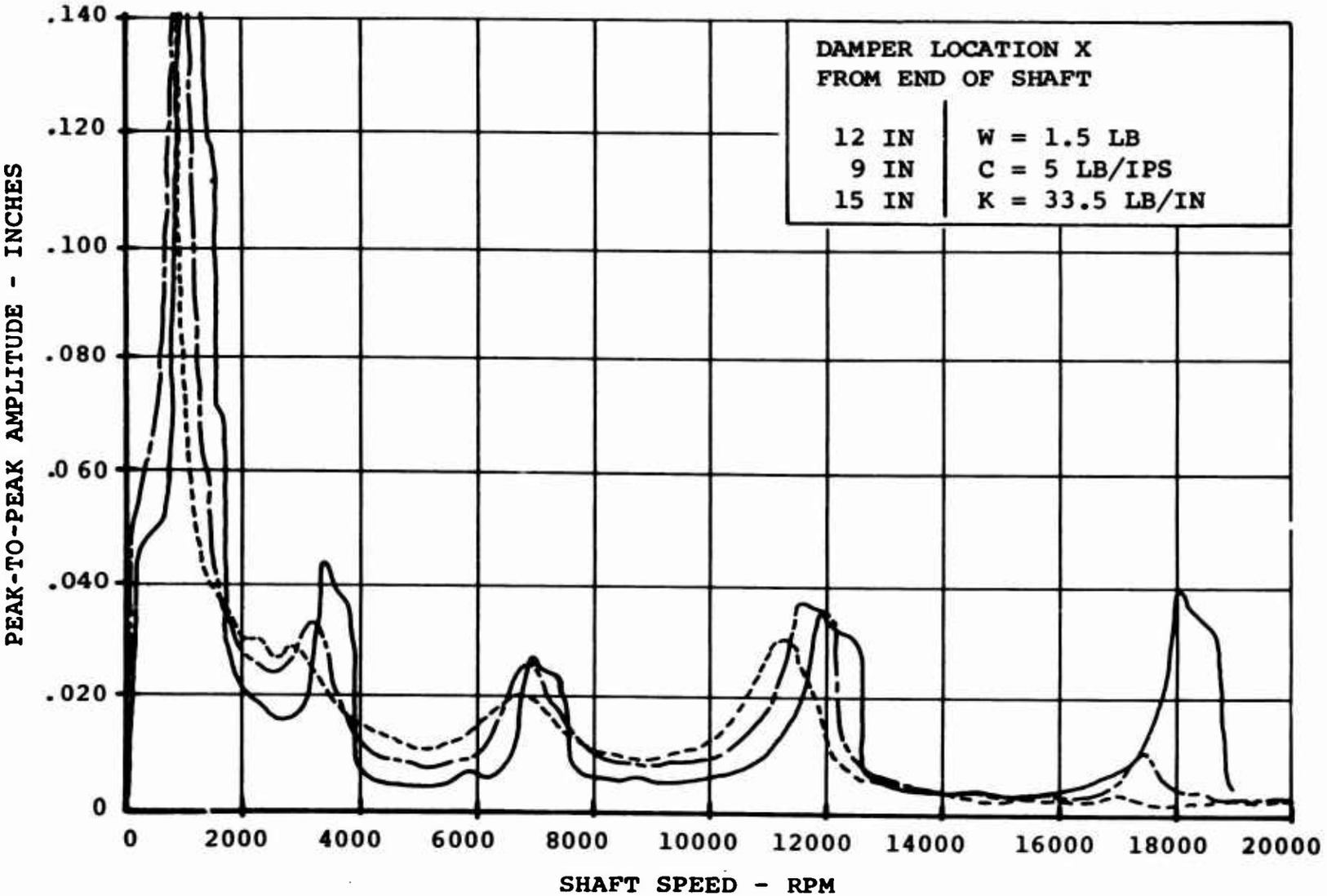

FIGURE 30. DAMPER LOCATION 2.

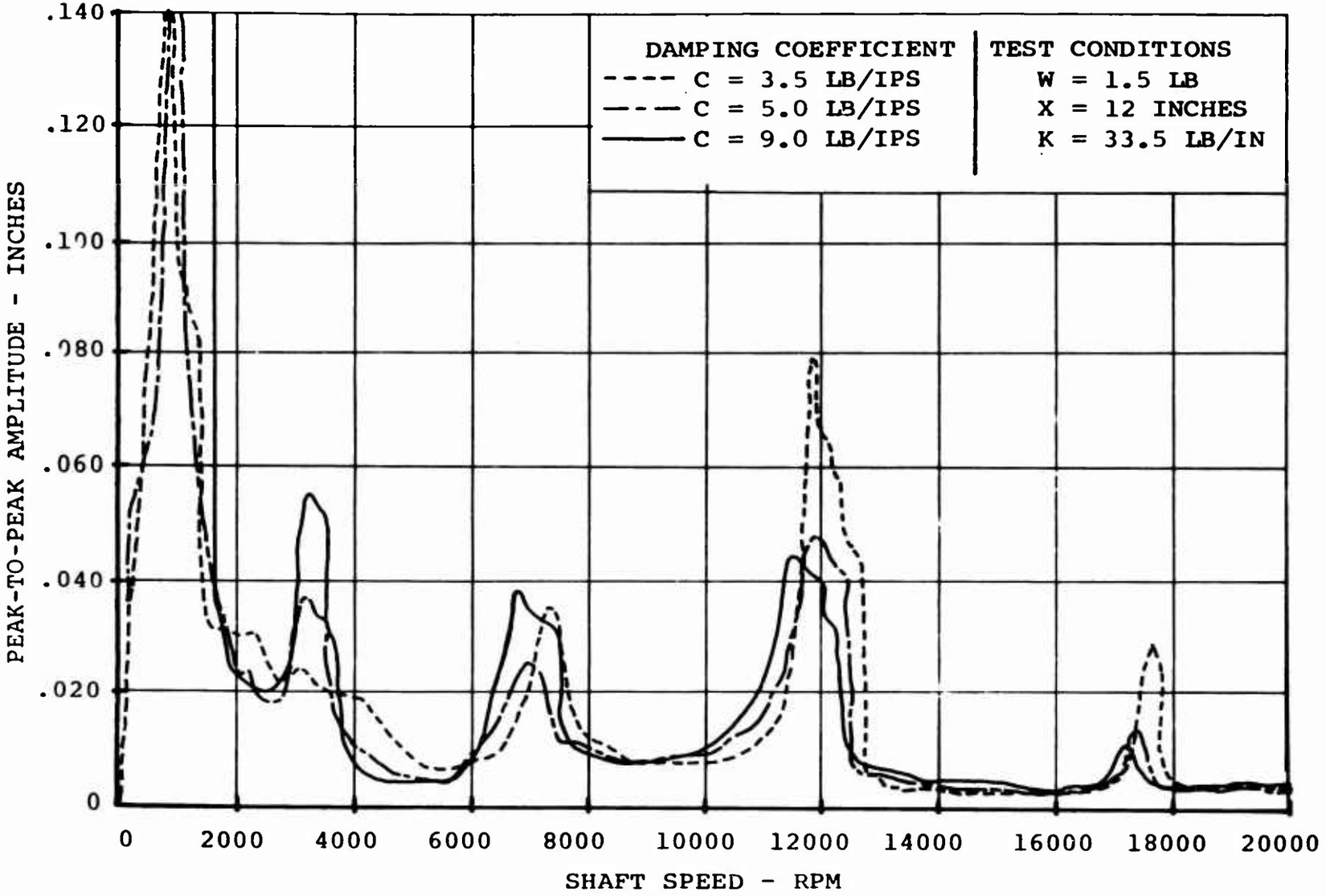

FIGURE 31. DAMPING COEFFICIENT.

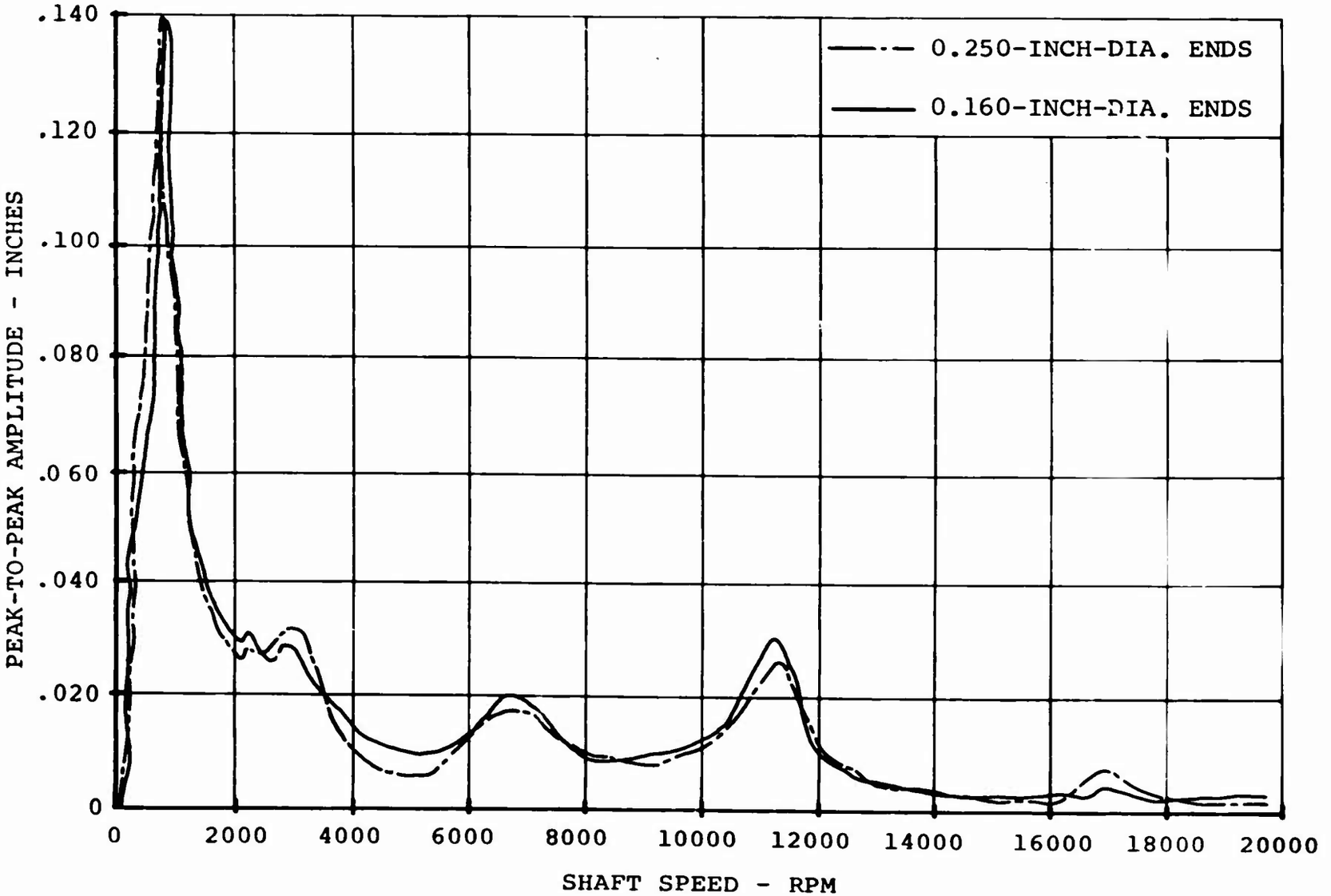

FIGURE 32. END STIFFNESS.

coupling, can be seen to reduce the amplitude at the fifth critical speed.

A comparison of two dampers and a single damper is given in Table V. For comparison, the result of the single damper with 0.160-inch diameter fixed-ended shaft is also included.

TABLE V
MODEL SHAFT PEAK-TO-PEAK VIBRATION AMPLITUDE, INCHES

Description of Configuration	Critical Speed Mode Number				
	1st	2nd	3rd	4th	5th
Single damper 0.250-inch fixed ends	.125	.110	.125	.024	.016
Double damper 0.250-inch fixed ends	.065	.038	0	0	.018
Single damper 0.160-inch fixed ends	.160	.028	.020	.030	.005

FULL-SCALE TESTS

Damper design variables investigated were as follows:

1. Damper coefficient
2. Damper weight
3. Damper support spring rate
4. Damper type

Environmental variables investigated were as follows:

1. Torque
2. Misalignment of end connection
3. Forced excitation of the damper

Balancing procedures were as follows:

1. Experimental method

2. Analytical method

The effects of damping coefficient variation are shown in Figures 33 and 34. Figure 33 indicates that the highest tested coefficient gave highest amplitudes at the third and fourth critical speeds. The sudden rise in this trace was due to a malfunction of the damper bearing spherical seat. After the malfunction was corrected, tests were rerun. The peak amplitudes were comparable to those of the previous runs.

The effects of added damper weight are shown in Figure 35. The damper weight was increased from 20 to 28.3 pounds. Amplitudes with increased damper weight were slightly higher at the higher speed antinodes and were lower at the damper. Spring rate results are shown in Figure 36. The difference in spring rates (168 to 2 pounds per inch) produced little change in shaft amplitude.

Damper type was investigated by substituting an immersion body damper, manufactured by Lord Manufacturing Company (shown in Figure 15), for the laboratory viscous shear damper. The maximum amplitudes experienced are shown in Table VI. It can be seen that the amplitudes are considerably higher at the first three critical apeeds but are more comparable at the fourth and fifth. Also, the first and second critical speeds occurred at lower revolutions per minute; these two speeds correspond to the undamped natural frequencies determined by vibrating the shaft.

TABLE VI
COMPARISON OF DAMPER PERFORMANCE

Critical Speed Mode No.	1		2		3		4		5	
	Ampl	rpm	Ampl	rpm	Ampl	rpm	Ampl	rpm	Ampl	rpm
Viscous Shear Damper (See Figure 58)	.192	303	.050	1524	.038	3200	.026	5400	.010	8300
Immersion Body Damper	Off Chart	250	.13	1050	.080	3450	.032	5700	.026	8200

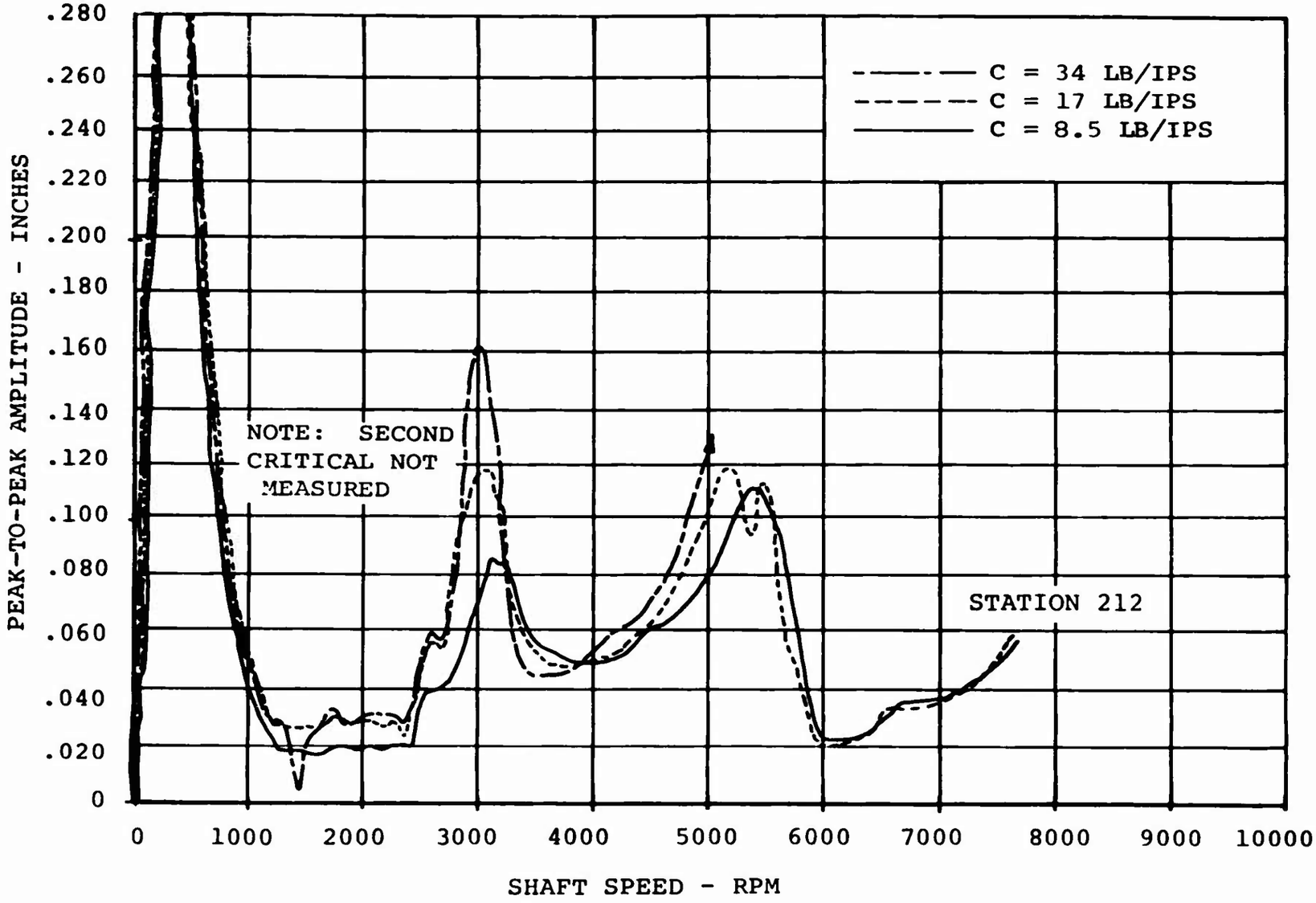

FIGURE 33. DAMPING COEFFICIENT.

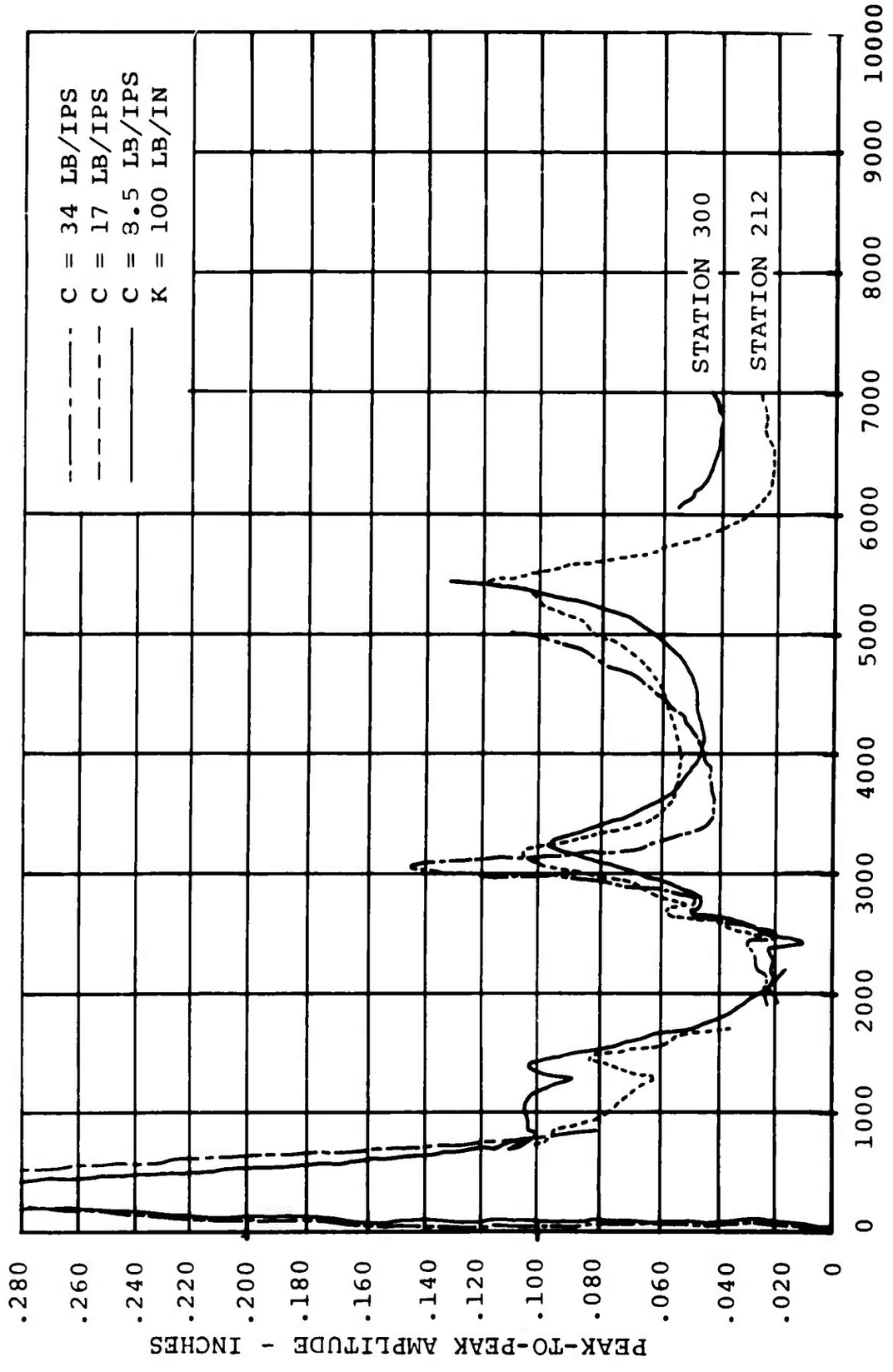

FIGURE 34. DAMPING COEFFICIENT.

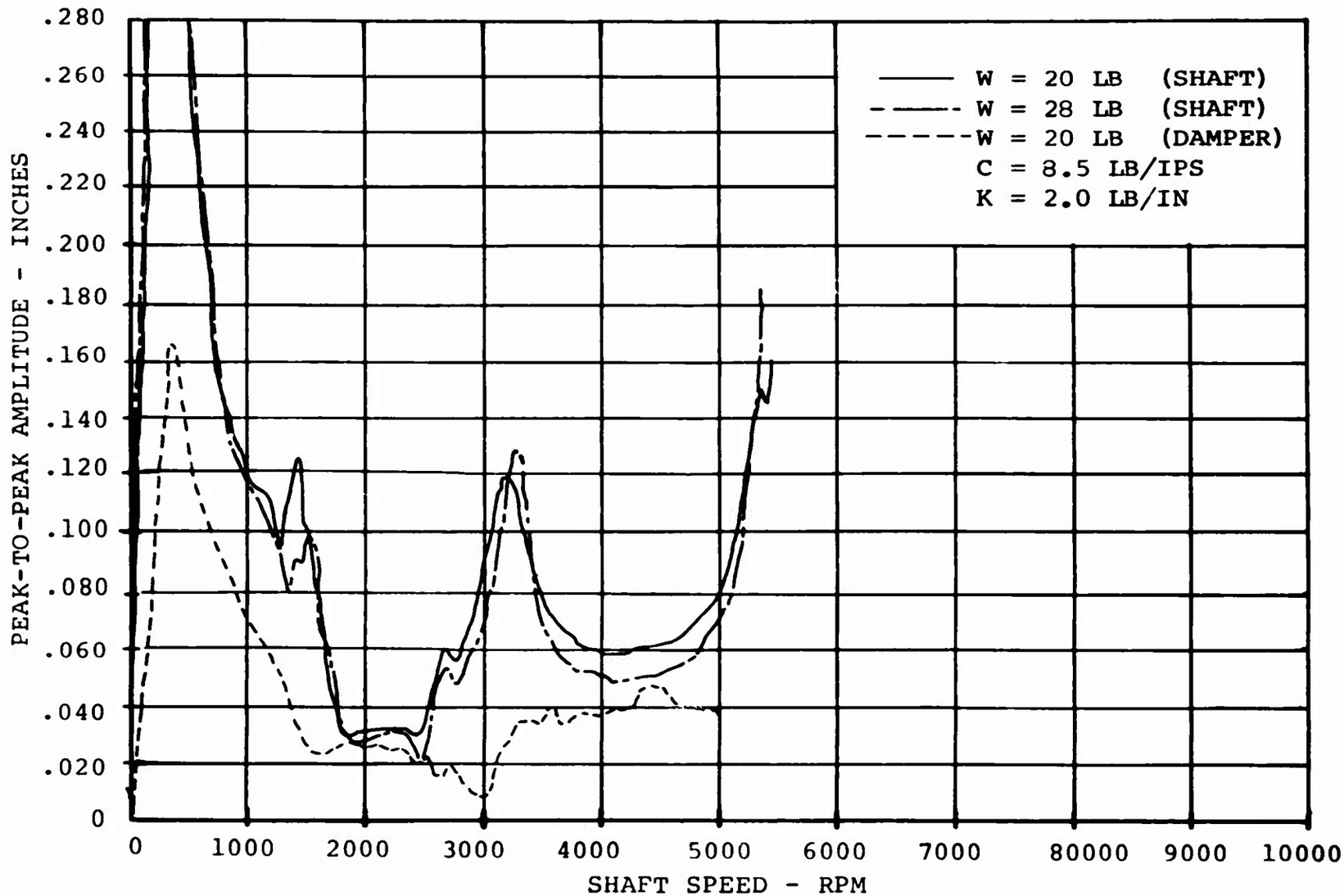

FIGURE 35. DAMPER WEIGHT.

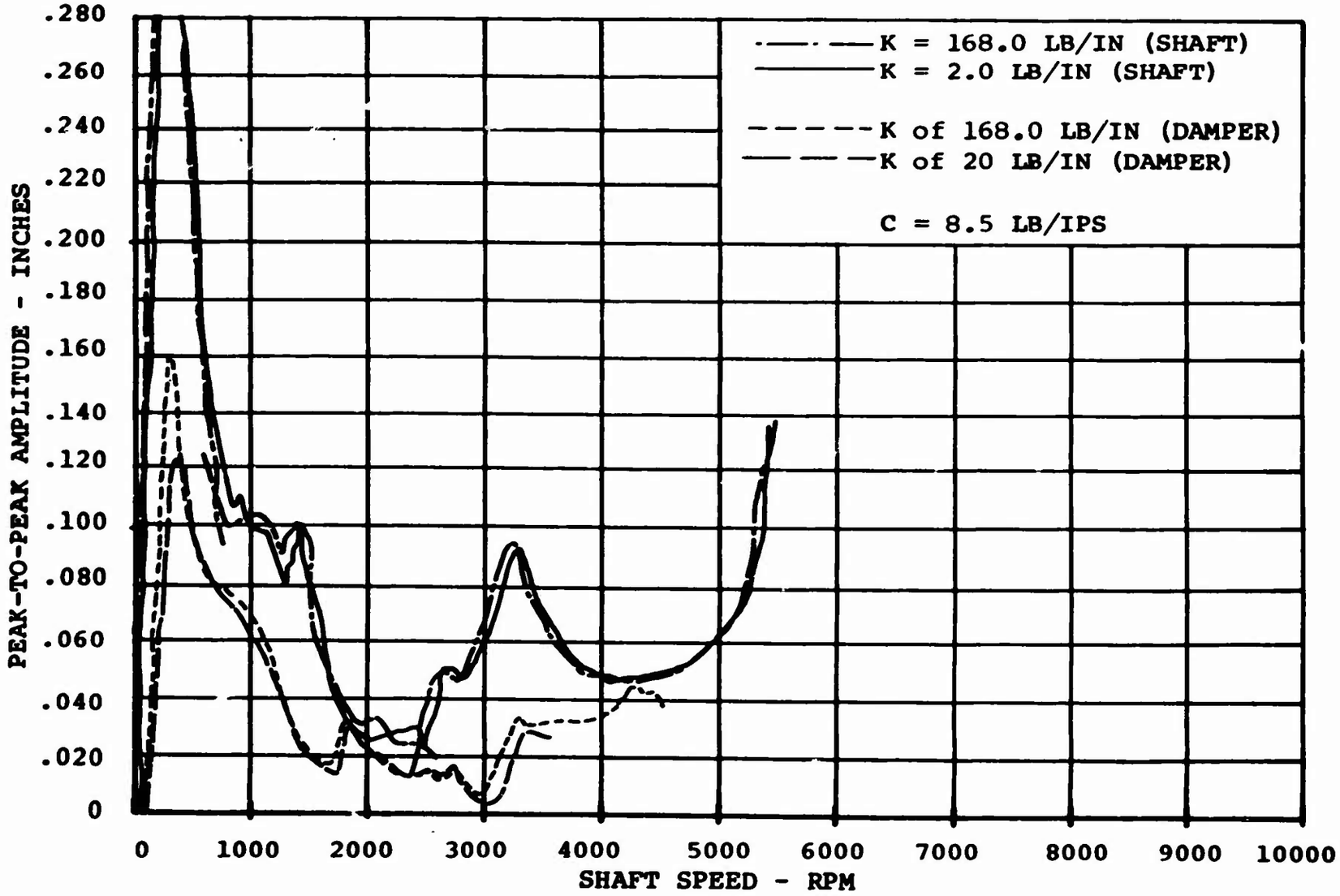

FIGURE 36. SUPPORT SPRING RATE.

ENVIRONMENTAL VARIABLES

The effect of torque is shown in Figures 37 through 42. These are composite figures giving amplitudes measured at the antinodes of the first four (in general) critical speeds. The amplitudes are maxima for each speed. Torque was varied from 0 to 15,000 inch-pounds measured at the shaft. Critical speeds were found to coincide with those found in the no-torque test stand. The effect of torque (at the fourth critical speed antinode Station 296) was to slightly reduce the amplitude through the speed range tested. The torque test stand was set for a maximum speed of 6300 revolutions per minute.

Misalignment of one-half degree in the flexible coupling at the end connection is shown in Figure 43. Two torque levels, zero and 10,000 inch-pounds, were tested. It can be seen that torque did not appreciably influence the shaft amplitude at the higher speeds.

Forced excitation of the damper mounting was performed under various torques and at varying frequencies. The effect of excitation at the fourth critical speed frequency is shown in Figure 44 (zero torque) and in Figure 45 (10,000-inch-pound torque). Figure 46 shows in a composite view the effects of excitation on the damper while operating at the various critical frequencies.

Figure 47 is a reproduction of an oscillograph tape typical of the records made during the Environmental Conditions tests. Recorded information was obtained from the optical pickup and from bending gages located at Station 296.

The first trace near the bottom of the sheet represents shaft revolutions per minute. The second trace from the bottom represents peak-to-peak amplitude as determined by the output of the optical pickup system. The measured amplitude is a function of the unbalance in the shaft and the location of the pickup unit. As the shaft starts to run, each revolution can be picked up from the trace, and the amplitude of the first revolution is caused by the initial band at the point of observation. As the first critical speed is approached, the amplitude increases. Each critical area can be picked from the trace and referenced to the speed trace directly below. A secondary peak or critical appears at about 2200 revolutions per minute. This would be the third critical speed of the shaft if the damper mass were not present. The actual third critical

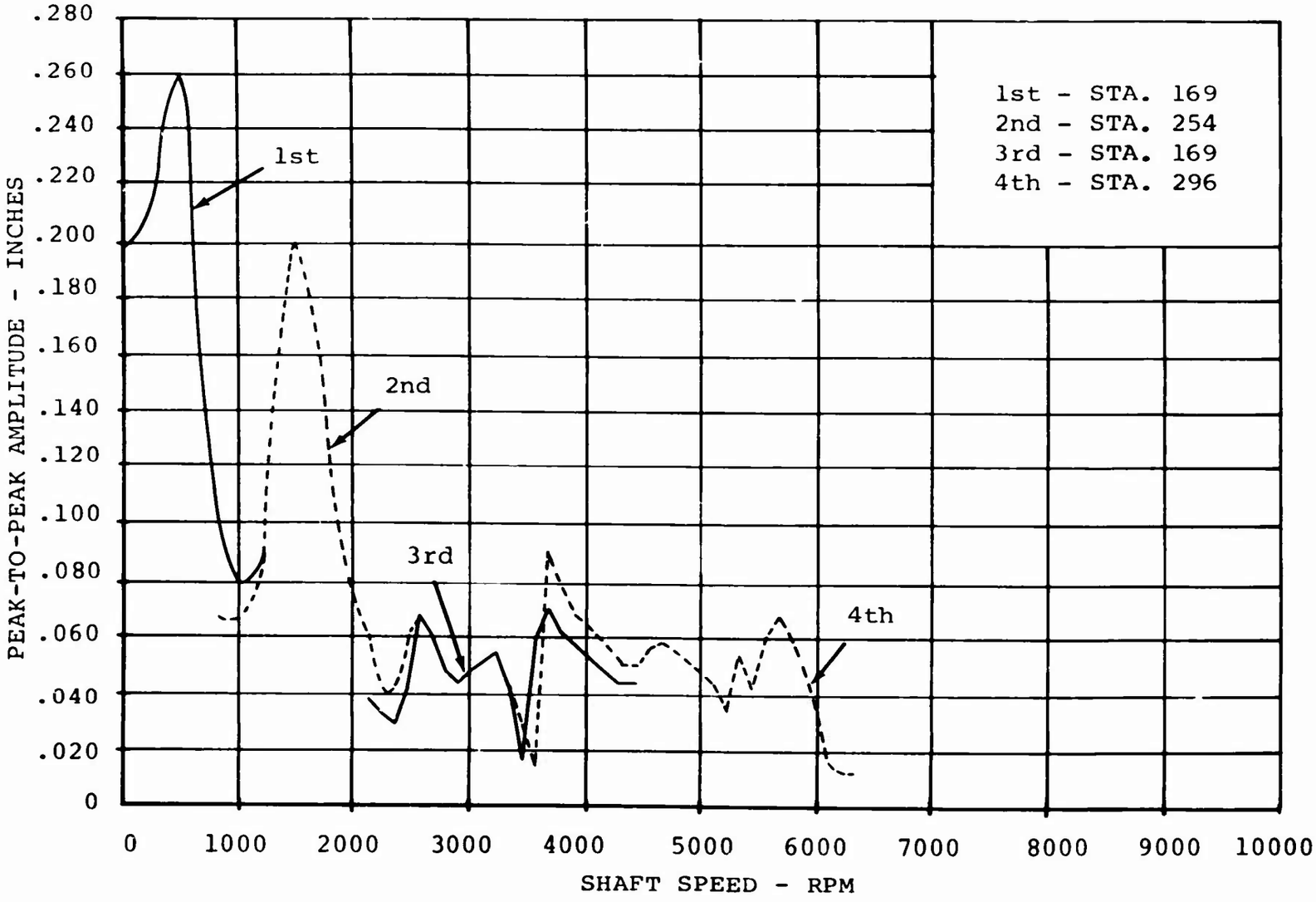

FIGURE 37. MAXIMUM DISPLACEMENT - ZERO TORQUE.

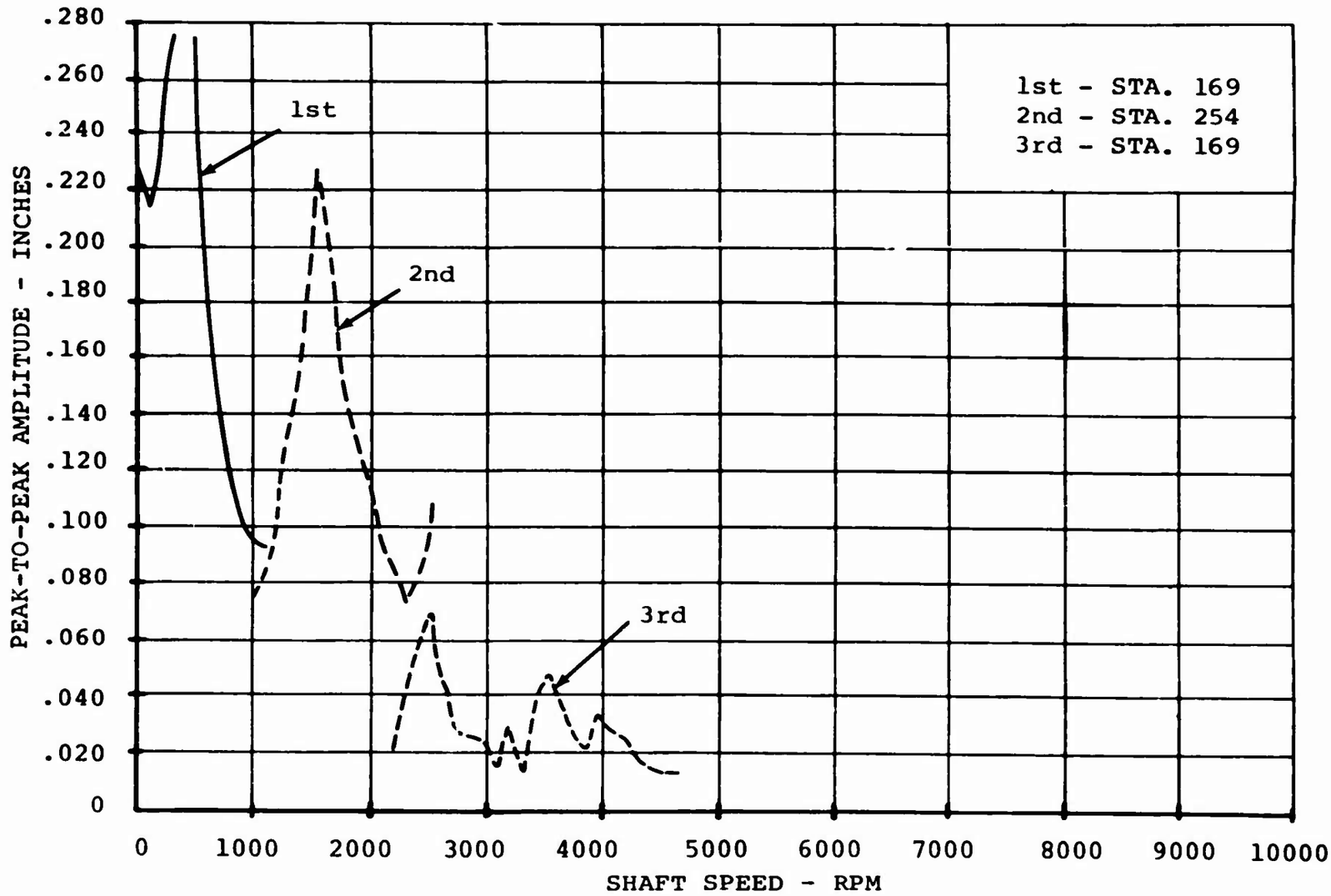

FIGURE 38. MAXIMUM DISPLACEMENT - 5000 IN-LB TORQUE.

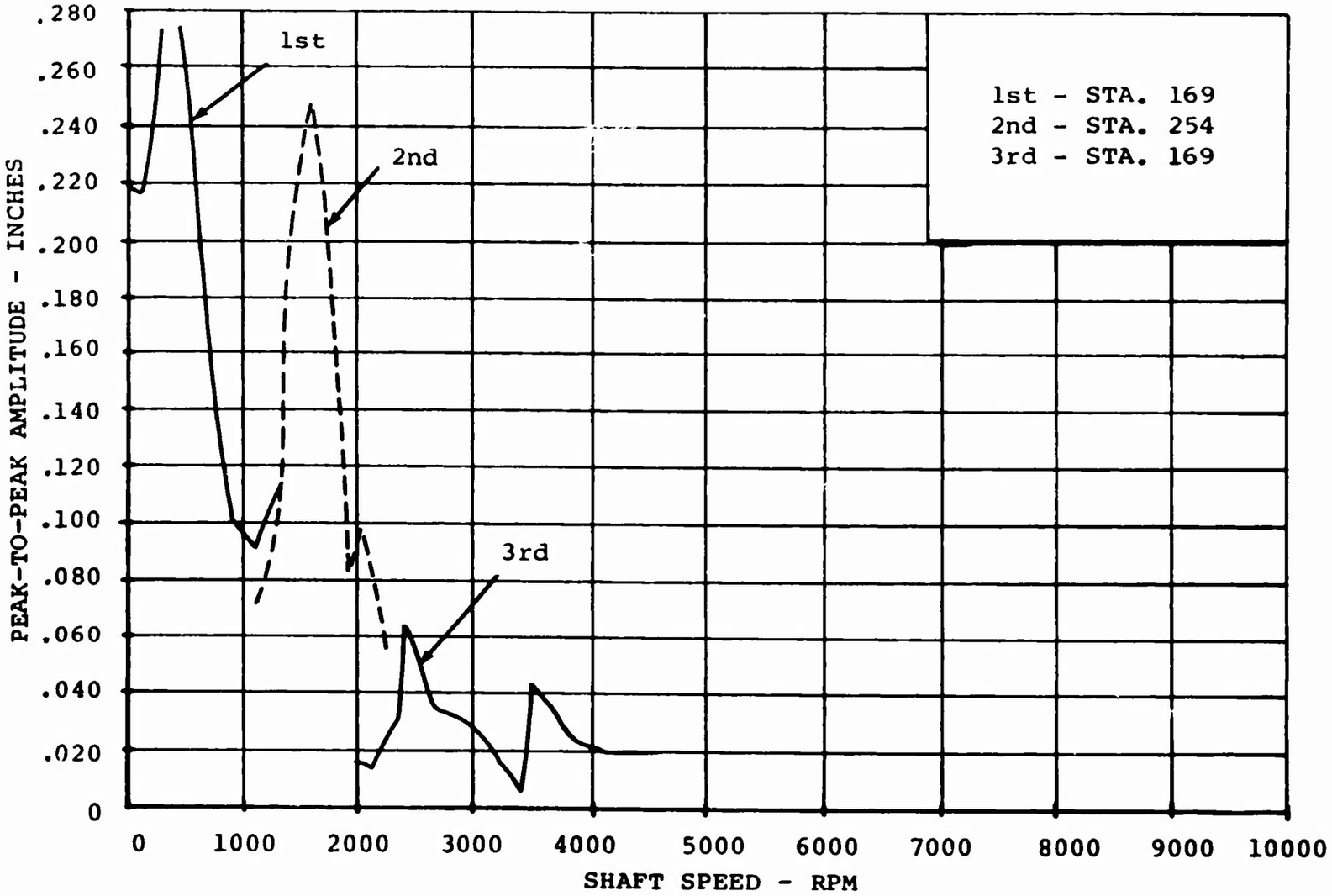

FIGURE 39. MAXIMUM DISPLACEMENT - 10,000 IN-LB TORQUE.

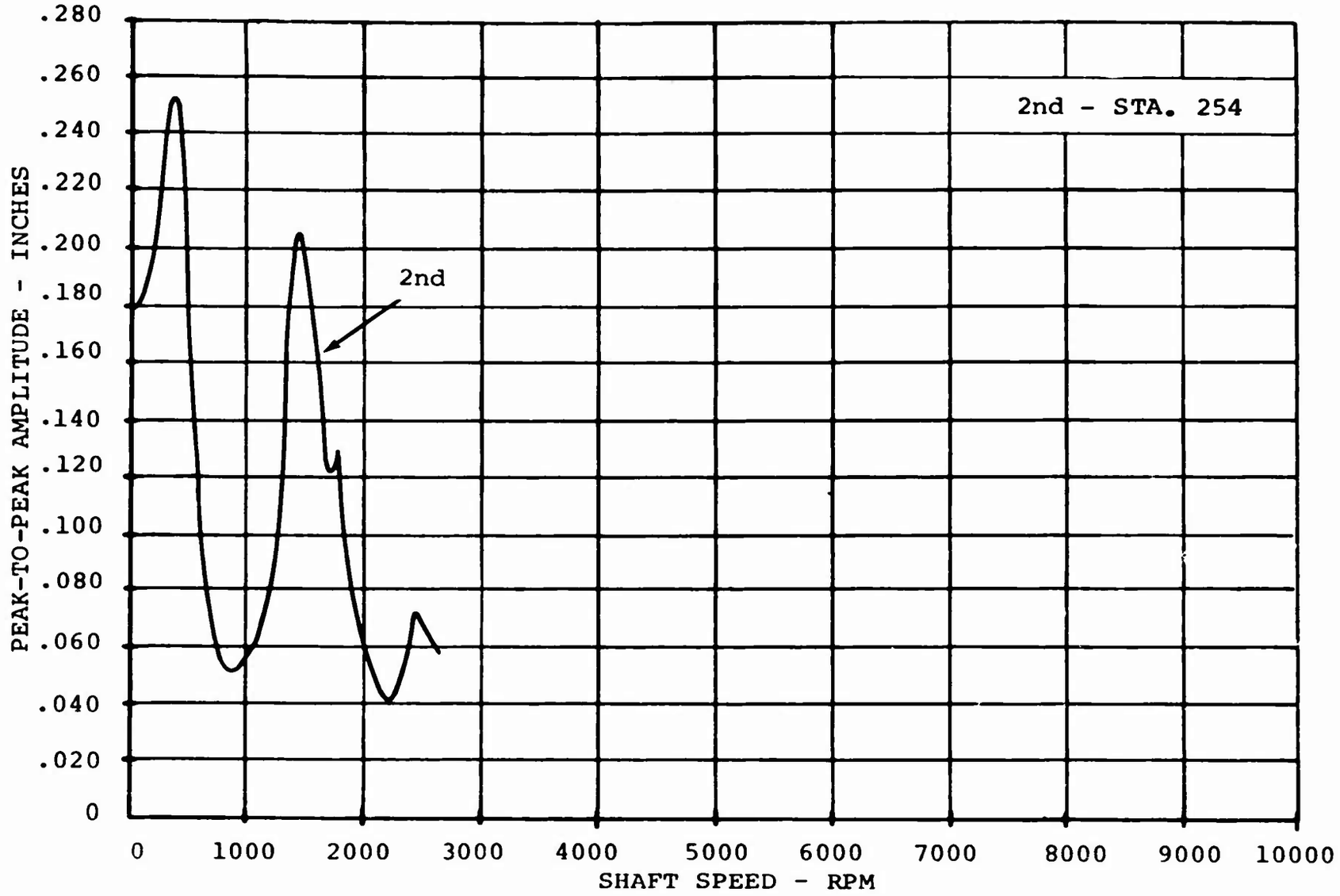

FIGURE 40. MAXIMUM DISPLACEMENT - 15,000 IN-LB TORQUE.

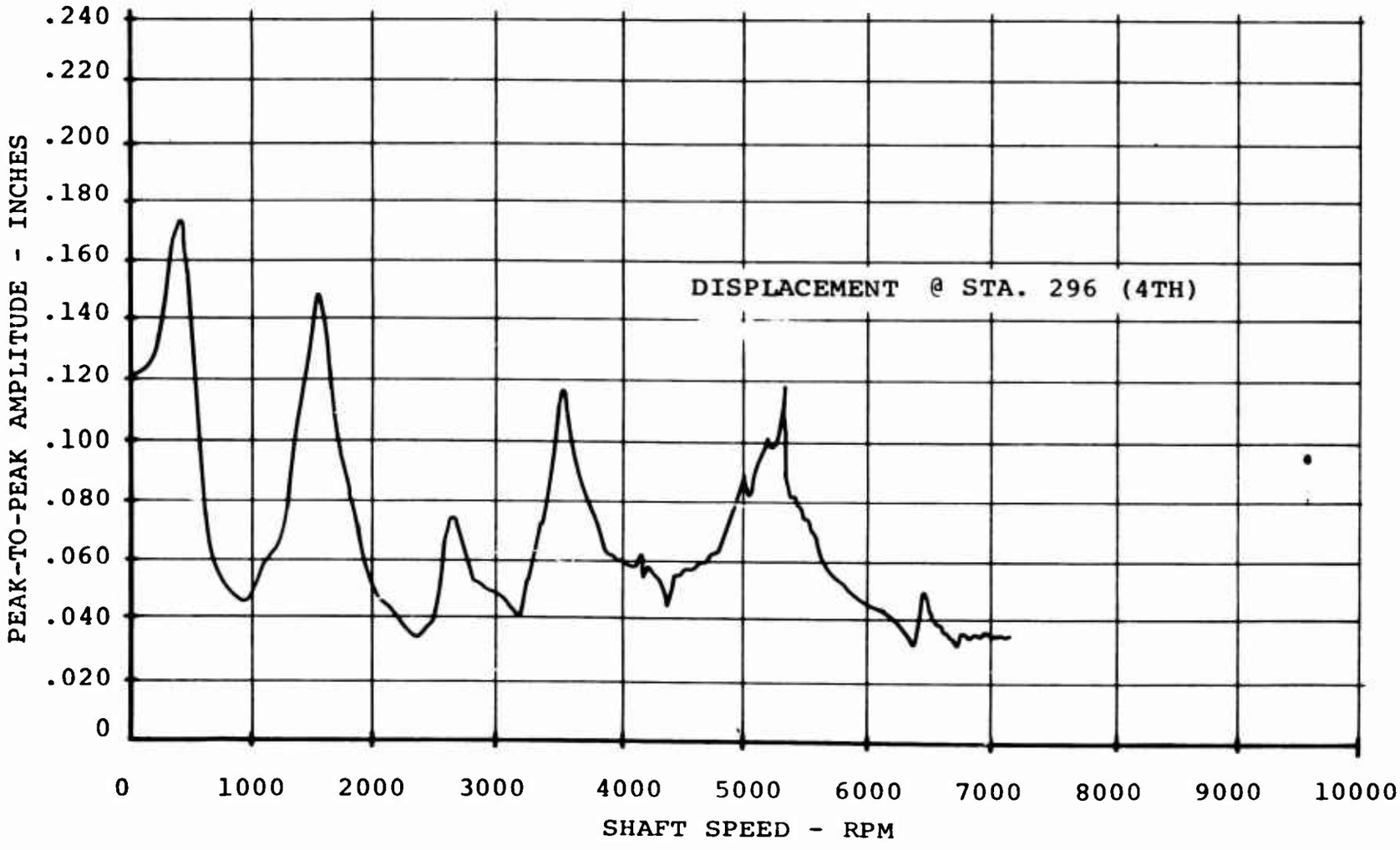

FIGURE 41. ZERO TORQUE.

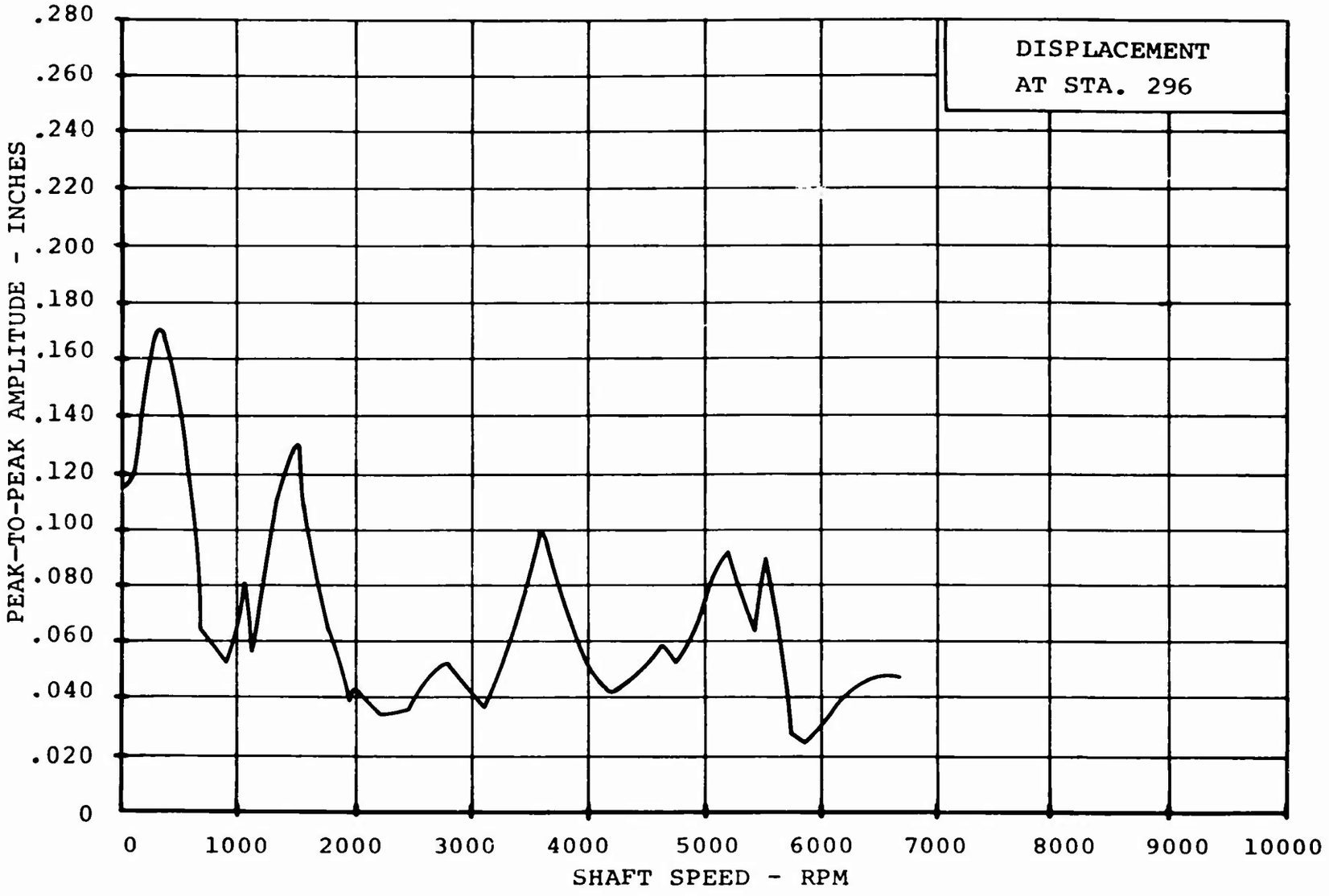

FIGURE 42. 10,000 IN-LB TORQUE.

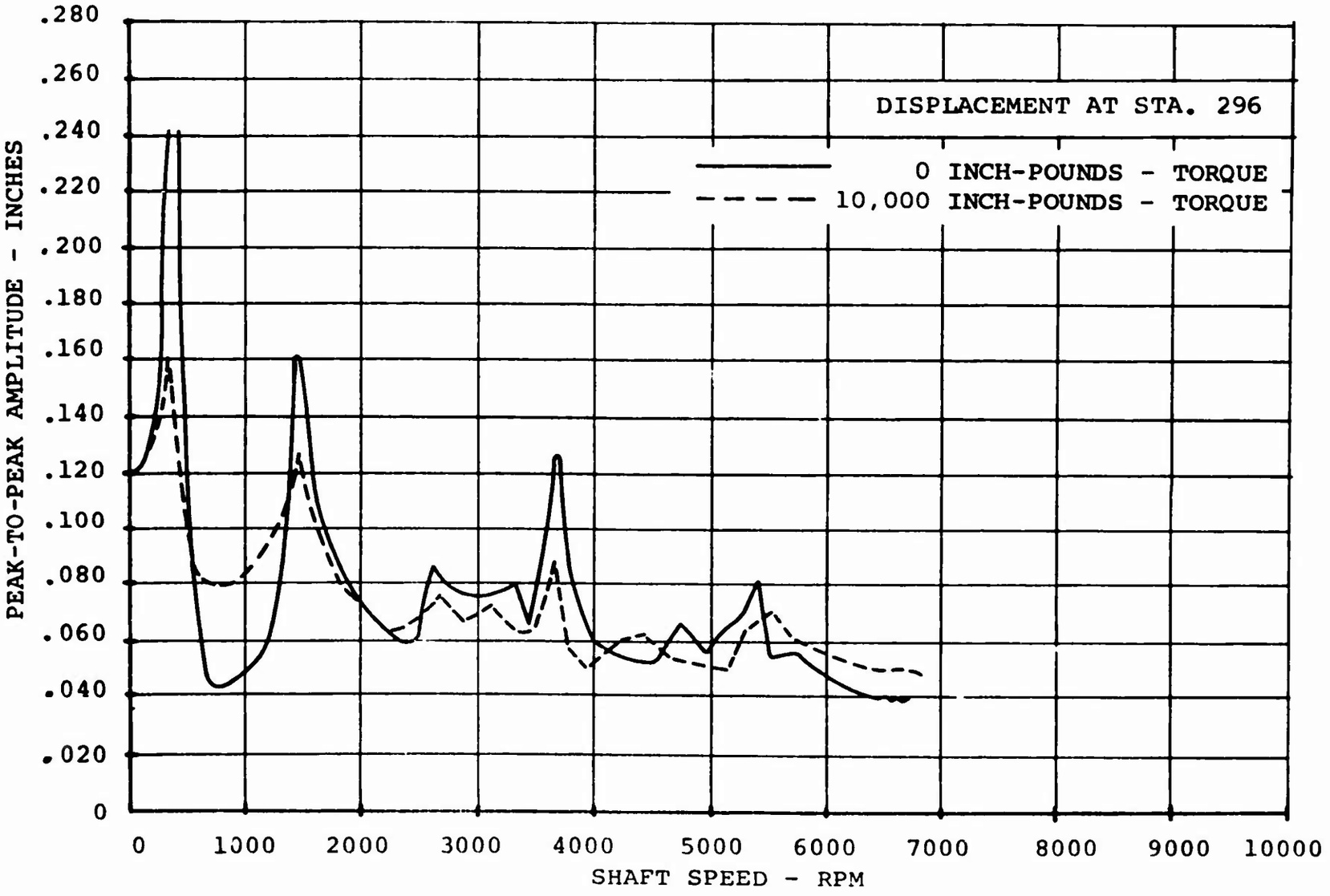

FIGURE 43. MISALIGNMENT.

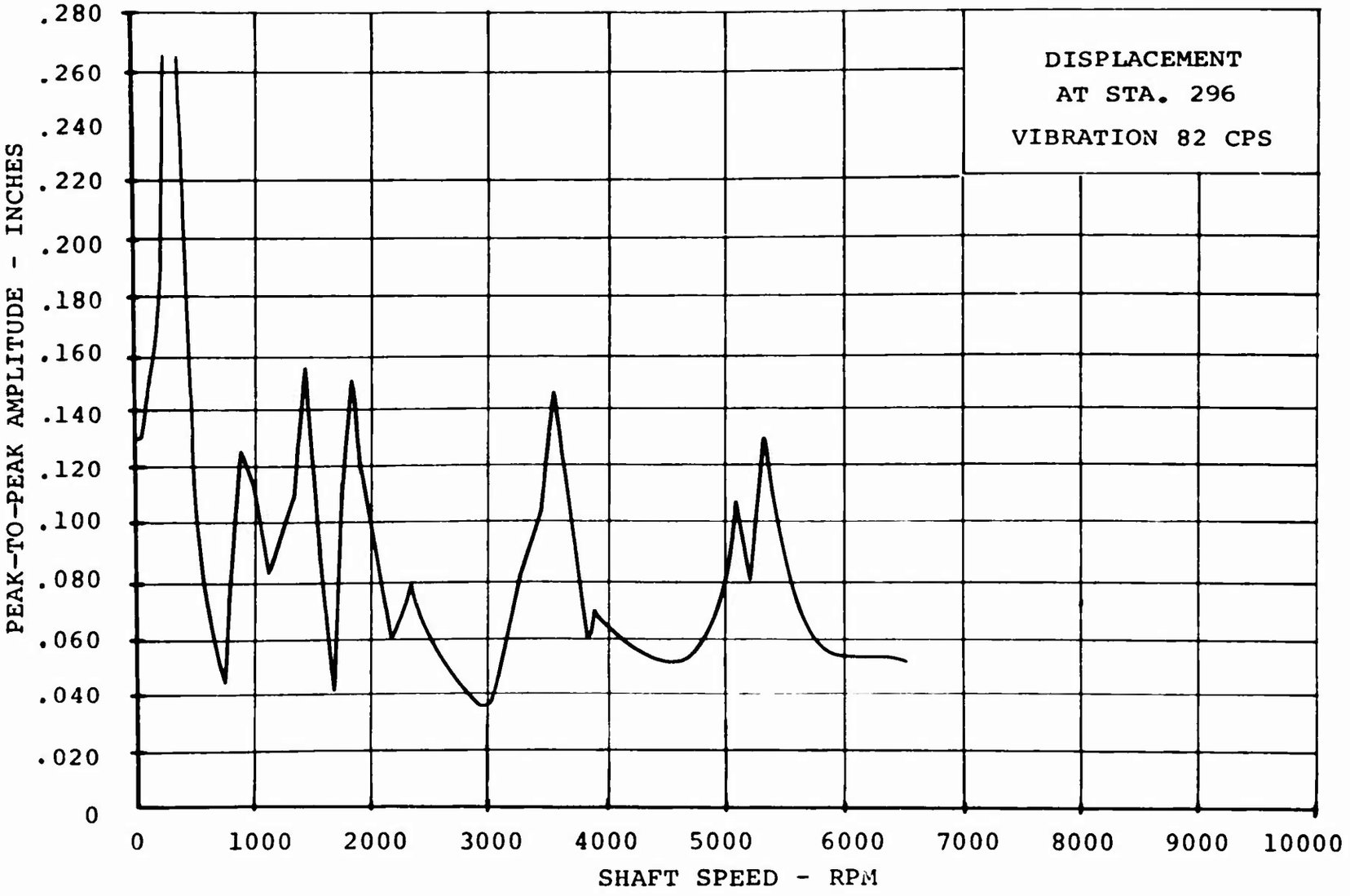

FIGURE 44. FORCED EXCITATION - NO TORQUE.

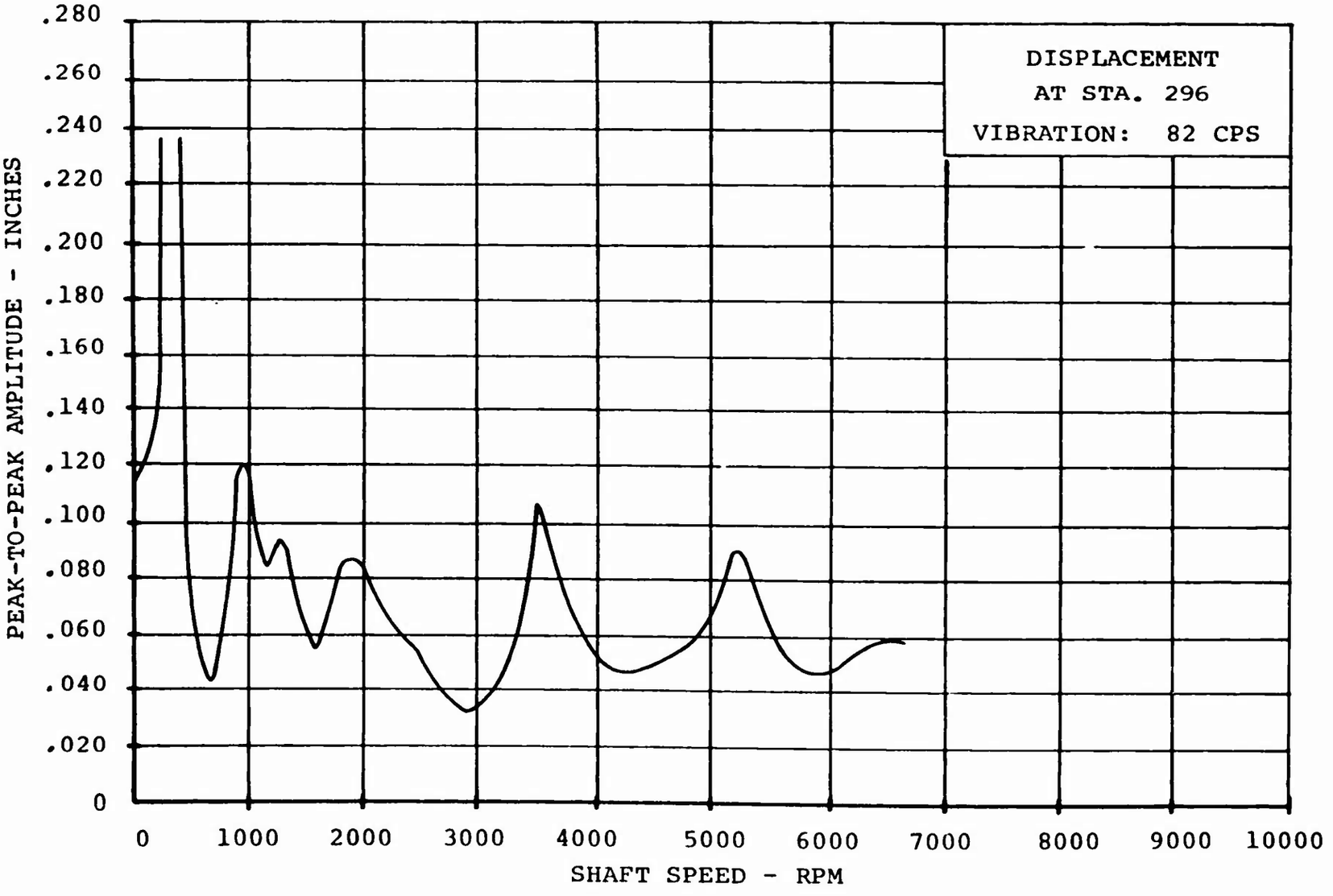

FIGURE 45. FORCED EXCITATION - 10,000 IN-LB TORQUE.

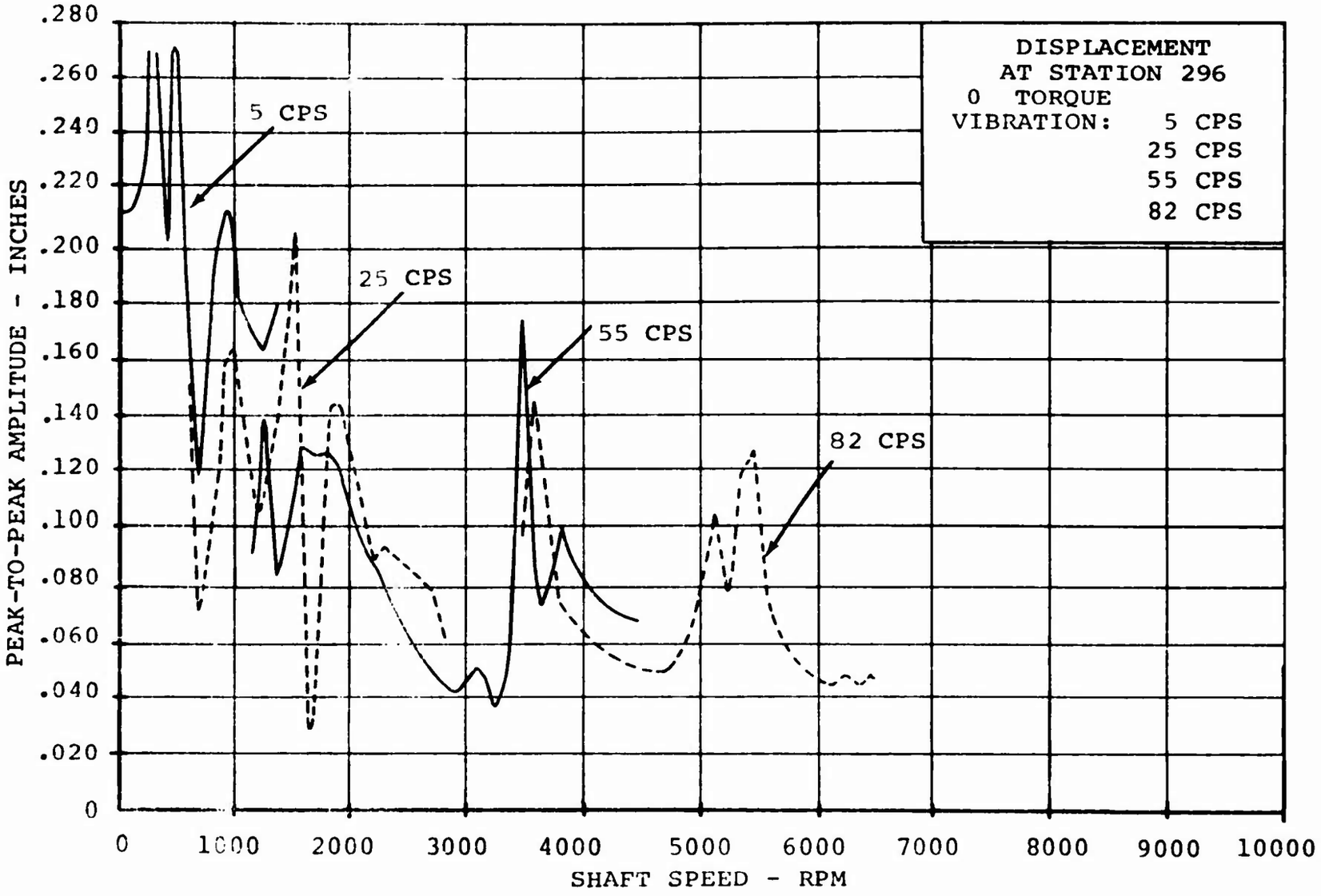

FIGURE 44. FORCED EXCITATION - VARIOUS FREQUENCIES.

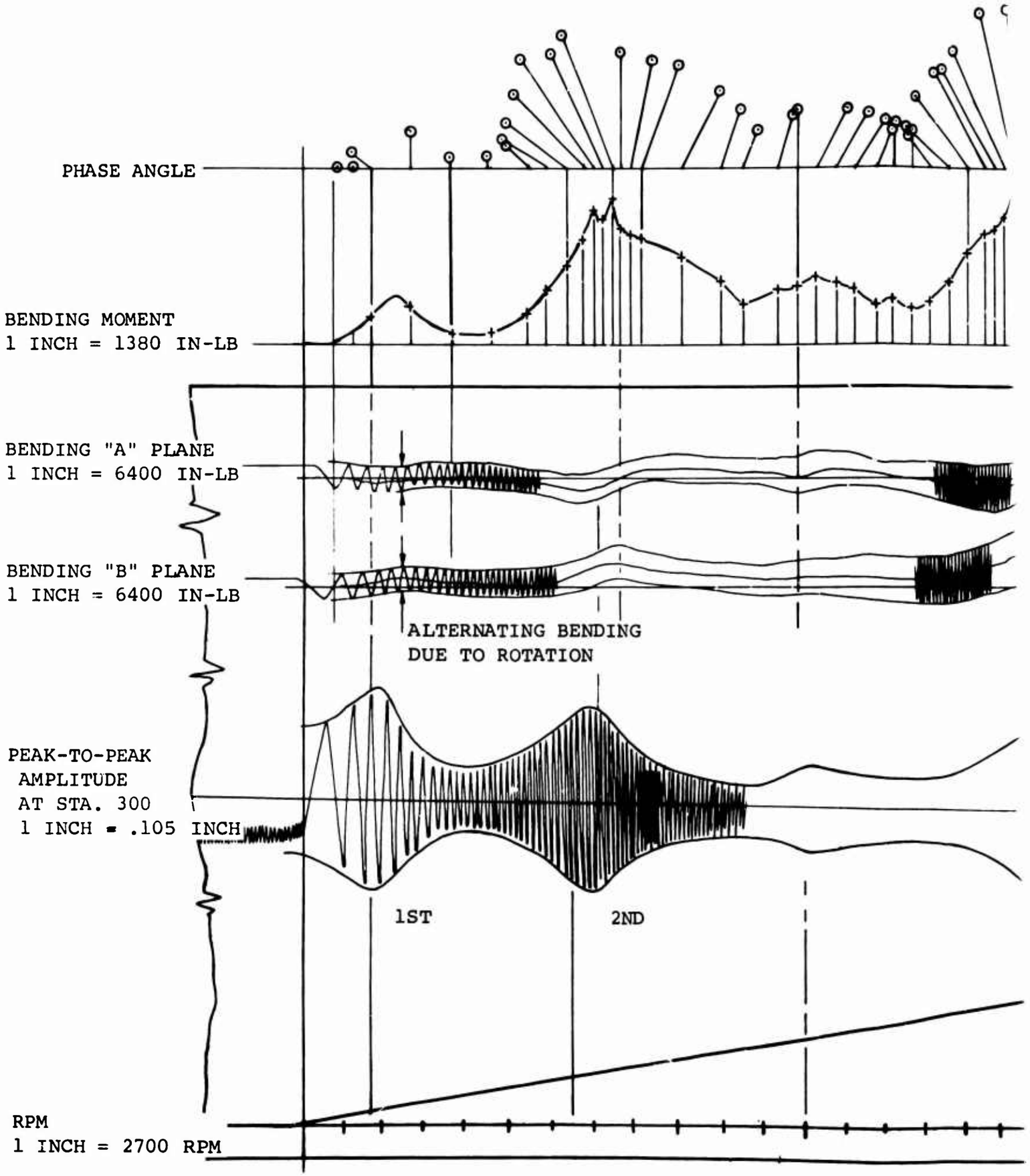

FIGURE 47. OSCILLOGR

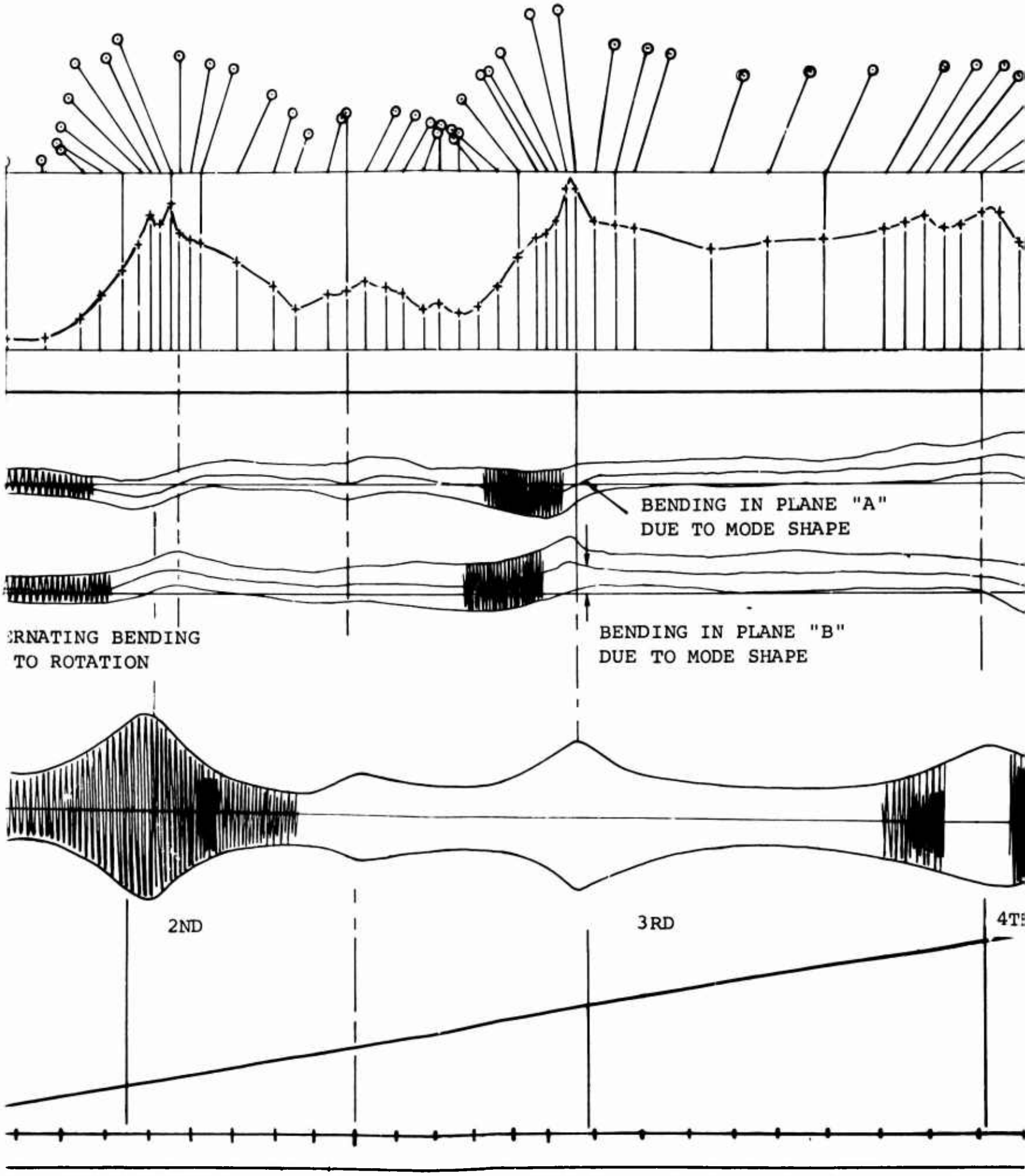

FIGURE 47. OSCILLOGRAPH RECORD.

B

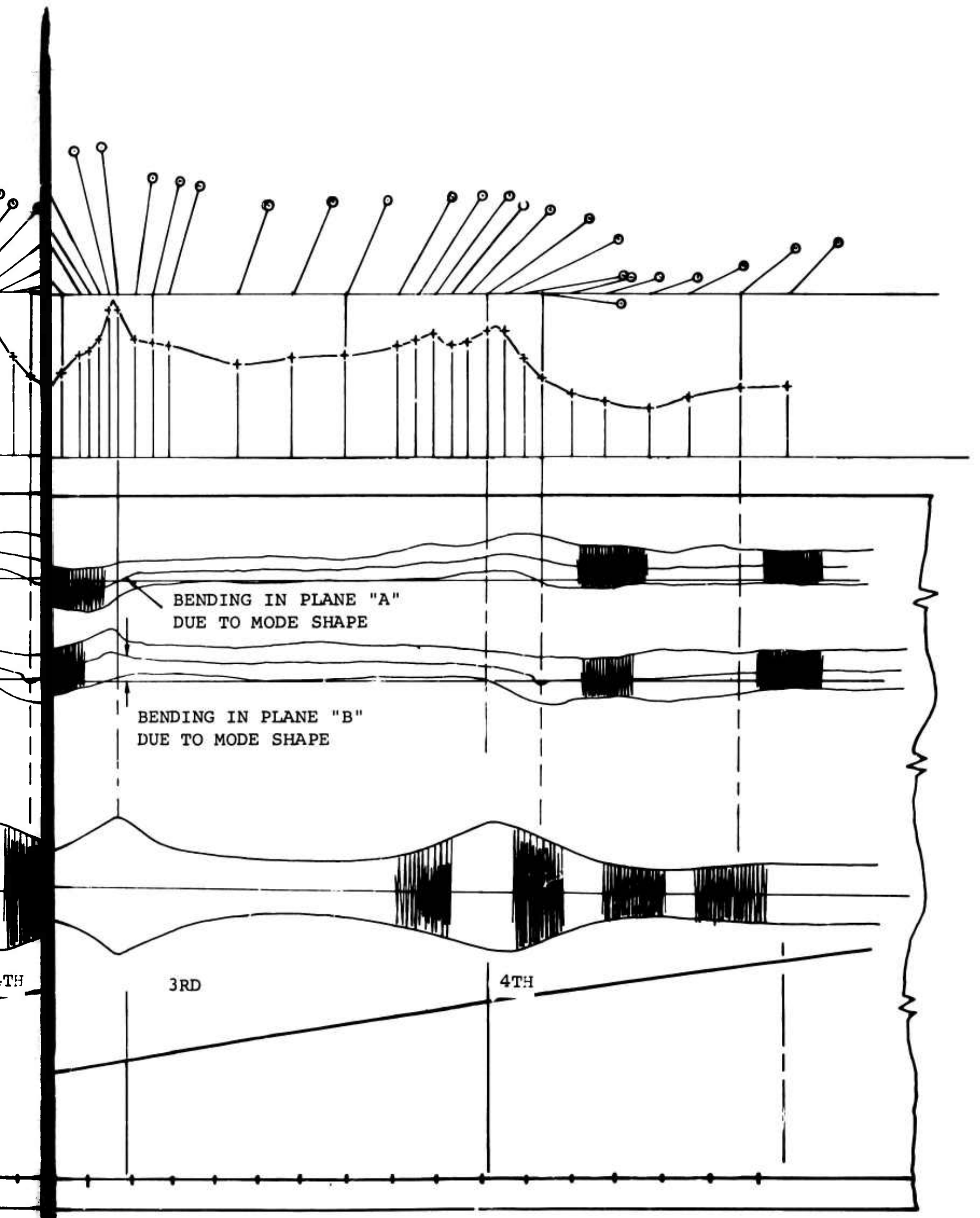

LLOGRAPH RECORD.

C

appears at 3400 revolutions per minute. A point of interest is the shift of the center of the trace with increased speed. The interpretation of this is that the normal sag of the shaft is decreasing with speed of rotation. The shaft has a tendency to straighten with speed. It is believed that this phenomenon is a reaction of the hysteresis of the shaft material due to the stresses caused by the sag with rotation. The shaft rise at the center of the span has been calculated to be .0795 inch at 6400 revolutions per minute.

The top two traces on the tape represent bending in two planes from strain gages on the shaft. The peak of one trace coincides with the center, or zero position, of the adjacent trace as the gages are 90 degrees apart on the shaft. This can be seen more easily at the lower speeds. The alternating bending in each trace is a result of gravity force on the rotating shaft. The magnitude of bending is dependent on the shaft station from which the measurements were taken. Calculated gravity bending stresses agree with the calibrated shaft strain outputs.

The center of each trace is taken as the base; deviation of the center from the base, with a change in speed, is an indication of the whirl mode bending in the plane being investigated. When the bending in both planes is added vectorially, the result is shown in the bending-moment curve plotted just above the tape data.

The shift of the center of each strain gage trace was related to an arbitrary X-Y coordinate system. This provides a description of the angle of the whirl mode bending plane at any speed and is shown in the final line at the top of the chart. Note the rapid angular change of this plane as the critical speeds are passed, and also note that the plane is at basically the same angle for the first three criticals. These dynamic data indicate the location of the unbalance in the shaft. Plotted as shown, the data also indicate the magnitude of unbalance.

The data obtained from the strain gages illustrate the basis for the shaft balance theory and the use of angular displacement, or phase angle, as an indicator for proper placement of shaft balance weight.

EXPERIMENTAL BALANCING METHOD

The maximum speed that could be attained during damper parameter tests was curtailed by sharp increases in amplitude approaching the fifth critical speed. To attain the desired speed range, a balancing method was devised and successfully applied. The result of initial balancing is shown in Figure 48. A significant reduction in amplitudes in the higher range was shown. The weights applied are shown in Table VII.

TABLE VII
PERMANENT BALANCE WEIGHTS
(Effective Radius = 2.375 Inches)

Weight (grams)	Station (inches)	Phase Angle (degrees)
16	120	180
16	140	30
16	193	340
16	194	270
16	224	210
16	266	180

Following completion of the Environmental Conditions tests, a refinement of the experimental method was successfully attempted. A trial balance at the first critical speed required 550 grams at 310 degrees at Station 200 to reduce the amplitude from 0.400 to 0.040. The phase of this weight indicates that the first mode unbalance is caused by the shaft crookedness and not by mass unbalance. The second mode was balanced independently by the addition of 80 grams at 130 degrees at the antinode, Station 120.

Table VIII shows dynamic data from the shaft with the balance weights shown in Table VII installed. It shows phase angles at various speeds and at a number of shaft stations. The stations agree with the antinodes at the respective critical speeds. Figures 49 through 52 show amplitude versus speed for a number of stations.

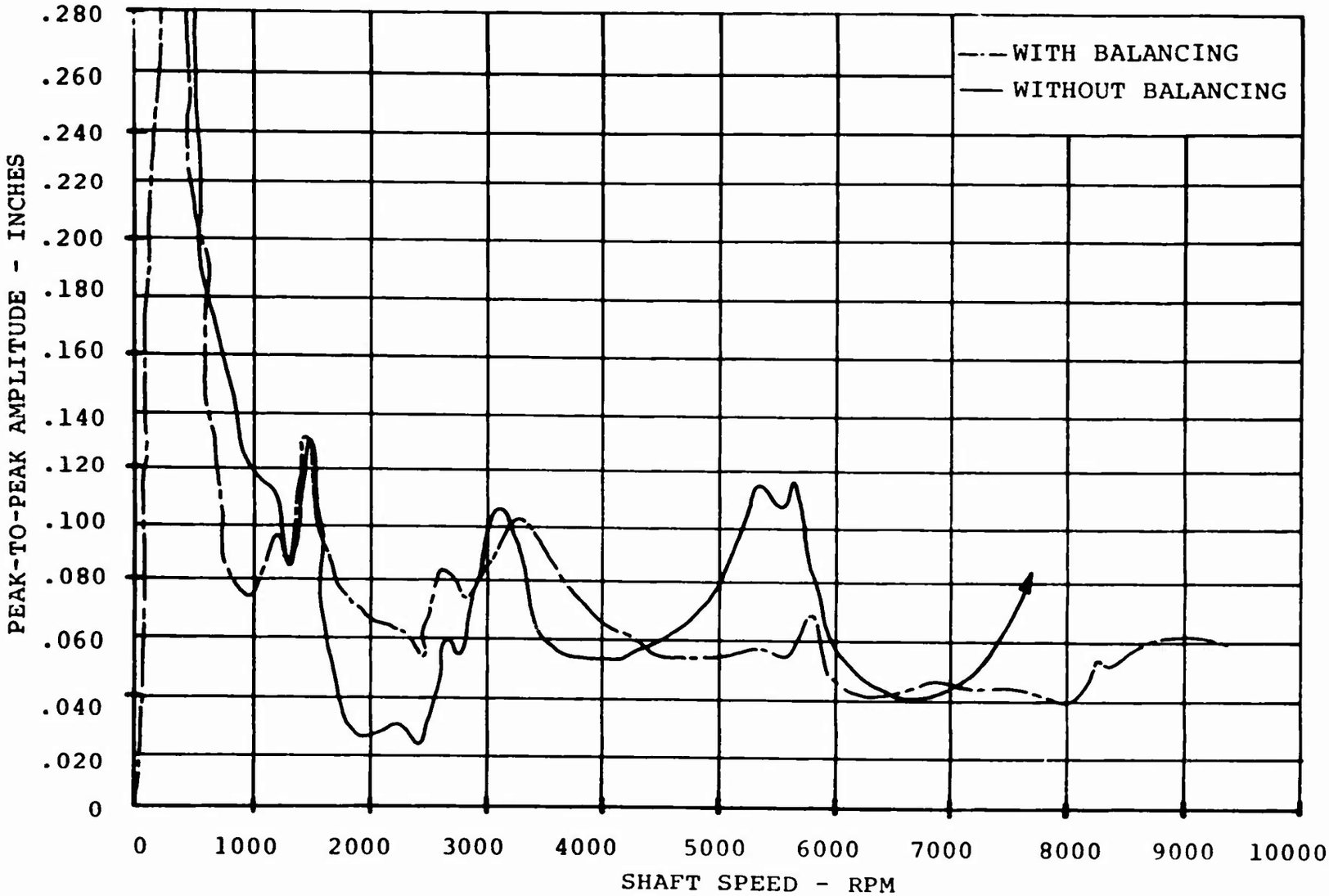

FIGURE 48. EFFECT OF BALANCE.

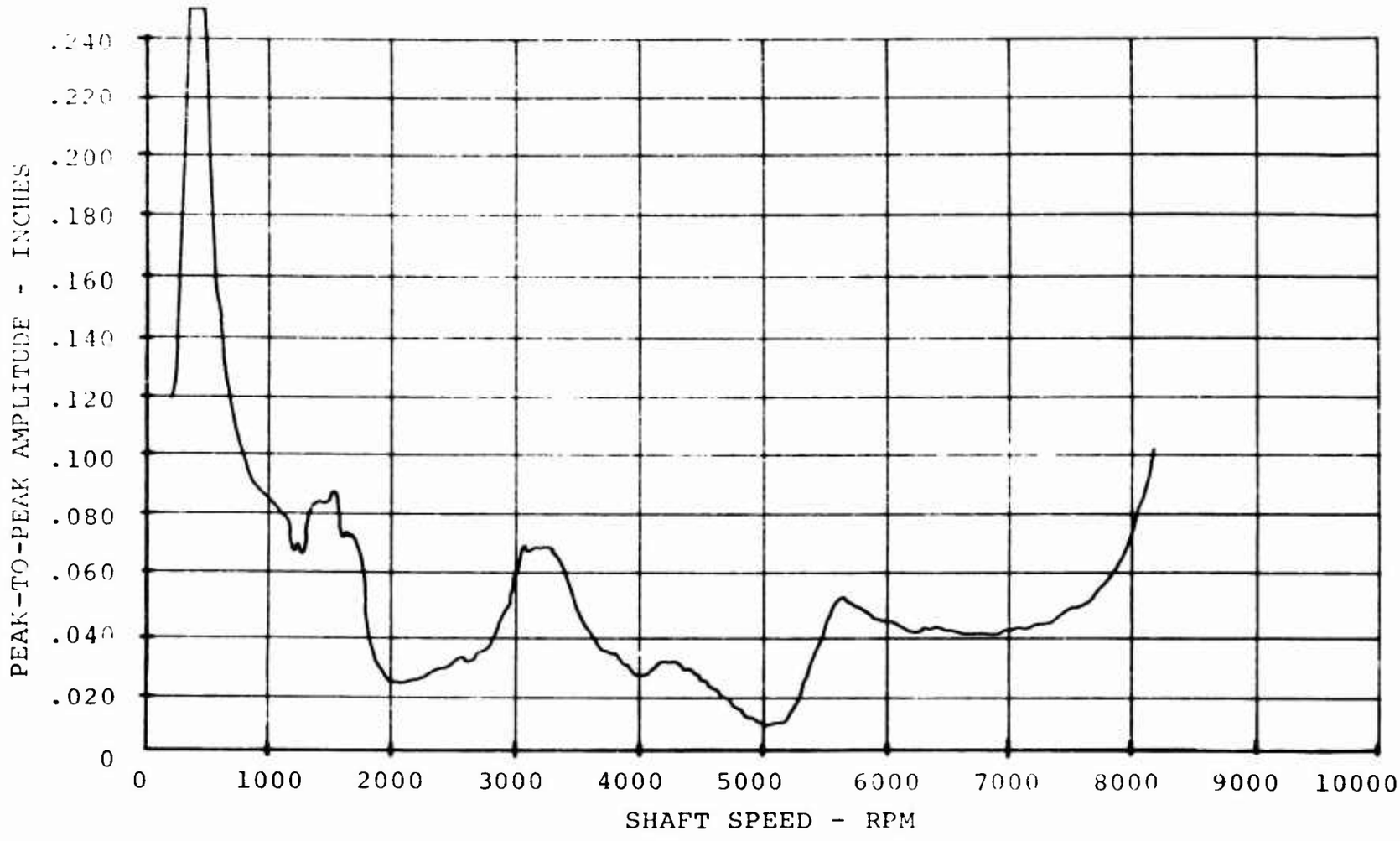

FIGURE 49. DISPLACEMENT - STATION 70 - EXPERIMENTAL BALANCING METHOD - TABLE VII WEIGHTS.

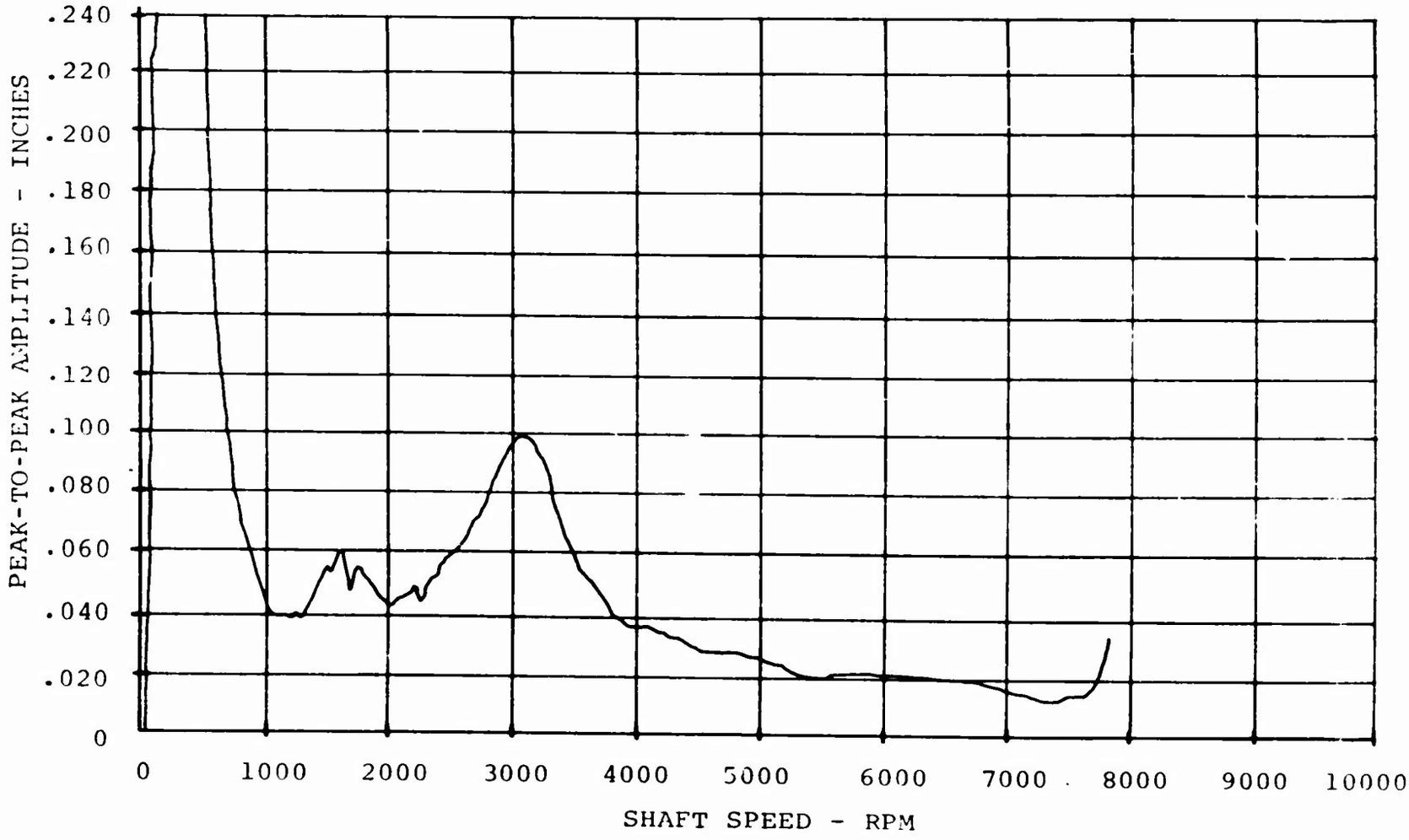

FIGURE 50. DISPLACEMENT - STATION 195 - EXPERIMENTAL BALANCING METHOD - TABLE VII WEIGHTS.

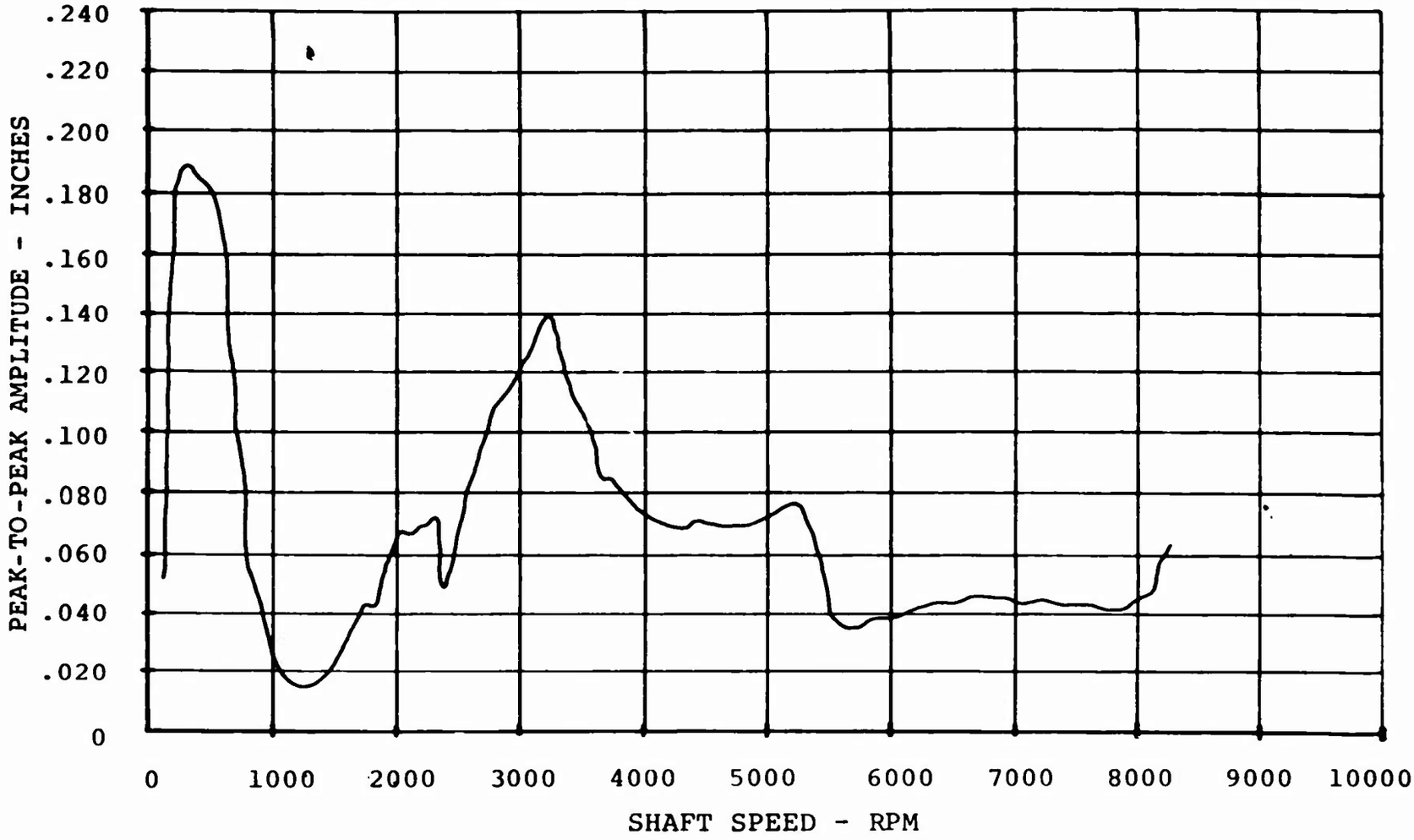

FIGURE 51. DISPLACEMENT - STATION 212 - EXPERIMENTAL BALANCING METHOD - TABLE VII WEIGHTS.

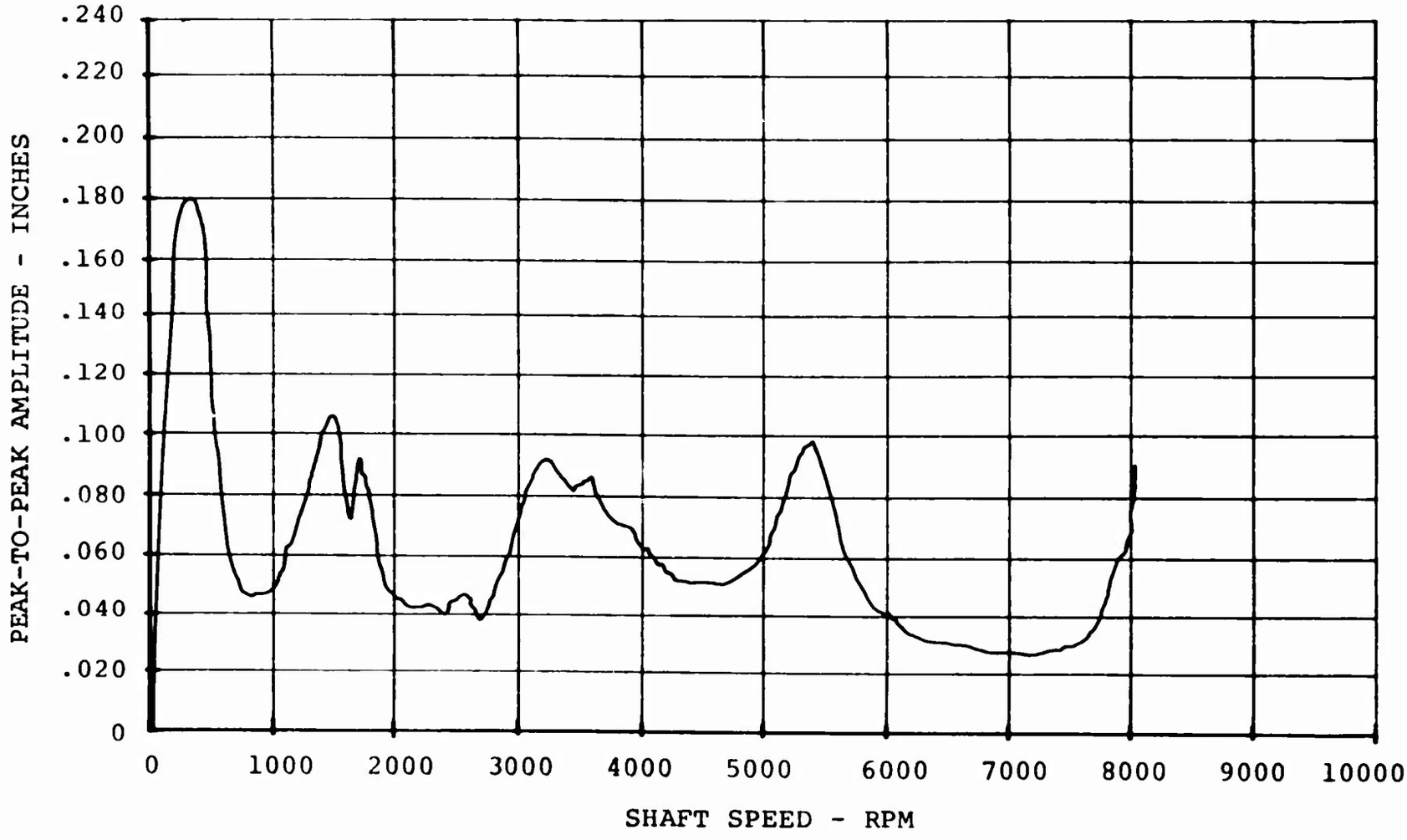

FIGURE 52. DISPLACEMENT - STATION 300 - EXPERIMENTAL BALANCING METHOD - TABLE VII WEIGHTS.

The experimental balancing procedure was applied to the shaft with deflections as reported in Table VIII and with small balance weights added for controlling the fifth critical speed only. These small weights did not affect the other critical speeds. The results of this application can be seen in Figure 53, which shows amplitude measurements taken at several shaft stations.

After the above successful experimental balancing of the shaft, all the weights, including the permanent balance weights, were removed. The shaft now presented a new balancing problem. Figures 54 and 55 show the unbalance shaft deflection at Stations 212 and 300, respectively. Table IX gives the phase angles for the distortion at Stations 212 and 300.

TABLE VIII
PHASE ANGLE LOCATING SHAFT DISTORTION PLANE

Shaft Speed (rpm)	Shaft Station (inches)	Phase Angle (degrees)
300	200	155
1380	120	37
	260	242
3260	80	306
	210	90
	280	316
5570	80	232
	150	25
	220	160
	290	20
8000	70	335
	130	138
	180	--
	230	90
	300	340

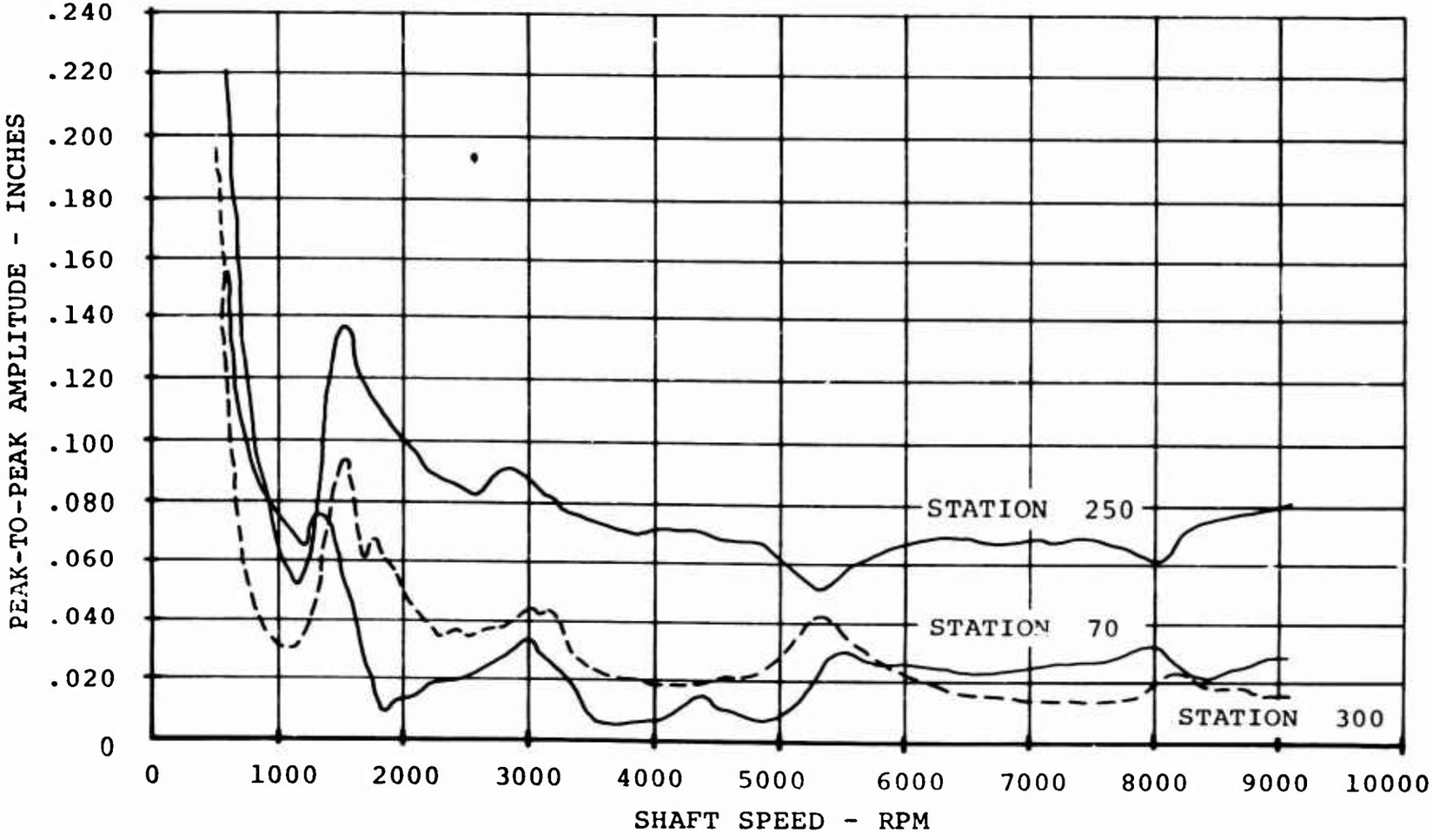

FIGURE 53. DISPLACEMENT - VARIOUS STATIONS - EXPERIMENTAL BALANCING METHOD.

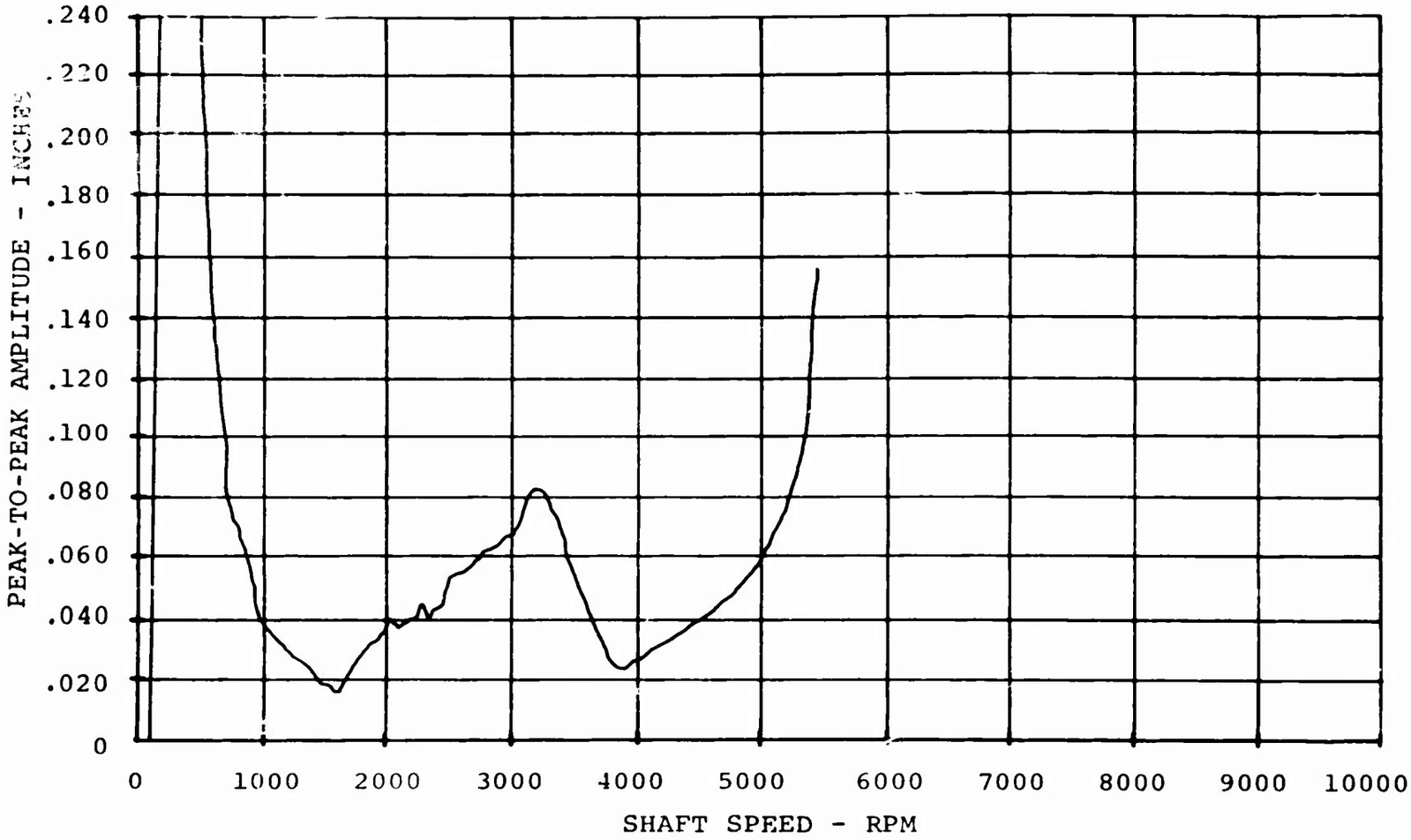

FIGURE 54. DISPLACEMENT - STATION 212 - NO BALANCING.

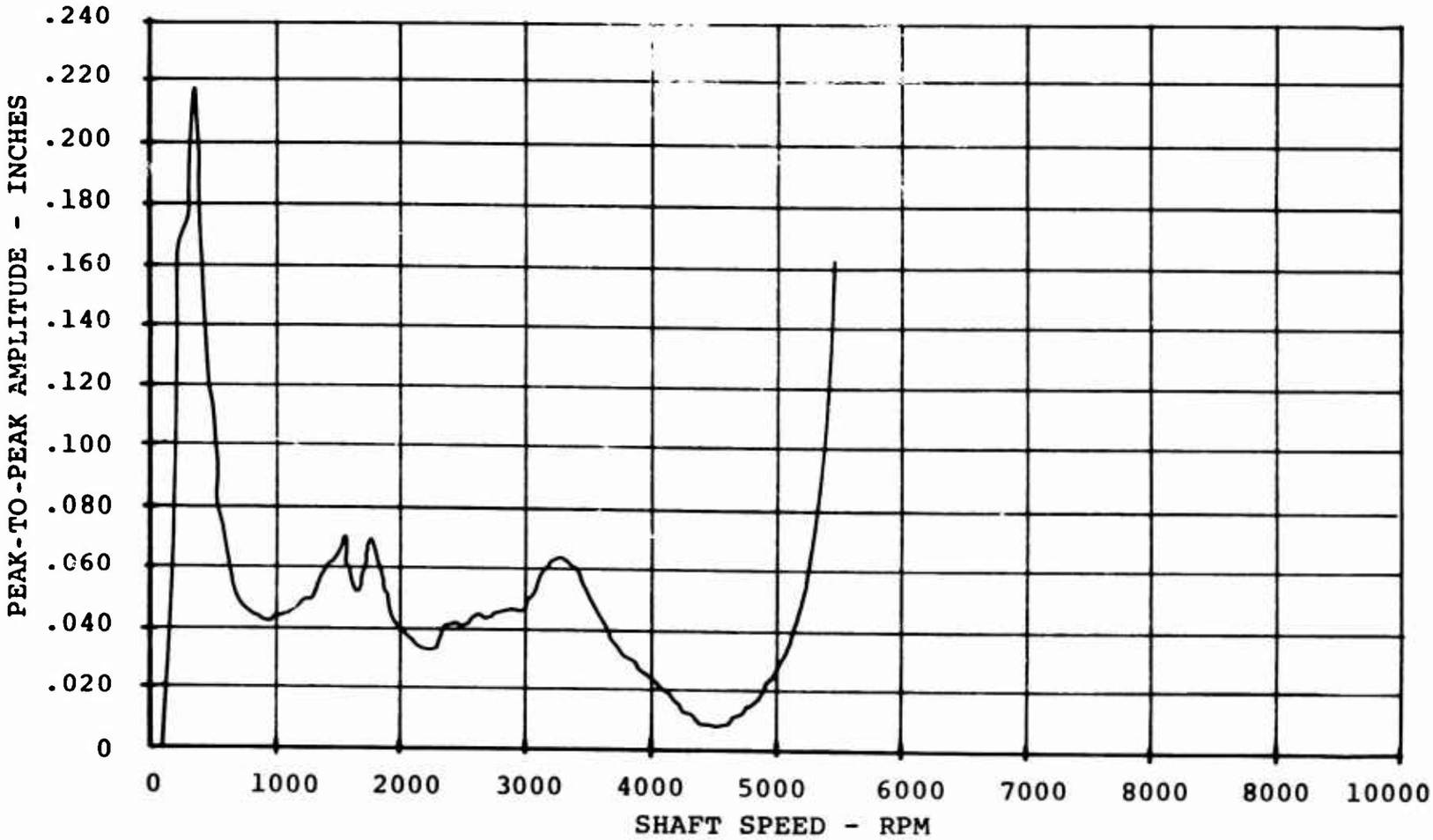

FIGURE 55. DISPLACEMENT - STATION 300 - NO BALANCING.

TABLE IX

PHASE ANGLE OF DISTORTION MEASURED AT STATIONS 212 AND 300 FOR UNBALANCED SHAFT

Speed (rpm)	Phase Angle at Station 212 (degrees)	Phase Angle at Station 300 (degrees)
300	--	181
1524	--	278
3200	127	338
5000	92	245
5300	85	253

Figure 56 shows the effect of adding one weight for the third critical speed (Run 171). A summary of the step-by-step procedure is given in Table X; all the required data and numbers of the runs are listed.

TABLE X

RUN SCHEDULE FOR EVALUATION OF EXPERIMENTAL BALANCE PROCEDURE

Run No.	Speed (rpm)	e Angle at Station 300 (degrees)	Balance Weight Added Before This Run (grams)
171	5376	260	10/215° - 185"
173	5363	315	32/160° - 222"
174	7100	180	32 gm. moved to 220°
175	7800	180	16 gm./140° - 140" & 222"
176	3200	41	16 gm./140° - 140" & 222"
	5400	35	
	8200	333	
177	3200	54	10/230° - 140" & 222"
	5400	64	
	8200	245	
178	3200	46	16/292° - 185"
	5400	11	
	8200	40	
180	5400	43	16/284° - 140" & 222"
181	--	--	6/300° - 222"

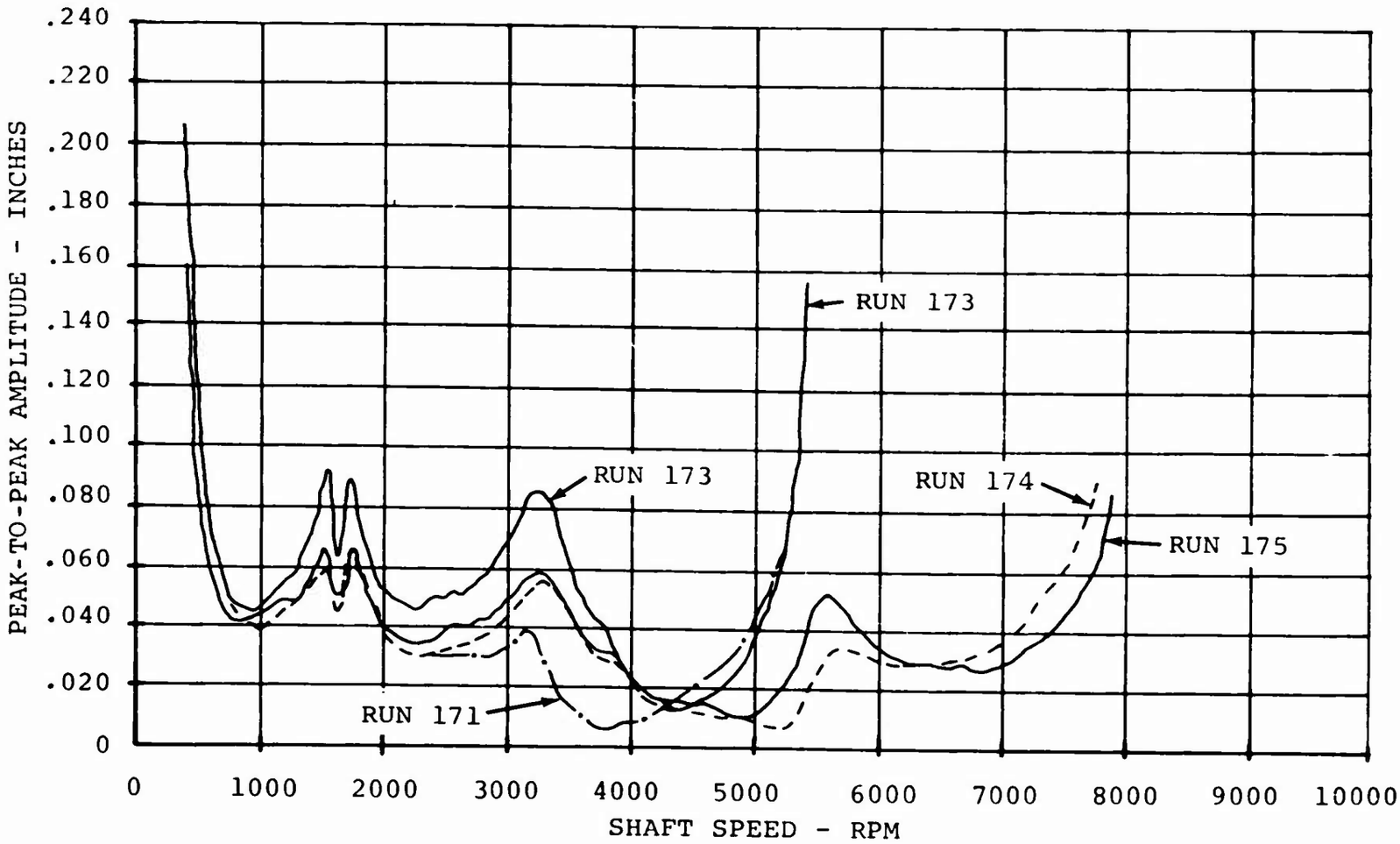

FIGURE 56. DISPLACEMENT - STATION 300 - EXPERIMENTAL BALANCING METHOD.

Figure 57 shows performance amplitudes of the shaft with the refined experimental approach.

Figure 58 shows a comparison of the balanced and unbalanced shaft.

Figures 59 and 60 show shaft response amplitudes when measured at different stations.

Table XI gives the total resultant weights for each station.

TABLE XI
TOTAL EFFECTIVE BALANCE WEIGHTS FROM
EXPERIMENTAL PROCEDURE

Shaft Station	Weight (grams)	Weight Angle (degrees)	Mode
140	27	185	5
185	21	262	3
222	29	230	4
	27	185	5

MODE SHAPES

The results of mode shape investigation are presented in tables and figures included in this report. The shaft was excited with a shaker to determine the mode shapes at resonance of the undamped shaft (Table XII) and the damped shaft (Table XIII). These same data are presented in graph form in Figure 61 for the undamped shaft and in Figure 62 for the damped shaft.

The mode shapes with the shaft rotating and the initial permanent balance weights in place are shown in Figure 63 (same data as in Table VIII).

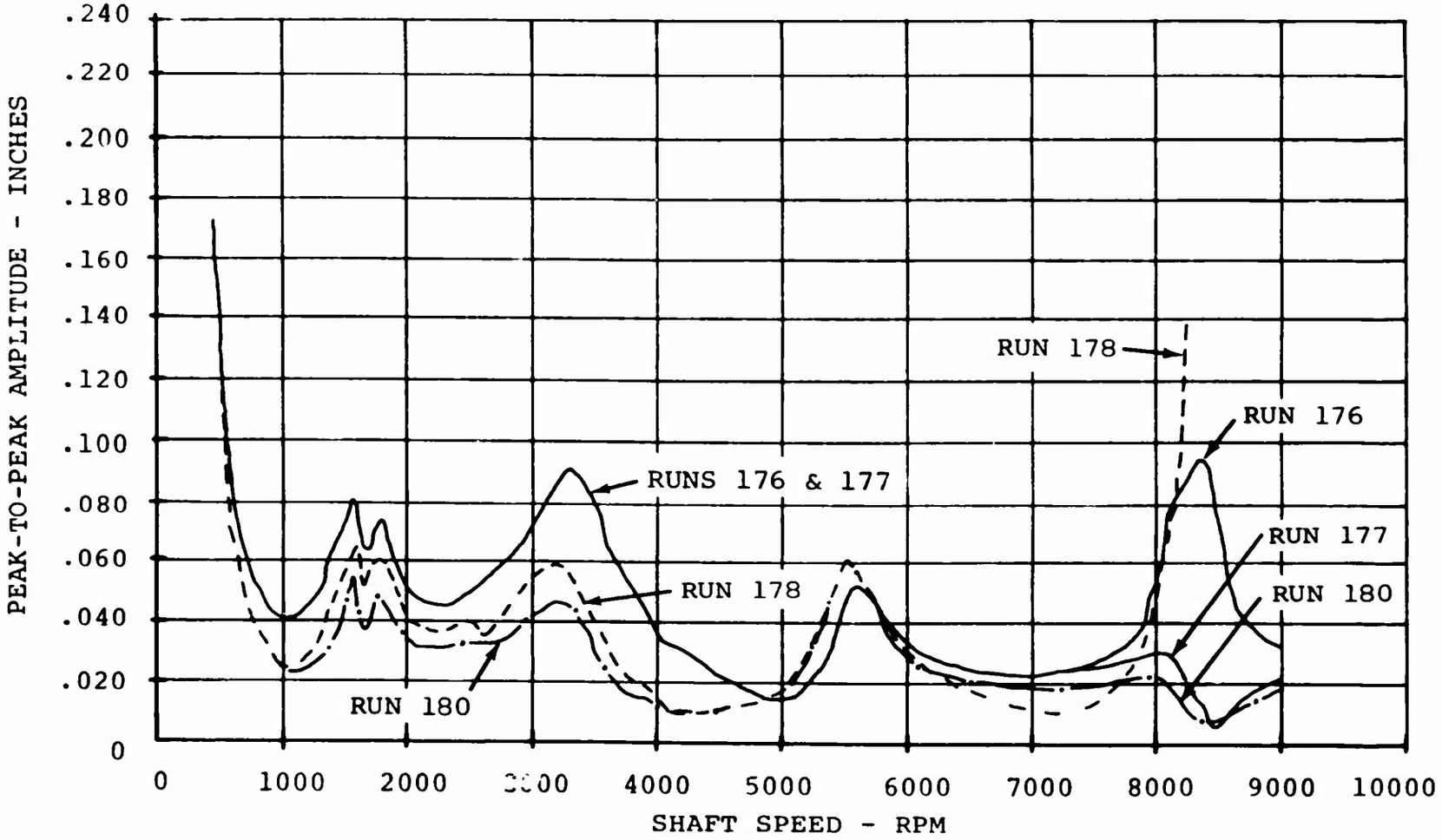

FIGURE 57. DISPLACEMENT - STATION 300 - EXPERIMENTAL BALANCING METHOD.

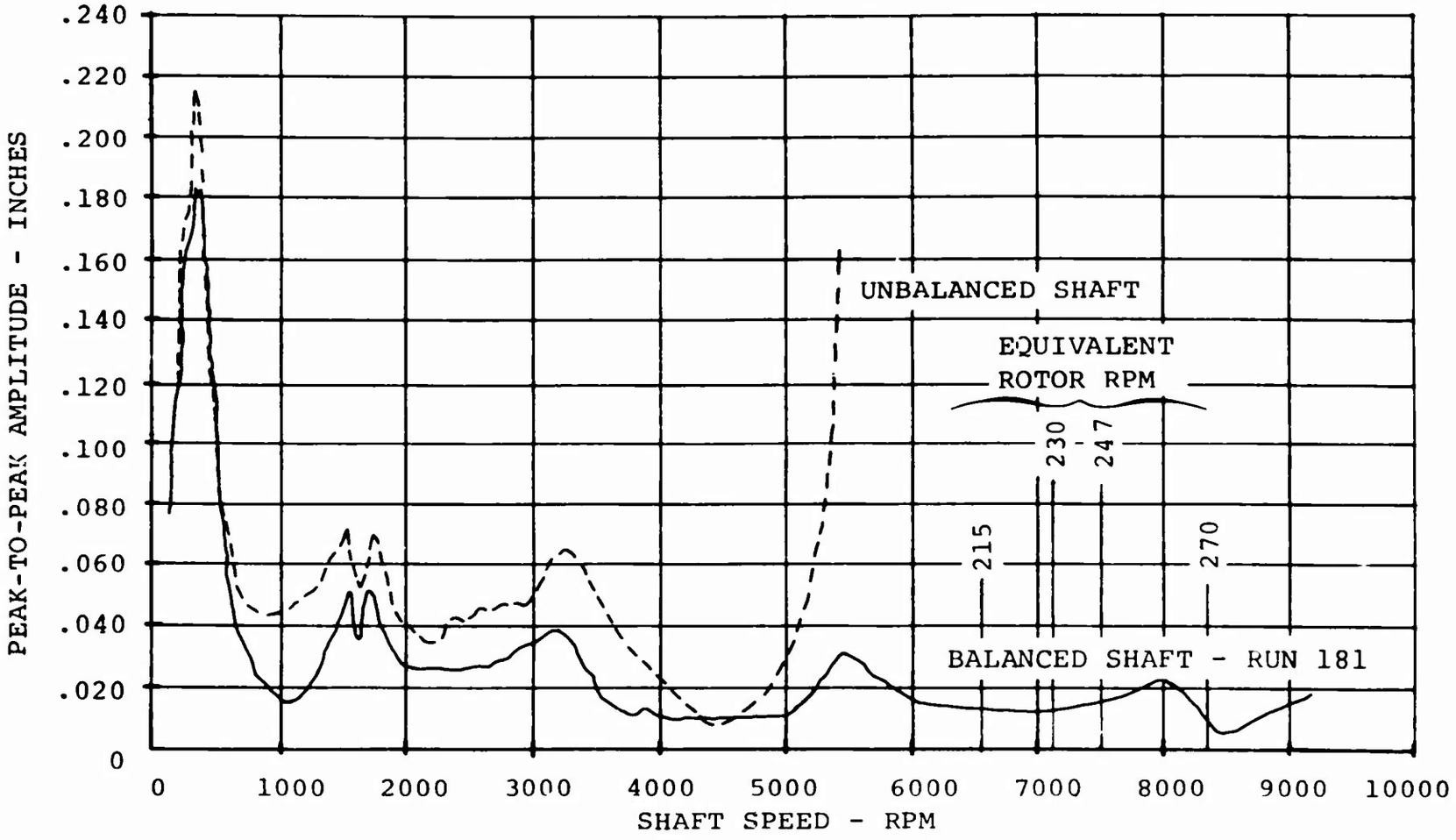

FIGURE 58. COMPARISON OF BALANCING RESULTS - STATION 300.

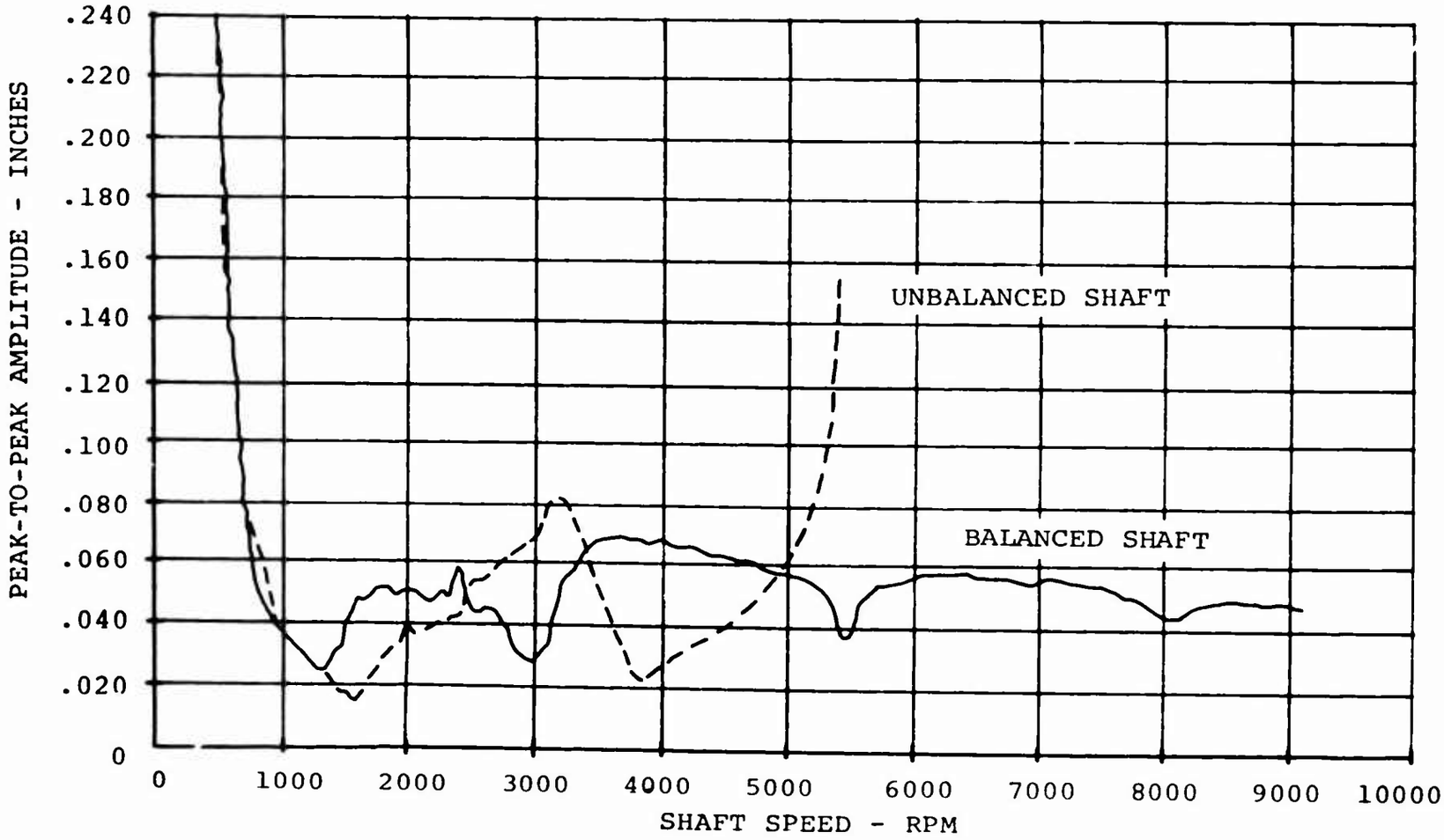

FIGURE 59. COMPARISON OF BALANCING RESULTS - STATION 212.

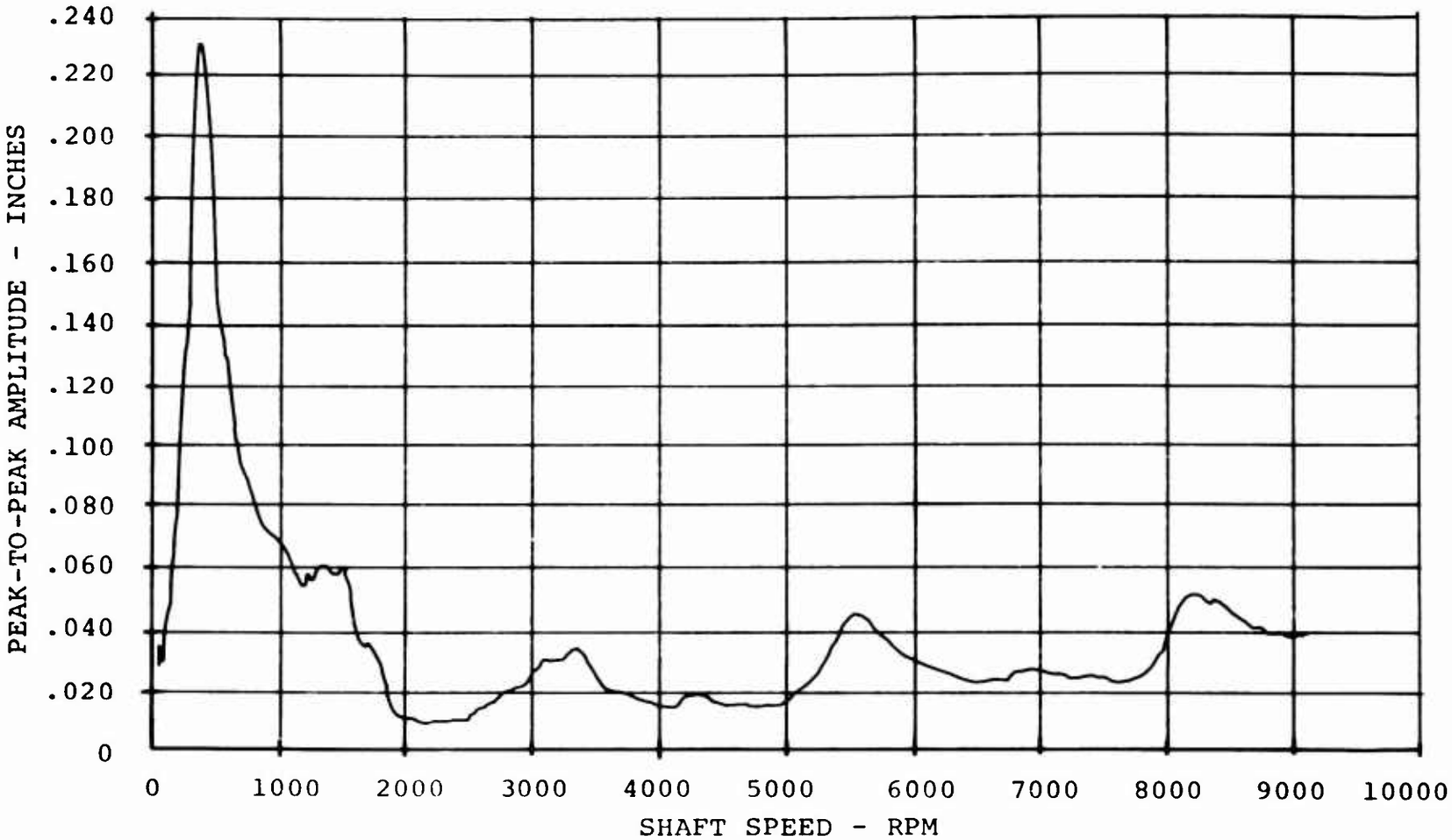

FIGURE 60. DISPLACEMENT - STATION 70 - EXPERIMENTAL BALANCING METHOD.

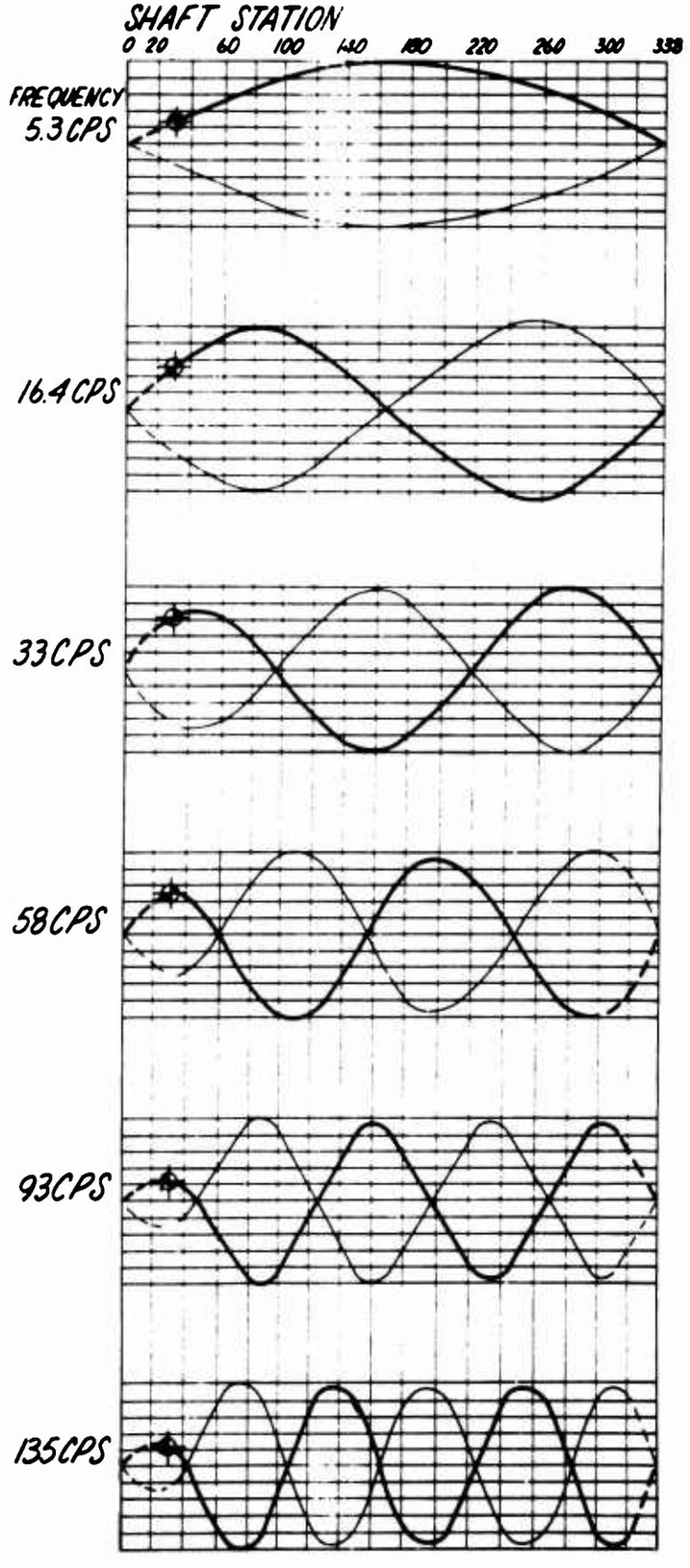

FIGURE 61. VIBRATED MODE SHAPES - UNDAMPED.

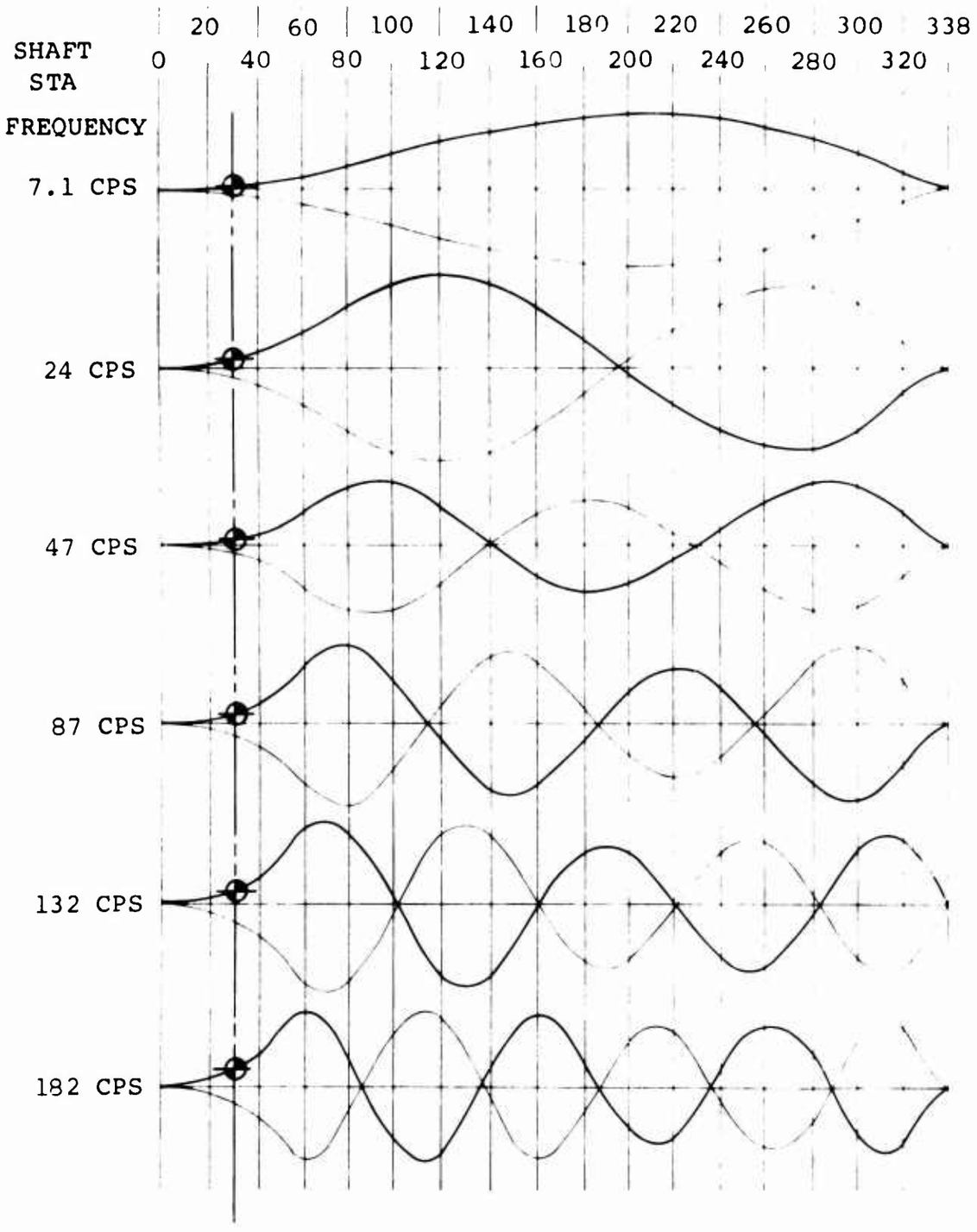

FIGURE 62. VIBRATED MODE SHAPES - DAMPED.

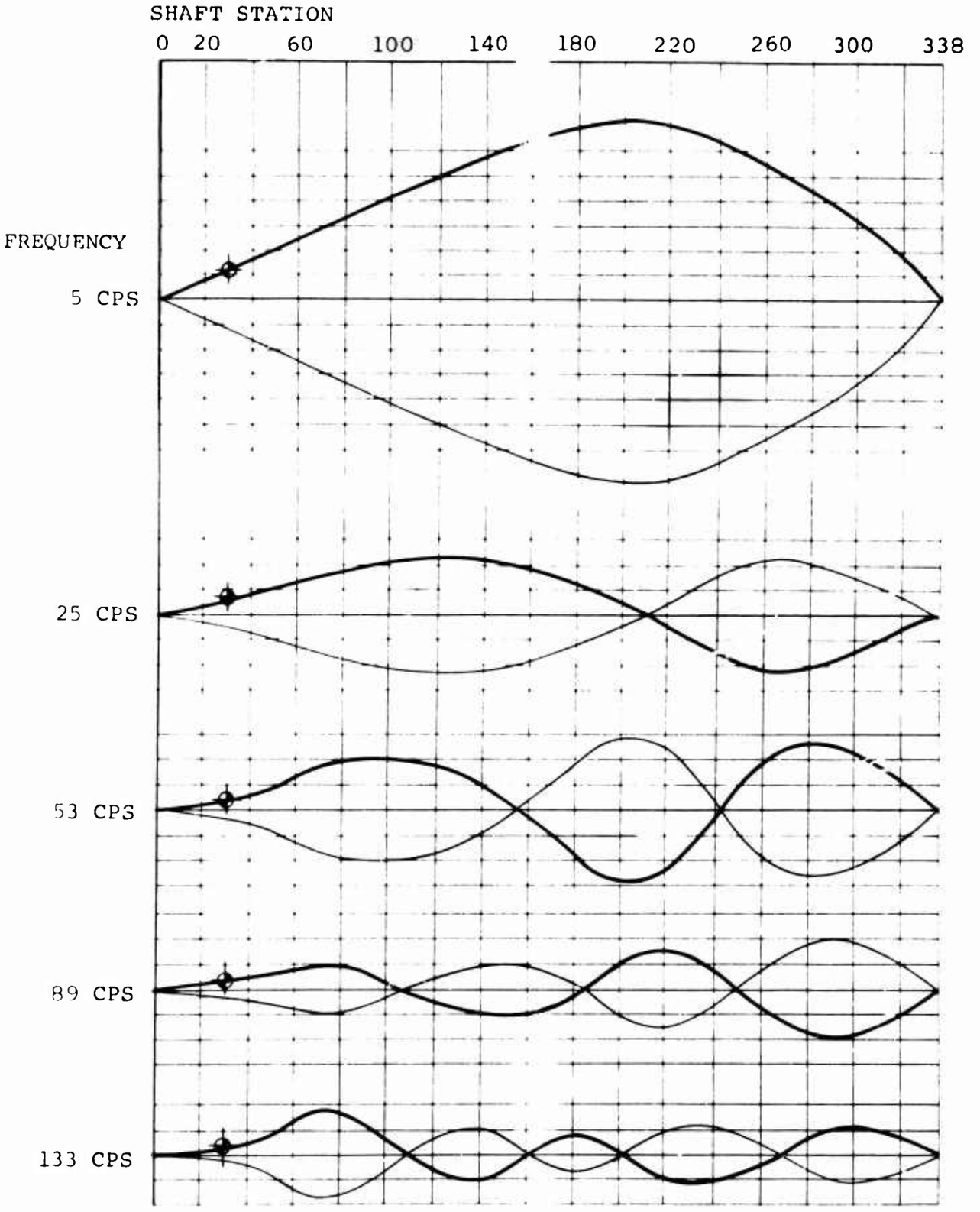

FIGURE 63. ROTATED MODE SHAPES.

All weights were removed, and the rotating mode shapes were recorded for the safe speeds under this condition. Figure 64 shows the mode shapes (same conditions as shown in Table IX above).

Experimental balancing produced a shaft with satisfactory amplitude characteristics. Table X gives the phase angle, speed, and conditions of the test run to achieve the desired balance result. Figure 65 displays the mode shapes associated with the experimentally balanced shaft.

A graphical presentation of the mode shape information, together with phase angle of the deflection given for the shaft with all balance weights removed, is shown in Figure 66 (same data as in Table IX).

TABLE XII
RESONANT FREQUENCIES AND LOCATIONS OF VIBRATION NODES AND ANTINODES OF UNDAMPED SHAFT

Resonant Frequency (cps)	Node Stations (inches)					Antinode Stations (inches)					
5.3	--					165					
16.6	165					80	255				
33	95	218				45	155	280			
58	60	155	246			30	110	196	295		
93	46	124	196	267		24	85	160	232	302	
135	40	104	163	222	282	22	73	133	192	250	308

TABLE XIII
RESONANT FREQUENCIES AND LOCATION OF VIBRATION NODES AND ANTINODES OF DAMPED SHAFT

Resonant Frequency (cps)	Node Stations (inches)				Antinode Stations (inches)				
7.1	--				200				
24	195				120	275			
47	140	223			92	182	288		
87	115	186	258		80	148	222	296	
132	102	160	220	283	70	130	190	255	310

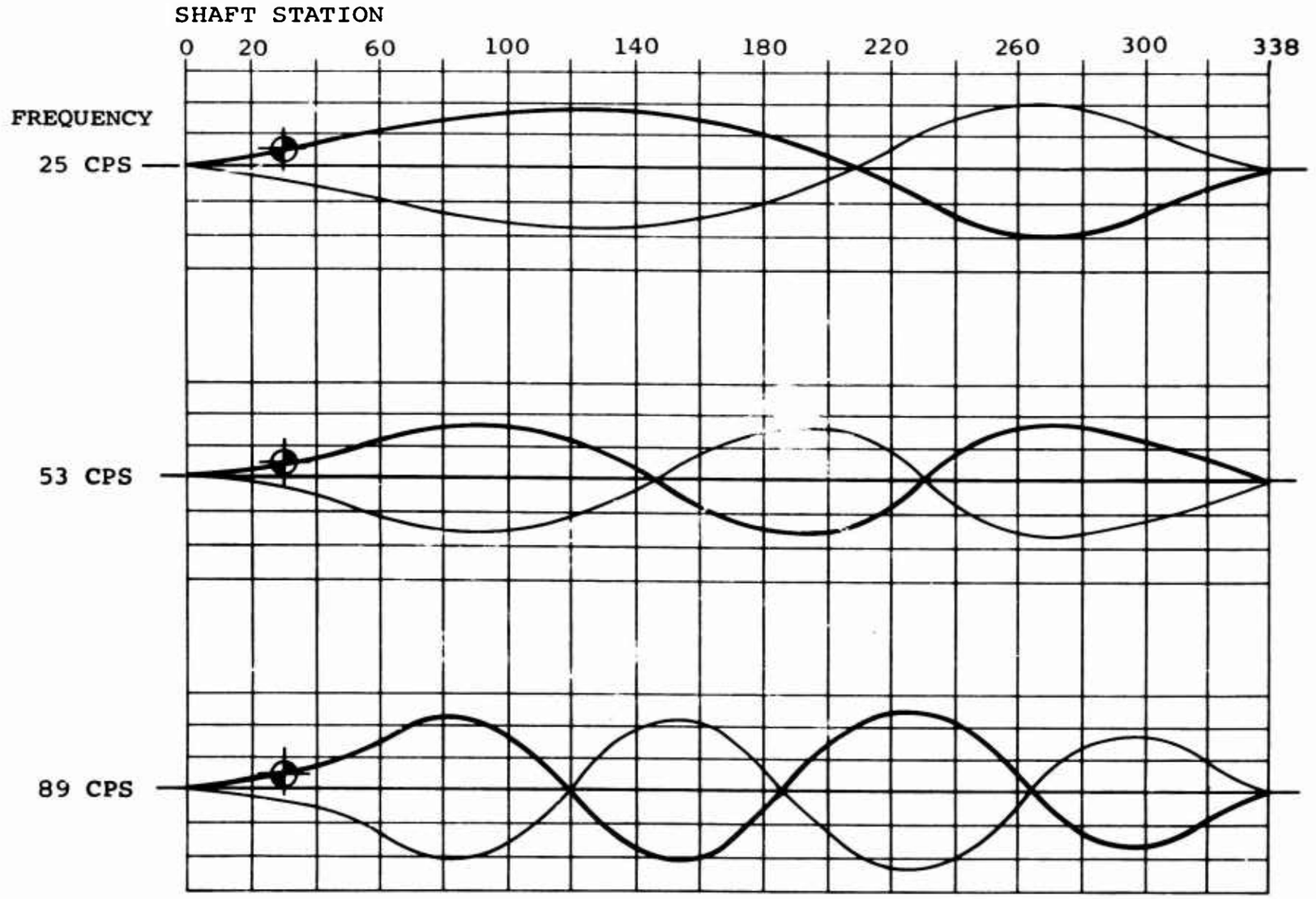

FIGURE 64. ROTATED MODE SHAPES - NO BALANCING.

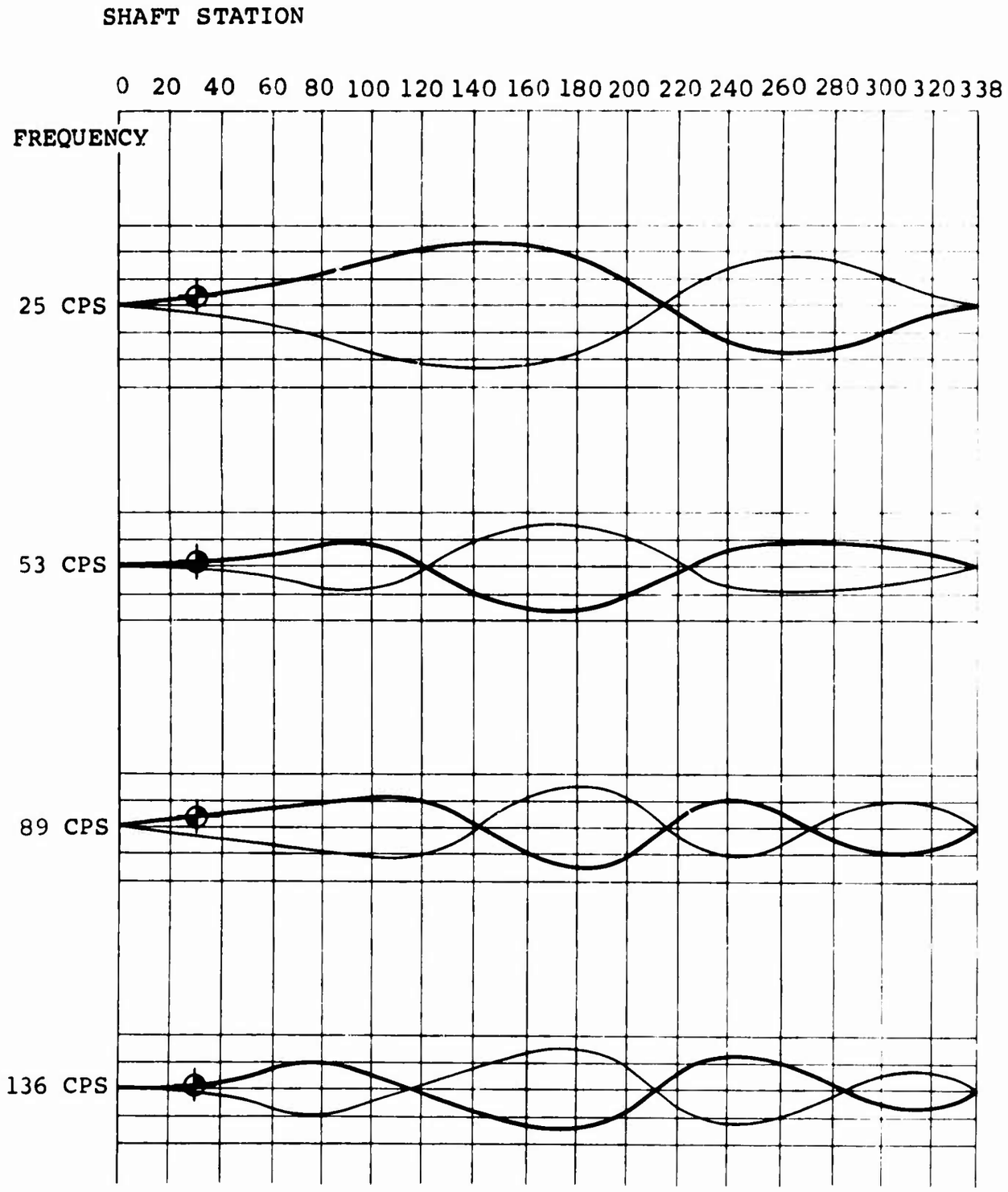

FIGURE 65. ROTATED MODE SHAPES - EXPERIMENTAL BALANCING METHOD.

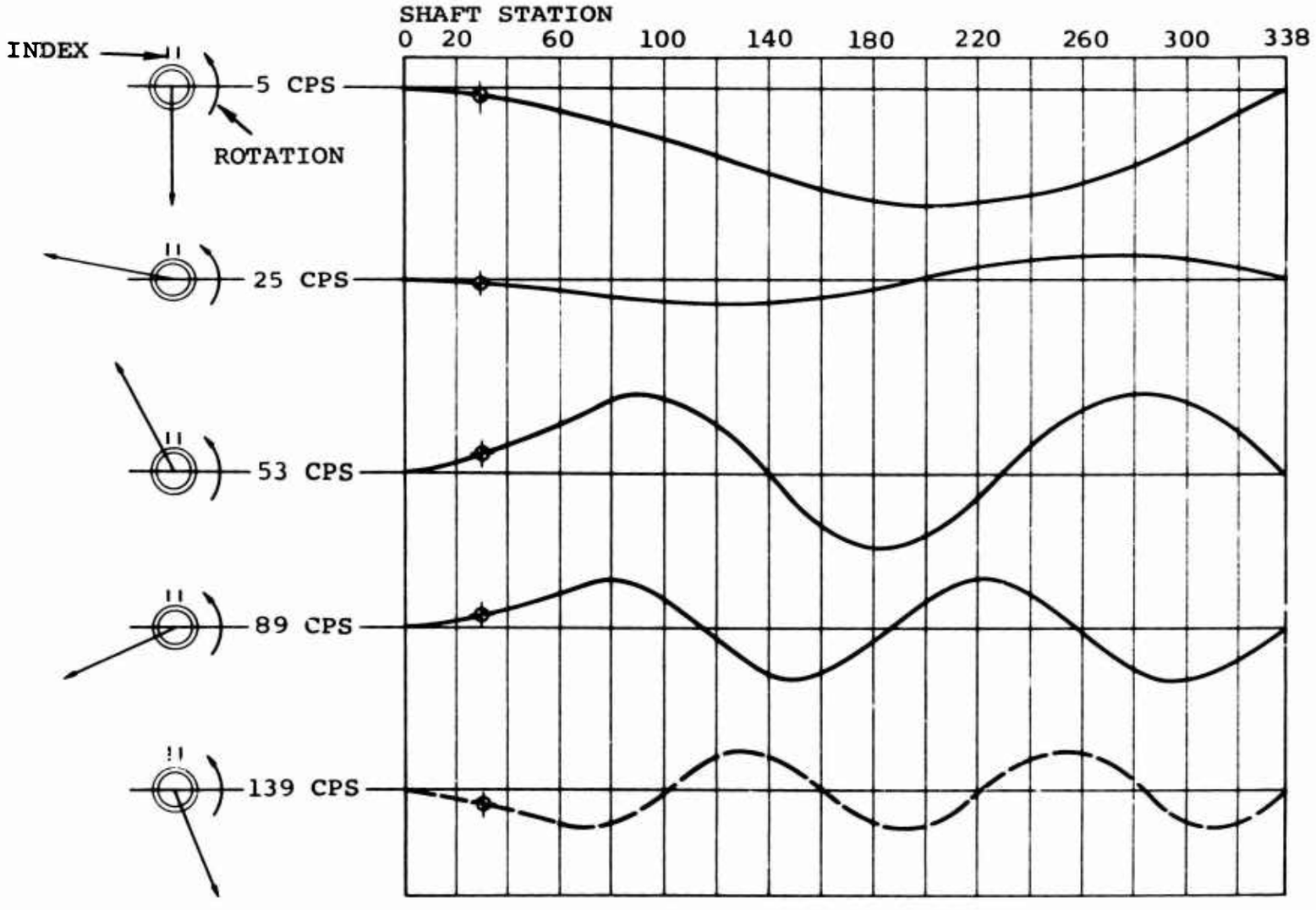

FIGURE 66. PHASE ANGLE - NO BALANCING.

ANALYTICAL BALANCING RESULTS

The analytical balancing procedure was applied to a shaft with the weights shown in Table VII in place. The results of three runs, with increasing balance weight magnitude, are shown in Figure 67. The mode shape associated with the final run of this series is given as Figure 68. A reduction in amplitude at the critical speed, and successful operation to the maximum speed, was obtained in this trial of the analytical method.

Table XIV and Figures 69 and 70 show the result of analytical effort to balance the entire range of critical speeds when the shaft condition included the weights shown in Table VII. All weights were removed, returning the shaft to the condition shown in Table IX. The analytical approach was used to solve this new balance problem. Test results and phase angle are given in Table XV, and the relative amplitudes are shown in Figure 71. It will be noted that operation beyond 5200 revolutions per minute was not possible.

TABLE XIV
PHASE ANGLE OF DISTORTION MEASURED AT STATION 300
DURING DEVELOPMENT OF ANALYTICAL BALANCING PROCEDURE

Speed (rpm)	Phase Angle at Station 300			
	Run 155	Run 156	Run 157	Run 158
1500	266°	274°	265°	285°
3200	308°	263°	258°	234°
5300	20°	350°	342°	318°
8000	--	190°	269°	--

	Run 167	Run 168	Run 169
1524	286°	290°	286°
3200	308°	293°	267°
5000	280°	285°	283°

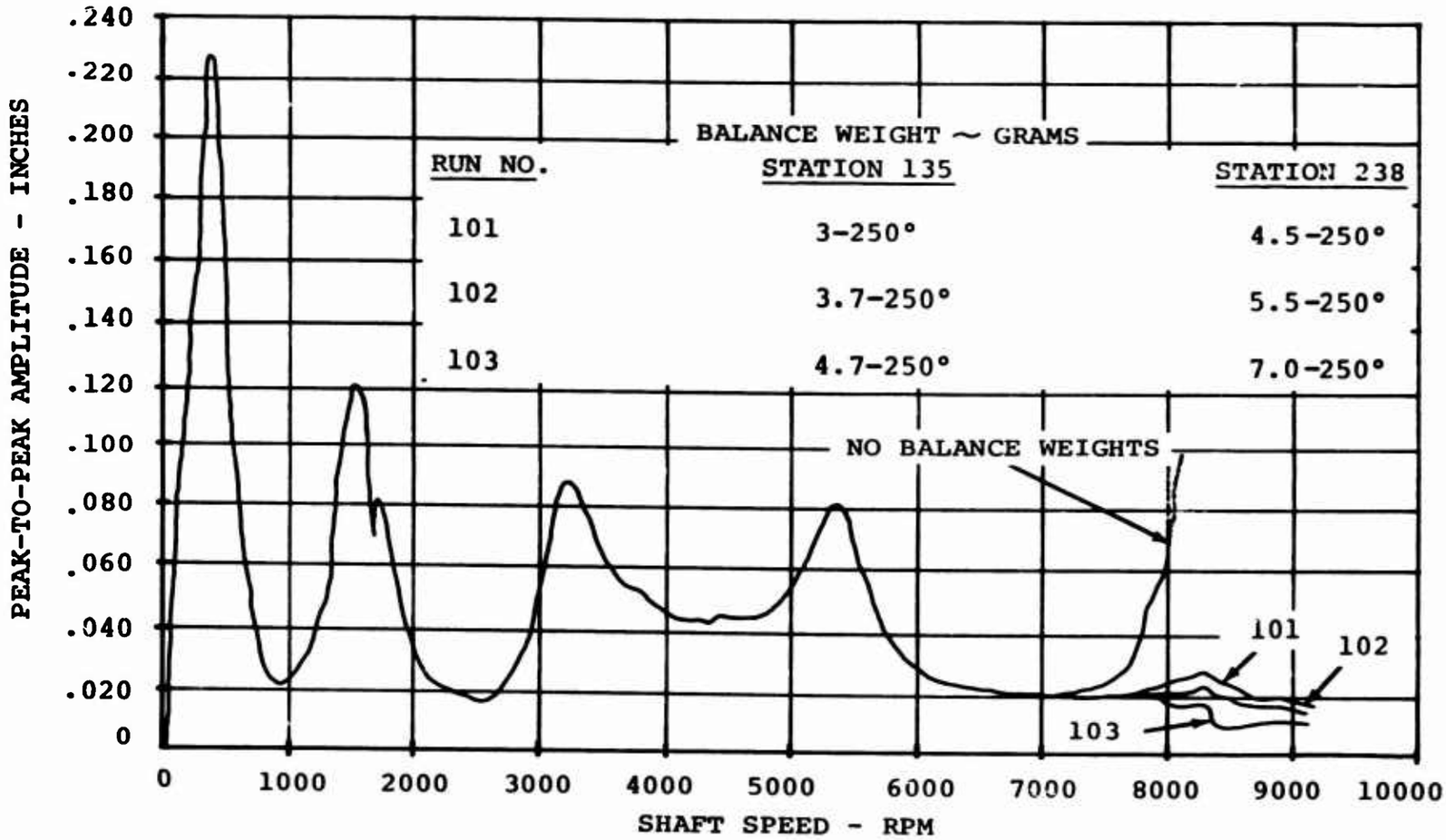

FIGURE 67. DISPLACEMENT - STATION 300 - ANALYTICAL BALANCING METHOD.

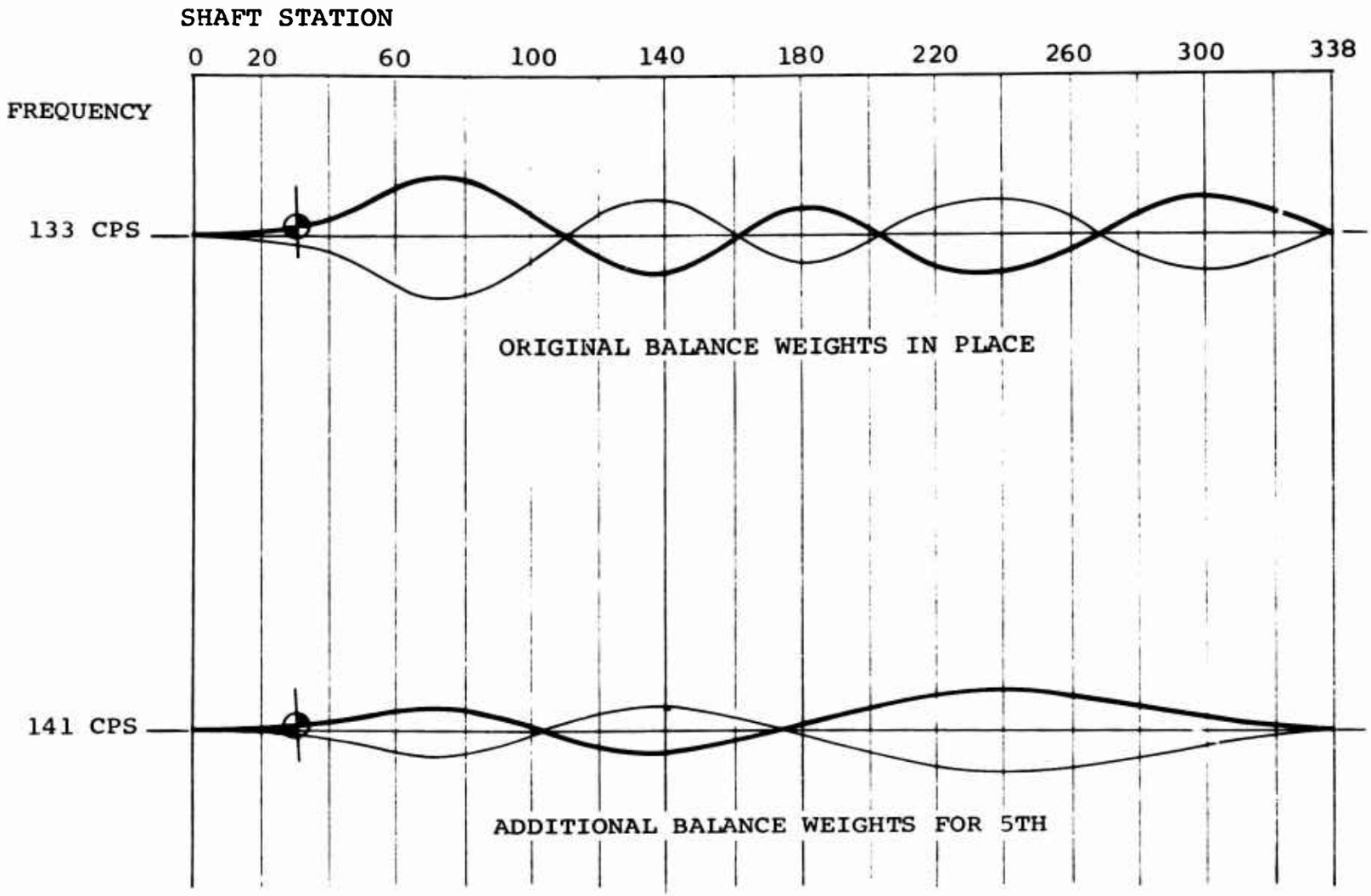

FIGURE 68. COMPARISON OF MODE SHAPES.

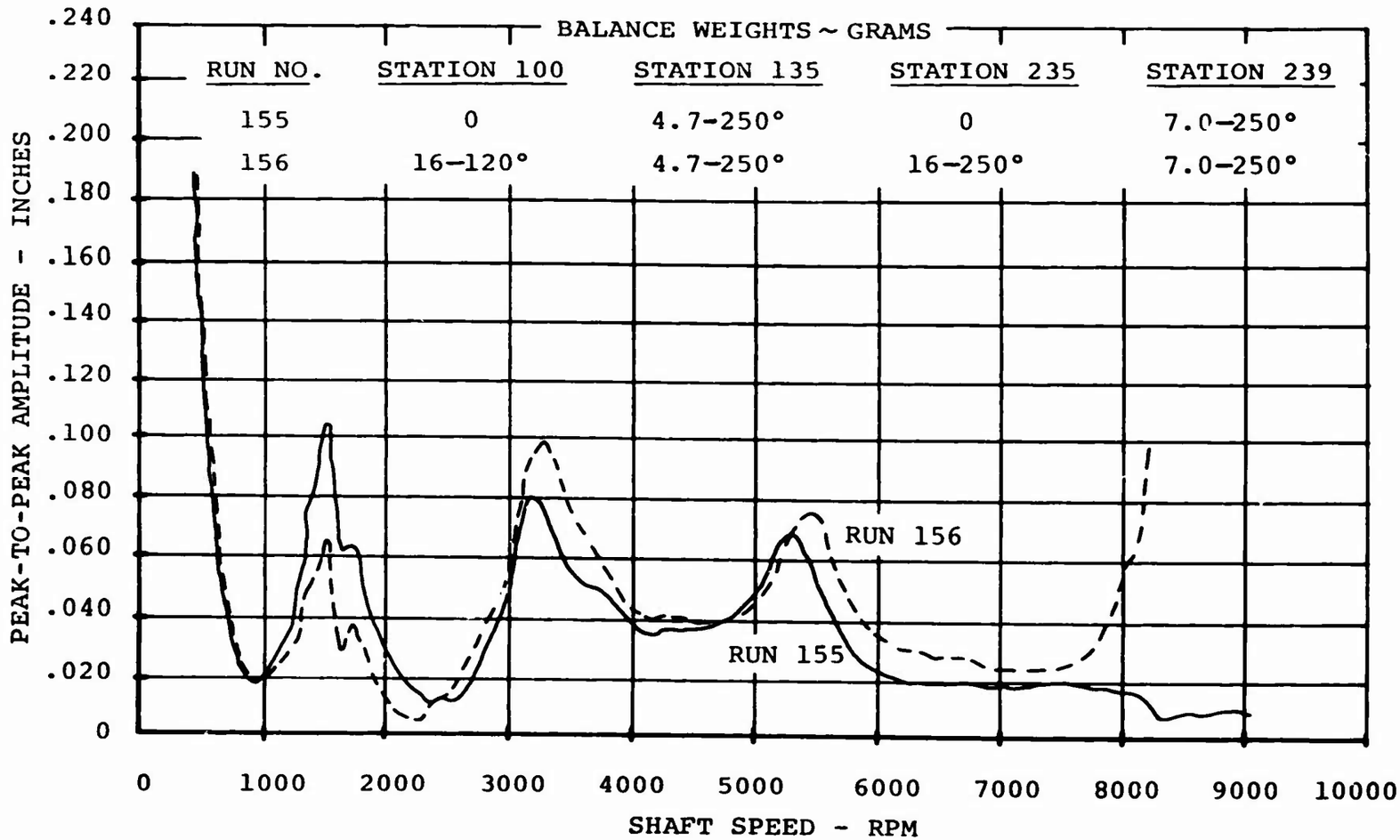

FIGURE 69. DISPLACEMENT - STATION 300 - ANALYTICAL BALANCING METHOD.

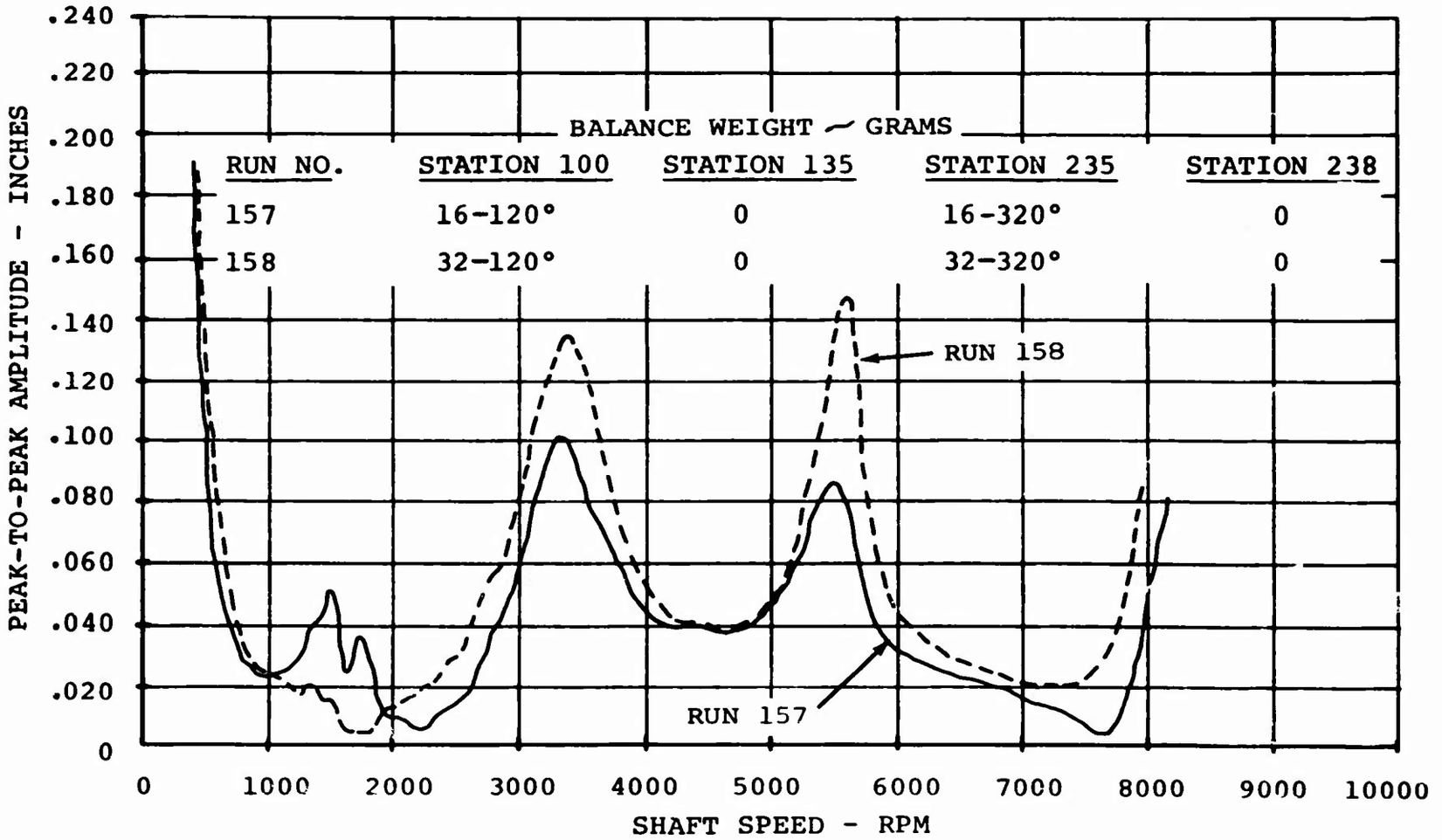

FIGURE 70. DISPLACEMENT - STATION 300 - ANALYTICAL BALANCING METHOD.

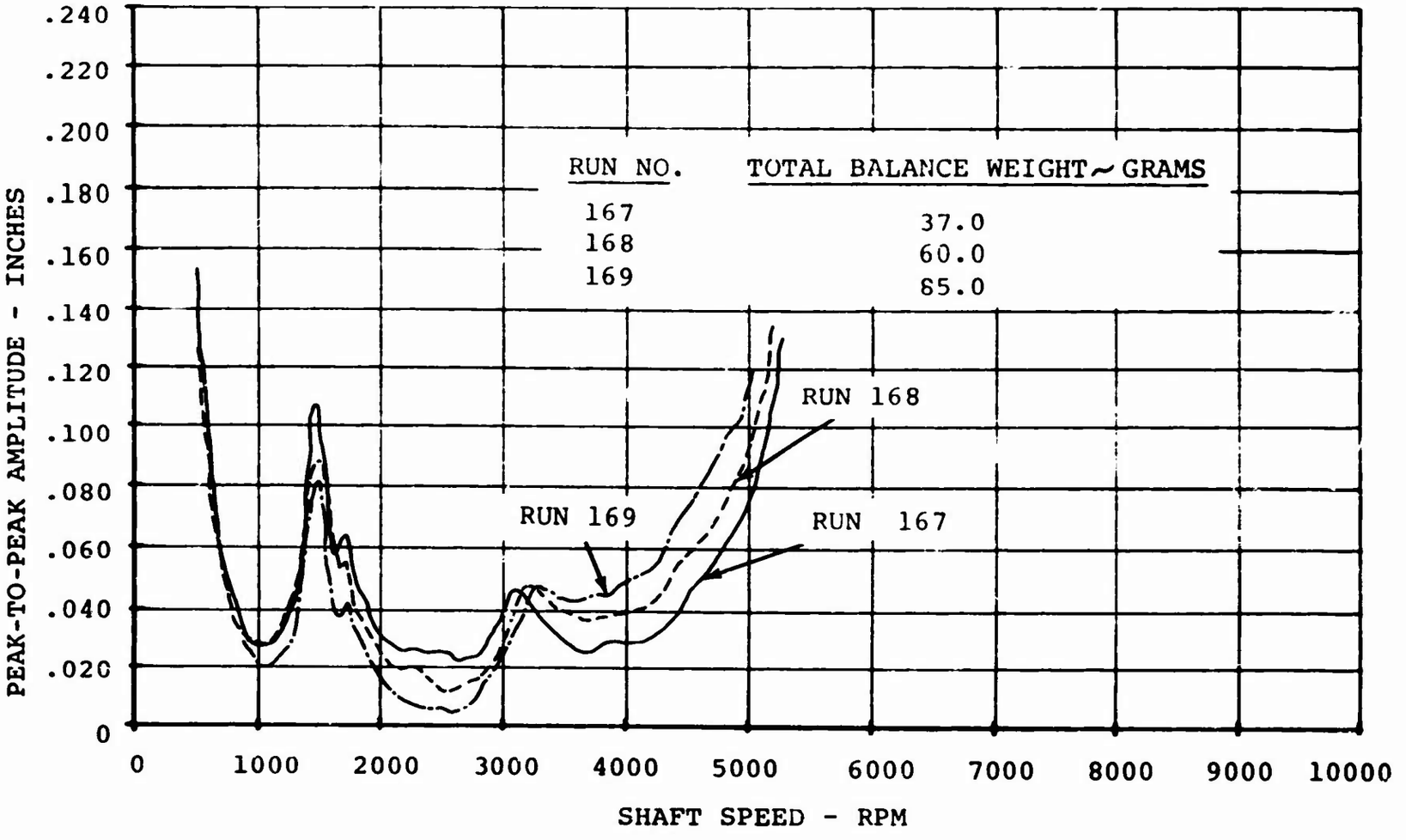

FIGURE 71. DISPLACEMENT - STATION 300 - ANALYTICAL BALANCING METHOD.

EVALUATION

SUMMARY

The supercritical shaft program consisted of design and test phases. Evaluation of both phases is included in this section. The test results are analyzed to indicate the applicability of the design to helicopter use.

A summation of program results is listed below. All trends indicated should be referred to the range of values actually tested and are drawn from the specific test specimens of this program.

1. The effect of balancing was the most significant variable imposed in the test program. Balancing was necessary in order to achieve the required maximum rotational speed.

2. Damping coefficient was the next most significant variable.

3. Damper moving weight should be minimized for minimum amplitude shaft operation.

4. Damper support spring rate has insignificant effect.

5. The viscous shear damper produced a smooth-running shaft, although shaft operation was satisfactory with immersion body damper.

6. The environmental variables of torque and misalignment did not greatly affect shaft amplitudes. The addition of forced excitation to the damper resulted in a total shaft amplitude which was the sum of the normal whirl amplitude plus the forced amplitude with no observed amplification.

7. Criteria for satisfactory aircraft operation established by maximum stress levels, structural loads, and damper heating were met or bettered by the balanced shaft.

8. Review of the design indicates that improvement in shaft operation is probable by redesigning the damper adapter section to improve centering and to reduce the moving weight.

MODEL TESTS

The design phase of the program was preceded by the testing and analysis of a dynamic scaled model supercritical shaft using the methods developed by Battelle Memorial Institute.

The results of the model tests determined the location of the damper on the full-size shaft. They also influenced the range of design damping coefficients for the full-size damper. Further, the values of the various critical speeds were determined by model tests and were scaled to the full-size shaft.

The following observations are drawn in evaluating the effectiveness of model test results in providing design information which led to optimum performance of the full-size shaft.

1. A workable damper location was established by the model tests. Whether this was an optimum location was not established since the full-size shaft design did not permit variation of this parameter.

2. The best overall control of shaft amplitude on the model required considerably larger damping coefficients than those found to give best results on the full-size shaft.

3. Numerical values for the critical speeds were predicted accurately from the model tests; they were different from those calculated originally.

4. The damper support spring rate had very little effect on model shaft performance. Similar results were observed in the full-size shaft test.

5. The model did not accurately predict the amplification factor (Ref. p. 129) and therefore could not establish the dynamic performance of the full-size shaft.

A comparison of damper motions indicates a possible reason for the difference in performance characteristics between model and full-size shafts. Refer to the apparent damper motion shown by the figure on page 183 of Reference 4 and the general comment that the damper motion is usually about one-half the maximum amplitude of the shaft. The figure bears out this statement at the fifth critical speed.

Now refer to the apparent damper motion shown by Figure 65, which shows the balanced full-size shaft at the fifth critical speed. It can be seen that the motion here is less than one-tenth the maximum amplitude of the shaft.

The change in the ratio of damper motion to unsuppressed amplitude would indicate a decrease in effectiveness of full-size shaft damping as compared to the model.

A change may be indicated in the method of relating the physical characteristics of the model to the full-size shaft to obtain a closer relationship in dynamic performance. This may enable a prediction of the threshold where balancing becomes necessary for higher speeds.

The recommended long-term solution to performance prediction is establishment of a rigorous theoretical treatment which includes the effect of mass unbalance and amplification factor. A partial approach to this is presented in the Analytical Balancing solution.

FULL-SCALE TESTS

Damping Coefficient

Damping coefficients were evaluated in a 2-to-1 range on either side of the optimum predicted by electrical analogy. The predicted coefficient was found to best restrain shaft amplitudes in the entire range of critical speeds. It appeared that the lowest coefficient tested (8.5) was least satisfactory at the higher speeds. The same trend was more clearly indicated by the model shaft, where it was possible to run through the entire speed range during the evaluation of this variable. The full-size tests were made before balancing, and the maximum safe speed was therefore curtailed.

The damping coefficient can vary over a limited range and still provide satisfactory operation of the shaft. Changes in

damping coefficient due to the temperature effect on viscosity can be absorbed within this range. Correction is required for viscosity changes which produce damping coefficients outside this limited range.

Damper Mount Spring Rate

Previous analysis had shown that the damper mount spring rate affected shaft action only when the resonant frequency of the damper spring-mass system was at or above the shaft rotational frequency. In order to make a 16-pound weight resonate at frequencies above the shaft's operating speed range (above 100 cps), a spring rate of over 16,000 pounds per inch would be required, which is impractically high. The resonant frequency of a 16-pound mass supported by springs having practical rates of 100 to 500 pounds per inch would be in the range of 8 to 18 cps. Therefore, it was concluded that a practical spring rate was of little importance to the dynamic behavior of the full-scale shaft in the normal operating speed range. Spring rate can, therefore, be subordinate to other design considerations.

Damper Moving Weight

Amplitudes with increased damper weight were higher at the higher speed antinodes and lower at the damper. This indicates that higher damper weight makes the damper less effective; a sufficiently high moving weight would create a nodal point at the damper, with a probable catastrophic effect on shaft behavior. Therefore, the previous recommendations of minimum damper weight should be carefully observed. The ratio of damper weight to shaft weight was one-third in the test specimen. This is the maximum recommended ratio and should preferably be reduced.

TORQUE

The maximum torque applied during test was 15,000 inch-pounds, resulting in a tube shear stress of 4800 psi. The effect of torque was, in general, to slightly reduce the shaft amplitude as shown in Figure 72. From previous tests of model shafts under transient torques, it was concluded that there was no noticeable effect in shaft amplitude within the normal design stress range. One explanation of the slight reduction observed is that the torque loading within the end gearboxes increased the gear shaft bearing lateral spring rate (preload effect). Since the supercritical shaft was supported at one end from

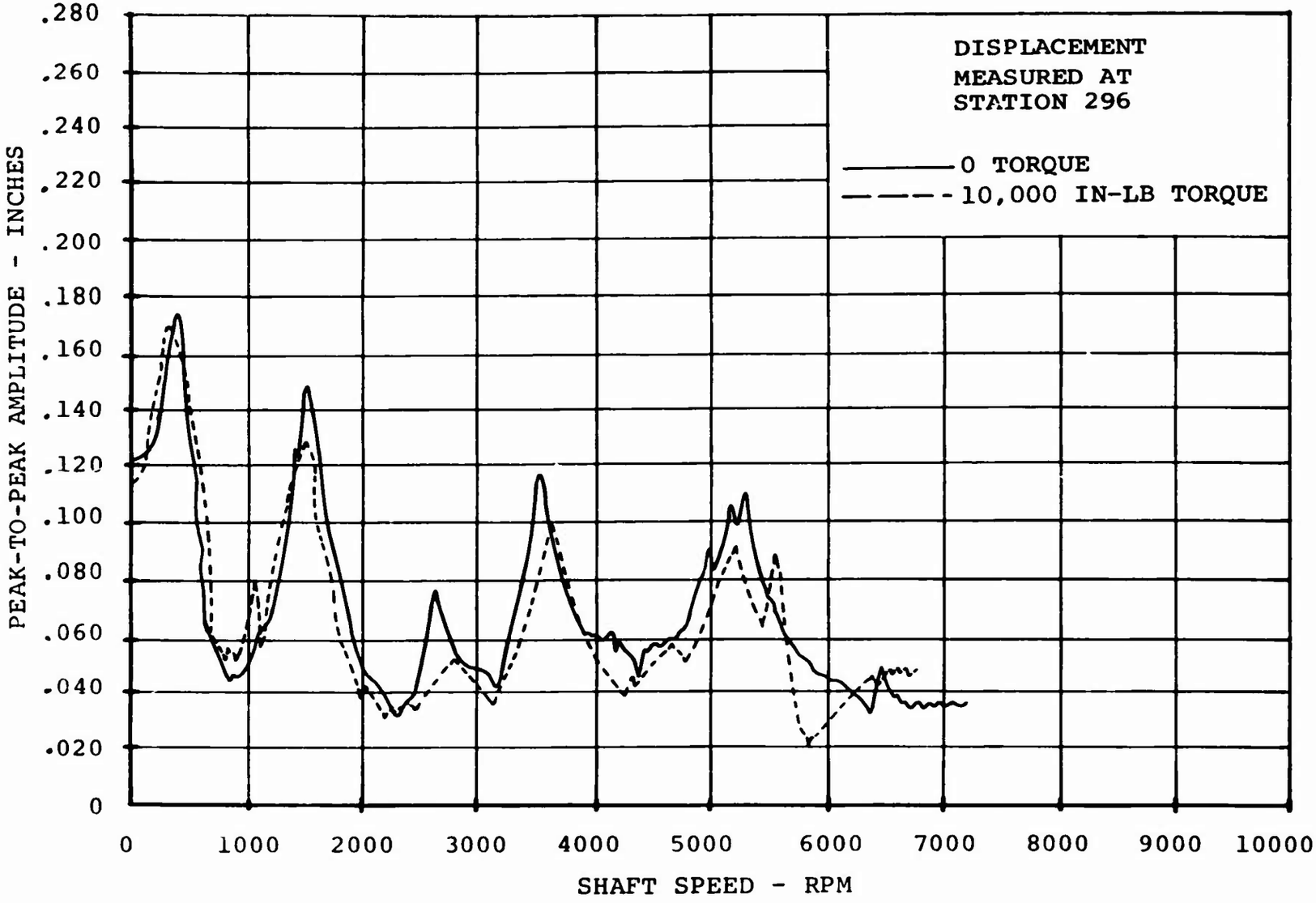

FIGURE 72. EFFECT OF TORQUE.

the gearbox shaft, this effect would tend to provide a slight decrease in shaft amplitude.

Misalignment

Misalignment was added at one end of the shaft by moving the test machine support shaft. Amount of misalignment was one-half degree, measured as a line-of-sight, without reference to the shaft static droop. The strain gages showed a marked reduction in shaft moment as a result of the moment added by misalignment. However, there was no significant reduction in whirling amplitudes (see Figure 73).

Forced Excitation

Forced excitation of the damper support resulted in the same effects noted with previous model testing, in which the end of the shaft was vibrated with an external shaker. The measured amplitudes with excitation were a summation of the dynamic unbalanced and the forced deflection. Figure 74 compares various conditions. No amplification of vibration was noticed, even when the damper was shaken at a shaft critical frequency.

Balancing

The initial balancing effort was a direct development of the results obtained during the initial test runs of the full-size shaft. It appeared to the investigators that modal balance could be accomplished once the phase angle relationship at, or near, the critical speed was established. Further, it seemed likely that more than one mode could be balanced if the corrections could be placed at points of minimum influence to successive modes. This procedure was attempted for the fourth and fifth critical speeds, with the result that the shaft finally ran successfully through the fifth critical and to a maximum 9300 revolutions per minute, while the unbalanced shaft had become increasingly violent beyond 7500 revolutions per minute.

Balancing, therefore, has appeared to be the most important single variable. To further develop and refine this, a balance program was advocated and performed. The following evaluation is concerned with the two methods investigated.

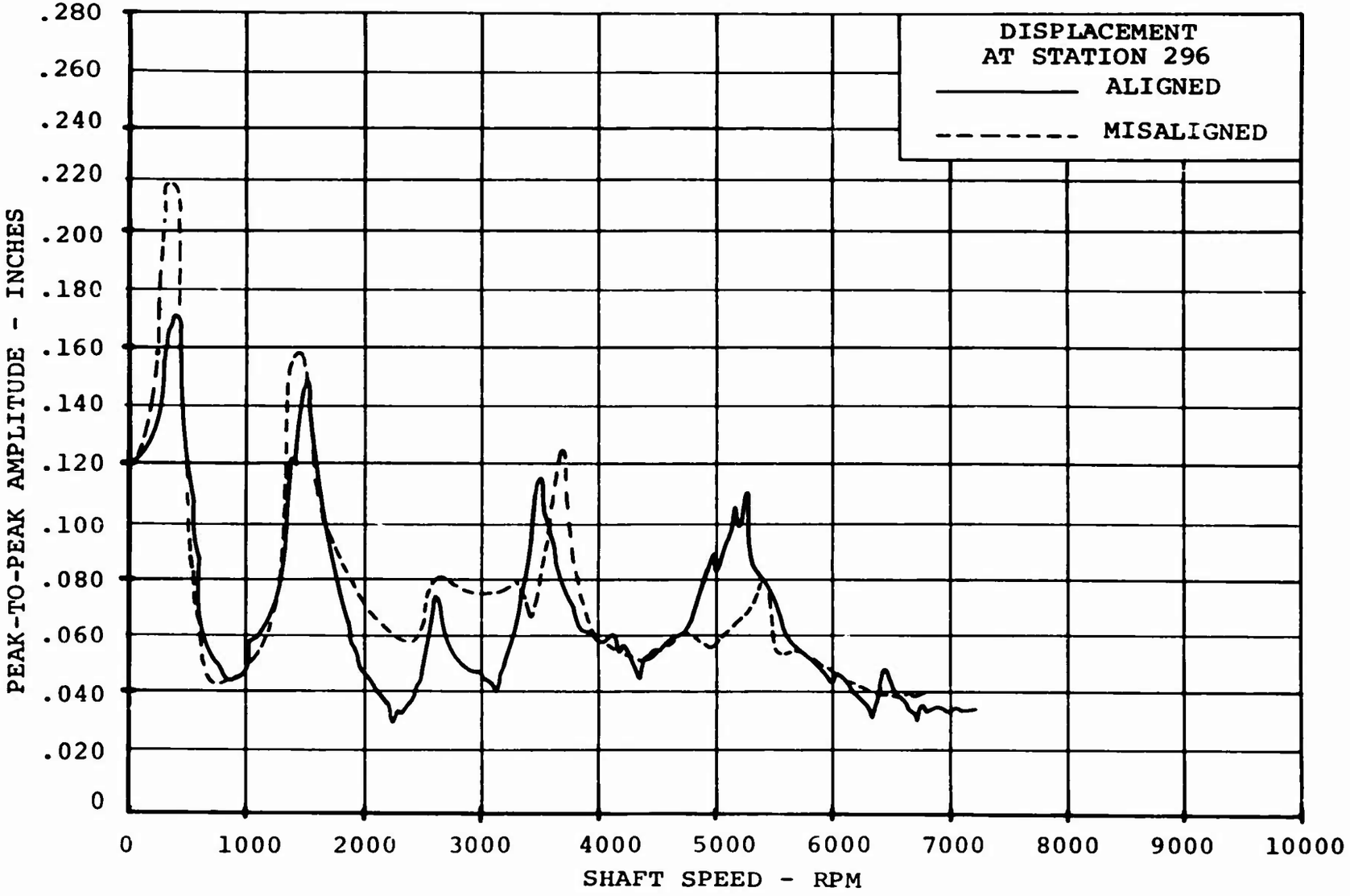

FIGURE 73. EFFECT OF MISALIGNMENT.

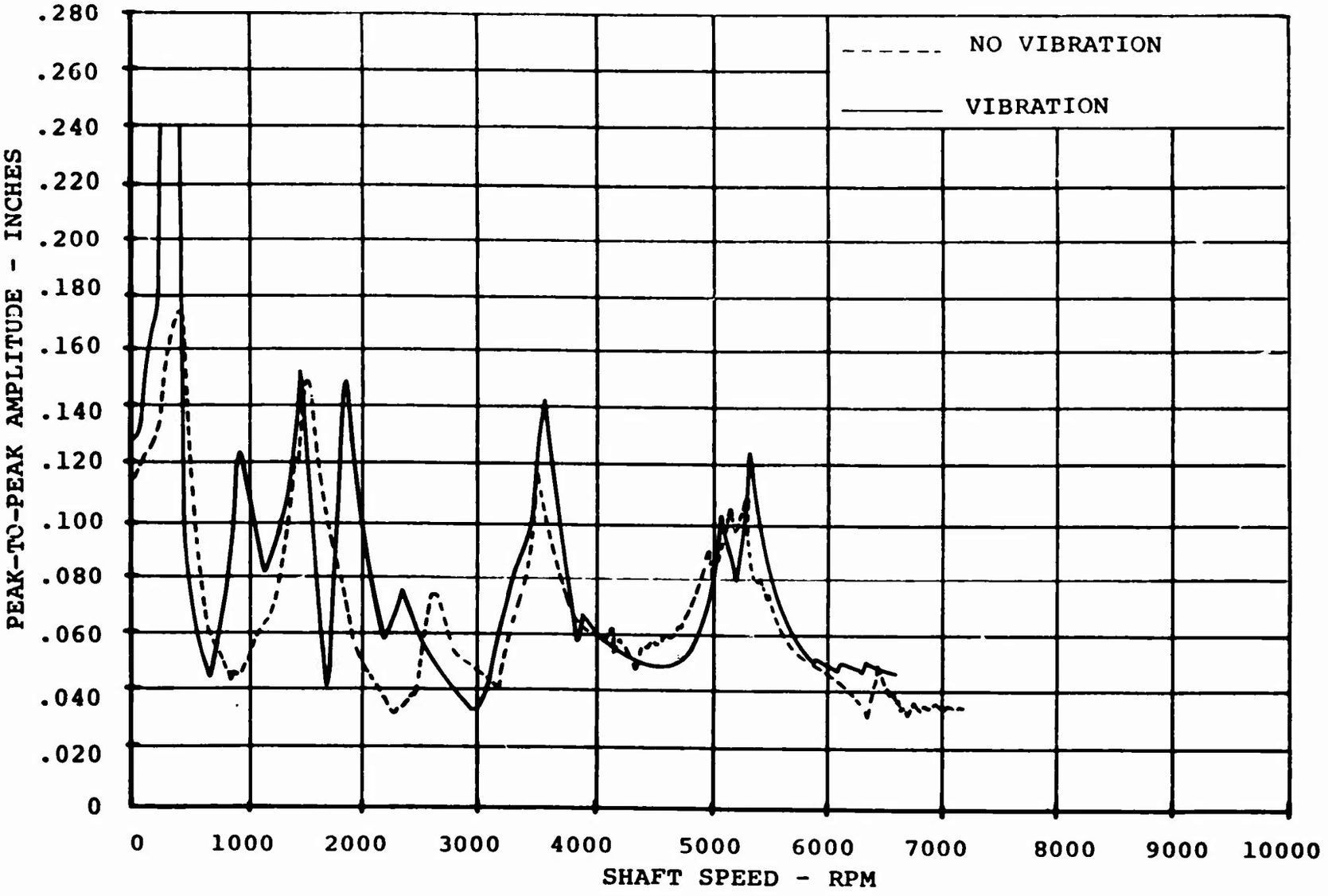

FIGURE 74. EFFECT OF FORCED EXCITATION.

Experimental Balancing

Results indicate that this balancing method is practical and effective. There is high confidence that this method can be applied to any supercritical shaft. There are, however, limitations in the number of critical speeds that can successfully be balanced by the present technique.

The experimental balancing technique for mode-by-mode correction becomes increasingly more difficult with the number of modes that are in need of correction.

The balance weights should be located at stations that affect only the mode of interest, leaving all other modes unaffected. Locating stations that meet these requirements for more than three modes has not been accomplished. At present, when balance of more modes is included, the interaction between modes destroys effectiveness, and unsatisfactory shaft performance results.

Practical considerations used in selecting the three highest modes for correction were: first, that these modes produce the most severe shaft bending stresses; and second, that the magnitude of correction required have little influence on the two lower modes.

To strengthen the conclusions as to the applicability of the experimental method, the shaft was tested in two initial dynamic configurations.

First, the shaft with the balance weights previously installed during the first balancing attempt was experimentally corrected, and improved performance was obtained.

Following this, all weights were removed to produce a dynamically new problem. Again the experimental procedure was applied, and satisfactory performance was also obtained.

The performance of the shaft balanced by the experimental method can be observed by referring to Figure 58, which shows the level of vibration at Station 300.

The difference in deflected shape of the balanced shaft and the unbalanced shaft can be seen in Figure 64.

The unbalanced shaft most resembles the classical mode shapes

produced by vibration tests. The deflection of the balanced shaft (Figure 65) bears little resemblance to this classical shape. The conclusion is that balancing out one mode allows the influence of adjacent modes to appear (modal coupling).

Because of modal coupling, there appeared to be a certain minimum level of vibration which could not be entirely eliminated. When level of vibration was reduced to zero at one station, the amplitude would increase at another. The best overall balance was achieved when the amplitude at a critical speed was reduced to this minimum level. The magnitude of this minimum level should not limit successful operation of the shaft, as evidenced by the Criteria of Successful Operation.

MODE SHAPES

Mode shapes were obtained by vibrating the shaft and by rotational tests. The vibrating modes were obtained both with and without damping. The rotational tests were necessarily all damped, but with various degrees of balancing, ranging from unbalanced to the balance obtained after application of the experimental and analytical methods.

The damped and vibrated shaft demonstrated resonant frequencies nearly identical to those found in the rotating tests using the same viscous damper. Accurate prediction of natural frequencies could therefore be made before a full-size shaft is rotated. On the other hand, there was a frequency shift with the undamped shaft, whose resonant frequencies were generally 70 percent of those of the damped shaft. When one compares data on the unbalanced rotated shaft and the damped vibrated shaft, a similarity in deflected shape is noted.

As previously noted, the mode shapes of the balanced shaft are distorted when compared to the clearly defined modes of both the vibrated and unbalanced shafts. In fact, the actual fifth mode, Figure 65, bears a resemblance to a fourth mode. Again, the conclusion is that modal coupling is evident when the balance weights have sufficiently suppressed the primary mode. The effect of the damper in suppressing the amplitude of the shaft in its vicinity can be clearly seen in the vibrated mode shapes.

The orientation of the mode shape plane and the change in angle as the critical speeds change can be noted in Figure 66.

ANALYTICAL BALANCING

The first task of the analytical method was to provide a balance correction for the fifth critical speed.

The solution of the equations indicated that two weights would be required and that these should be placed at points which the analysis indicated to be the most effective to counteract the mass distribution. The inputs to the equations were obtained from rotating test data acquired from the shaft while in the initial test condition. The total balance correction weight used was determined by repetitive testing. The calculated balance correction weights were larger than those actually found to provide satisfactory balance.

A further investigation (Figures 69 and 70) was conducted to improve all the remaining modes except the first. The first was considered primarily due to initial bend. Calculations for removal of the deflection indicated that a very large weight would be required. The test results for this set of numbers show an improvement of the second critical speed but an increased amplitude at the third, fourth, and fifth critical speeds.

A final evaluation of the analytical balancing method resulted in data which indicated clearly that all deflection shapes were distorted. At 1524 rpm (second critical), 3200 rpm (third critical), and 5000 rpm, the deflection shape was close to the first critical, with maximum amplitudes near Station 200. (Graphical presentation is not included in this report.)

The existence of a stable first mode rotating at a higher-than-first-mode rpm is not reasonable on the basis of calculated loads from measured deflection. It is therefore hypothesized that the observed shape either was rotating at first mode speed or was a planar vibration. In either event, the shaft alternating stresses were low (approximately 300 psi). This is far below the stress level of a fifth mode shape with the same amplitude. Therefore, it is believed that the observed deflection did not represent the high bending stresses to be assumed by comparison to deflection amplitudes more usual to the higher critical speeds.

Review of the initial analytical balance trial indicates a successful balance of the fifth critical speed. In further

trials, the mode shapes associated with the critical speeds to be corrected were erased in favor of a suspected non-synchronous first mode. The test results do not indicate a smooth-running shaft for this reason. As has been seen, the amplitudes recorded are not indicative of shaft bending and are probably not indicative of rotating unbalance.

Existence of a non-synchronous first mode shape is presently unsubstantiated by test data. An experimental continuation of the analytical balancing method would attempt to define this motion. Application of the previously used bending strain gages would be particularly useful in correctly analyzing the condition.

AMPLIFICATION FACTOR

The amplification factor is defined here as the ratio of calculated to actual unbalance in the system. The actual unbalance causes the amplitudes observed. The calculated unbalance causes equal deflection in a critically damped system. In a critically damped system, there is no amplification (ratio of 1).

The actual unbalance is obtained from test results wherein a known weight removes all amplitude.

The balance weights of Table XV were calculated from observed deflection at all criticals except the fifth.

Amplitudes approaching the fifth critical speed were excessive, and the test was halted when stresses reached 10,000 psi. Calculated balance weight for this condition is about 400 grams. However, the balance weight at the actual fifth critical speed would have been much greater than 400 grams.

TABLE XV
BALANCE WEIGHTS

Mode	1	2	3	4	5
Calculated unbalance	1770	146	78	335	400 plus
Actual unbalance from test	550	80	15*	35*	11

*Indicated actual unbalance weight obtained by applying amplification factor from Figure 75.

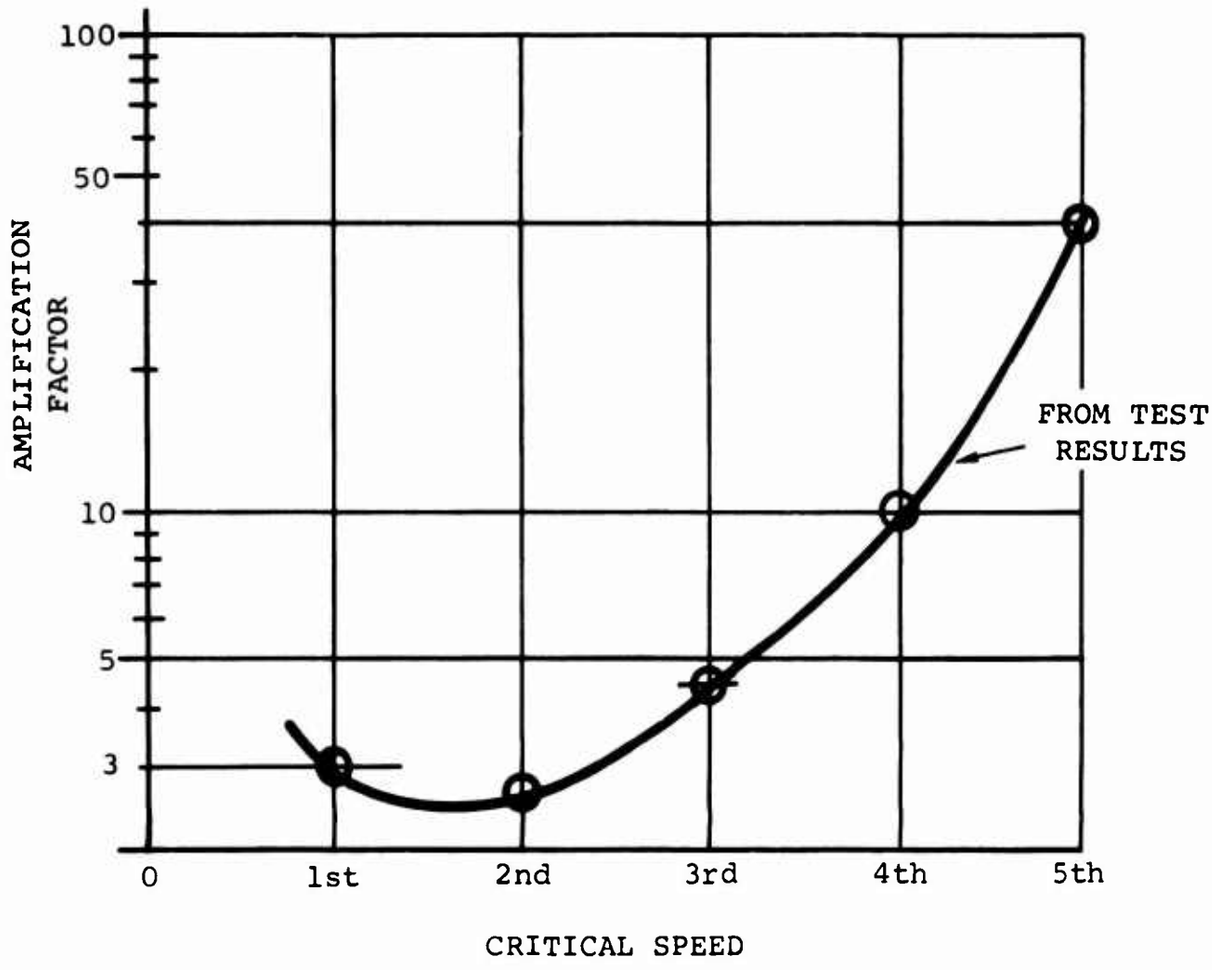

FIGURE 75. AMPLIFICATION FACTOR.

The effect of the amplification factor is to make the shaft sensitive to unbalances. The balancing technique was adequate to control the amplitude in the test shaft and resulted in a supercritical speed shaft system feasible for an aircraft test installation.

If, however, the present amplification factor curve is extrapolated, it is apparent that at still higher critical speeds the tolerable degree of unbalance becomes much less. Therefore, with any given degree of balancing refinement, there would be a limitation in the number of critical speeds that could be safely traversed. For this reason, reduction of the amplification factor appears to be highly important, both to make possible less sensitive production balancing requirements and also to attain the future goal of high-speed (engine rpm) interconnect shafts. The test shaft would be required to negotiate seven critical speeds if operated at engine rpm.

CRITERIA OF SUCCESSFUL OPERATION

Continuous safe operation of a supercritical shaft implies that the following conditions exist:

1. Shaft stress levels are below the fatigue endurance limit for the reliability desired.

2. Loads from shaft to structural supports are of a magnitude that will not necessitate the redesign of these supports to ensure adequate fatigue life and that will not create a significant vibration input to the structure.

3. Damper power absorption is sufficiently low that the heat can be dissipated without a circulatory cooling system and that the power absorption does not represent a significant power-loss weight penalty.

Tests of the balanced full-scale shaft show that these conditions are met. Figure 76 indicates the magnitude of several of the parameters of interest and shows the effects of balancing.

This figure is a multiple cross-plot of end load versus deflection for various speeds. The load on the damper is related to this data and is included. Shaft amplitudes indicative of test

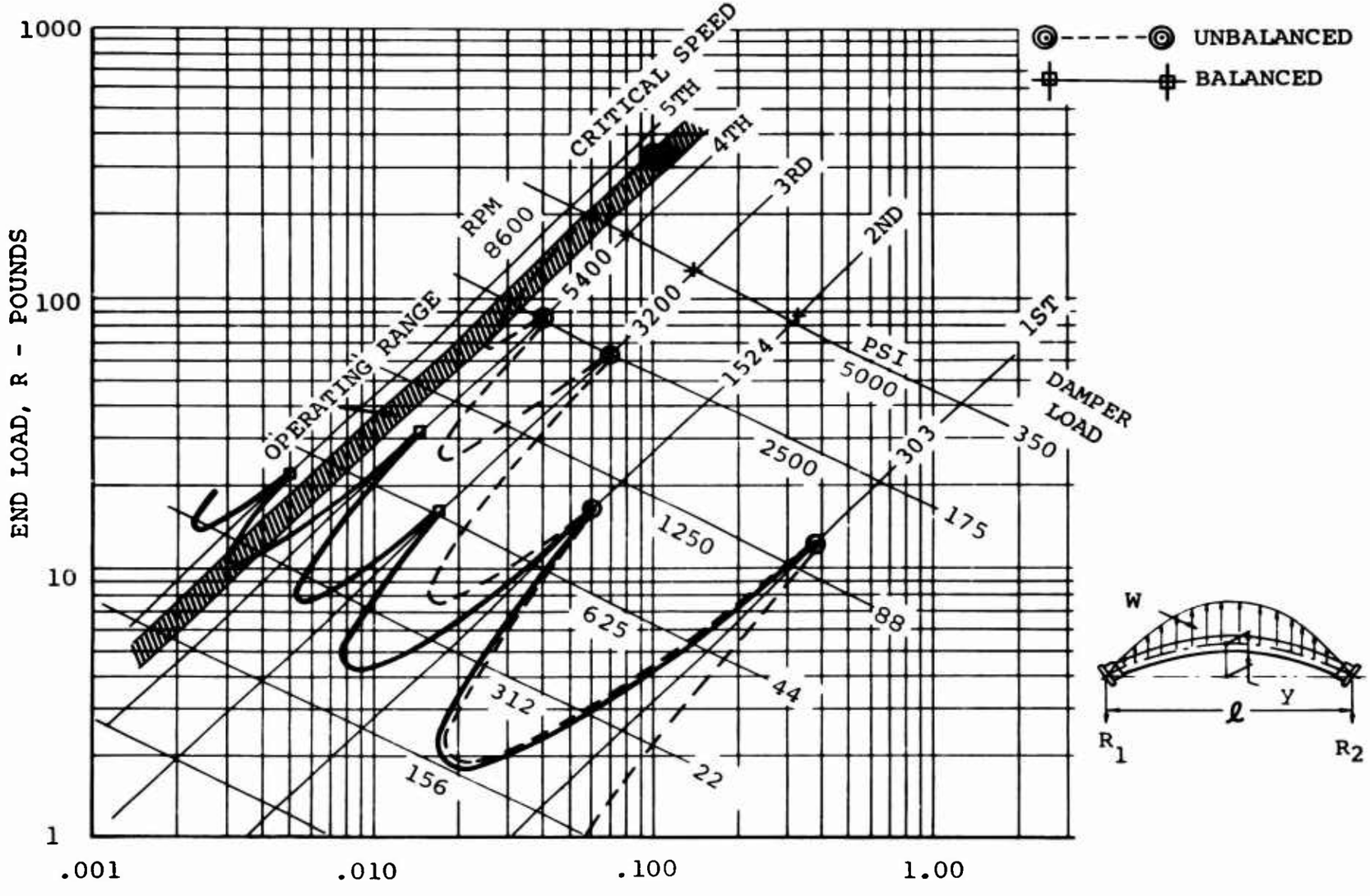

FIGURE 76. STRESSES AND LOAD LEVELS.

results from balanced and unbalanced shafts have been superimposed. The operational range between the fourth and fifth critical speeds is also shown.

The amplitude at each critical represents a bend in the shaft which whirls at shaft speed. Shaft bending stress is calculated from the amplitude and the mode shape.

End load (R) is the resulting orbiting load transmitted to the supporting transmission output shaft. Damper load (L) is the orbiting load transmitted to the damper bearing.

The following information is obtained from the figure:

1. The operational speed range falls between criticals. Continuous operation, therefore, occurs at less than the amplitudes experienced at critical, which enables the ambient vibration level to become the design condition.

2. Maximum shaft bending stress is below 1250 pounds per square inch. Since this is from a synchronous whirl condition, the stress is not cyclic fatigue. Cyclic bending stresses are imposed by the static sag of the shaft. The magnitude of this stress was approximately 1200 pounds per square inch in the test shaft.

3. Damper bearing load is at a maximum at the first critical speed and is approximately 100 pounds. The most severe bearing fatigue condition is at the fourth critical speed where the load is 75 pounds at 5400 revolutions per minute. Bearing life from this condition is in excess of 100,000 hours B-10. It is realized that this load is not the only one imposed on the bearing during operation (shaft weight and damper inertia are additive). Consideration of all these gives evidence that expected bearing life will be consistent with other transmission system components.

DESIGN REVIEW

The full-size supercritical shaft test specimen was designed using, as background information, Boeing-Vertol's extensive experience with shafting operating below the first lateral mode and with the knowledge gained from previous subscale shaft testing.

Experience with the full-scale shaft has led to conclusions relevant to improved design approaches for operational shafts. One area which has appeared to be of particular importance is the damper joint. This section allows disassembly of the shaft, and must also permit a bearing size which is consistent with loads, speeds, and lubrication available. The model shafts did not require such a section, and this may be part of the reason for the divergence of the full-scale shaft. The damper joint is heavier than an unbroken tube. This characteristic is believed to affect the shaft performance adversely.

The damper moving weight as tested was comprised of 75 percent necked section and 25 percent actual damper parts. The sensitivity to balance correction evidenced at the fifth critical is believed to result from the relatively high damper moving weight in comparison to tube weight. A refinement of the damper joint to reduce weight has been studied, and it is possible to remove 5 pounds from the configuration as tested while maintaining equal bending stiffness. However, the optimum design solution in this area would be to continue the shaft at full diameter through the damper. The problem of providing a bearing around this diameter would then require solution. Design studies of roller supports, fluid-film, and ball bearing shaft mountings have been advanced recently. Indications are that a fluid film or ball bearing surrounding a full diameter shaft can reduce damper moving weight to 20 percent of the configuration tested. The design problem centers about the lubrication system required for the bearings.

PROGRAM ACHIEVEMENTS

The requirement set forth for this program was to produce a shaft which would operate supercritically while transferring 2000 (or more) horsepower 28 feet and at speeds to 8900 rpm. This requirement was accomplished. The shaft was designed, fabricated, and tested. Stable operation at supercritical speeds was demonstrated. Maximum speed attained was in excess of the design maximum. The reduction in number of major shaft components (couplings, support bearings, adapters) was as predicted. This reduction represents a significant calculable weight saving, as well as a potential improvement in reliability.

To accomplish these results, it was necessary to develop a method of dynamic balancing during the program. Based upon

the performance demonstrated during the tests, the following is concluded:

1. Supercritical shafting is feasible for helicopter operation

2. Supercritical ft design will be advantageous to the helicopter.

3. Supercritical shaft development should proceed toward an evaluation in the CH-47A helicopter.

CONCLUSIONS

1. Satisfactory operation of the full-size, damped, supercritical speed shaft has been demonstrated. The test shaft ran successfully through five critical speeds and beyond the normal operation speeds.

2. The shaft was operated directly at each critical speed for extended periods of time, and the tests demonstrated that no operational speeds need be avoided.

3. Dynamic balancing of the full-size shaft assembly was necessary to obtain satisfactory performance with a single damper.

4. The effect of balancing was more significant to shaft operation than the effect of any other variable in the range of variables investigated.

5. Existing analytical methods satisfactorily determined such design information as damper coefficient and damper spring rate.

6. Scale-model shaft testing was required to predict accurately optimum damper placement and critical speeds.

7. Neither analytical nor scale-model test techniques were able to predict full-size shaft dynamic performance.

8. A viscous damper appears to be a good choice for an aircraft type damper, but the effect of viscosity change with temperature must be considered in this type of design.

BIBLIOGRAPHY

1. Bishop, R. E. D., and Gladwell, G. M. L., "The Receptances of Uniform and Non-Uniform Rotating Shafts," Journal of Mechanical Engineering Science, 1(1), pp. 78-91 (1959).

2. Bishop, R. E. D., and Gladwell, G. M. L., "The Vibration and Balancing of an Unbalanced Flexible Rotor," Journal of Mechanical Engineering Science, 1(1), pp. 66-77 (1959).

3. Bishop, R. E. D., "The Vibration of Rotating Shafts," Journal of Mechanical Engineering Science, 1(1), pp. 50-65 (1959).

4. Design Criteria for High-Speed Power-Transmission Shafts, Technical Documentary Report No. ASD-TDR-62-728, Part II, Air Force Systems Command, Wright-Patterson Air Force Base, Ohio, December 1964.

5. Design Manual - Supercritical-Speed Power-Transmission Shafts, Battelle Memorial Institute, Columbus, Ohio, 1965.

6. Parkinson, A. G., Jackson, K. L., and Bishop, R. E. D., "Some Experiments on the Balancing of Small Flexible Rotors: Part I - Theory," Journal of Mechanical Engineering Science, 5(1), pp. 114-128 (1963).

7. Parkinson, A. G., Jackson, K. L., and Bishop, R. E. D., "Some Experiments on the Balancing of Small Flexible Rotors: Part II - Experiments," Journal of Mechanical Engineering Science, 5(2), pp. 133-145 (1963).

8. USAAML Technical Report 65-34, An Investigation of the Behavior of Floating Ring Dampers and the Dynamics of Hypercritical Shafts on Flexible Supports, U.S. Army Aviation Materiel Laboratories, Fort Eustis, Virginia, June 1965.

DISTRIBUTION

US Army Materiel Command	10
US Army Mobility Command	5
US Army Aviation Materiel Command	6
Chief of R&D, DA	1
US Army Aviation Materiel Laboratories	30
US Army R&D Group (Europe)	2
US Army Human Engineering Laboratories	1
US Army Test and Evaluation Command	1
US Army Engineer Waterways Experiment Station	1
US Army Combat Developments Command, Fort Belvoir	2
US Army Combat Developments Command Transportation Agency	1
US Army Aviation School	1
US Army Tank-Automotive Center	2
US Army Aviation Test Board	3
US Army Aviation Test Activity	2
Air Force Flight Test Center, Edwards AFB	2
US Army Transportation Engineering Agency	1
Air Force Aeropropulsion Laboratory	1
Air Force Flight Dynamics Laboratory, Wright-Patterson AFB	1
Systems Engineering Group (RTD), Wright-Patterson AFB	4
Bureau of Naval Weapons, DN	22
Chief of Naval Research	2
David Taylor Model Basin	1
Commandant of the Marine Corps	1
Marine Corps Liaison Officer, US Army Transportation School	1
Ames Research Center, NASA	1
Lewis Research Center, NASA	1
NASA Representative, Scientific and Technical Information Facility	2
NAFEC Library (FAA)	2
Federal Aviation Agency, Washington, D. C.	1
Defense Documentation Center	20

APPENDIX I

HIGH-SPEED SHAFTING DESIGN BY ELECTRICAL ANALOGY METHOD

The design of the high-speed shaft by the electrical analogy method utilizes the information contained in this appendix.

Follow the outline beginning on Page 30 of Reference 4. Copies can be obtained from the Defense Documentation Center (DDC), Cameron Station, Bldg. 5, 5010 Duke Street, Alexandria, Virginia, 22314. Use the known shaft and damper parameters:

ℓ = 338.8 inches

D = 4.50 inches

d = 4.26 inches

W = 20 lb

K = 100 lb/inch

1. From equation (17), page 8, Reference 4,

$$f_{ss} = \sqrt{\frac{\pi}{2} \frac{g\,EI}{L^4 w} n^2}$$

$$= \frac{\pi}{2} \sqrt{\frac{386\ (10.6^{x10^6})\ 4\pi(4.50^4 - 4.26^4)}{(338.8)^4 (0.10)\ 64\pi(4.50^2 - 4.26^2)}}\ 5^2$$

= 107 cps (8)

2. From equation (33), page 19, Reference 4,

$$\lambda = 2\,L/n$$

$$= 2\ (338.8)/5$$

= 135 inches (9)

3. From equation (50), page 22, Reference 4,

$$Z_s = 0.109 f^{\frac{1}{2}} (D^2 - d^2)(D^2 + d^2)^{\frac{1}{4}}$$

$$= 0.109\ (107)^{\frac{1}{2}}\ (4.5^2 - 4.26^2)\ (4.5^2 + 4.26^2)^{\frac{1}{4}}$$

$$= 5.7 \text{ lb/ips} \qquad (10)$$

4. From equation (51), page 22, Reference 4,

$$X_m = + j\ 2\ \pi\ f\ W/g$$

$$= + j\ (2\pi)\ 107\ (20)/386$$

$$= + j\ 34.9 \qquad (11)$$

5. From equation (52), page 22, Reference 4,

$$X_k = - j\ K/2\ \pi f$$

$$= - j\ (100)/2\pi 107$$

$$= - j\ 0.1486 \qquad (12)$$

6. Combining the spring and mass reactances and dividing by the characteristic shaft impedance give the normalized impedance of the damper.

$$X_n = (X_k + X_m)\ Z_s$$

$$= (+ j\ 34.9 - j\ 0.1486)/6.0$$

$$= + j\ 5.8 \qquad (13)$$

7. To cancel reactances, the damper must be placed such that the end of the shaft (which is a universal joint having an infinite reactance) looks to the damper like a reactance of -j 5.8. Note that this is the negative of the damper reactance. The Smith chart shows that a normalized reactance of -j 5.8 corresponds to 0.222λ, while an infinite reactance corresponds to 0.250λ.

8. Therefore, the damper must be placed at 0.250λ - 0.222λ, or 0.028λ from one end of the shaft.

9. Converting from damper location in wavelengths to inches gives

$$X = 0.028\lambda$$

$$= 0.028\ (135)$$

$$= 3.7 \text{ inches} \qquad (14)$$

The basic damper parameters as established by this procedure are summarized as follows:

Number of dampers	1	
Damper location	3.7 in. from end	X
Damper coefficient (Approx. 3 x Z_{ss})	18.0 lb/ips	C
Damper weight	20.0 lb	W
Damper spring rate	100 lb/in.	K

APPENDIX II

HIGH-SPEED SHAFTING DESIGN BY USE OF THE DESIGN MANUAL, REFERENCE 5

The previous example illustrates the solution of a relatively simple shaft system by the use of the Electrical Analogy method. The pin-ended shaft immediately eliminates much of the work relating fixed ends, or equivalent cantilever ends, to a configuration that can be handled by the electrical power transmission line theory. Even with this simplification, it is apparent that further improvement in the application of the theory would be desirable. The design manual was prepared by Battelle because the need for improvement of design procedure was recognized.

The design manual contains empirical data obtained from a great number of tests and is presented in chart form so that a designer has merely to pick the desired values from the charts based on the known information of his system.

There is no reference to the electrical transmission line theory or the Smith chart for the solution of the voltage standing wave ratios, although it should be remembered that this procedure was instrumental in obtaining successful shaft operation from which the charts were made.

The application of the design manual charts to determine the characteristics of the full-size shaft and damper is now illustrated in the following example:

1. The first critical speed of the shaft can be calculated using formula (3), page 6, Reference 5,

$$N_{ss} = 60 \frac{\pi}{2} \sqrt{\frac{g\ EI}{L^4 w}}\ n^2 \qquad (15)$$

or it can be picked from the chart on page 9, Reference 5, by using the known diameter and length and reading the rpm; in this case, 28 ft & 4.50 in. OD x 4.26 in. ID.

$$d/D = 4.26/4.50 = .95 \text{ ratio} \qquad \boxed{260 \text{ rpm}} \qquad (16)$$

2. Other critical speeds can be obtained from the first by the ratio of rpm at first x n^2 for any other speed, or use chart on page 11, Reference 5.

Mode	1st	2nd	3rd	4th	5th
rpm	260	1040	2340	4160	6500

3. Damper parameters

a. Location along the shaft, χ

Refer to Table 2, page 14, Reference 5, and opposite the range of criticals 1 - 5 read the number of dampers required, 1, and in the next column the location from one end of the shaft, 0.05L.

.05 x 338.8 = $\boxed{16.94}$ inches from end of shaft (17)

b. Damping coefficient, C

Refer to Table 3, page 16, Reference 5, and opposite the shaft diameter of 4.50 inches and in column for a d/D ratio of .95, read $\boxed{1.665}$ as a constant.

Multiply the constant by the square root of the shaft rotational speed in revolutions per second to obtain the damping coefficient of the damper.

5th critical speed = 6500 rpm = 108 RPS

$\sqrt{108}$ x 1.665 = $\boxed{17.3 \frac{\text{lb/sec}}{\text{in.}}}$ C (18)

c. Damper weight, W

See page 18, Reference 5, where it is recommended that the damper weight should not exceed 1/3 the weight of the shaft. Refer to Table 5, page 19, Reference 5, and again opposite shaft diameter of 4.5 inches and in column d/D ratio of .95, read $\boxed{1.861}$ as weight constant.

Multiply the weight constant by the shaft length in feet to obtain the shaft weight.

$1.861 \times 28 = 52.2$ lb

$1/3 \times 52.2 =$ **17.4 lb damper wt.** W (19)

d. Damper spring rate, K

General statement here indicates that the spring rate should be kept low to reduce the load transmitted to the structure.

An arbitrary value will be used:

100 lb/inch K

The basic damper parameters have been established and can be summarized as follows:

Number of dampers	1	
Damper location	17 inches from end	X
Damping coefficient	17.3 lb/sec/in.	C
Damper weight	17.4 lb	W
Damper spring rate	100 lb/in.	K

APPENDIX III

EXPERIMENTAL BALANCING THEORY

MODAL BALANCING THEORY

In the series of papers by Bishop, Gladwell, et al, References 1,2,3,6, and 7, the response of a rotating shaft is expressed as an infinite summation of modal responses. The stead-state deflection of the geometric centerline of the shaft is

$$\bar{w}(x,t) = \sum_{n=1}^{\infty} \bar{\xi}_n(t)\,\psi_n(x) \tag{20}$$

where the vector displacement, $\bar{w}$, is referred to a fixed set of axes with origin at the bearing centerline, and the series of functions, $\psi_n(x)$, is a set of orthogonal mode shapes for the shaft.

The modal response vector, $\bar{\xi}_n(t)$, resulting from both mass unbalance and shaft runout is

$$\bar{\xi}_n(t) = \frac{\left(\bar{a}_n\Omega^2 + \bar{\epsilon}_n\omega_n^2\right)\epsilon^{i(\Omega t - \xi_n)}}{\sqrt{\left[\left(\omega_n^2 - \Omega^2\right)^2 + 4\mu_n^2\omega_n^2\Omega^2\right]}} \tag{21}$$

where

$$\xi_n = \tan^{-1}\left(\frac{2\mu_n\omega_n\Omega}{\omega_n^2 - \Omega^2}\right)$$

μ_n = n^{th} mode damping ratio (external damping)

ω_n = n^{th} mode natural frequency

Ω = shaft rotational speed.

The displacement of the mass axis from the geometric axis of the shaft is a vector given by

$$\bar{a}(x) = \sum_{n=1}^{\infty} \bar{a}_n\psi_n(x), \tag{22}$$

and the displacement of the elastic axis of the shaft from the bearing centerline, referred to as shaft runout or elastic unbalance, is the vector function

$$\bar{\varepsilon}(x) = \sum_{n=1}^{\infty} \bar{\varepsilon}_n \psi_n(x). \tag{23}$$

The forcing function from the mass and elastic unbalance can be considered a general defect with both magnitude and angular phase that are frequency dependent. Let

$$\bar{F}_r(\Omega) = \bar{a}_n \Omega^2 + \bar{\varepsilon}_n \omega_n^2; \tag{24}$$

then

$$\bar{\varepsilon}_n(t) = \frac{\bar{F}_n(\Omega) e^{i(\Omega t - \xi_n)}}{\sqrt{\left[\left(\omega_n^2 - \Omega^2\right)^2 + 4\mu_n^2 \omega_n^2 \Omega^2\right]}}. \tag{25}$$

Discrete masses, m_i, attached to the shaft at an axial station, x_i, at a distance from the geometric axis of the shaft, r_i, are represented as a mass distribution.

$$m(x)b(x) = \sum_i m_i r_i \, \delta(x - x_i), \tag{26}$$

which has a model series representation

$$b(x) = \sum_{n=1}^{\infty} b_n \psi_n(x) \tag{27}$$

where

$$b_n = \frac{1}{M_n} \sum_i m_i r_i \psi_n(x_i)$$

$$M_n = \int_0^L m(x) \quad [\psi_n(x)]^2 \quad dx$$

$m(x)$ = mass per unit length of shaft.

From equation (20), the component of shaft distortion due to a single mode lies entirely in one axial plane, although both the orientation of this plane with respect to the shaft and the orientation of the forcing function, $\bar{F}_r(\Omega)$, with respect to the shaft are functions of frequency. To balance the shaft in the n^{th} mode at $\Omega = \omega_n$ requires that the plane of the forcing function with respect to the shaft be located and that the balance weights be adjusted so that

$$M_n \left| \bar{F}_n(\omega_n) \right| + \sum_i m_i r_i \psi_n(x_i) \omega_n^2 = 0. \tag{28}$$

When the balance weights are selected according to equation (28), the residual vibration is given by

$$\bar{\xi}_n(t) = \frac{\bar{\varepsilon}_n \left(\omega_n^2 - \Omega^2 \right) e^{i(\Omega t - \xi_n)}}{\sqrt{\left[\left(\omega_n^2 - \Omega^2 \right)^2 + 4\mu_n^2 \omega_n^2 \Omega^2 \right]}} . \tag{29}$$

This result is important because it indicates that balance weights can be used to remove the modal component of the mass unbalance completely and to cancel the elastic unbalance at any particular speed, i.e., $\Omega = \omega_n$. However, there will always be a residual vibration when $\Omega \neq \omega_n$ resulting from the elastic unbalance.

Equation (28) also indicates that any single mode can be balanced by one weight located at any position on the shaft so long as it does not correspond to a node. The location requiring the smallest amount of weight is obviously an antinode, and at any other position the effectiveness of a balance weight is determined by the mode shape at that location.

However, a single applied weight will, in general, affect the balance of all other modes as well as the one for which the weight is intended. It can be shown that in order to balance one mode and also to make sure that k other modes are not affected requires a minimum of (k + 1) balance weights and locations. These weights and locations must satisfy the following set of (k + 1) simultaneous equations:

$$\sum_{i=1}^{(k+1)} m_i r_i \psi_n(x_i) = - \frac{M_n}{\omega_n^2} |F(\omega_n)| \qquad (30)$$

$$\sum_{i=1}^{k+1} m_i r_i \psi_j(x_i) = 0 \quad , \qquad (31)$$

where the subscript n is the number of the mode being balanced and the subscript j represents each of the k other modes. In practice, the equation (31) determines the relative magnitudes of the weights at each of the balancing stations, and their magnitude is found by experimentally balancing the shaft, thereby satisfying equation (30).

APPLICATION OF THEORY FOR CH-47A SHAFT

As discussed previously in the report, the balancing procedure for the CH-47A shaft is intended to balance only the third, fourth, and fifth critical speeds without regard to the effect of the applied weights on the first or second critical speeds. It was also found from experience that in order to minimize the required balancing, it was desirable to use balance weights and positions to accomplish the following:

1. Balance the third mode and not affect the fourth.

2. Balance the fourth mode and not affect the third or fifth.

3. Balance the fifth mode and not affect the third or fourth.

Since there are a total of three different modes, three balance positions were required. These positions were selected with the goals of having one position at an antinode of each

of the modes for maximum effectiveness and also to reduce the modal coupling as much as possible to simplify the solution of equations (30) and (31). The selected positions were:

$$X_1 = 185 \text{ inches}$$

$$X_2 = 222 \text{ inches}$$

$$X_3 = 140 \text{ inches}$$

The mode shapes used for these positions were:

3rd Mode	4th Mode	5th Mode
$\psi_3(x_1) = 1.0$	$\psi_4(x_1) = 0$	$\psi_5(x_1) = -1.0$
$\psi_3(x_2) = 0$	$\psi_4(x_2) = 1.0$	$\psi_5(x_2) = 0$
$\psi_3(x_3) = 0$	$\psi_4(x_3) = -1.0$	$\psi_5(x_3) = +1.0$

If we denote $m_{\alpha\beta}$ as the balance mass placed at Station X_β to balance the α mode, equations (30) and (31) for the third mode when all balance weights have the same effective radius, $r_i = R$, become

$$m_{31}\psi_3(x_1) + m_{32}\psi_3(x_2) = -\frac{M_3}{\omega_3^2 R}\left|\bar{F}(\omega_3)\right| \qquad (32)$$

$$m_{31}\psi_4(x_1) + m_{32}\psi_4(x_2) = 0 \ . \qquad (33)$$

There will be a unique solution to this set of equations as long as the determinant of the coefficient is not equal to zero.

$$\begin{vmatrix} \psi_3(x_1) & \psi_3(x_2) \\ \psi_4(x_1) & \psi_4(x_2) \end{vmatrix} \neq 0 . \tag{34}$$

The solution to the above equations for the listed data is

$$m_{31} = \frac{-M_3 \, |\bar{F}(\omega_3)|}{\omega_3{}^2 R}$$

$$m_{32} = 0, \tag{35}$$

thereby requiring a single weight at Station 185. No weight is calculated for Station 140, since no effort was made to uncouple the third and fifth modes.

Similar calculations for the fourth and fifth modes give

$$m_{41} = m_{43} = 0$$

$$m_{42} = \frac{-M_4 \, |\bar{F}(\omega_4)|}{\omega_4{}^2 R} \tag{36}$$

to allow balancing at the fourth mode without affecting the third or fifth and

$$m_{51} = 0$$

$$m_{52} = m_{53} = \frac{M_5 \, |\bar{F}(\omega_4)|}{\omega_4{}^2 R} \tag{37}$$

to balance the fifth mode without disturbing the third or fourth modes. It can be seen that the fifth mode is balanced by the weight at Station 140, m_{53}; and since this station is also an antinode for the fourth mode, it is necessary to use an equal weight at Station 222, m_{52}, to maintain the fourth mode balance.

Since the sign convention for the mode shapes is arbitrary, the absolute sign of the solution for the masses has no meaning; but a change in sign for the mass at different locations indicates that weight should be placed on the opposite side of the shaft from the reference weight. The angular placement of the reference mass must be determined from the orientation of the plane of unbalance for that node.

APPENDIX IV

MOTION AND BALANCING OF A FLEXIBLE SHAFT WITH DISTRIBUTED UNBALANCE AND INITIAL IMPERFECTIONS

INTRODUCTION

The data included in this appendix were prepared for the Vertol Division by Maurice A. Brull, Engineering Consultant.

The purpose of the present work is to provide an analytical theory for predicting the motion and stresses in a shaft operating at critical or hypercritical speeds and to furnish a theoretical basis for the development of a suitable dynamic balancing procedure. This report contains the theoretical analysis which will later be correlated to the experimental effort.

In this preliminary report, the equations of motion for a flexible shaft with distributed unbalance and arbitrary initial imperfections are developed; these equations are formulated in general terms to allow the use of any convenient coordinate system. These equations are then specialized for a special rotating coordinate system which will be convenient for use in interpreting experimental data. A solution to the equations is then obtained which shows the relationships between the unbalance and initial deflection and the amplitudes of the various whirling modes.

DERIVATION OF THE GENERAL EQUATIONS

The equations of motion are now developed for the rotating shaft, expressed in a general rotating or nonrotating coordinate system. Referring to Figure 77, page 153, the following is noted:

0 denotes the line between the end supports of the shaft.

0' is the position (at rest) of the center of any cross section.

0" is the position at any instant of the center of the

cross section when an elastic displacement has taken place.

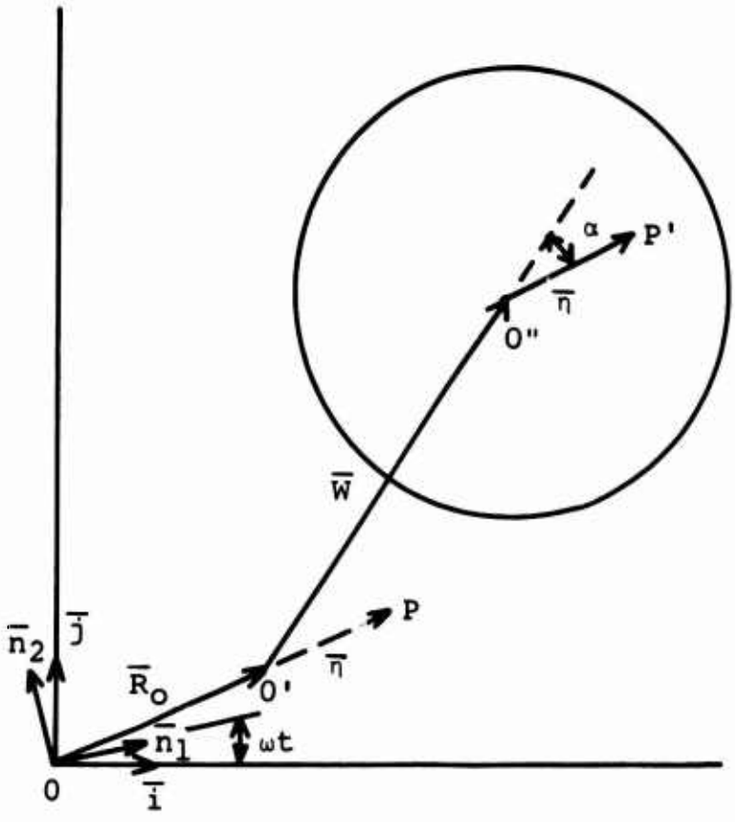

FIGURE 77. DIAGRAM ILLUSTRATING MOTION OF TYPICAL SHAFT CROSS SECTION.

P is the position of the mass-center of the cross section when no elastic displacement is present.

P' is the instantaneous deflected position of the cross-center of the cross section. The following notation is adopted:

$\bar{R}_o$ = position vector of cross-section center with respect to line of support due to initial deflection

$\bar{W}$ = displacement vector of cross-section center due to shaft flexibility

$\bar{R}$ = position vector of mass-center of cross section at any instant

$\bar{\eta}$ = position vector of mass-center of cross section with respect to center of cross section

t = time

$\bar{V}_o$ = absolute velocity of geometric center of cross section

$\bar{V}$ = absolute velocity of mass-center of cross section

$\bar{a}$ = absolute acceleration of mass-center of cross section

A = cross-sectional area

ρ = mass-density of shaft material

E = Young's modulus

I = moment of inertia of shaft about a diameter

$\bar{F}_e$ = net elastic force vector acting on a unit span of shaft

c = damping coefficient per unit span of shaft

x = coordinate along line of supports of shaft

$\bar{i},\bar{j},\bar{k}$ = a set of unit vectors fixed in space, with $\bar{k}$ along the line of supports

$\bar{n}_1,\bar{n}_2$ = unit vectors fixed in the shaft and rotating with it

$\bar{\Omega}$ = angular velocity vector for shaft

$\bar{\Omega}_f$ = angular velocity vector for any rotating frame of reference

ω = rate of rotation of shaft

It should be noted that $\bar{W}$ does not include any sag due to the shaft weight, since elastic forces induced by this sag will be in equilibrium with the dead weight.

The instantaneous position vector $\bar{R}$ of the mass-center of an arbitrary cross section may be expressed as

$$\bar{R} = \bar{R}_o + \bar{W} + \bar{\eta} \quad , \tag{38}$$

and the absolute velocity of the mass-center is therefore

$$\bar{V} = \frac{d\bar{R}}{dt} \tag{39}$$

where the differential operator $\frac{d(\ )}{dt}$ is with respect to a Newtonian frame of reference (i.e., fixed in space); in the present case, the frame of reference $\bar{i}$, $\bar{j}$, $\bar{k}$ is suitable. It is well known that if we choose to express the vectors $\bar{R}$ and $\bar{V}$ (or any other vector function) in a frame of reference which is rotating with angular velocity $\bar{\Omega}_f$ with respect to fixed space, the absolute differential operator may be expressed as

$$\frac{d(\ )}{dt} = \frac{\partial(\ )}{\partial t} + \bar{\Omega}_f \times (\ ) \tag{40}$$

where $\frac{\partial(\ )}{\partial t}$ now denotes differentiation with respect to the rotating frame of reference. From equations (38), (39), and (40)

$$\bar{V} = \frac{\partial R_o}{\partial t} + \frac{\partial \bar{W}}{\partial t} + \frac{\partial \bar{\eta}}{\partial t} + \bar{\Omega}_f \times (\bar{R}_o + \bar{W} + \bar{\eta}) \tag{41}$$

is obtained.

It should be noted that the velocity of the cross-section center

can be obtained by setting $\bar{\eta}$ equal to zero in equation (41). Then

$$\bar{V}_o = \frac{\partial \bar{R}_o}{\partial t} + \frac{\partial W}{\partial t} + \bar{\Omega}_f X(\bar{R}_o + \bar{W}) . \tag{42}$$

The absolute acceleration of the cross-section mass-center is obtained as

$$\bar{a} = \frac{d\bar{V}}{dt} = \frac{\partial \bar{V}}{\partial t} + \bar{\Omega}_f X \bar{V} , \tag{43}$$

and substituting equation (41) in equation (43) gives

$$\bar{a} = \frac{\partial^2 \bar{R}_o}{\partial t^2} + \frac{\partial^2 \bar{W}}{\partial t^2} + \frac{\partial^2 \bar{\eta}}{\partial t^2} + 2\bar{\Omega}_f X\left[\frac{\partial \bar{R}_o}{\partial t} + \frac{\partial \bar{W}}{\partial t} + \frac{\partial \bar{\eta}}{\partial t}\right] +$$

$$\frac{\partial \Omega_f}{\partial t} X(\bar{R}_o + \bar{W} + \eta) + \bar{\Omega}_f X[\bar{\Omega}_f X(\bar{R}_o + \bar{W} + \bar{\eta})] . \tag{44}$$

The equation of motion for an element of shaft of length dx in the spanwise direction may then be written in the form

$$\bar{F}_e dx - C(X)\bar{V}_o dx = \rho A \bar{a} dx . \tag{45}$$

Substituting for $\bar{a}$ and $\bar{V}_o$ from equations (42) and (45) gives

$$\bar{F}_e - C(X)\left[\frac{\partial \bar{R}_o}{\partial t} + \frac{\partial \bar{W}}{\partial t} + \Omega_f X(\bar{R}_o + \bar{W})\right]$$

$$= \rho A\left[\frac{\partial^2}{\partial t^2}(\bar{R}_o + \bar{W} + \bar{\eta}) + 2\bar{\Omega}_f X\frac{\partial}{\partial t}(\bar{R}_o + \bar{W} + \bar{\eta}) +\right.$$

$$\left.\frac{\partial \bar{\Omega}_f}{\partial t} X(\bar{R}_o + \bar{W} + \bar{\eta}) + \bar{\Omega}_j X\{\bar{\Omega}_f X(\bar{R}_o + \bar{W} + \eta)\}\right] . \tag{46}$$

Note that C(X) is the damping coefficient per unit span of shaft. For the damper design of interest here, the damping force is proportional to the velocity of the cross-section center, given by equation (42). If it is assumed that the elastic

center of the cross section is located at the geometric center, the elastic force (per unit span) which may be obtained from elementary beam theory for a slender shaft is given by

$$\bar{F}_e = -EI\frac{\partial^4 \bar{W}}{\partial x^4} \cdot \tag{47}$$

For a short, stubby shaft or very thin-walled hollow shafts, it may be necessary to account for the transverse shear deformation and modify equation (47) according to the Timoshenko beam theory. This is, however, not important for the cases of interest here, and the general equation of motion is now obtained by substituting equation (47) in equation (46) and rearranging forms. The result is

$$EI\frac{\partial^4 \bar{W}}{\partial x^4} + C(X)\left[\frac{\partial \bar{W}}{\partial t} + \bar{\Omega}_f X \bar{W}\right] + \rho A\left[\frac{\partial^2 \bar{W}}{\partial t^2} + 2\Omega_f X\frac{\partial \bar{W}}{\partial t} + \right.$$

$$\left.\frac{\partial \bar{\Omega}_f}{\partial t} X \bar{W} + \bar{\Omega}_f X(\bar{\Omega}_f X \bar{W})\right] = -\rho A\left[\frac{\partial^2}{\partial t^2}(\bar{R}_o + \bar{\eta}) + 2\bar{\Omega}_f X\frac{\partial}{\partial t}(\bar{R}_o + \bar{\eta}) + \right.$$

$$\left.\frac{\partial \bar{\Omega}_f}{\partial t} X(\bar{R}_o + \bar{\eta}) + \bar{\Omega}_f X\{\bar{\Omega}_f X(\bar{R}_o + \bar{\eta})\}\right] - C(X)\left[\frac{\partial \bar{R}_o}{\partial t} + \bar{\Omega}_f X \bar{R}_o\right] \cdot \tag{48}$$

Equation (48) is valid for any coordinate system provided the correct angular velocity vector $\bar{\Omega}_f$ of the reference frame is used wherever indicated. This equation is equally valid whether the shaft is whirling (i.e., deflection of constant magnitude in time) or undergoing a combination of whirling and vibration. It can therefore be used to study the transient behavior as well as the steady-state characteristics of rotating shafts.

The problem of interest here is that of whirling shafts, and several different coordinate systems are suitable for use. Thus, the unit vectors $\bar{i},\bar{j},\bar{k}$, which are fixed in space, may be used, or any convenient frame of reference rotating with the shaft may be used. Since the experimental program measures various quantities with respect to axes fixed in the shaft, it is particularly convenient to use such a frame of reference, since it will make the interpretation of theory and experiment considerably easier. We therefore select the reference frame $\bar{n}_1,\bar{n}_2,\bar{k}$, in which $\bar{k}$ is along the line of supports, while $\bar{n}_1$ and $\bar{n}_2$ are fixed in the shaft cross section and therefore rotate with the shaft at an angular rate ω. It should be noted that

the use of vector analysis requires that the reference frames used be right-handed. It also follows that ω is positive when clockwise about the $\bar{k}$ axis. At time zero, $\bar{n}_1$ and $\bar{n}_2$ coincide with $\bar{i}$ and $\bar{j}$; and at any subsequent instant, $\bar{n}_1$ and $\bar{n}_2$ are rotated by an angle ωt from $\bar{i}$ and $\bar{j}$. For this particular frame of reference, clearly

$$\bar{\Omega}_f = \bar{k}\omega \, . \tag{49}$$

It is clear that, with respect to the frame of reference, the initial deflection is constant with time, so that $(\partial \bar{R}_o/\partial t) = 0$ and $\bar{R}_o$ may be expressed as

$$\bar{R}_o = \bar{n}_1 u_0 + \bar{n}_2 v_0 \tag{50}$$

where u_0 and v_0 are functions of X only. Similarly, the mass unbalance vector $\bar{\eta}$ is also constant with time in the reference frame, and

$$\bar{\eta} = \bar{n}_1 \eta_1 + \bar{n}_2 \eta_2 \tag{51}$$

can be written.

Finally, note that the elastic deflection $\bar{W}$ may be expressed as

$$\bar{W} = \bar{n}_1 u + \bar{n}_2 v \tag{52}$$

and note that, for whirling, the magnitude of $\bar{W}$ is constant and $(\partial \bar{W}/\partial t) = 0$. The equation of motion (48) therefore reduces to

$$EI\frac{d^4 W}{dx^4} + C(X)\omega \bar{k}x\bar{W} + \rho A\omega^2 \bar{k}x(\bar{k}x\bar{W})$$

$$= -\rho A\omega^2 \bar{k}x[\bar{k}x(\bar{R}_o + \bar{\eta})] - C(X)\omega \bar{k}x\bar{R}_o \, . \tag{53}$$

Now, substitute equations (50), (51), and (52) in equation (53) and note that from the definition of vector product, $\bar{k}x\bar{n}_2 = -\bar{n}_1$ can be written (see Figure 77). Thus, a vector equation with components in the $\bar{n}_1$ and $\bar{n}_2$ directions is obtained, and by setting each component equal to zero, the following two equations for unknowns elastic displacements u and v are obtained:

$$EI\frac{d^4u}{dx^4} - \rho A\omega^2 u - \omega C(x)v = \rho A\omega^2(u_o + \eta_1) + \omega C(x)v_o \quad (54)$$

$$EI\frac{d^4v}{dx^4} - \rho A\omega^2 v + \omega C(x)u = \rho A\omega^2(v_o + \eta_2) - \omega C(x)u_o . \quad (55)$$

Equations (54) and (55) are the governing equations to be solved for the unknown functions u(x) and v(x), which give the amplitude and orientation of the whirling shape as functions of the unbalance and initial deflections.

SOLUTION FOR ELASTIC DISPLACEMENTS

It is convenient, because of the form of equations (54) and (55), to obtain their solution in the form of an infinite series in terms of the bending mode shapes for a beam having the boundary conditions prescribed for the whirling shaft. It should be emphasized that the use of these eigenfunctions for beam bending vibrations does not imply in any way that the shaft is undergoing lateral vibrations. Rather, these functions are simply convenient on a purely mathematical basis to use as building blocks for the solution of the differential equations. It is also pointed out that, for the case of zero damping, equations (54) and (55) decouple and each beam mode shape becomes a homogeneous solution of the equations. This indicates that the allowed whirling shapes (i.e., whirling eigenfunctions) are identical to the lateral vibration modes, but, again, this does not imply that bending vibrations are present.

Therefore, the eigenfunctions $X_n(x)$ will be used for lateral beam vibrations, which are defined by the equation

$$X_n^{lv} - \frac{\rho A}{EI}\omega n^2 X_n = 0, \quad (56)$$

together with appropriate boundary conditions. For example, in the case of true simple support on the ends $x = o_1 L$, the functions become

$$X_n(x) = \sin\frac{n\pi x}{L} \quad (n = 1,2....) . \quad (57)$$

It should be noted that ω_n are the critical speeds of the shaft in radians per second, which happen to coincide with the bending

natural frequencies. For the case of simple end supports, it is clear from equations (56) and (57) that these critical speeds are given by

$$\omega_n = \sqrt{\frac{EI}{\rho A}\frac{n^2\pi^2}{L^2}} \tag{58}$$

The solution of equations (54) and (55) may easily be carried out for arbitrary damping distribution c(x) by using the mode shapes of equation (56) together with the Galerkin method. This will, however, lead to coupled algebraic equations for the coefficients in the series for u(x) and v(x) which will add unnecessary complexity to the numerical work. An alternate, approximate procedure suggests itself, which will lead to a much simpler solution and still yield good accuracy. Thus, if it is assumed that the shaft is whirling in its mode, with unit amplitudes, it is easily shown that the total damping force over the entire shaft is given by

$$\bar{F}_{td} = \bar{n}_1\omega \int_0^L c(x)X_n(x)dx - \bar{n}_2\omega\int_0^L c(x)X_n(x)dx \,. \tag{59}$$

It follows, therefore, that the average damping force per unit length of shaft for a unit amplitude in the n^{th} mode is given by

$$\bar{F}_d^{\,k} = \bar{n}_1\omega c_n - \bar{n}_2\omega c_n \tag{60}$$

where

$$c_n = 1/L \int_0^L c(x)X_n^{\,2}(x)dx^* \,. \tag{61}$$

Equation (60) indicates that, for each mode, the variable damping coefficient c(x) of equations (54) and (55) may be replaced by an equivalent constant damping c_n given by equation (61). It should be noted that, if the damping is provided by a single damper of coefficient k at $x = \zeta$, the fraction c(x) may be written in the form

$$c(x) = k\,(x - \zeta) \tag{62}$$

*This is a weighted average force calculated so that the dissipation of energy due to damping keeps its true value.

where $\delta(x - \zeta)$ is the Dirac delta function at ζ. Equation (61) then gives

$$c_n = (K/L)X_n^2(\zeta) . \tag{63}$$

Similarly, for a number m of dampers located at coordinates ζ_i,

$$c_n = \sum_{i=1}^{m} (k_i/L)X_n^2(\zeta_i)$$

where k_i are the constants of individual dampers.

If the equivalent uniform damping coefficient of equation (61) is now substituted in equations (54) and (55),

$$EI\frac{d^4u}{dx^4} - \rho A\omega^2 u - \omega c_n v = \rho A\omega^2(u_0 + \eta_1) + \omega c_n v_0 \tag{64}$$

$$EI\frac{d^4v}{dx^4} - \rho A\omega^2 v + \omega c_n u = \rho A\omega^2(v_0 + \eta_2) - \omega c_n u_0 . \tag{65}$$

Now a solution is sought for u and v in the form of an infinite series in terms of the functions $X_n(x)$ defined previously; thus, write

$$u(x) = \sum_{n=1}^{\infty} AnXn(x)$$

$$v(x) = \sum_{n=1}^{\infty} BnXn(x). \tag{66}$$

It is convenient to expand the functions u_0, v_0, η_1 and η_2 in series in terms of the functions $X_n(x)$. This is possible because of the completeness and orthogonality of these eigenfunctions. Then

$$u_o(x) = \sum_{n=1}^{\infty} a_n X_n(x), \qquad a_n = \frac{\int_o^L u_o(x) Xn(x)\,dx}{\int_o^L Xn^2(x)\,dx}$$

$$\nu_o(x) = \sum_{n=1}^{\infty} b_n X_n(x), \qquad b_n = \frac{\int_o^L \nu_o(x) Xn(x)\,dx}{\int_o^L X_n^2(x)\,dx} \qquad (67)$$

$$\eta_1(x) = \sum_{n=1}^{\infty} e_n X_n(x), \qquad e_n = \frac{\int_o^L \eta_1(x) Xn(x)\,dx}{\int_o^L X_n K(x)\,dx}$$

$$\eta_1(x) = \sum_{n=1}^{\infty} g_n X_n(x), \qquad g_n = \frac{\int_o^L \eta_2(x) Xn(x)\,dx}{\int_o^L X_n K(x)\,dx} \qquad (68)$$

Substituting equations (66), (67), and (68) in equations (64) and (65) gives, after making use of equations

$$\sum_{n=1}^{\infty} \{A_n \rho A(\omega_n^2 - \omega^2) - \omega C_n B_n\} X_n(x) = \sum_{n=1}^{\infty} \{\rho A \omega^2 (a_n + e_n) + \omega C_n b_n\} X_n(x),$$

$$\sum_{n=1}^{\infty} \{B_n \rho A(\omega_n^2 - \omega^2) + \omega C_n A_n\} X_n(x) = \sum_{n=1}^{\infty} \{\rho A \omega^2 (b_n + y_n) - \omega C_n a_n\} X_n(x).$$

Since these equations must be satisfied for all values of x within the interval $o \le x \le L$, coefficients of like terms must be equated; thus, algebraic equations are obtained for each of the sets of coefficients A_n and B_n. After dividing by ρA, these equations may be written in the form

$$(\omega_n^2-\omega^2)A_n - \omega\gamma_n B_n = \omega^2(a_n+e_n)+\omega\gamma_n b_n$$

$$\omega\gamma_n A_n+(\omega_n^2-\omega^2)B_n = \omega^2(b_n+y_n)-\omega\gamma_n b_n \qquad (69)$$

where γ_n is a reduced damping ratio defined as

$$\gamma_n = \frac{Cn}{\rho A} . \qquad (70)$$

Equations (69) are easily solved for the elastic displacement amplitudes; the result is

$$A_n = \frac{(\omega_n^2-\omega^2)[\omega^2(a_n+e_n)+\omega\gamma_n b_n]+\omega^2\gamma_n[\omega(b_n+g_n)-\gamma_n a_n]}{(\omega_n^2-\omega^2)^2+\omega^2\gamma_n^2} \qquad (71)$$

$$B_n = \frac{(\omega_n^2-\omega^2)[\omega^2(b_n+gn)-\omega\gamma_n a_n]-\omega^2\gamma_n[\omega(a_n+e_n)+\gamma_n b_n]}{(\omega_n^2-\omega^2)^2+\omega^2\gamma_n^2} . \qquad (72)$$

The substitution of equations (71) and (72) in Equations (66) yields the complete solution for u(x) and v(x). It is seen that, if the unbalance vector $\bar{n}(x)=\bar{n}_1\eta_1(x)+\bar{n}_2\eta_2(x)$ and the initial deflection vector $\bar{R}_0(x)=\bar{n}_1U_0(x)+\bar{n}_2V_0(x)$ are known, the coefficients A_n and B_n are easily obtained from the coefficients a_n, b_n, e_n and g_n which represent the modal contributions of the functions u_o, v_o, η_1, and η_2.

INTERPRETATION OF EXPERIMENTAL MEASUREMENTS

As has been shown previously, the determination of whirling amplitudes is relatively easy when the unbalance and initial deflection are known. The solution of the problem, however, does not stop here, because the distributed unbalance and the initial deflection are not necessarily known. In fact, the real problem is to determine these initial imperfections from experimental data and to balance the shaft in such a way as to minimize their effects. Thus, the coefficients a_n, b_n, e_n, and g_n must now be determined from suitable measurements. It is clear at the outset that only a limited number of these coefficients can be determined, and it is logical to limit the values of n considered to the number of critical speeds contained within the speed range of interest. Thus, if a shaft which will operate at speeds up to the fifth critical is to be balanced, it is likely that only the modal contributions up to the fifth mode in the unbalance and initial deflection will be of importance. Thus, if the shaft is to be operated up to the m^{th} critical speed, A_m coefficients corresponding to the modal contributions in the first m modes of the four "imperfection" functions u_o, v_o, η_1, and η_2 must be determined. Note that the functions u_o and v_o (and therefore the coefficients a_n and b_n) may be determined from static measurements of the initial deflection in two planes fixed with respect to the shaft. This reduces the number of unknown coefficients to 2m. It is clear that if the shaft is operated at m different speeds within the range of interest and the deflections u and v are measured at a representative point, a set of 2m simultaneous equations which will relate the coefficients e_n and g_n to the measured amplitudes may be written with the aid of equations (66), (71), and (72). It is therefore possible, in principle, to determine the unknown unbalance from experimental data if the initial deflection can first be obtained from static measurements. The m speeds selected for the measurements should cover, insofar as possible, the entire range of operation of the shaft. In fact, it may be advantageous to make all measurements at the critical speeds, as this may, in some cases, simplify the calculations. The values of the coefficients A_n and B_n of equations (71) and (72) are now denoted by A_{nk} and B_{nk} when the speed ω is chosen equal to the k^{th} critical shaft speed. It is clear from equations (71) and (72) that, when we operate at the k^{th} critical speed, the other modes of deformation will still be present. (If this were not so, it would be possible to show that $A_{nk}=B_{nk}=o$ for $n \neq k$.) It may be possible, however, that for a specific problem, the amplitude of modes other than that

corresponding to the operating critical speed will be small. This would be expressed by the inequalities

$$\begin{aligned} A_{nk} &<< A_{kk} \\ B_{nk} &<< B_{kk} \end{aligned} \tag{73}$$

In such a case, it would be permissible to neglect all modes except the k^{th}, and the deflections would be given by

$$\begin{aligned} U_k(x) &= \frac{1}{\gamma k} [\omega_k(b_k+g_k) - \gamma_k a_k] X_k(x) \\ V_k(x) &= \frac{1}{\gamma k} [\omega_k(a_k+e_k) + \gamma_k b_k] X_k(x). \end{aligned} \tag{74}$$

It is clear that, if U_k and V_k are measured at the critical speed ω_k, and if a_k and b_k (k=1,2..m) are known from the static measurements, then equation (74) can be used to solve for the modal unbalance coefficients e_k and g_k. Furthermore, the solution is now very easy to carry out, since each one of equation (74) only involves one of the unknowns and the solution of simultaneous equations is no longer required. This great simplification hinges upon the satisfaction of the inequalities (73), which in turn depends on the shaft properties.

It has been shown that the determination of the unbalance is possible but requires both static deflection measurements and dynamic measurements. The experimental determination of the static deflection in two planes is a fairly simple matter under laboratory conditions, but it may be difficult to accomplish in production. It would therefore be desirable to eliminate this step so that only a dynamic deflection measurement would be required. An obvious possibility is the case in which the whirling is the result primarily of the critical deflection, while the actual mass unbalance is small. In such a case, the coefficients e_n and g_n may be neglected compared to a_n and b_n in equations (71) and (72) or (74). As a result, the dynamic deflection measurements may be used to solve for a_n and b_n for as many harmonics as desired. As before, the problem is simplified considerably if the inequalities (73) hold. Of course, this situation in which the initial deflection is the dominant effect is more likely in a solid shaft than in the hollow shafting of interest here. A different approach may be used to accomplish the same result, however, as will be shown below.

Referring to equations (69), note that the combination of coefficients (a_n+e_n) and (b_n+g_n) appears on the right-hand side.

If the damping coefficient is small, so that $\gamma_n << \omega$, it is permissible to add the term $\omega\gamma_n g_n$ to the right-hand side of the first of equations (69) and to subtract $\omega\gamma_n e_n$ from the right-hand side of the second. It is noted that if g_n and e_n are small compared to a_n and b_n, these modifications are again possible so that this new approximation contains the previous special case. With these changes, equations (69) may be written in the form

$$\begin{aligned}(\omega_n^2-\omega^2)A_n-\omega\gamma_n B_n &= \omega^2 r_n+\omega\gamma_n s_n \\ \omega\gamma_n A_n+(\omega_n^2-\omega^2)B_n &= \omega^2 s_n-\omega\gamma_n r_n\end{aligned} \tag{75}$$

where

$$\begin{aligned}r_n &= a_n + e_n \\ s_n &= b_n + g_n.\end{aligned} \tag{76}$$

The shaft imperfections are now described by the two sets of coefficients r_n and s_n rather than by four sets as before. Since the ultimate goal is to decrease the amplitudes A_n and B_n, it is unnecessary to distinguish between the effects of initial deflections and those of mass unbalance. In fact, this approximate method is equivalent to defining "an effective unbalance" described by the functions

$$\begin{aligned}u_o(x)+\eta_1(x) &= \sum_{n=1}^{\infty} r_n X_n(x) \\ v_o(x)+\eta_2(x) &= \sum_{n=1}^{\infty} s_n X_n(x).\end{aligned} \tag{77}$$

Equations (75) may be solved with the result

$$A_n = \frac{\omega^2(\omega_n^2-\omega^2-\gamma_n^2)r_n+\omega\omega_n^2\gamma_n s_n}{(\omega_n^2-\omega^2)^2+\omega^2\gamma_n^2} \tag{78}$$

$$B_n = \frac{\omega^2(\omega_n^2-\omega^2-\gamma_n^2)s_n-\omega\omega_n^2\gamma_n r_n}{(\omega_n^2-\omega^2)^2+\omega^2\gamma_n^2}. \tag{79}$$

Equations (78) and (79) may be substituted into equations (66) to obtain the deflection functions $u(x)$ and $v(x)$ in terms of the effective modal unbalance coefficients r_n and s_n. Then, if

measurements of u and v are obtained at any point for m different operating speeds, these data may be used to compute the coefficients r_n and s_n for n=1,2,...m. Thus, the first m modal contributions of the effective unbalance are determined without any need for a static initial deflection measurement. It should be noted that, as before, there is an advantage if the operating speeds chosen to make measurements are the first m critical speeds. If the coefficients obey the inequalities (73),

$$u_k(x) = \frac{\omega_k s_k - \gamma_k r_k}{\gamma k} X_k(x)$$

$$v_k(x) = \frac{\gamma_k s_k + \omega_k r_k}{\gamma k} X_k(x) \qquad (80)$$

is obtained immediately, and equations (80) may easily be solved for r_k and s_k.

Therefore, it has been shown that if $\gamma_k << \omega$, the effective unbalance can be determined from one dynamic measurement of the whirling amplitude. The computations are greatly simplified again if the inequalities (73) are satisfied; this point can, of course, be checked quite easily for any particular shaft design.

DETERMINATION OF BALANCE CORRECTIONS

The perturbing force caused by the effective unbalance may be obtained from equations (64) and (65). Thus, the perturbing force per unit length of shaft is given by

$$\bar{F}_p = \bar{n}_1 \rho A \omega^2 (u_o + \eta_1) + \bar{n}_2 \rho A \omega^2 (v_o + \eta_2). \qquad (81)$$

Substituting for the effective unbalance from equations (67), (68), and (76),

$$\bar{F}_p = \sum_{n=1}^{\infty} \rho A \omega^2 (n_1 r_n + \bar{n}_2 s_n) X_n(x). \qquad (82)$$

The problem of balancing a given shaft when r_n and s_n have been determined is now reduced to the determination of balance corrections which will produce a suitable corrective force $\bar{F}^*$. This correction force $\bar{F}^*$ must, insofar as possible, cancel out

the effect of the disturbing force $\bar{F}_p$ in as many modes as necessary to cover the design range of ω.

Now, assume that balance corrections are introduced by attaching at k points ξ_i concentrated masses M_i at distances ε_i from the geometric axis and at angles θ_i with respect to the unit vector $\bar{n}_1$. The unbalance force per unit length due to such concentrated masses may be written in the form

$$\bar{F}^* = \sum_{i=1}^{k} M_i \varepsilon_i \omega^2 [\bar{n}_1 \cos\theta_i + \bar{n}_2 \sin\theta_i] \delta(x-\xi_i) \tag{83}$$

where $\delta(x-\xi_i)$ is the Dirac delta function at ξ_i. It is convenient to expand this expression in a series in terms of the mode shapes of the shaft; thus,

$$\bar{F}^* = \sum_{n=1}^{\infty} \frac{\omega^2 X_n(x)}{N_n} \sum_{i=1}^{k} M_1 - \varepsilon_i [\bar{n}_1 \cos\theta_i + \bar{n}_2 \sin\theta_i] X_n(\xi_i) \tag{84}$$

where $N_n = \int_0^L X_n^2(x)\,dx$.

Adding equations (82) and (84) gives the net disturbing force per unit length resulting from both the initial unbalance and the correction masses; the result is

$$\bar{F}_p + \bar{F}^* = \omega^2 \sum_{n=1}^{\infty} \{\rho A(\bar{n}_1 r_n + \bar{n}_2 s_n) + \frac{1}{N_n} \sum_{i=1}^{k} M_1 - \varepsilon_i (\bar{n}_1 \cos\theta_i + \bar{n}_2 \sin\theta_i)\ X_n(\xi_i) . \tag{85}$$

It is clear from equation (85) that in order to eliminate the disturbing force in a given mode, the coefficient of $X_n(x)$ for the mode must be made to vanish. Since these coefficients are themselves vectors with components in the $\bar{n}_1$ and $\bar{n}_2$ directions, two equations relating the correction masses to the unbalance are obtained for each mode; thus

$$\sum_{i=1}^{k} M_i \varepsilon_i X_n(\xi_i) \cos\theta_i = -\rho A N_n r_n \tag{86}$$

$$\sum_{i=1}^{k} M_i \varepsilon_i X_n(\xi_i) \sin\theta_i = -\rho A N_n s_n . \tag{87}$$

It is now clear that for each mode which must be suppressed, two equations must be written in the unknowns $M_i\varepsilon_i\cos\theta_1$ and $M_i\varepsilon_i\sin\theta_i$. Also note that ε_1 is determined by the shaft radius and method of attachment of the mass correction, so that the only true unknowns are each mass M_i and the angle θ_i at which the mass must be mounted. For convenience, the notation

$$M_i\varepsilon_i\cos\theta_i = p_{i1}$$
$$M_i\varepsilon_i\sin\theta_i = p_{i2} \tag{88}$$

is introduced; equations (86) and (87) may then be written

$$\sum_{i=1}^{k} p_{i1}X_n(\xi_i) = \rho AN_n r_n$$
$$\sum_{i=1}^{k} p_{i2}X_n(\xi_i) = \rho AN_n s_n . \tag{89}$$

It is now clear that for each mode that is to be eliminated, two equations can be written in two unknowns, which determine one mass balance correction. In fact, if the first k modes are to be suppressed, a system of k masses <u>can always</u> be determined from equations (89) which will accomplish the purpose. From a design viewpoint, however, this may not be the most advantageous system of balance weights, and it may be desirable to attempt a correction of m modes with k masses where $k<m$. In such a case, the problem of satisfying 2m equations [yielded by equations (89)] for 2k unknowns would arise. The correction can be made by making the system of equations (89) linearly dependent to a suitable degree so that the number of independent equations is reduced to the number of unknowns. There may be a method to optimize the way in which this reduction is carried out, but this is outside the scope of the present report. The fact is that a solution can be found by prescribing a suitable number (i.e., m-k) of relations between the functions $X_n(\xi_i)$ $(n=1,2...m,\ i=1,2...k)$, and this is accomplished in practice by shifting the stations at which correction masses are to be attached. Thus, the problem of determining the position and magnitude of corrections can be handled analytically. Two additional remarks must be made, however, in connection with the selection of correction masses. First, when the calculations for unbalance are carried out by hand, it is

convenient and accurate to use theoretical modes; but when modal information is used in equations (89), it is necessary to use actual modes because the corrections are sensitive to the coefficients $X_n(\xi_i)$, which could be in error if theoretical and actual modes deviate appreciably. Second, it has been found by experience that equations (89) tend to overestimate the correction needed. This is probably due to the fact that when measurements are made at critical speed, the effective damping of the shaft is small so that the unbalance is overestimated. Thus, the proper balancing procedure until an improvement can be made would consist of locating the masses by the above method but trying an initial balancing with a fraction (of the order of 20 percent) of the calculated magnitude and retesting the shaft, monitoring the amplitude and phase angle. It should be noted that the whirling behavior becomes more and more sensitive to small balance changes in the higher modes (because of larger amplification factors).

Unclassified

Security Classification

DOCUMENT CONTROL DATA - R&D

(Security classification of title, body of abstract and indexing annotation must be entered when the overall report is classified)

1 ORIGINATING ACTIVITY (Corporate author) THE BOEING COMPANY, VERTOL DIVISION Morton, Pennsylvania	2a. REPORT SECURITY CLASSIFICATION Unclassified 2b GROUP None

3 REPORT TITLE

DESIGN AND TEST EVALUATION OF A SUPERCRITICAL SPEED SHAFT

4 DESCRIPTIVE NOTES (Type of report and inclusive dates)

Final Report

5 AUTHOR(S) (Last name, first name, initial)

Baier, Robert, and Mack, John

6. REPORT DATE	7a TOTAL NO. OF PAGES	7b. NO. OF REFS
June 1966	186	8

8a CONTRACT OR GRANT NO. DA 44-177-AMC-161(T) b. PROJECT NO. Task 1M121401D14414 c. d.	9a ORIGINATOR'S REPORT NUMBER(S) USAAVLABS Technical Report 66-49 9b. OTHER REPORT NO(S) (Any other numbers that may be assigned this report) R-458

10. AVAILABILITY/LIMITATION NOTICES

Distribution of this document is unlimited.

11. SUPPLEMENTARY NOTES	12. SPONSORING MILITARY ACTIVITY
	U.S. Army Aviation Materiel Laboratories, Fort Eustis, Virginia

13. ABSTRACT

This report describes the research, evaluation, experimental procedures, and conclusions from a study of the feasibility of the use of a supercritical speed interconnecting shaft in helicopters and other aircraft that require interconnecting drive shafts. The program was centered around the design, construction, and test of a full-scale supercritical speed shaft with dimensions compatible with the Boeing-Vertol CH-47A helicopter. Particular emphasis was placed on the design and development of suitable dampers for supercritical speed shaft installations, and on the development of shaft balancing procedures suitable for production application. The test shaft was operated successfully through a speed range from 0 to 9500 revolutions per minute, and subsequent analysis showed that the supercritical speed shaft offers a number of advantages over the subcritical speed shafts that are now used. All methods, procedures, and results are thoroughly documented with substantiating data, and firm conclusions and recommendations are presented. Four mathematical appendixes are provided.

DD FORM 1 JAN 64 1473

Unclassified

Security Classification

14. KEY WORDS	LINK A		LINK B		LINK C	
	ROLE	WT	ROLE	WT	ROLE	WT
SUBCRITICAL SPEED SHAFT						
SUPERCRITICAL SPEED SHAFT						
INTERCONNECTING DRIVE SHAFT						
HELICOPTER						
VTOL						
DAMPER						
BALANCE						
FEASIBLE						
ADVANTAGEOUS						

INSTRUCTIONS

1. ORIGINATING ACTIVITY: Enter the name and address of the contractor, subcontractor, grantee, Department of Defense activity or other organization *(corporate author)* issuing the report.

2*a*. REPORT SECURITY CLASSIFICATION: Enter the overall security classification of the report. Indicate whether "Restricted Data" is included. Marking is to be in accordance with appropriate security regulations.

2*b*. GROUP: Automatic downgrading is specified in DoD Directive 5200.10 and Armed Forces Industrial Manual. Enter the group number. Also, when applicable, show that optional markings have been used for Group 3 and Group 4 as authorized.

3. REPORT TITLE: Enter the complete report title in all capital letters. Titles in all cases should be unclassified. If a meaningful title cannot be selected without classification, show title classification in all capitals in parenthesis immediately following the title.

4. DESCRIPTIVE NOTES: If appropriate, enter the type of report, e.g., interim, progress, summary, annual, or final. Give the inclusive dates when a specific reporting period is covered.

5. AUTHOR(S): Enter the name(s) of author(s) as shown on or in the report. Enter last name, first name, middle initial. If military, show rank and branch of service. The name of the principal author is an absolute minimum requirement.

6. REPORT DATE: Enter the date of the report as day, month, year; or month, year. If more than one date appears on the report, use date of publication.

7*a*. TOTAL NUMBER OF PAGES: The total page count should follow normal pagination procedures, i.e., enter the number of pages containing information.

7*b*. NUMBER OF REFERENCES: Enter the total number of references cited in the report.

8*a*. CONTRACT OR GRANT NUMBER: If appropriate, enter the applicable number of the contract or grant under which the report was written.

8*b*, 8*c*, & 8*d*. PROJECT NUMBER: Enter the appropriate military department identification, such as project number, subproject number, system numbers, task number, etc.

9*a*. ORIGINATOR'S REPORT NUMBER(S): Enter the official report number by which the document will be identified and controlled by the originating activity. This number must be unique to this report.

9*b*. OTHER REPORT NUMBER(S): If the report has been assigned any other report numbers *(either by the originator or by the sponsor)*, also enter this number(s).

10. AVAILABILITY/LIMITATION NOTICES: Enter any limitations on further dissemination of the report, other than those imposed by security classification, using standard statements such as:

(1) "Qualified requesters may obtain copies of this report from DDC."

(2) "Foreign announcement and dissemination of this report by DDC is not authorized."

(3) "U. S. Government agencies may obtain copies of this report directly from DDC. Other qualified DDC users shall request through _____."

(4) "U. S. military agencies may obtain copies of this report directly from DDC. Other qualified users shall request through _____."

(5) "All distribution of this report is controlled. Qualified DDC users shall request through _____."

If the report has been furnished to the Office of Technical Services, Department of Commerce, for sale to the public, indicate this fact and enter the price, if known.

11. SUPPLEMENTARY NOTES: Use for additional explanatory notes.

12. SPONSORING MILITARY ACTIVITY: Enter the name of the departmental project office or laboratory sponsoring *(paying for)* the research and development. Include address.

13. ABSTRACT: Enter an abstract giving a brief and factual summary of the document indicative of the report, even though it may also appear elsewhere in the body of the technical report. If additional space is required, a continuation sheet shall be attached.

It is highly desirable that the abstract of classified reports be unclassified. Each paragraph of the abstract shall end with an indication of the military security classification of the information in the paragraph, represented as *(TS)*, *(S)*, *(C)*, or *(U)*.

There is no limitation on the length of the abstract. However, the suggested length is from 150 to 225 words.

14. KEY WORDS: Key words are technically meaningful terms or short phrases that characterize a report and may be used as index entries for cataloging the report. Key words must be selected so that no security classification is required. Identifiers, such as equipment model designation, trade name, military project code name, geographic location, may be used as key words but will be followed by an indication of technical context. The assignment of links, rules, and weights is optional.